UNIVERSIDAD MICHOACANA DE
SAN NICOLÁS DE HIDALGO

Facultad de Ingeniería Eléctrica
División de Estudios de Posgrado

"MODELING AND ANALYSIS OF INTEGRATED NATURAL GAS AND ELECTRICITY NETWORKS"

by

JOSÉ LUIS SÁNCHEZ GARDUÑO

THESIS

REQUIREMENT FOR THE DEGREE OF

DOCTOR OF SCIENCE IN ELECTRICAL ENGINEERING

ADVISOR:

CLAUDIO RUBÉN FUERTE ESQUIVEL, PhD.

MORELIA, MICHOACÁN FEBRUARY, 2021

MODELING AND ANALYSIS OF INTEGRATED NATURAL GAS AND ELECTRICITY NETWORKS

Los Miembros del Jurado de Examen de Grado aprueban la Tesis de **Doctorado en Ciencias en Ingeniería Eléctrica, Opción en Sistemas Eléctricos** de ***José Luis Sánchez Garduño.***

Dra. Elisa Espinosa Juárez
Presidente del Jurado

Dr. Claudio Rubén Fuerte Esquivel
Director de Tesis

Dr. J. Jesús Rico Melgoza
Vocal

Dr. J. Aurelio Medina Rios
Vocal

Dr. César Ángeles Camacho
Revisor Externo (UNAM)

Dr. Roberto Tapia Sánchez
Jefe de la División de Estudios de Posgrado de la Facultad de Ingeniería Eléctrica. UMSNH
(Por reconocimiento de firmas)

UNIVERSIDAD MICHOACANA DE SAN NICOLÁS DE HIDALGO
Febrero 2021

Dedicatoria

A Dios por darme vida, salud y la oportunidad de perseguir mi sueños.

A mi padre José Luis Sánchez Aguilar, a quién durante este proceso Dios llamó a su lado, pero que fue pilar fundamental en la realización de éste y todos los logros de mi vida. A ti, mi más profunda y eterna gratitud. Te querré por siempre papá!!

A mi madre Ma. de los Ángeles Garduño Rodríguez, la piedra angular de todo lo que soy, y mi más puro y eterno amor.

A mis queridos hermanos Ulises y Ramses, mis compañeros de vida.

A mi abuela Josefina Rodríguez Cano, mi querida mamá grande.

A mis tíos, David, José y Betty.

A mi compañera, mi amiga y mi novia, Brenda Anais Sánchez Ledesma, y...

a mis hermanos por elección, Goyo, Química, Miguel y César.

"Nunca consideres el estudio como una obligación,
sino como una oportunidad para penetrar en el bello y maravilloso mundo del saber"
Albert Einstein

Abstract

Among the main challenges faced by current energy systems is the need to design analysis strategies that guarantee the continuity of the energy supply, while considering the increasingly random nature of electrical systems. Even though there is a fundamental trend in integrating renewable sources in electrical systems, in countries like Mexico and United States, this integration has also increased the dependence on the use of natural gas as a primary energy source for the production of electricity. The increasing use of gas-fired generators has motivated research about how electricity and natural gas transmission networks interact between them. Within this context, a novel approach to the comprehensive formulation of the electricity and natural gas flows problem is proposed in this thesis, which allows addressing the interaction between both energy systems from a steady- and quasi-steady-state viewpoint.

Regarding the natural gas system, a new mathematical model is proposed to represent the steady state and transient state of the gas that flows through the pipelines. Unlike the models developed so far that approximate gas flows by an average value that depends on the pipeline length, the proposed model allows calculating the inlet and outlet gas flow in a pipeline. This proposal applies to different operating regimes of gas flows and any pressure level in natural gas transportation systems.

On the other hand, the electrical system is modeled from a power flow model that considers the effect of primary frequency regulation on generation as well as the voltage and frequency dependence of the loads. The interdependence between the electricity and natural gas systems is considered from the electrical power consumption of the compression stations and the gas consumption by the gas-fired generators, where the latter may be limited by gas

availability. The multi-energy system operational interdependence is evaluated considering disturbances in both systems, which could result in an unfeasible operating point in terms of the electric frequency value. A proposed control action is performed to bring the system towards a feasible equilibrium point that guarantees that the electric system operates within an established frequency band. Since each generator active power with primary regulation changes concerning its original programmed power, the reactive power limits must also change according to the value of that generation. Hence, a set of equations is proposed to determine the generator reactive power limits as a function of its active power generation.

Based on all technical aspects mentioned above, the proposed approach allows a better evaluation of the existing interdependence between energy infrastructures and their real operating conditions. The effectiveness and validity of the proposal are numerically demonstrated through the case studies reported in this thesis.

Keywords— Electricity infrastructure, frequency regulation, gas and power flow analysis, natural gas infrastructure, nodal gas flow injections.

Resumen

Entre los principales retos a los que se enfrentan los sistemas energéticos actuales se encuentra la necesidad de diseñar estrategias de análisis que garanticen la continuidad del suministro de energía considerando la naturaleza cada vez más aleatoria de los sistemas eléctricos. Aunque existe una tendencia fundamental en la integración de fuentes renovables en los sistemas eléctricos, en países como México o Estados Unidos, esta integración también ha incrementado la dependencia sobre el uso del gas natural como fuente de energía primaria para la producción de electricidad. El creciente uso de generadores a gas ha motivado la investigación sobre cómo las redes de transporte de electricidad y de gas natural interactúan entre sí. En este contexto, en esta tesis se propone un enfoque novedoso para la formulación integral del problema de flujos de electricidad y gas natural que permite abordar la interacción entre ambos sistemas energéticos desde un punto de vista de estado estacionario y cuasi estacionario.

En cuanto al sistema de gas natural, se propone un nuevo modelo matemático para representar el estado estacionario y el estado transitorio del gas que fluye a través de los gasoductos. A diferencia de los modelos desarrollados hasta ahora, que aproximan los flujos de gas mediante un valor promedio que depende de la longitud del gasoducto, el modelo propuesto permite calcular el flujo de gas a la entrada y a la salida del gasoducto. Esta propuesta se aplica a diferentes regímenes de funcionamiento y a cualquier nivel de presión en los sistemas de transporte de gas natural.

Por otro lado, el sistema eléctrico es modelado a partir de un modelo de flujo de potencia que considera el efecto de la regulación primaria de frecuencia en la generación, así como la dependencia de la tensión y la frecuencia de las cargas. La interdependencia entre los

sistemas eléctrico y de gas natural se considera a partir del consumo de energía eléctrica de las estaciones de compresión y del consumo de gas por parte de los generadores de gas, donde este último puede estar limitado por la disponibilidad de gas. La interdependencia operativa del sistema multi-energético se evalúa considerando perturbaciones en ambos sistemas, lo que podría resultar en un punto de operación infactible en términos del valor de la frecuencia eléctrica. En este contexto, se propone una acción de control para llevar el sistema hacia un punto de equilibrio factible que garantice que el sistema eléctrico opere dentro de una banda de frecuencia establecida. Dado que la potencia activa de cada generador con regulación primaria cambia respecto a su potencia original programada, los límites de potencia reactiva también deben cambiar en función del valor de dicha generación. Por ello, se propone un conjunto de ecuaciones para determinar los límites de potencia reactiva del generador en función de su generación de potencia activa.

Con base en todos los aspectos técnicos mencionados, el enfoque propuesto permite una mejor evaluación de la interdependencia existente entre las infraestructuras energéticas y sus condiciones reales de operación. La eficacia y la validez de la propuesta se demuestran numéricamente a través de los casos de estudio reportados en esta tesis.

Palabras clave— Análisis de flujos de gas y electricidad, infraestructura de gas natural, infraestructura eléctrica, inyecciones nodales de flujo de gas, regulación de frecuencia.

Acknowledgments

I am very grateful to my research advisor, Dr. Claudio Rubén Fuerte Esquivel, for allowing me to work under his guidance. For all the knowledge shared, for the teachings, and continuous learning, but above all, I thank him for all the support, understanding, trust, and friendship he has given me. All my admiration and respect.

I thank the graduate department of the UMSNH faculty of engineering for opening the doors for me and allowing me to do my doctoral studies, in addition, I want especially to thank the academic staff for sharing their knowledge.

Thanks to the National Council for Scientific and Technological Research (CONACyT), Mexico, for the financial support received under grant 571370, which facilitated the completion of my doctoral degree.

I especially thank my parents and brothers for all their effort, trust, love, and unconditional support throughout this journey.

I thank my girlfriend Brenda and all of my friends for their support, motivation, and encouragement in achieving my goals.

Thanks to my friends and classmates, Romay, Uriel, Jaque, Ricardo, Iván, my great friend Josué Guadalupe, and everyone who supported this effort.

Finally, I thank God for giving me life, health, and the grand fortune of being able to pursue my dreams!

"They who dream by day are cognizant of many things
which escape those who dream only by night."
Edgar Allan Poe, Eleonora

Contents

Abstract V

Resumen VII

Acknowledgements IX

Contents XI

List of Figures XV

List of Tables XVII

Acronyms XIX

Nomenclature XXI

Publications XXV

1 Introduction 1
- 1.1 Introduction . . . 1
- 1.2 Justification . . . 2
- 1.3 State of the art . . . 3
  - 1.3.1 Modeling of volumetric flows in gas networks . . . 4
  - 1.3.2 Static power flow analysis of integrated natural gas and electricity networks . . . 9
  - 1.3.3 Multi-period power flow analysis of integrated natural gas and electricity networks . . . 13
- 1.4 Hypothesis . . . 15
- 1.5 Objectives . . . 16
  - 1.5.1 Particular objectives . . . 16
- 1.6 Contributions . . . 17
- 1.7 Methodology . . . 18
- 1.8 Thesis outline . . . 19

2 Gas flow equations in steady state 21
2.1 Introduction . . . 21
2.2 Nodal flow injection equations . . . 22
2.2.1 Compressibility factor . . . 26
2.2.2 Friction factor . . . 28
2.2.3 Linepack and Δ_q . . . 31
2.3 Validation of proposed equations . . . 31
2.4 Comparison of gas flow equations . . . 33
2.5 Conclusions . . . 45

3 Modeling of natural gas and electricity networks 47
3.1 Introduction . . . 47
3.2 Natural gas network . . . 47
3.2.1 Pipeline . . . 48
3.2.2 Compressor stations . . . 49
3.2.3 Network model . . . 50
3.2.4 Case studies . . . 53
3.3 Electricity network . . . 61
3.3.1 Electric generators . . . 62
3.3.2 Electric loads . . . 64
3.3.3 Mismatch equations . . . 65
3.3.4 Case study . . . 66
3.4 Conclusions . . . 70

4 Static power flow analysis of integrated natural gas and electricity networks 73
4.1 Introduction . . . 73
4.2 Coupling between natural gas and electricity networks . . . 74
4.3 Integrated natural gas and power flow methodology . . . 75
4.3.1 Case study . . . 76
4.3.2 Case study 2 . . . 83
4.4 Preventive control of electric frequency methodology . . . 90
4.4.1 Case study . . . 93
4.4.2 Case study 2 . . . 97
4.5 Conclusions . . . 108

5 Multi-period power flow analysis of integrated natural gas and electricity networks 111
5.1 Introduction . . . 111
5.2 Transient natural gas flow modeling . . . 112
5.2.1 Multi-period AFE model . . . 114
5.2.2 Multi-period NFI model . . . 115
5.2.3 Compressor stations . . . 117
5.2.4 Network model . . . 118
5.2.5 Case study . . . 120
5.2.6 Case study 2 . . . 127
5.3 Integrated natural gas and power flow methodology . . . 132

5.3.1 Natural gas network 133
5.3.2 Electricity network 133
5.3.3 Coupling between natural gas and electricity networks 134
5.3.4 Unified multi-period electricity and natural gas network model . . . 135
5.4 Conclusions 150

6 General conclusions and future work 153
6.1 General conclusions 153
6.2 Future work 155

A Deductions 159
A.1 Deduction of nodal flow injection equations 159
A.2 Deduction of Δq equation 164

B Systems' data 167
B.1 Electrical networks 167
B.1.1 3-bus test system 167
B.2 Gas networks 169
B.2.1 Belgium network 169
B.2.2 15-node network 171
B.2.3 Network of 11 nodes for low pressure 172

Bibliography 175

List of Figures

2.1 Forces acting on a volume of gas circulating through a pipeline. 23
2.2 Scheme of nodal gas flow injections. 24
2.3 Extra high pressure. 39
2.4 High pressure. 40
2.5 Medium pressure. 41
2.6 Low pressure. 42
2.7 Compressibility factor. 42
2.8 Comparison of flows. 44

3.1 Balance of gas flow at the k-th node. 50
3.2 Belgium natural gas network. 53
3.3 Nodal pressure. 55
3.4 Compressibility factor. 56
3.5 Gas flows with the NFI model considering the elevation of nodes. 56
3.6 Distribution of Δq among the connection nodes of a pipeline. 57
3.7 Gas flows. 58
3.8 Difference between the inlet and outlet gas flows. 59
3.9 Nodal pressures. 59
3.10 Compressibility factor. 59
3.11 Low pressure gas network. 60
3.12 Three-bus network. 67

4.1 The 20-node gas network coupled with a 3-bus electrical network. 76
4.2 Nodal pressures. 82
4.3 Compressibility factor. 82
4.4 The 15-node gas network coupled with the IEEE-118 network. 84
4.5 Gas flows in the pipelines. 88
4.6 Linepack in the pipelines. 89
4.7 Nodal pressures. 89
4.8 Nodal compressibility factor. 89
4.9 Flow chart of the implemented algorithm. 91
4.10 The 15-node gas network coupled with the IEEE-118 network. 98
4.11 Reactive power generated. 101

4.12 Nodal pressure. 105
4.13 Gas flows in the pipelines. 105
4.14 Difference between inlet and outlet gas flows in the pipelines. 106
4.15 Linepack in the pipelines. 106

5.1 AFE multi-period model. 114
5.2 NFI multi-period model. 115
5.3 Pipeline diagram of the Belgium gas network. 120
5.4 Natural gas demand characteristic for a 24-hour period. 121
5.5 Natural gas flows from node "k" to node "m". 122
5.6 Natural gas flows from node "m" to node "k". 123
5.7 Difference between inlet and outlet gas flows by pipeline. 124
5.8 Nodal pressures. 125
5.9 Compressibility factor by node. 126
5.10 Total linepack in the network. 126
5.11 Natural gas flows from node "k" to node "m". 127
5.12 Natural gas flows from node "m" to node "k". 128
5.13 Difference between inlet and outlet gas flows by pipeline. 129
5.14 Nodal pressures. 130
5.15 Compressibility factor by node. 131
5.16 Total linepack in the network. 131
5.17 Natural gas source in node 1. 132
5.18 The 15-node gas network coupled with the IEEE 118-bus network. 136
5.19 Electric power load characteristic for a 24-hour period. 137
5.20 Electrical system frequency. 138
5.21 Active power supplied by system units. 138
5.22 Reactive power supplied by system units. 139
5.23 Gas consumption by gas-fired generators. 140
5.24 Natural gas flows from node "k" to node "m". 140
5.25 Natural gas flows from node "m" to node "k". 141
5.26 Difference between inlet and outlet gas flows by pipeline. 141
5.27 Nodal pressures. 142
5.28 Total linepack in the network. 143
5.29 Electric power load characteristic for a 24-hour period. 144
5.30 Electrical system frequency. 145
5.31 Active power supplied by generators in primary frequency regulation. 146
5.32 Reactive power supplied by generators in primary frequency regulation. . . 147
5.33 Natural gas flows from node "k" to node "m". 148
5.34 Natural gas flows from node "m" to node "k". 148
5.35 Difference between inlet and outlet gas flows by pipeline. 149
5.36 Nodal pressures. 149
5.37 Total linepack in the network. 150

List of Tables

2.1 Chemical composition of natural gas 27
2.2 Comparison of gas flow equations 38

3.1 Comparison of gas flows $[SCMH] \times 10^3$ 54
3.2 Gas supplied by node 1 $[SCMH] \times 10^3$ 55
3.3 Comparison of results in compressor stations 57
3.4 Comparison of gas flows $[SCMH]$ 61
3.5 Gas supplied, gas demanded and nodal pressures 61
3.6 Generators' description 67
3.7 Active power generated [MW] 68
3.8 Frequency magnitudes 68
3.9 Reactive power generated [MVARs] - FRPF model 69
3.10 Electric power load 70

4.1 Results for electric generators 78
4.2 Nodal voltages 79
4.3 Gas supplied by node 1 $[SCMH] \times 10^3$ 79
4.4 Results in the gas pipelines 80
4.5 Gas demanded $[SCMH] \times 10^3$ 81
4.6 Results in the compressor station 82
4.7 Generators in primary frequency regulation 84
4.8 Frequency magnitudes 85
4.9 Compressor stations' results 86
4.10 Gas demanded $[SCFH] \times 10^6$ 86
4.11 Total network values 87
4.12 Gas supplied by sources $[SCFH] \times 10^6$ 87
4.13 Economic dispatch and conventional flows' results 94
4.14 Results for electric generators 94
4.15 Gas demanded $[SCMH] \times 10^3$ 95
4.16 Gas supplied by node 1 $[SCMH] \times 10^3$ 95
4.17 Nodal voltages 95
4.18 Electric power demands 96
4.19 Results in the gas pipelines 96

4.20 Compressor stations' results 97
4.21 Generators in primary frequency regulation 98
4.22 Frequency magnitudes 98
4.23 Economic dispatch and conventional flows results for the $\Delta P > 0$ case . . . 99
4.24 Economic dispatch and conventional flows results for the $\Delta P < 0$ case . . . 99
4.25 Active power generated 100
4.26 Reactive power generated 101
4.27 Gas demanded $[SCFH] \times 10^6$ 103
4.28 Gas supplied by sources $[SCFH] \times 10^6$ 103
4.29 Total network values 104
4.30 Compressor stations' results 107

B.1 Generator data 167
B.2 Transmission lines' data 167
B.3 Loads' data 168
B.4 Shunt compensators' data 168
B.5 Node data 169
B.6 Pipelines' data 170
B.7 Compressor stations' data 170
B.8 Node data 171
B.9 Pipelines' data 171
B.10 Compressor stations' data 172
B.11 Node data 172
B.12 Pipelines' data 173

Acronyms

AFE average flow equation.

AGA American gas association.

BHP brake horsepower.

CFE Comisión Federal de Electricidad.

FRPF frequency regulated power flows.

GFE general flow equation.

MP-AFE multi-period average flow equation.

MP-NFI multi-period nodal flow injection.

MSCF million standard cubic feet.

MSCFD mullion standard cubic feet per day.

MSCFH million standard cubic feet per hour.

NFI nodal flow injection.

RMS root mean square.

SCMD standard cubic meters per day.

SCMH standard cubic meters per hour.

Nomenclature

Constants

g	Gravitational constant $\left(32.1742\frac{ft}{s^2}, 9.81\frac{m}{s^2}\right)$.
GHV	Gross heating value $\left(1015\frac{BTU}{SCF}, 37.81\frac{MJ}{SCM}\right)$.
R_{air}	Specific air constant $\left(1716\frac{ft-lb}{slug\cdot^\circ R}, 286.9\frac{N\cdot m}{kg\cdot^\circ K}\right)$.

Sets and indices

^{avg}	Average value.
^{cal}	Calculated value.
^{gau}	Gauge pressure.
^{iny}	Injection.
^{max}	Maximum limit.
^{min}	Minimum limit.
^{nom}	Nominal value.
^{sch}	Scheduled value.
$_0$	Standard conditions.
$_D$	Discharge node.
$_S$	Suction node.
$_{comp}$	Compressor station.

$_{gl}$ Gas load.

$_{gs}$ Gas source.

$_{G}$ Electric generator.

$_{L}$ Electric load.

$_{ref}$ Reference value.

$_{Tot}$ Total network value.

$_{i,j}$ Buses in the electrical system.

$_{k,m}$ Nodes in the natural gas system.

Parameters

α, β, γ Compressors gas consumption coefficients.

ϵ Pipeline efficiency (*dimensionless*).

η Compression process efficiency (*dimensionless*).

κ Isentropic coefficient (*dimensionless*).

μ Dynamic viscosity ($poise, Pa \cdot s$).

ε Roughness of the inner wall of the pipe (in, mm).

A Cross-sectional area of pipeline $\left(ft^2, m^2\right)$.

a, b, c Heat rate coefficients for coupled nodes.

a_Q, b_Q Coefficients of reactive generation control characteristics (*dimensionless*).

CR Compression ratio (*dimensionless*).

D Inner diameter of pipeline (in, mm).

E Compressor's parasitic efficiency (*dimensionless*).

G Specific gravity (*dimensionless*).

h Nodal height (ft, m).

K_{pc}, K_{qc} Portion of total load proportional to n-th power of voltage (*dimensionless*).

K_{pf}, K_{qf} Frequency characteristics of load (*dimensionless*).

K_{pp}, K_{qp} Portion of total load proportional to constant power load (*dimensionless*).

K_{pz}, K_{qz} Portion of total load proportional to constant impedance load (*dimensionless*).

K_{reg} Turbine steady-state regulation setting $(p.u.)$.

L Pipeline length $(miles, km)$.

Nc Number of compressor stations.

Ne Number of buses in the electrical system.

Ng Number of nodes in the gas system.

nG Number of electric generators.

nL Number of electric loads.

T Temperature $(^\circ R, ^\circ K)$.

Variables

$\dot{m}$ Gas mass flow rate $(lb/s, Kg/s)$.

λ Friction factor (*dimensionless*).

ρ Density $\left(lb/ft^3, kg/m^3\right)$.

τ Gas extracted by the compressor $(SCFH, SCMH)$.

θ Voltage angle $(^\circ)$.

υ Flow speed rate $(ft/s, m/s)$.

f Frequency (Hz).

LP Gas storage in the pipeline (SCF, SCM).

P	Active power ($p.u.$).
p	Pressure ($psia, bar$).
Q	Reactive power ($p.u.$).
q	Volumetric flow rate ($SCFH, SCMH$).
Re	Reynolds number ($dimensionaless$).
S	Apparent power ($p.u.$).
t	Time (s).
v	Voltage magnitude ($p.u.$).
v_a, v_b	Complementarity variables ($p.u.$).
z	Compressibility factor ($dimensionless$).

Publications

Journal Papers

- Tovar-Ramírez, C. A., Fuerte-Esquivel, C. R., Martínez Mares, A., Sánchez-Garduño, J. L. (2019). A generalized short-term unit commitment approach for analyzing electric power and natural gas integrated systems. Electric Power Systems Research, 172, 63–76.

Conference papers:

- J. L. Sánchez-Garduño and C. R. Fuerte-Esquivel, "Integrated analysis of electrical and gas transmission networks considering primary frequency control," 2020 IEEE PES Transmission & Distribution Conference and Exhibition - Latin America (T&D LA), Montevideo, Uruguay, 2020, pp. 1-6.

- J. L. Sánchez-Garduño and C. R. Fuerte-Esquivel, "Preventive power rescheduling for electric frequency enhancement in integrated energy systems," 2020 IEEE International Autumn Meeting on Power, Electronics and Computing (ROPEC), Ixtapa, Mexico, 2020, pp. 1-6.

- O. Romay, J. L. Sánchez-Garduño and C. R. Fuerte-Esquivel, "Unified state estimation in integrated natural gas and electricity networks," 2020 IEEE International Autumn Meeting on Power, Electronics and Computing (ROPEC), Ixtapa, Mexico, 2020, pp. 1-6.

Chapter 1

Introduction

1.1 Introduction

The evolution and change that energy systems have undergone worldwide have motivated the study of how different energy systems interact with each other. Such is the case of studies performed to determine the electrical power systems operation, where the systems responsible for transporting the primary energy sources and the energy conversion process used to be excluded. In this case, the existing operational interdependence between the primary energy transport systems and the electrical systems was neglected. It has been demonstrated, however, that the safe, reliable and economic operation of an electric energy system depends not only on its proper operation and control but also on its ability to take advantage of the different types of primary energies used to generate electricity.

Among the different types of primary energies used to generate electricity, the global use of natural gas as a primary energy source to produce electricity has dramatically increased in the last decade. This has motivated the study of existing interdependencies between electricity and natural gas transmission networks in a unified framework of analysis.

1.2 Justification

One of the significant challenges that current energy systems face is the need to design strategies of analysis that guarantee the continuity of the energy supply, taking into account the increasingly random nature of electrical systems. The background mentioned above requires generators with fast responses to change their production levels and provide sufficient reserve margins to guarantee the safe and reliable operation of the energy system.

On the other hand, natural gas is an essential energy source for the future. Low greenhouse gas emissions and relatively low capital costs place it in a competitive position within most energy sectors and above other energy sources, particularly for new electric power generation facilities. Global projections of natural gas reserve levels are also clear indicators of the increasingly important role that it will play in supporting growth in markets through 2035 [Ríos-Mercado15].

In Mexico, for example, the demand for natural gas by the Mexican electricity sector in the last decade has shown an increase of 62.3%, rising from 2,389.6 MSCFD in 2006 to 3,878.5 MSCFD in 2016, mainly because of the strategy implemented by the Comisión Federal de Electricidad (CFE) to replace costly and polluting fuels with more efficient and sustainable fuels such as natural gas. In this context, natural gas is expected to have an 82% share of the total fuel consumption by 2031, which will help regulate the sustainable use of energy and meet the obligations in terms of clean energy, as well as reduce polluting emissions from the electricity industry [SENER17a].

Even though there is indeed an essential trend in the integration of renewable sources into the national interconnected system (NIS), note that of the 317,278 GWh of electrical energy produced in Mexico in 2018, 51% was produced by combined cycle generators, while 3.9 % was produced by wind energy, 0.7% by photovoltaic energy and 0.2% by bioenergy [CENACE19]. It is expected that by 2031 the combined cycle units will continue to contribute 44.6% of the 456,683 GWh forecast, compared with 14.8% from wind energy and

22.6% produced jointly from bioenergy, nuclear, efficient generation, solar photovoltaic, and geothermal energy [SENER17b].

Based on the information mentioned above, gas production has had a significant impact on deploying new infrastructures, especially in countries such as Mexico or the United States, where the installed capacity of gas-fired power plants has increased enormously in recent years. It is expected that this tendency will increase in the coming years [SENER17a, Pambour17, Ríos-Mercado15]. Under these circumstances, the independent planning, operation and control of each energy infrastructure is no longer acceptable because of the growing interdependency between different energy systems. Therefore, the studies associated with electric power and natural gas networks operation must be carried out under a comprehensive reference framework that allows a better assessment and evaluation of the complex interdependence between these two subsystems.

Finally, regarding the gas transport system modeling, there are many proposals to calculate the gas flow through pipelines; however, all these equations assume that the gas flow through the entire pipeline can be modeled from an average model. This model main drawback is its assumption that the gas flow at the inlet and outlet ends of a pipeline are equal. Therefore, the models developed so far are limited to specific operating conditions, which could be insufficient and imprecise to describing the behavior of flows in a natural gas transportation system.

1.3 State of the art

The growing interest in analyzing the operational interdependence of integrated natural gas and electricity systems has encouraged many proposals that describe the steady state and/or the transient state of the multi-energy system from multiple approaches. The description of these works is given below.

1.3.1 Modeling of volumetric flows in gas networks

The efficient and effective movement of natural gas from producing regions to points of consumption is a crucial activity for the gas industry, and although different means of transportation can be applied, pipelines represent the most efficient and economical means of transporting large quantities of natural gas. Therefore, gas pipeline networks have stretched thousands of kilometers around the world in recent decades [Ríos-Mercado15].

Since a gas network is typically managed and operated from control centers to ensure reliability and the security of the supply, it is vital to have the correct models of the gas grid components and to use suitable computational tools to assess the system operating state [Osiadacz87]. A large number of works have focused on the analysis of the behavior of natural gas transport networks. For example, [Olorunniwo81] proposes a methodology for the optimal network design and expansion, and [Wong68, Wu00, Ríos-Mercado06] present optimization techniques to minimize the cost of fuel consumed by compression stations, while [Moller04, Tomasgard07, Tabkhi07, Borraz-Sánchez10, Bermúdez15, Arumugam15] propose methods to minimize operating costs or optimize flow capacity in transmission networks. These concepts are applied in [Mikolajková18] to a distribution system. Even though the analysis of these optimization problems is beyond the scope of this work, this is not the case for the models used to describe the strong dependence between the flow rate in pipelines and the pressure drop along the pipeline, which is commonly considered by the so-called general flow equation (GFE) or derivations of it.

The GFE is obtained by solving the partial differential equations that describe the energy balance in a pipeline under the following assumptions: i) a stable and isothermal flow, ii) a neglectable change of kinetic energy in the pipeline, iii) constant gas compressibility along the entire network, iv) constant friction force in each pipeline, and v) the validity of the Darcy friction loss relationship. Despite all these assumptions, the GFE, also called the fundamental flow equation, has been universally accepted to computing the steady-state volumetric flow rate of fluids [Ríos-Mercado15, Menon05].

Many other mathematical expressions have been derived from the GFE over the last century to approximate the average magnitude of compressible gas flows through large pipelines under specific conditions. Examples of these are the Weymouth (1912), Spitzglass (1912), Panhandle A (1940) and Panhandle B (1956) equations. The works of [Crane Company88], [Osiadacz87] and [Modisette00] provide complete details about these equations. Since each of these equations has a range of validity based on the considerations made in their deductions, their results do not coincide in the effect of flow, friction or pipe diameter on pressure drop. Hence, using one or another equation will influence the results obtained from analyzing a gas transmission grid.

It is a common practice to group all the physical properties and/or parameters of the pipeline and gas into a constant "C" or "K" , referred to as the resistance of the pipeline, to simplify the model [Menon05]. Based on this simplification and the equations mentioned above, several formulations have been proposed for the analysis, modeling and simulation of natural gas transportation networks. The gas network is modeled as an electrical circuit in [Tao98, Ke00], where the Weymouth equation is used to represent the electrical resistance. The same idea is used in [Taherinejad14], but the author considers the equations of Panhandle B, Weymouth, AGA, Colebrook-White and Gersten to have different electrical resistance models according to the operating conditions. In [Narváez99], gas flows are solved using a linear nodal balance model derived from the GFE linearization. [De Wolf17] analyzes the mathematical properties of various formulations of the gas transmission problem taking into account the nonlinear relationship between the gas flow and drop pressure from the Weymouth equation. The transmission network is simulated in [Woldeyohannes09] and [Abdolahi07] by the GFE considering different exponents and values of the constant "C". On the other hand, [Arumugam15, Bamzah10] use different equations (e.g., Panhandle A, Weymouth, Cox, and Lacey equations), for the analysis of gas flows depending on the pressure level or operating regime to which the gas is subjected. In [Woldeyohannes11] a simulation model is proposed for the analysis of transmission pipeline network system (TPNS) based on the GFE but incorporating detailed characteristics of compressor sta-

tions. [Olatunde12] analyzes the behavior of the GFE considering different friction factors. On the other hand, the Lacey's equation is used in [Abeysekera16] to perform a steady-state analysis of a low-pressure network considering the properties of gas composition and gas quality. The existence of a solution for a mathematical model of the gas transport system considering a non-flat topology is reported in [Bermúdez17], where an alternative form of the GFE is analytically demonstrated.

Many of the works mentioned above disregard that the pipeline resistance depends not only on the characteristics of the pipe but also on the conditions to which the fluid is subjected. By way of example, the gas compressibility depends on the temperature and pressure conditions it is subjected to, which vary throughout the transmission system. Furthermore, the average gas flow model neglects the inherent difference between the inlet and outlet gas flows at the pipeline, as well as the impact of this difference on the gas storage at each pipeline. This difference exists, however, because of the slow gas dynamics, the difference in altitude between the interconnecting nodes, the frictional force opposing the free movement of the fluid and the gas compressibility condition. Therefore, the average gas flow model could only be valid in situations where the pipe is full and the compressibility factor is close to 1, the pipe dimensions are very small, the coefficient of friction tends to be 0 and/or the gas travels at high speeds.

On the other hand, to model and efficiently calculate the gas flows through a natural gas transmission network, it is necessary to consider its topology in the problem formulation. The works of [Wu00, Ríos-Mercado06, De Wolf17, Tabkhi07, Szoplik12, Bermúdez15, Bermúdez17, Farzaneh-Gord16] make use of the so-called "incidence matrix" proposed in [Osiadacz87], which relates the different links between the elementary sections of a network. In this formulation, the interconnection points are defined as "nodes" with the network's active and passive elements called "arcs." The number of rows of the incidence matrix corresponds to the number of nodes and the number of columns to the number of branches. Lastly, the matrix k-th element is 1 if the arc is from node k, -1 if the arc is to node k and 0 if the arc is not connected to node k. Hence, a gas flow direction is preassigned to

each pipe, which may or may not coincide with the real gas flow direction of the gas flowing through the arc.

In addition to the hypothetical predefined direction of gas flow, it is necessary to consider its possible bidirectionality. Hence, the arcs must be duplicated in the incidence matrix to consider both possible directions. Another way to include this possible bidirectionality was proposed in [Tomasgard07], where additional equations of the form $(1 - \alpha)$ were added to determine the gas flow direction inside the pipeline. Similarly, two binary variables are imposed as constraints in [Mikolajková18], and only one of these variables can be active. To consider this bidirectionality without duplicating or adding variables to the model, [De Wolf17, Munoz03, Taimin Gindalan10, Martinez-Mares12] define the flow direction from a sign function, which depends on the difference between the quadratic nodal pressures of each pipe.

A drawback of this approach is that the gas flow direction must be verified for each pipe at each iteration of the solution process. Note also that determining the gas flow direction based on the difference between the quadratic nodal pressures might not always be valid. For example, a suction node "k" may have a lower pressure than a discharge node "m" if the height at which the "k" node is located is greater than the one associated with the "m" node. As a consequence of the interaction with the force of gravity, the resulting fluid circulation could be from the "k" node to the "m" node because of the gas natural circulation from the highest point to the lowest point. Note, however, that the force of gravity effect on the gas flow circulation does not occur if all nodes are at the same height, as assumed in [Woldeyohannes09, Woldeyohannes11, Farzaneh-Gord16, Munoz03]. Lastly, some works consider the effect of altitude changes on the pipeline: the potential energy, either from an adjustment factor that relates gravity to the difference in the height of the nodes [Taherinejad14, Abeysekera16, Martinez-Mares12] or from the pipeline's angle of inclination [Pambour17, Abdolahi07, Bermúdez17], which has a direct impact on the nodal pressure magnitudes.

Even though there are many proposed equations for calculating steady-state isothermal gas flow in pipelines, all these equations assume that the gas flow through the entire pipeline can be modeled by an average magnitude calculated at half of the pipeline's length. Therefore, these formulations do not consider the inherent difference between the inlet and outlet gas flows from a pipeline at a given instant of time.

Hence, the present work proposes a new mathematical model representing the steady-state behavior of gas flows through pipelines. This model consists of two equations developed from the concept of nodal flow injections, which allow calculating the inlet and outlet gas flows as well as the pressure drop in a pipe. These equations also implicitly consider the possible bidirectionality of gas flows. Other factors that the proposed equations take into account are the following. First, the strong dependence of the compressibility factor on the pressure and temperature conditions at which the gas is subjected at each node. Second, the potential energy effect on the gas flows because of the gravitational force acting on the pipeline inclination. Similarly, the dependence of gas flow magnitudes on the pipelines characteristics, e.g., length and diameter. Likewise, the equations proposed in this work consider the different operating regimes to which the gas may be subjected based on adequately selecting the friction coefficient relationship. Hence, these equations can be applied to different operational regimes and at any pressure level of natural gas transportation systems. Therefore, these equations solve the problem of using multiple equations to calculate gas flows according to the operating conditions or the type of study to be performed.

When using the average-based gas flow equations, the maximum gas flow is achieved when the pressure drop is maximum, which implies that the discharge node's pressure tends to be 0. Note that this is physically inconsistent since, in such a case, there can be no gas flow circulating through the discharge node. This statement is validated with the proposed nodal injection-based gas flow equations. It is also observed that the greater the pressure drop is, the greater the difference between the inlet and outlet gas flows.

In conjunction with the gas compression state, the relationships mentioned above directly

impact the stored gas and the storage capacity of the pipelines. From a steady-state gas flow model, however, it is impossible to consider the gas storage changes inside each pipeline and the impact of these changes on the behavior of gas flows and the nodal pressures of the entire network. Under this premise, from the nodal gas flow injection equations proposed for the steady state, new nonlinear algebraic nodal gas flow equations are derived to satisfy the energy and mass balance inside each pipe transiently. Therefore, the transient-state solution of a natural gas network for hourly sub periods is obtained by solving a set of nonlinear algebraic equations instead of a set of nonlinear space-time partial differential equations.

1.3.2 Static power flow analysis of integrated natural gas and electricity networks

Among the different types of primary energies used to generate electricity, the use of natural gas as a primary energy source to produce electricity has dramatically increased in the last decade, which has motivated an increasing number of works regarding the operational interdependence between natural gas and electricity infrastructures. From the steady-state operational interdependence viewpoint, a natural gas and electric power flow program should offer a very useful tool for system planners and system operators for evaluating how these two energy infrastructures interact with each other. There have been several proposals that can be broadly classified into two main categories: sequential [Beyza19, Massrur18, Meng19] and unified [An03, Martinez-Mares12, Zeng16, Shi17, Men17] solution methods.

Sequential solutions are rather attractive because the operating state associated with each energy infrastructure is independently determined by considering the effect of the electricity (resp. gas) infrastructure as a fixed demand of gas (resp. electric power). In the case of having gas compressors driven by electric motors and gas-fired power units, an electric power flow study is first performed by considering an initial guess of the power demanded by the gas compressors. The operating state of the gas network is then obtained for the fuel required by the gas-fired units. The sequential solution of both problems is performed

until both infrastructures' operating states do not change between iterations. On the other hand, the unified methods combine the set of equations representing the steady operating state of each energy infrastructure for a unified, iterative solution through a linearization technique.

The differences between the proposed sequential approaches are given by how the system components are modeled and the numerical methods used for obtaining the operating state of each energy infrastructure. A similar line of reasoning applies to the unified approaches. A common characteristic of the sequential and unified approaches, however, proposed in [Beyza19, Massrur18, Meng19] and [An03, Zeng16, Shi17, Men17], respectively, is that the electricity network is mathematically modeled by using the conventional formulation of the power flow problem. Hence, the gas and electricity networks are only coupled via the slack generator's active power if this generator is represented by a gas-fired unit. Note that in this case both infrastructures become fully independent if gas compressors do not use electric power from the electrical network, so there is no need to formulate and solve a unified model. On the other hand, using a single gas-fired slack generator in the unified approach could be impractical since potentially introducing misleading operating conditions for the gas part of the model. This drawback is overcome in [Martinez-Mares12] by allowing an arbitrary number of gas-fired generators to have variable active power by using the concept of distributed slack nodes.

From the operational perspective, many works address the possibility of jointly modeling and analyzing the natural gas and electricity networks from different approaches. For example, in [An03, Unsihuay07] unified models are presented for calculating the optimal flows of electric power and natural gas from the consumption of gas by units operating with this fuel. The interdependence of the two infrastructures is assessed in terms of the impact of gas market prices on the commitment and dispatch of units, i.e., on the production costs of natural gas generating plants. In [Quelhas Alves de Freitas06], both networks are represented by graph theory. The links have both capacity and efficiency restrictions, and weighting factors represent energy losses through the links so that the networks' technical

operating parameters are omitted from the model. In [Geidl07], the coupling between the different infrastructures is explicitly studied through the concept of energy centers, which are modeled by converter devices between the different primary energy sources, excluding the transport system itself from the analysis. The maximum amount of energy supplied by the natural gas system to each combined cycle electric generator is calculated in [Munoz03] by considering these generators as natural gas loads, so the electricity transmission grid is not considered in the study. Lastly, a unified model that considers the effect of temperature on the operation of the natural gas system is presented in [Martinez-Mares12].

On the other hand, proposals such as [Liu09, Liu11, Chaudry08] consider the transmission grid through a DC model, which results in limitations in determining the safety of the operating state of the electrical system, such as those associated with voltage and reactive generation control. A similar idea is applied to the modeling of the gas transport system (e.g. [Munoz03, Liu09]), where the flow equation is considered as a function of the resistance of the pipe "C" or "K", which is constant and includes all gas and pipeline parameters.

Many of the proposals mentioned above consider the nodal mismatch power and gas equations and the nodal voltages and nodal pressures as state variables. All these proposals, however, consider the gas flow circulating through the pipelines from the general flow equation or derivations of it (e.g. Weymouth, Panhandle A and B, Spitzglass, among others), which are based on average gas flow magnitudes.

In practice, several generators can continually modify their generation to participate in the frequency regulation. Under these operating circumstances, changes in the frequency will produce adjustments in the active power output of generators according to their prime motors static response and, therefore, in the natural gas demand. Furthermore, the amount of electric power demanded by loads is affected by fluctuations in both nodal voltages and frequency. Hence, the consideration of these characteristics permits a better assessment of the interdependence between then interconnected natural gas and electricity networks. In this context, works such as those performed by

[Ćalović81, Restrepo05, Ferreira A.18, Saadat79] analyze primary frequency regulation to evaluate its effect on the generation dispatch or the system response to the occurrence of pre-established contingencies, which also consider frequency and voltage-dependent load models. None of these formulations, however, presents a unified analysis that shows how primary regulation affects the behavior of the natural gas transportation system when variations in demand or contingencies occur in the electrical system.

Under these principles, and from the mathematical models developed for natural gas flows, a new unified formulation suitable for the steady-state analysis of a multi-energy system composed of the natural gas and electricity networks is proposed.

The formulation developed in a single frame of reference allows an integrated gas and power flow analysis, where the primary regulation of frequency, as well as the voltage and frequency dependence of loads, are fully considered. In addition, the gas availability for generators participating in the frequency regulation is also taken into account based on a new restriction that limits the active power supplied by those generators. Considering all those technical aspects permits a better representation of the interaction between energy infrastructures and their actual operating conditions.

Since the active power supplied by each generator with primary regulation changes with respect to its original scheduled power, the reactive power limits must also change according to the value of that generation. Hence, a set of equations is proposed, based on the generator's capability curve, to determine the generator's reactive power limits as a function of its generation of active power. Within this context, an advanced way to handle the reactive power limits is adopted in this work based on the concepts of complementarity constraints and the Fischer-Burmeister function. In this case, the inequality constraints associated with these limits are transformed into equality constraints, which are directly added to the gas and power flow formulation. This permits the automatic checking of reactive power limits and, when applicable, automatic enforcement of limits during the iterative solution process.

Finally, under the occurrence of a critical disturbance that produces a large imbalance between load and generation in an electric power system, the primary regulation control may not be sufficient to bound the steady-state error of the frequency deviation within its normal operating range. This also affects the steady-state operational interdependence of multi-energy systems; however, to the best of the author's knowledge and belief, this topic has not been addressed.

To overcome this drawback, a control action is proposed in this thesis to obtain a gas and power flow solution where the electrical frequency is within limits. The proposal consists of sequentially solving two related subproblems: the gas and power flow problem and the economic dispatch problem. First, the natural gas and power flow problem is solved considering the primary regulation of generators. Suppose the multi-energy system's equilibrium point is declared unfeasible because the steady-state frequency error is beyond its normal operating range. In that case, an economic dispatch study is performed to obtain a new dispatch of active powers in those generators that participate in frequency regulation. From this new set of scheduled active powers, the gas and power flow problem with primary regulation is newly solved to obtain a feasible equilibrium point for the critical disturbance. This equilibrium point guarantees that the system operates within the established frequency band and that the generators' reactive power limits are consistent with their corresponding generation of active power.

1.3.3 Multi-period power flow analysis of integrated natural gas and electricity networks

With the growing interest in analyzing the integrated natural gas and electricity system from a dynamic interdependence perspective, some studies have been carried out from the steady-state or successions of steady state formulations to model the dynamic behavior of electricity and natural gas systems.

Since natural gas and electricity systems' dynamics evolve on very different time scales, reflecting both systems' dynamic behavior in a unified framework of analysis is not easy. In

this context, the gas system reacts more slowly to changes in the network because of the speed at which the gas travels as well as the forces acting on it. The most basic formulation for the gas transportation system consists of a steady-state representation of the natural gas system, assuming that the study period's discretization is long enough to ignore the dynamic behavior of the gas flow [Liu09, Mohtashami09]. Since the steady-state gas models developed so far do not consider the impact of variations in the pipeline linepack, these models are inadequate to describe the dynamic behavior of gas systems, and they are even less accurate when the supply and demand of gas change over time [Pambour17].

Conventional methods for the analysis of transient gas flow in pipe networks are typically applied to find the numerical solution of the partial differential equations of continuity and moment; however, solving these equations is a complex and cumbersome process. To overcome this drawback, the use of the electrical analogy method is expanded in [Ke00], and a set of first-order ordinary differential equations for the transient analysis of isothermal gas flows in the pipe network is derived. Solving the proposed first-order ordinary differential equation, however, is still not an easy problem. Within this context and given that gas dynamics evolve over large time scales, the analysis period can be discretized into sub periods of time, e.g., 1 hour. Under this principle and given that electricity travels at the speed of light, a steady-state model for modeling the electricity infrastructure is sufficient for studying short-term planning, as has been shown in [Royo01, Murillo-Sánchez00]. Considering that gas flows through the networks at speeds of 60 to 90 km/hr, however, the behavior of the slow dynamics must be modeled in detail.

The set of nonlinear partial differential equations of moment and continuity is solved using a finite difference method [Liu11, Aalto08]. The size of the discretization step in time and space is a critical parameter for the analysis's precision and computational burden. On the other hand, models with greater computational efficiency at the expense of accuracy propose gas pipelines' representation using a transfer function [Behbahani-Nejad08, Kralik84]. Some other authors choose to discretize the continuity and moment equations but add another equation to the formulation of the gas flow problem, e.g., [Tabkhi07, Moritz07].

Lastly, the multi-period analysis of natural gas and electricity flows is approached from the unit commitment perspective in [Liu11, Tovar-Ramírez19]. Both proposals, however, are formulated based on the Weymouth average gas flow equation. On the other hand, a unified optimization model of gas and electricity systems based on mixed-integer linear programming (MILP) approach is proposed in [Correa-Posada15]. The issue of flexibility and reliability that the gas system can provide to the electric power system is addressed in this proposal. The electrical network is linearly modeled through a DC power flow formulation, while the gas dynamics are represented from a linearization of the general flow equation implemented in the continuity equation. Under the principles assumed to derived the steady-state mathematical models of natural gas flows, a new formulation for the quasi-steady-state analysis of integrated natural gas and electricity networks is proposed.

1.4 Hypothesis

All practical equations used to compute the gas flow through a pipeline assume an average model where the gas flows at both pipeline ends are equal. After reviewing how different types of parameters affect the gas flow, it is assumed that a comprehensive steady state and transient gas flow model can be derived from the concept of nodal gas injections to reflect the fact that the inlet and outlet gas flows in a pipeline are different.

In practical electric power systems, there is no slack generator to compensate system losses, such that power systems do not necessarily operate at nominal frequency. Hence, developing a unified approach to assessing electricity and natural gas networks' interdependency in terms of electric frequency variations is possible.

An integrated formulation of the existing interdependence between natural gas and electricity systems can be derived to quantitatively assess how natural gas availability affects the safe and reliable operation of the electrical system.

1.5 Objectives

This doctoral project overall objective focuses on developing a new unified methodology to analyze and quantify more efficiently and realistically the complex operational interdependence between natural gas and electricity power infrastructures. This formulation is performed considering a quasi-stationary operating state and the gas infrastructure's dynamics.

1.5.1 Particular objectives

In order to achieve the main objective mentioned above, it is necessary to establish the following specific objectives.

- To develop a new model that describes more accurately, for the steady state and transient operating states, the behavior of the forces that interact in the gas flow through a pipeline.
- To develop a model that implicitly considers the bidirectionality of gas flows inside a pipeline.
- To implement a model of electric power flows that considers the effect of primary frequency regulation in the presence of variations in electricity demand, preserving the frequency and power generation within their established operating limits.
- The integration of the models developed for each infrastructure into a comprehensive model that allows analyzing and calculating the operational interdependence in steady state and quasi-steady state, from the behavior of gas-fired generators and compression stations.
- To implement a unified model to assess the existing interdependence between natural gas and electricity infrastructures in both steady state and transient operating states.

1.6 Contributions

The main contributions of this thesis are the following:

- A new and general mathematical model is proposed to represent in a more realistic way the steady-state behavior of isothermal gas flows through pipelines. Unlike all other proposals reported in the open literature, the proposed model consists of two equations developed from the concept of nodal flow injections, which allow calculating the inlet and outlet gas flows as well as the pressure drop in a pipe.

- New nonlinear algebraic nodal gas flow equations are derived from the proposed steady-state nodal gas flow injection equations to satisfy the momentum and mass balance inside each pipe transiently. Therefore, the transient-state analysis of a natural gas network is performed by solving a set of nonlinear algebraic equations instead of a set of nonlinear space-time partial differential equations.

- A novel approach to achieve a better representation of the operational interaction between both energy infrastructures is proposed by considering the generator-governor characteristics and the voltage and frequency dependence of loads in the electric power flow problem.

- Since the active power supplied by each generator with primary regulation changes with respect to its original scheduled power, the reactive power limits must also change according to the value of that generation. Hence, a set of equations is proposed, based on the generator's capability curve, to determine the generator's reactive power limits as a function of its generation of active power.

- The gas availability for generators participating in the frequency regulation is taken into account based on a new restriction limiting the active power supplied by those generators.

- A new, practical preventive control action to maintain the electric frequency inside an established operating band is proposed within the context of the steady-state interdependency between gas and electricity infrastructures.

1.7 Methodology

The methodology that has been adopted in this thesis is described as:

- A full review of previous works in the formulation of the natural gas flows through pipelines in both steady and transient operating states. A survey is also done regarding the formulation of the operational interdependency between electricity and natural gas networks.
- To develop a set of nonlinear equations that better represent the steady and transient states of gas flows through pipelines.
- To perform a comparative study of steady-state gas flow equations already proposed in the literature with respect to the proposed equations to determine how effective the proposal is.
- To develop a digital program that solves the gas flow problem with the proposed gas flow models.
- To develop a digital program that solves the electric power flow problem considering the primary frequency regulation and the voltage and frequency dependence of loads.
- To develop a unified framework to perform steady and quasi-steady-state analysis of electricity and natural gas networks to better represent the operational interaction between both energy infrastructures.
- To formulate a new practical control action in a multi-energy system for maintaining a steady-state error of frequency deviation within the electrical frequency operating limits.
- To test the proposed approaches considering multi-energy systems of different sizes and topological structures.

1.8 Thesis outline

To the best of the author's knowledge and belief, the approaches described above have not been previously addressed in any research work, and will be developed in detail in the rest of this thesis, which is constituted as follows.

In Chapter 2 two new equations are derived from the momentum and state equations of gases referred to as nodal flow injection (NFI) equations to calculate the of steady-steady gas flows through a pipeline. From the NFI equations, a new equation to calculate the average gas flows in a pipe, referred to as the average flow (AFE) equation, is obtained and used to derive the general flow equation. The effectiveness and applicability of the proposed equations are numerically demonstrated by comparing their results with respect to the ones obtained by the equations most commonly used in practice.

A general steady-state model for calculating gas flows and nodal pressures in a natural gas transport system is presented in Chapter 3. The advantages of having a model based on nodal injections are numerically demonstrated. Lastly, the modeling for the electrical power system is also presented in this chapter considering the primary frequency regulation and loads dependent on the voltage and frequency. In this case, a new equation to relate active and reactive power generation limits is proposed based on the generator capability curve. Based on the above, the power flow problem is formulated and its performance is compared to the conventional power flow model.

An integrated formulation to simultaneously analyze natural gas and electricity systems is developed in Chapter 4. This proposal is validated by analyzing the response of generators with frequency regulation to changes in electrical load and their impact on the natural gas transportation system. A control scheme that preserves the value of frequency within the established operating limits is also proposed. Lastly, the impact of gas availability on primary frequency regulation and unit dispatch is analyzed in this chapter.

A model to describe the transient-state of gas flows from the NFI equations is derived in Chapter 5. The proposed model's effectiveness is validated by analyzing its performance against the behavior of the AFE-based gas flow model for a time horizon of 24 hrs. The transient-state gas flow model is then integrated into the electrical model with frequency regulation to obtain a quasi-stationary multi-period model that allows assessing the operating state of a multi-energy system for an hourly time horizon. The response of the multi-energy system to load shedding and abrupt increments of power demand are analyzed, highlighting once again the relevance of considering the availability of gas in the operational interdependence of the multi-energetic system.

Finally, Chapter 6 presents the general conclusions of the research work developed in this thesis as well as suggestions for future works associated with this topic.

Chapter 2

Gas flow equations in steady state

2.1 Introduction

A gas network is normally managed and operated from control centers according to the data received from a supervisory control and data acquisition system. In order to ensure the reliable and secure operation of this network through the processing of these data, the correct modeling of the gas components composing the transmission network and the calculation of the natural gas flows are of paramount importance [Osiadacz87].

Several mathematical equations have been proposed for the calculation of steady-state isothermal gas flow in pipelines. All these proposals, however, assume that the natural gas flowing through the entire pipeline can be modeled by an average magnitude calculated in the middle of the segment or length of the pipe. This implies that the flow going into one end of the duct is exactly equal to the one that is extracted from the other end, and, therefore, details of what is happening inside the pipeline are not being considered.

In other words, these formulations do not consider the inherent difference between the incoming and outgoing flow through a pipeline at a given instant of time. In practice, this difference exists and is due to the compressibility and storage of the gas, the speed at which the gas travels through the pipeline, the friction force, the inclination of the pipeline, among

other factors. Neglecting this difference of the amount of gas could cause an inaccuracy in the network calculations of the amount of gas at the inlet and outlet nodes of a pipeline, which is spread throughout the network. This results in an incorrect assessment of the steady-state operating state of the entire gas transmission network.

Based on the information mentioned above, a new mathematical model that represents in a more realistic way the behavior of the gas transport systems operating in a stationary state is proposed in this chapter. In this case, two new equations are proposed to relate the gas flow and the pressure drop through a pipe based on the concept of "*nodal flow injections*."

2.2 Nodal flow injection equations

The dynamics acting on a natural gas transport system are predominantly determined by the flow through the pipelines, so the set of nonlinear partial differential equations describing the transient gas flow within a pipeline are derived from the mass, momentum and energy conservation laws, as well as from the equation of state for gases [Pambour17]. Applying these laws to an infinitesimal control volume of a general pipeline with a constant cross-sectional area "A" and an infinitesimal length "dx," as shown in Figure 2.1, results in a set of fundamental partial differential equations that describe the behavior of the one-dimensional compressible gas flow through a pipeline. This set of equations are described below.

1. **The continuity equation or mass conservation equation** states that mass can neither be created nor destroyed, i.e., if gas is contained in a certain volume, the mass will remain constant unless some gas is removed or added to the container:
$$\frac{\partial \dot{m}}{\partial x} + A\frac{\partial \rho}{\partial t} = 0. \tag{2.1}$$

2. **The momentum equation** corresponds to Newton's second law and describes the sum of all forces acting on a gas particle within a pipe:
$$\frac{\partial p}{\partial x} + g\rho\frac{\partial h}{\partial x} + \frac{\lambda\,|\upsilon|\,\upsilon}{2D}\rho + \frac{1}{A}\frac{\partial \dot{m}}{\partial t} + \frac{\partial\left(\rho\upsilon^2\right)}{\partial x} = 0. \tag{2.2}$$

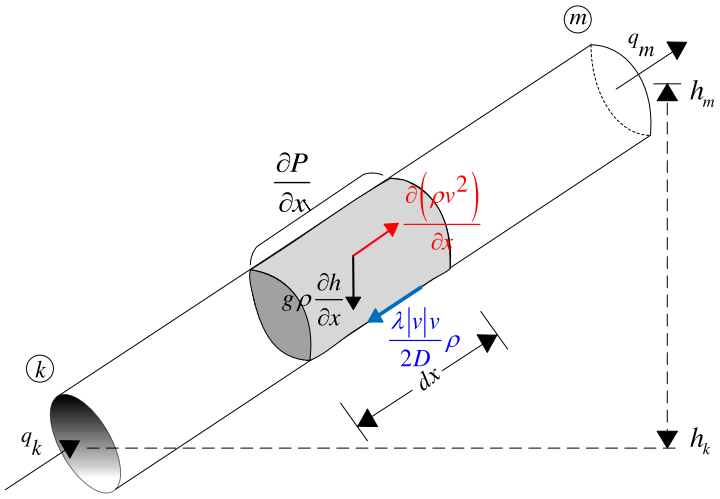

Figure 2.1: Forces acting on a volume of gas circulating through a pipeline.

3. **The energy equation** represents the heat addition from the soil to the gas, which corresponds to the law of conservation of energy during the transportation process. In this case, "W" is the heat addition (per mass flow and time):

$$\frac{\partial}{\partial t}\left[(\rho A dx)\left(c_v T + \frac{v^2}{2} + gdh\right)\right] + \frac{\partial}{\partial x}\left[(\rho v A dx)\left(c_v T + \frac{P}{\rho} + \frac{v^2}{2} + gdh\right)\right] = W(\rho A dx). \quad (2.3)$$

4. **The equations of state for gases** relate to the pressure, temperature and the density of the gas:

$$\rho = \frac{p}{zR_{gas}T} \quad and \quad \rho_0 = \frac{p_0}{z_0 R_{gas} T_0}. \quad (2.4)$$

In order to obtain a steady-state model that describes the behavior of the gas flow that circulates through a pipe, the temporal variations of the flow were not considered, so the effects of (2.1) and the fourth term of (2.2) were negligible. Furthermore, by assuming that the heat exchange between the ground and the pipe is very small and remains constant, the energy Eq. (2.3) can also be neglected.

Establishing that the gas flow through a pipeline can be modeled by flow injections at both ends of the pipeline, as shown in Figure 2.2, and if this principle is considered when the moment (2.2) and state (2.4) equations are discretized by the implicit scheme of Euler, the expressions (2.5) and (2.6) are finally obtained. This set of equations is referred to as "the nodal flow injection equations" (NFI equations):

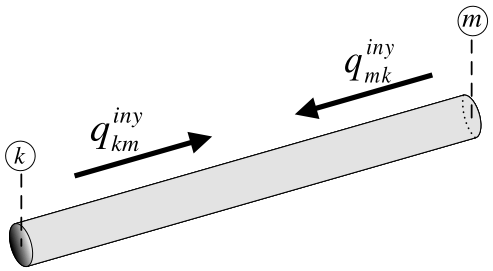

Figure 2.2: Scheme of nodal gas flow injections.

$$
\begin{aligned}
q_{km}^{iny}\left|q_{km}^{iny}\right| &= \frac{D_{km}^5\pi^2 z_0^2 T_0^2}{8Gp_0^2 L_{km}^2\lambda_{km}^2 z(p_k,T_k)^2 T_k^2}\times \\
&\Big[p_k^2\big(z\left(p_k,T_k\right)T_k\lambda_{km}L_{km}R_{air}+gG\left(2D_{km}+\lambda_{km}L_{km}\right)\left(h_k-h_m\right)\big) \\
&-p_k p_m\frac{z\left(p_k,T_k\right)T_k}{z\left(p_m,T_m\right)T_m}\times\big(z\left(p_m,T_m\right)T_m\lambda_{km}L_{km}R_{air}+2gGD_{km}\left(h_k-h_m\right)\big)\Big]
\end{aligned}
\tag{2.5}
$$

$$
\begin{aligned}
q_{mk}^{iny}\left|q_{mk}^{iny}\right| &= \frac{D_{km}^5\pi^2 z_0^2 T_0^2}{8Gp_0^2 L_{km}^2\lambda_{km}^2 z(p_m,T_m)^2 T_m^2}\times \\
&\Big[p_m^2\big(z\left(p_m,T_m\right)T_m\lambda_{km}L_{km}R_{air}+gG\left(2D_{km}+\lambda_{km}L_{km}\right)\left(h_m-h_k\right)\big) \\
&-p_k p_m\frac{z\left(p_m,T_m\right)T_m}{z\left(p_k,T_k\right)T_k}\times\big(z\left(p_k,T_k\right)T_k\lambda_{km}L_{km}R_{air}+2gGD_{km}\left(h_m-h_k\right)\big)\Big].
\end{aligned}
\tag{2.6}
$$

Equation (2.5) calculates the volumetric gas that flows from the "k" inlet node to the "m" outlet node. Similarly, Eq. (2.6) is associated with the amount of gas arriving at the "m" outlet node coming from the "k" inlet node. Note that these equations implicitly consider the effects of gravity on gas circulation, the speed of the fluid, the distance traveled, the compression state of the gas, the pressure losses due to friction, among others factors. See Appendix A.1 for details about their mathematical deduction.

In order to represent the NFI equations in a more compact form, the parameters of (2.5) and (2.6) can be grouped into global constants α and β (as seen in Appendix A.1) such that these expressions can be rewritten in the form of (2.7) and (2.8), which only depends on nodal pressures:

$$q_{km}^{iny}\left|q_{km}^{iny}\right| = \alpha\big(p_k^2\beta_{k1}-p_k p_m\beta_{k2}\big) \tag{2.7}$$

$$q_{mk}^{iny}\left|q_{mk}^{iny}\right| = \alpha\big(p_m^2\beta_{m1}-p_k p_m\beta_{m2}\big). \tag{2.8}$$

Note that the product on the left-hand side of equations (2.7) and (2.8) is the gas flow times its absolute value, so the square of the gas flow can be either a positive or a negative value. From a physical viewpoint, this condition represents the possible bi-directionality of the gas within a pipeline, i.e., the possibility of gas circulating from a "k" node to an "m" node in one operating state and from the "m" node to the "k" node in a different operating state.

Based on the information mentioned above and to preserve the equality equation and effect of the absolute value, Eq. (2.7) can be separated into two terms (2.9) and (2.10):

$$q_{km}^{iny} = \alpha^{\frac{1}{2}} \left(p_k^2 \beta_{k1} - p_k p_m \beta_{k2}\right)^{\frac{1}{2}} \tag{2.9}$$

$$\left|q_{km}^{iny}\right| = \alpha^{\frac{1}{2}} \left|\left(p_k^2 \beta_{k1} - p_k p_m \beta_{k2}\right)\right|^{\frac{1}{2}}. \tag{2.10}$$

From (2.9) and (2.10), the following conclusions can be drawn:

$$if \ \ \left(p_k^2 \beta_{k1} > p_k p_m \beta_{k2}\right) \Rightarrow q_{km}^{iny} \left|q_{km}^{iny}\right| = \left(q_{km}^{iny}\right)^2 \tag{2.11}$$

$$if \ \ \left(p_k^2 \beta_{k1} < p_k p_m \beta_{k2}\right) \Rightarrow q_{km}^{iny} \left|q_{km}^{iny}\right| = -\left(q_{km}^{iny}\right)^2. \tag{2.12}$$

Finally, if (2.10) is substituted in Eq. (2.7), the expression (2.13) is obtained. A similar analysis is performed for Eq. (2.8), which results in (2.14):

$$q_{km}^{iny} = \alpha^{\frac{1}{2}} \frac{\left(p_k^2 \beta_{k1} - p_k p_m \beta_{k2}\right)}{\left|p_k^2 \beta_{k1} - p_k p_m \beta_{k2}\right|^{\frac{1}{2}}} \epsilon \tag{2.13}$$

$$q_{mk}^{iny} = \alpha^{\frac{1}{2}} \frac{\left(p_m^2 \beta_{m1} - p_k p_m \beta_{m2}\right)}{\left|p_m^2 \beta_{m1} - p_k p_m \beta_{m2}\right|^{\frac{1}{2}}} \epsilon. \tag{2.14}$$

Note that the efficiency factor "ϵ" has been included in equations (2.13) and (2.14), with a value defined by the time that the pipeline has been in service. Typically, efficiency factors can range from 0.6 to 0.92 depending on the liquid content of the pipeline, the age of the pipeline that determines its grade of corrosion and the operating conditions [Mokhatab19].

Finally, (2.13) and (2.14) are the final form of the NFI equations and represent two new expressions that relate the pressure drop to the volumetric flow rate of the gas flowing through a pipeline in stationary state. These equations allow calculating the amount of gas flow injected and received at both ends of the pipeline, which are not necessarily of equal magnitude. In addition, these equations implicitly consider the possible bidirectionality of the gas flow in their formulation, which always circulate in opposite directions, i.e. if $q_{km}^{iny}\left|q_{km}^{iny}\right| > 0$ then $q_{mk}^{iny}\left|q_{mk}^{iny}\right| < 0$, and conversely if $q_{km}^{iny}\left|q_{km}^{iny}\right| < 0$ then $q_{mk}^{iny}\left|q_{mk}^{iny}\right| > 0$.

2.2.1 Compressibility factor

Equations (2.13) and (2.14) are a function of the compressibility factor "z," which is defined as the ratio of the gas volume at a given temperature and pressure to the volume of an ideal gas at the same temperature and pressure [Menon05].

Nevertheless, even though the gas flow is subjected to different conditions at each pipeline of the network, many proposals use a constant value for the compressibility factor. Nonetheless, while the value of this factor is $z = 1$ for an ideal gas, for a real gas this factor depends on both the chemical composition of gas and the pressure and temperature to which the gas is subjected. Thus, if the compressibility factor increases, the molecules expand, and the flow decreases. On the contrary, if this factor decreases, the molecules collide and compact such that the gas flow increases. This behavior justifies the importance of considering the compressibility factor as a function of the gas pressure and the temperature.

Even though there is no exact theoretical determination of this relationship, several empirical approaches have been developed. In this work, the American Gas Association (AGA) empirical equation [AGA85] is adopted, i.e.:

$$z\left(p,T\right) = 1 + 0.257p_r - 0.533\frac{p_r}{T_r}, \tag{2.15}$$

where

- p_r corresponds to the relative pressure given by the quotient between its value at the node and its pseudo-critical magnitude

$$p_r = \frac{p}{p_{pc}}$$

- and T_r corresponds to the relative temperature given by the quotient between its value at the node and its pseudo-critical magnitude

$$T_r = \frac{T}{T_{pc}}.$$

On the other hand, the pseudo-critical pressure and temperature values can be calculated from Kay's rule given by the expressions (2.16) and (2.17), respectively [Mokhatab19]:

$$p_{pc} = \sum_{i=1}^{N} p_{c_i} y_i, \tag{2.16}$$

$$T_{pc} = \sum_{i=1}^{N} T_{c_i} y_i, \tag{2.17}$$

where

- y is the mole fraction of the hydrocarbon that makes up the mixture,
- T_c is the critical temperature of the hydrocarbon, and
- p_c is the critical pressure of the hydrocarbon.

For this work, the chemical composition of natural gas presented in Table 2.1 was considered, with which the following pseudo-critical pressure and temperature values were obtained:

$$p_{pc} = 681.882\,[psi] \quad and \quad T_{pc} = 406.9362\,[R]\,.$$

Table 2.1: Chemical composition of natural gas

Hydrocarbon	y_i
Methane	70 %
Ethane	10 %
Propane	7%
Butane	3 %
Carbon dioxide	6 %
Nitrogen	4 %

2.2.2 Friction factor

The loss of energy due to the existing friction between the internal wall of the pipeline and the fluid, which opposes the circulation of the gas flow and causes a gradual loss of pressure along the pipeline, must be considered for calculating the gas flow. This loss of pressure caused by friction force is commonly considered in fluid dynamics from a dimensionless parameter known as The Darcy coefficient of friction [Menon05], which is represented by the term "λ" in the NFI equations. This parameter depends on the magnitude of the relative roughness of the internal wall of the pipe "ε" and on the magnitude of a dimensionless number known as the Reynolds number given by (2.18). This number permits characterizing the nature of the fluid according to its operating regime:

$$\mathrm{Re} = \frac{\upsilon D \rho}{\mu}. \tag{2.18}$$

Four types of flows have been established: laminar, critical, in transition or partially turbulent and fully turbulent. Even though natural gas pipelines are normally operated in the partially and fully turbulent region [Mokhatab19], the applicability of the proposed equations to any regime and/or to other compressible fluids is possible by considering a different correlation of the friction coefficient for each operating regime, based on the friction coefficient formulation, its region of validity, as well as its acceptance in practice and academia.

Laminar flow

A gas fluid with a small Reynolds number (< 2000) is considered laminar because it has a high viscosity and/or because it moves at low speeds. This gas flow travels strictly in one direction such that the friction factor shows a sharp dependency on the flow rate and the gas viscosity, and therefore the roughness of the duct is negligible [Mokhatab19]. The expression for calculating the friction factor in this regime is defined by the Hagen-Poiseuille Eq. (2.19):

$$\lambda = \frac{64}{Re}. \tag{2.19}$$

Critical flow

For Reynolds numbers in the range of $2000 < Re < 4000$, the flow is known as critical. In this relatively low flow zone is not possible to know what is happening between the laminar and partially turbulent zones because part of the laminar flow is unstable. Therefore, in this region multiple behaviors are observed, and it is not possible to establish a correlation for the coefficient of friction that describes such behavior [Schroeder01].

If a smooth-walled pipe is considered with a relative roughness $\varepsilon/D < 1 \times 10^{-7}$, however, the coefficient of friction can be approximated by

$$\frac{1}{\sqrt{\lambda}} = 1.3273 Re^{0.1596}. \tag{2.20}$$

Partially turbulent flow

A flow is considered partially or totally turbulent when it has a high Reynolds number (> 4000). In this case, the flow is characterized by being chaotic because of its low viscosity and/or because it travels at high speed. Under these operating conditions, the Colebrook-White equation is the most accepted equation for the estimation of the friction factor in the partially turbulent regime [Mokhatab19]. This equation contemplates both smooth and rough pipes, being valid for the zone known as the transition zone, where $4000 < Re < 1E8$, and for values of relative roughness given by $\varepsilon/D < 0.05$.

The Colebrook-White equation is given by (2.21). The friction factor λ, however, is implicit in it, preventing its factorization and complicating its use, for which the use of numerical methods is required:

$$\frac{1}{\sqrt{\lambda}} = -2 \log \left[\frac{\varepsilon/D}{3.7} + \frac{2.51}{Re\sqrt{\lambda}} \right]. \tag{2.21}$$

To face this problem, many explicit equations have been proposed particularizing their application to a certain operating regime or to a certain range of validity. Hence, if a flow has a turbulent behavior and circulates through a smooth-walled pipeline with a relative roughness of $\varepsilon/D < 1 \times 10^{-7}$, the coefficient of friction can be calculated from the Drew,

Koo and McAdams equation:

$$\frac{1}{\sqrt{\lambda}} = \frac{1}{\sqrt{0.0056 + \frac{0.5}{Re^{0.32}}}}. \tag{2.22}$$

On the other hand, if the gas flow circulates through a rough pipe, the coefficient of friction can be calculated from (2.23), which is a very good approximation with respect to the experimental values obtained by the Colebrook-White equation [Camaraza Medina11]:

$$\frac{1}{\sqrt{\lambda}} = \left[-2\log\left(\left(\frac{\varepsilon}{3.7D}\right) - \frac{A_1}{B_1}\right)\right], \tag{2.23}$$

where

- $A_1 = 2.296\log\left[\frac{47.5}{\mathrm{Re}^2} + \frac{3.27}{\mathrm{Re}}\left(\frac{\varepsilon}{D}\right)^{1.12} + \frac{1}{18.26}\left(\frac{\varepsilon}{D}\right)^{2.25}\right]$
- and $B_1 = \mathrm{Re}\left[\log\left(\mathrm{Re}^{2.5}\right)\left(\frac{\varepsilon}{D}\right)^{1.12}\right]^{0.01}$.

Fully turbulent flow

When the Reynolds number has values greater than 1×10^8, the flow is considered to be in a state of complete turbulence. Under this operating state and considering hydraulically smooth conditions, the coefficient of friction is only a function of the Reynolds number, so that it is independent of the relative roughness and can be approximated by the Blasius equation [Abdolahi07]:

$$\frac{1}{\sqrt{\lambda}} = 1.777Re^{0.125}. \tag{2.24}$$

In contrast, for a full turbulent flow flowing through a rough-walled pipe, the friction factor shows no dependence on flow, and the numerical value of the Reynolds number no longer influences the friction factor. In this operational state, the coefficient of friction becomes constant and depends only on the value of the relative roughness of the pipe through which the fluid circulates. For this regimen of operation, the coefficient of friction can be approximated by using the Nikuradse equation [Mokhatab19]:

$$\frac{1}{\sqrt{\lambda}} = 2\log\left({}^{D}/_{\varepsilon}\right) + 1.14. \tag{2.25}$$

2.2.3 Linepack and Δ_q

The gas storage inside a pipeline, referred to as "*linepack*," is a key factor in the ability of the gas transport system to supply gas to demand nodes. From the equation of state for gases (2.4), it is possible to relate the physical volume of the pipeline with the volume of the gas contained in it, which results in (2.26) [Menon05]. Once the operating state of the gas network has been computed at a given instant of time, Eq. (2.26) is used to calculate the amount of stored gas inside a pipeline connecting nodes "k" and "m":

$$LP_{km}^{avg} = \frac{T_0}{p_0} \frac{p_{km}^{avg}}{z_{km}^{avg} T_{km}^{avg}} \frac{\pi}{4} D_{km}^2 L_{km}, \tag{2.26}$$

where p_{km}^{avg} corresponds to the root mean square of nodal pressures, T_{km}^{avg} is the arithmetic mean of nodal temperatures and z_{km}^{avg} is calculated by replacing p_{km}^{avg} and T_{km}^{avg} in Eq. (2.15).

On the other hand, the difference between the inlet and outlet flows of a pipeline, i.e., Δ_q^{pipe}, is related to the friction force, the speed and compressibility of the gas flowing through the pipe, the pressure drop and the physical properties of the pipeline. All these factors cause an increase or a decrease in the stored gas given by (2.26): a variation in the linepack. Note that the proposed NFI equations directly permit calculating the difference between the inlet and outlet flow at the pipeline ends by using (2.27), which will be implicitly considered in the network model:

$$\Delta_q^{pipe} = q_{km}^{iny} + q_{mk}^{iny}. \tag{2.27}$$

From these proposed equations, it is also possible to deduce an analytical expression to calculate the value of Δ_q^{pipe}. Substituting Eq. (2.5) and Eq. (2.6) into (2.27) and performing algebraic operations results in (2.28). See Appendix A.2 for more information about the derivation of this equation:

$$\Delta_q^{pipe} = \frac{D_{km}^{2.5} \pi T_0}{p_0} \sqrt{\frac{R_{air} \left(p_k - p_m\right)}{8 L_{km} \lambda_{km} G T_{km} z}} \left(p_k^{\frac{1}{2}} - p_m^{\frac{1}{2}} \right). \tag{2.28}$$

2.3 Validation of proposed equations

Based on the theoretical concepts described in [Osiadacz87] and [Menon05], it is possible to express the gas flow, gas pressure and gas storage in a pipeline as average values

at the center of the pipeline. Hence, the average value of a gas flow through a pipeline connected between nodes "k" and "m" is obtained by applying the concept of *root mean square* (RMS) [Triola09] to equations (2.13) and (2.14):

$$q_{RMS} = q_{km}^{avg} = \sqrt{\frac{\left(q_{km}^{iny}\right)^2 - \left(q_{mk}^{iny}\right)^2}{2}}. \tag{2.29}$$

By developing Eq. (2.29), the expression (2.30) is obtained, which represents a new equation for calculating the average flow that circulates through a pipe in steady state:

$$\begin{aligned} q_{km}^{avg} = \frac{D_{km}^{2.5}\pi}{4\sqrt{G}L_{km}\lambda_{km}}\left(\frac{T_0}{p_0}\right) \times \Bigg[& \frac{p_k^2}{z(p_k,T_k)^2 T_k^2}\begin{pmatrix} z\left(p_k,T_k\right)T_k\lambda_{km}L_{km}R_{air}+ \\ gG\left(2D_{km}+\lambda_{km}L_{km}\right)\left(h_k-h_m\right)\end{pmatrix} \\ & -\frac{p_m^2}{z(p_m,T_m)^2 T_m^2}\begin{pmatrix} z\left(p_m,T_m\right)T_m\lambda_{km}L_{km}R_{air}- \\ gG\left(2D_{km}+\lambda_{km}L_{km}\right)\left(h_k-h_m\right)\end{pmatrix} \\ & +\frac{p_k p_m}{z\left(p_k,T_k\right)z\left(p_m,T_m\right)T_k T_m}\times\begin{pmatrix} \lambda_{km}L_{km}R_{air}\left(z\left(p_k,T_k\right)T_k - z\left(p_m,T_m\right)T_m\right) \\ -4gGD_{km}\left(h_k-h_m\right)\end{pmatrix}\Bigg]^{\frac{1}{2}}. \end{aligned} \tag{2.30}$$

Grouping the general parameters according to (2.31), the expression (2.30) can be rewritten only as a function of nodal pressures:

$$\begin{aligned} q_{km}^{avg} = \underbrace{\frac{D_{km}^{2.5}\pi}{4\sqrt{G}L_{km}\lambda_{km}}\left(\frac{T_0}{p_0}\right)}_{\alpha} \times \Bigg[& p_k^2 \underbrace{\frac{\begin{pmatrix} z\left(p_k,T_k\right)T_k\lambda_{km}L_{km}R_{air}+ \\ +gG\left(2D_{km}+\lambda_{km}L_{km}\right)\left(h_k-h_m\right)\end{pmatrix}}{z(p_k,T_k)^2 T_k^2}}_{\beta_k} - \\ & -p_m^2 \underbrace{\frac{\begin{pmatrix} z\left(p_m,T_m\right)T_m\lambda_{km}L_{km}R_{air}- \\ -gG\left(2D_{km}+\lambda_{km}L_{km}\right)\left(h_k-h_m\right)\end{pmatrix}}{z(p_m,T_m)^2 T_m^2}}_{\beta_m} + \\ & +p_k p_m \underbrace{\frac{\begin{pmatrix} \lambda_{km}L_{km}R_{air}\left(z\left(p_k,T_k\right)T_k - z\left(p_m,T_m\right)T_m\right) \\ -4gGD_{km}\left(h_k-h_m\right)\end{pmatrix}}{z\left(p_k,T_k\right)z\left(p_m,T_m\right)T_k T_m}}_{\beta_{km}}\Bigg]^{\frac{1}{2}}. \end{aligned} \tag{2.31}$$

Lastly, the bidirectionality of the gas flow can be also considered by applying a theory similar to the one used in the derivation of NFI equations, from which the Eq. (2.32) is finally obtained. This equation is referred to as the "*average flow equation*" (AFE), and it is a new way to calculate the steady-state average flow of gas that circulates through a pipe. Note that this proposed equation considers the impact of the force of gravity on the inclination of the gas pipeline, the compressibility factor as a function of the nodal magnitudes of pressure and temperature, and the implicit direction in which the gas circulates inside the pipeline:

$$q_{km}^{avg} = \alpha \frac{\left(p_k^2 \beta_k - p_m^2 \beta_m + p_k p_m \beta_{km}\right)}{\left|p_k^2 \beta_k - p_m^2 \beta_m + p_k p_m \beta_{km}\right|^{\frac{1}{2}}} \epsilon. \tag{2.32}$$

Finally, under the assumption that the pipe is completely horizontal and that the compressibility factor is known and remains constant, the expression (2.33) is directly derived from (2.30). This equation corresponds to the *"general flow equation"* (GFE) from which other types of equation, e.g. the Weymouth, Panhandle and Lacey equations, can be derived. Note that these equations have been widely used by industry and researchers around the world to approximate the average steady-state isothermal volumetric gas flow circulating in a flow line through a general pipeline with a circular cross section:

$$GFE = q_{km}^{avg} = \frac{\pi}{4} \left(\frac{T_0}{p_0}\right) \epsilon \sqrt{\frac{\left(p_k^2 - p_m^2\right) D_{km}^5 R_{air}}{G T_{km} L_{km} \lambda_{km} z}}. \tag{2.33}$$

2.4 Comparison of gas flow equations

Since the friction factor varies over a wide range of values according to the Reynolds number, none of the current gas flow equations is universally applicable. Hence, in most cases the transport system operators personalize the gas flow equations to their particular pipes by means of measurements of gas flow, gas nodal pressures and temperature, with which an efficiency or an effective roughness for the pipe can be computed [Mokhatab19]. Based on this principle, many equations have been proposed to approximate steady-state gas flow by considering the properties and conditions of the gas and the pipeline, as well as the pressure drop along the pipeline [Johnson35, Menon05, Coelho07]. The most common ones are reported below within a unified framework of units in the international system

so that q is in standard cubic meters per day (SCMD), P is in kPa, D is in mm, L is in km, T is in $^\circ K$ and μ is in *poise*. On the other hand, the NFI equations and the AFE are expressed in their general form for facilitating their application and conversion to any system and type of consistent units.

1. **General flow equation (GFE) or fundamental equation** is adopted as the absolute or complete statement that relates the pressure drop to a steady-state isothermal flow that circulates through a pipe [Schroeder01]:

$$q = 1.1494 \times 10^{-3} \epsilon \left(\frac{T_0}{p_0}\right) \left[\frac{(p_k^2 - p_m^2)}{\lambda G T_{km} L_{km} z}\right]^{0.5} D_{km}^{2.5}. \tag{2.34}$$

   Note that (2.34) corresponds to Eq. (2.33) with a conversion factor to achieve the unit consistency described above.

2. **Panhandle B equation** is the most used for high pressure transmission systems ($>$ $7000\,[kPa]$) composed of pipelines with large diameters ($> 600mm$)and fully turbulent flow conditions defined by numerical values of Reynolds in the range from 4 to 40 million. This equation is given by

$$q = 1.002 \times 10^{-2} \epsilon \left(\frac{T_0}{p_0}\right)^{1.02} \times \left[\frac{p_k^2 - p_m^2}{G^{0.961} T_{km} L_{km} z}\right]^{0.51} D_{km}^{2.53}. \tag{2.35}$$

3. **Panhandle A equation** has been developed for its use in high pressure natural gas pipelines ($5500 - 10000\,[kPa]$) with diameters between 300-1500 mm. This equation implicitly incorporates a friction factor for a smooth partially turbulent regime with Reynolds numbers in the range of 5 to 11 million:

$$q = 4.5965 \times 10^{-3} \epsilon \left(\frac{T_0}{p_0}\right)^{1.0788} \times \left[\frac{p_k^2 - p_m^2}{G^{0.8539} T_{km} L_{km} z}\right]^{0.5394} D_{km}^{2.6182}. \tag{2.36}$$

4. **Weymouth equation** is used for high pressure systems ($700 - 3500\,[kPa]$), large flows and internal diameters between 150 and 300 mm. Even though the Weymouth equation is less accurate than other equations, it is normally used in the design of

primary distribution networks and fully turbulent regimes, as it overestimates the calculation of pressure drop and maximizes the pipe diameter required for a given mass flow rate. This equation is given by

$$q = 3.7435 \times 10^{-3} \epsilon \left(\frac{T_0}{p_0}\right) \left[\frac{p_k^2 - p_m^2}{G T_{km} L_{km} z}\right]^{0.5} D_{km}^{2.667}. \tag{2.37}$$

5. **Mueller equation** is used for intermediate pressure systems and in partially turbulent operating regimes. It considers the effects of the friction factor by directly including the dynamic viscosity of the gas in the equation:

$$q = 0.685 \times 10^{-3} \epsilon \left(\frac{T_0}{p_0}\right) \times \left[\frac{p_k^2 - p_k^2}{G^{0.74} T_{km} L_{km} \mu^{0.26}}\right]^{0.5747} D^{2.724}. \tag{2.38}$$

6. **IGT equation** was proposed by the Institute of Gas Technology to be used in distribution systems and, like the Mueller equation, depends on the value of the dynamic viscosity of the gas. Both equations share one common attribute: at a low flow they are conservative, while at a high flow they are overly optimistic [Schroeder01]. Lastly, the IGT equation is given by

$$q = 1.2822 \times 10^{-3} \epsilon \left(\frac{T_0}{p_0}\right) \times \left[\frac{p_k^2 - p_m^2}{G^{0.8} T_{km} L_{km} \mu^{0.2}}\right]^{0.555} D_{km}^{2.667}. \tag{2.39}$$

7. **Fritzsche equation** was developed in Germany and is widely used in gas and compressed air pipelines. The mathematical expression for this equation is

$$q = 1.4053 \times 10^{-3} \epsilon \left(\frac{T_0}{p_0}\right) \times \left[\frac{p_k^2 - p_m^2}{G^{0.858} T_{km} L_{km} \mu^{0.142}}\right]^{0.538} D_{km}^{2.69}. \tag{2.40}$$

8. **Spitzglass equation** is applied to an intermediate pressure range close to atmospheric ($108 - 300\,[kPa]$) and to diameters less than 100 mm. It is mainly used

in distribution systems with low pressure drop, small flow rates and fully turbulent operating regimes:

$$q = 1.0815 \times 10^{-2} \epsilon \left(\frac{T_0}{p_0}\right) \times \left[\frac{p_k^2 - p_m^2}{G T_{km} L_{km} z \left(1 + \frac{91.44}{D_{km}} + 0.0012 D_{km}\right)}\right]^{0.5} D_{km}^{2.5} \quad (2.41)$$

9. **Polyflo equation** is commonly used for medium pressure systems ($108.8 - 801.3\,[kPa]$), and it is given by

$$q = 0.574 \times 10^{-3} \epsilon \left(\frac{T_0}{p_0}\right) \left[\frac{p_k^2 - p_m^2}{\lambda G T_{km} L_{km}}\right]^{0.5} D_{km}^{2.5}, \quad (2.42)$$

with $\frac{1}{\sqrt{\lambda}} = 5.338 Re^{0.076}$.

10. **Cox equation** is also used in medium pressure systems ($108.8 - 801.3\,[kPa]$), but it assumes a constant coefficient of friction:

$$q = 1.282 \times 10^{-3} \epsilon \left[\frac{p_k^2 - p_m^2}{G L_{km}}\right]^{0.5} D_{km}^{2.5}. \quad (2.43)$$

11. **Spitzglass LP equation** is derived from (2.41) and is applicable to secondary distribution networks, which operate at low pressure levels ($0 - 6.9\,[kPa\ gauge]$), to small diameters of pipe ($< 100mm$) and in a fully turbulent regime. In this case, the gas flow is computed by

$$q = 25.956 \times 10^{-3} \epsilon \times \left[\frac{p_k - p_m}{G L_{km} z \left(1 + \frac{91.44}{D_{km}} + 0.0012 D_{km}\right)}\right]^{0.5} D_{km}^{2.5}. \quad (2.44)$$

12. **Lacey equation** given by (2.45) is the most used in secondary distribution networks for a pressure range of 0-7.5 $[kPa\ gauge]$, small diameters ($< 100mm$) and partially turbulent regimes:

$$q = 1.372 \times 10^{-3} \epsilon \times \left[\frac{(p_k - p_m) D_{km}^5}{G L_{km} \left(0.004 + \frac{0.1913}{D_{km}}\right)}\right]^{0.5}. \quad (2.45)$$

13. **Pole equation** is also used in secondary distribution networks, and it is derived from the Lacey equation by considering an overall diameter of 69.56 mm for the coefficient of friction in all pipes. The Pole equation is expressed as

$$q = 17.04 \times 10^{-3} \times \left[\frac{(p_k - p_m)\, D_{km}^5}{G L_{km}} \right]^{0.5}. \tag{2.46}$$

Note that all these equations have a numerical parameter in their definition with a value obtained by simplifying the magnitude of the parameters to the known standard conditions, the assumptions made for their deduction and the unit conversion factors. In this sense, note that for the case of low pressure equations the pressures are gauge pressures. This is because in their mathematical deduction it was assumed that

$$\frac{(p_k + p_m)}{2} \approx P_{km}^{avg} \approx p_0 + p_x, \tag{2.47}$$

where P_x equals $0.39\,[kPa]$ for the Lacey and Pole equations and equals $1.210\,[kPa]$ for the Spitzglass LP equation. Based on the aforementioned,

$$p_k^2 - p_m^2 = (p_k - p_m)\,(p_k + p_m) \approx \left(p_k^{gau} - p_m^{gau}\right) 2 p_{km}^{avg}. \tag{2.48}$$

To demonstrate the validity of NFI equations (2.13) and (2.14), as well as the AFE (2.32), the gas flow obtained under different operating conditions is compared against the ones obtained by the most commonly used equations that have been described above. For this purpose, the volumetric flow of gas through a single pipeline under four pressure conditions, i.e., extra high, high, medium and low pressure, was calculated with each equation, while considering pressure drops of 1%, 2%, 5%, 10%, 20% and 40% for each case as well as smooth and rough pipe conditions.

To validate the effectiveness of the proposed equations, the gas flow magnitudes obtained from the GFE, considering the implicit model of the Colebrook-White equation (2.21) for the friction coefficient, were taken as reference values. The reason for using the Colebrook-White equation is due to its close relation to the Moody chart, which was derived from thousands of experimental studies on commercial pipes. Note that currently this is the standard and most accepted equation for the estimation of the friction factor in the transition zone between

Table 2.2: Comparison of gas flow equations

Drop	GFE		Panh-B	Panh-A	Weymouth	Mueller	IGT	Polyflo		Cox	Spitz	Fritzsche	Spitz-LP	Lacey	Pole	AFE		q_{km}^{inj}		q_{mk}^{inj}	
pressure	Roug	Smooth						Rough	Smooth							Rough	Smooth	Rough	Smooth	Rough	Smooth
Extra high pressure, considering: $p_k = 9000\,[kPa]\,, L_{km} = 30\,[km]\,, D_{km} = 660.4\,[mm]\,, T_{km} = 300K, \varepsilon = 0.01524\,[mm]\,, z = 0.8, G = 0.6,\ q\ [SCMD] \times 10^6$																					
1%	7.1772	7.9927	8.0388	8.0295	6.8013	9.0142	7.4695	5.8026	5.8502	4.3018	4.8047	6.4489	0.5251	0.5024	0.4270	7.5523	8.1887	7.5785	8.2171	7.5261	8.1603
2%	10.1942	11.5733	11.4183	11.6382	9.5943	13.3866	10.9433	8.4067	8.4881	6.0683	6.7777	9.3395	0.7426	0.7105	0.6039	10.7140	11.7485	10.7882	11.8300	10.6392	11.6665
5%	16.1004	18.7728	18.0788	18.9216	15.0546	22.4676	18.0437	13.6572	13.8176	9.5219	10.6350	15.1680	1.1741	1.1234	0.9549	16.8703	18.7771	17.1640	19.1040	16.5715	18.4445
10%	22.5526	26.8397	25.4063	27.1175	21.0156	32.9667	26.1298	19.5596	19.8201	13.2923	14.8461	21.7206	1.6604	1.5887	1.3504	23.5276	26.4715	24.3525	27.3996	22.6727	25.5097
20%	31.1195	37.7801	35.1959	38.2789	28.9279	47.5974	37.2543	27.5907	28.0004	18.2967	20.4356	30.6371	2.3482	2.2467	1.9098	32.2257	36.6208	34.5190	39.2269	29.7562	33.8144
40%	41.5615	51.3763	47.1986	52.2087	38.5706	66.2503	51.2694	37.6055	38.2163	24.3956	27.2474	41.7573	3.3208	3.1774	2.7009	42.6284	48.8575	48.8934	56.0379	35.2675	40.4209
High pressure, considering: $p_k = 3000\,[kPa]\,, L_{km} = 30\,[km]\,, D_{km} = 254\,[mm]\,, T_{km} = 300K, \varepsilon = 0.01524\,[mm]\,, z = 0.9, G = 0.6,\ q\ [SCMD] \times 10^6$																					
1%	0.1769	0.1845	0.2201	0.1888	0.1672	0.1889	0.1726	0.1440	0.1445	0.1316	0.1489	0.1511	0.0282	0.0254	0.0226	0.1761	0.1841	0.1766	0.1846	0.1756	0.1836
2%	0.2548	0.2689	0.3126	0.2736	0.2359	0.2805	0.2528	0.2089	0.2097	0.1856	0.2101	0.2188	0.0399	0.0359	0.0320	0.2535	0.2680	0.2549	0.2694	0.2521	0.2665
5%	0.4088	0.4396	0.4949	0.4448	0.3701	0.4707	0.4169	0.3397	0.3416	0.2912	0.3296	0.3553	0.0630	0.0568	0.0506	0.4065	0.4366	0.4122	0.4427	0.4008	0.4304
10%	0.5782	0.6320	0.6955	0.6375	0.5167	0.6907	0.6037	0.4869	0.4902	0.4065	0.4602	0.5088	0.0891	0.0803	0.0715	0.5744	0.6249	0.5907	0.6427	0.5576	0.6066
20%	0.8041	0.8940	0.9635	0.8998	0.7113	0.9972	0.8607	0.6872	0.6928	0.5595	0.6334	0.7177	0.1261	0.1135	0.1012	0.7971	0.8787	0.8440	0.9304	0.7473	0.8238
40%	1.0801	1.2209	1.2921	1.2273	0.9483	1.3880	1.1845	0.9370	0.9458	0.7460	0.8445	0.9782	0.1783	0.1605	0.1431	1.0675	1.1914	1.2023	1.3419	0.9129	1.0189
Medium pressure, considering: $p_k = 300\,[kPa]\,, L_{km} = 30\,[km]\,, D_{km} = 254\,[mm]\,, T_{km} = 300K, \varepsilon = 0.01524\,[mm]\,, z = 1.0, G = 0.6,\ q\ [SCMD] \times 10^3$																					
1%	13.4625	13.5464	19.9169	14.8736	15.8643	13.3886	13.3953	11.8404	11.8459	13.1551	14.1278	12.6701	8.4565	8.0275	7.1528	13.5312	13.4925	13.5661	13.5260	13.4975	13.4575
2%	19.7599	19.9253	28.2899	21.5581	22.3791	19.8830	19.6251	17.1970	17.2079	18.5573	19.9295	18.3492	11.9593	11.3526	10.1156	19.8610	19.9013	19.9621	20.0022	19.7596	19.7993
5%	32.5421	32.9416	44.7919	35.0496	35.1153	33.3708	32.3584	28.0267	28.0527	29.1185	31.2717	29.8003	18.9094	17.9500	15.9942	32.7059	33.0138	33.1265	33.4390	32.2802	32.5847
10%	46.9553	47.7183	62.9465	50.2313	49.0197	48.9650	46.8596	40.2299	40.2792	40.6485	43.6541	42.6740	26.7419	25.3851	22.6193	47.1861	47.9243	48.4227	49.1804	45.9164	46.6349
20%	66.5600	67.9689	87.2010	70.9062	67.4754	70.6957	66.8094	56.8643	56.9549	55.9524	60.0897	60.1922	37.8187	35.8999	31.9885	66.8729	68.3615	70.5196	72.0895	63.0159	64.4188
40%	90.9375	93.3680	116.9389	96.7092	89.9672	98.4005	91.9433	77.6388	77.7946	74.6032	80.1196	82.0397	53.4838	50.7702	45.2385	91.3366	93.9746	102.1887	105.1406	79.0080	81.2902
Low pressure, considering: $p_k = 7\,[kPa]\,(gauge)\,, L_{km} = 0.3\,[km]\,, D_{km} = 76.2\,[mm]\,, T_{km} = 288.15K, \varepsilon = 0.01524\,[mm]\,, z = 1.0, G = 0.6,\ q\ [SCMD] \times 10^3$																					
1%	0.4794	0.4815	0.8879	0.5940	0.6007	0.4687	0.5035	0.4660	0.4662	0.5966	0.5566	0.4636	0.5422	0.5220	0.5386	0.4806	0.4757	0.4809	0.4750	0.4807	0.4748
2%	0.7149	0.7189	1.2642	0.8632	0.8493	0.6979	0.7396	0.6792	0.6795	0.8436	0.7871	0.6731	0.7667	0.7382	0.7617	0.7164	0.7083	0.7168	0.7084	0.7164	0.7079
5%	1.2058	1.2157	2.0162	1.4143	1.3423	1.1810	1.2291	1.1170	1.1176	1.3332	1.2439	1.1016	1.2123	1.1672	1.2044	1.2081	1.1987	1.2093	1.1994	1.2073	1.1975
10%	1.7832	1.8028	2.8688	2.0537	1.8967	1.7573	1.8042	1.6260	1.6273	1.8840	1.7577	1.5983	1.7144	1.6506	1.7032	1.7864	1.7806	1.7897	1.7832	1.7839	1.7774
20%	2.6266	2.6651	4.0786	2.9795	2.6780	2.6124	2.6459	2.3643	2.3669	2.6600	2.4817	2.3169	2.4246	2.3344	2.4087	2.6312	2.6385	2.6402	2.6467	2.6230	2.6295
40%	3.8497	3.9245	5.7889	4.3151	3.7750	3.8763	3.8732	3.4310	3.4360	3.7496	3.4983	3.3527	3.4289	3.3013	3.4064	3.8563	3.8958	3.8822	3.9210	3.8315	3.8698

laminar and turbulent flow, as well as for smooth and rough pipes. The results obtained from the study cases as well as the description of the conditions for each experiment are presented in the Table 2.2. Furthermore, the relative errors for each case are reported from Figure 2.3 to Figure 2.6. Note that the relative errors less than 25 % with respect to the reference values are the only ones reported in these figures.

The results reported in Table 2.2 and Figure 2.3 clearly show that for the smooth regime case the Panhandle A and IGT equations have the smallest divergence from the reference case. Note, however, that the Panhandle A equation has a better performance for low pressure drops, while the IGT equation improves as the pressure drop increases, just as the Fritzsche equation does for the rough regime case.

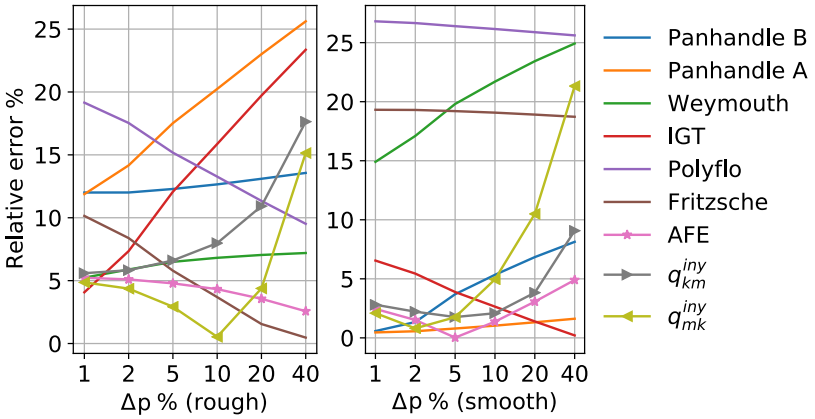

Figure 2.3: Extra high pressure.

On the other hand, the Panhandle B and Weymouth equations maintain constant relative errors as the pressure increases in the rough regime of operation. Note, however, that the first equation tends to be optimistic, while the second one is conservative with respect to the calculated magnitude of gas flow, which can be observed in Table 2.2.

The Panhandle B and Weymouth equations are commonly used in practice in natural gas transportation systems: the former is used for the analysis of operating conditions, while the latter is used in the design and planning stages of the gas network. This is because the Panhandle B equation overestimates the calculation of gas flow through a pipeline, while the Weymouth equation overestimates the pressure drop and maximizes the diameter of a

given flow by providing certain safety margins. From Table 2.2, it is observed that a similar behavior occurs with the NFI equations: gas flow magnitudes are above and below reference values when calculated by the equation q_{km}^{iny} and q_{mk}^{iny}, respectively, as a consequence of the pressure drop. Note, however, that the average of these equations is preserved in a consistent way following the behavior of the GFE.

Based on the aforementioned analysis, the NFI equations proposed in this work contribute to confronting the problem of having to use multiple equations for the different types of analysis that are required within the same gas transportation system.

The results obtained for the high pressure case are reported in Figure 2.4 . The results obtained by using the IGT equation present the smallest deviation with respect to the ones obtained by using the GFE when the operating condition corresponds to the rough case. Within this context, note that the flows calculated from the IGT equation and those obtained from the q_{km}^{iny} equation are very similar. On the other hand, the Mueller equation has the best performance at low pressure drops and a smooth regime of operation. As the pressure drop increases, however, the deviation from the reference values also increases. This behavior is the opposite of what is observed when using the Panhandle equations.

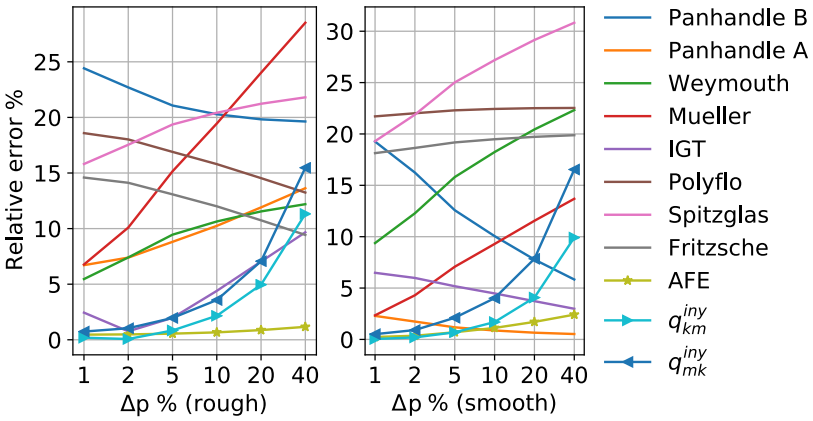

Figure 2.4: High pressure.

The case of medium pressure is reported in Figure 2.5. These results clearly show that the higher the pressure drop in the network the better approximation the Weymouth equation has in both smooth and rough regimes. The opposite occurs with the Cox, Spitzglass and Mueller equations, where the deviation from the reference values increases proportionally to the pressure drop. The equations commonly used in medium pressure systems are the Spitzglass and Mueller equations. The corresponding results of these equations are very similar to the ones observed when using the q_{mk}^{iny} and q_{km}^{iny} equations, respectively, as reported in Table 2.2. On the other hand, the Polyflo and Fritzsche equations (also used in medium pressure systems) present a relatively constant divergence from the reference values for both cases. Lastly the IGT equation is the one that best follows the behavior of the GFE in both cases.

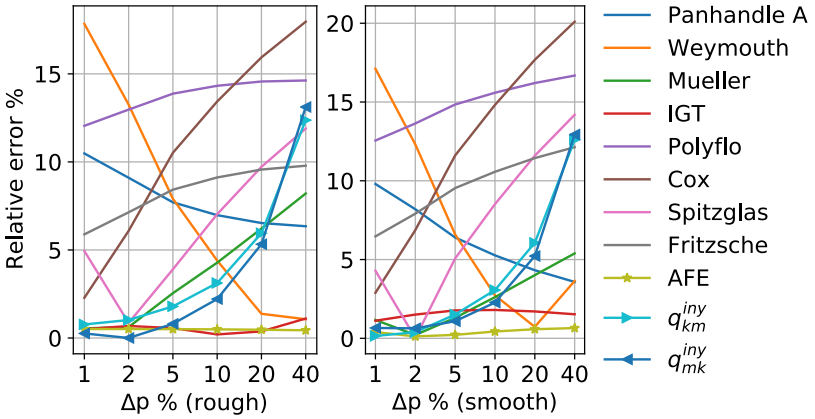

Figure 2.5: Medium pressure.

For the low pressure case, the results presented in Figure 2.6 show that the low pressure equations have a region of validity in the vicinity of pressure drops of approximately 5%. When the pressure drops are lower or higher than that value, the deviation from the reference case begins to increase. Hence, the low pressure equations are optimistic for low pressure drops and conservative for large pressure drops, this as a consequence of the assumptions made for their mathematical deductions. On the other hand, the results reported in Table 2.2 clearly show that the proposed NFI equations present the smallest difference in values between them $q_{km}^{iny} \approx q_{mk}^{iny} \approx AFE$. This is because the calculated compressibility factor is close to 1, which implies that in the pipeline the gas flow through it and the pressure drop are relatively small.

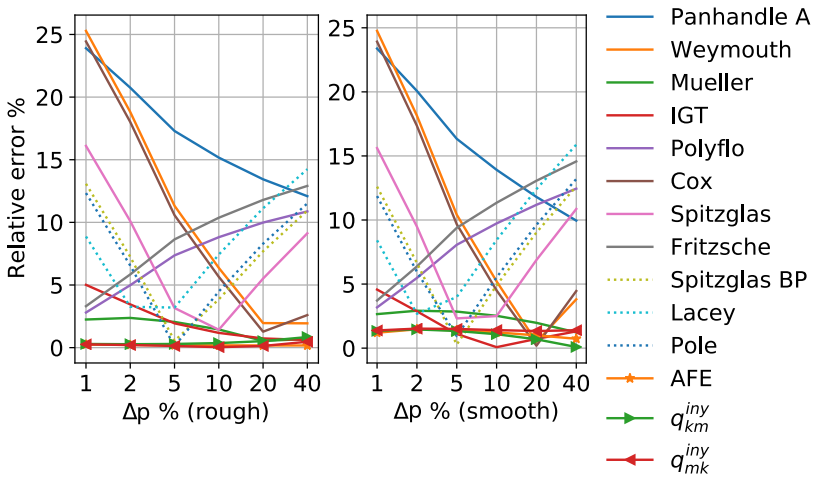

Figure 2.6: Low pressure.

From a general perspective, the AFE equation presents the best performance for all case studies, even though an explicit method was considered to calculate the friction coefficient. Note also that for the GFE a constant, known and typical compressibility factor was selected according to each pressure level, while for the AFE this coefficient was calculated according to the gas operating conditions. Hence, even though the assumed values for the compressibility factor were close to those calculated , as shown in Figure 2.7, the difference in values is the main reason for the variability between the results obtained by the GFE and AFE, so the correct selection of the compressibility factor has a significant impact on the magnitude of the calculated flow.

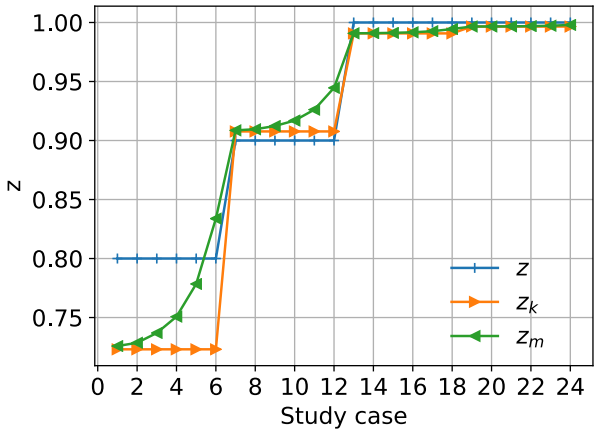

Figure 2.7: Compressibility factor.

From Figure 2.7, it is clear that the higher the nodal gas pressure is, the smaller the value of the compressibility factor. Hence, as the pressure drop increases along the pipeline the compressibility factor at the outlet node "m" also increases, indicating that the gas is expanding and that the amount of gas at the inlet and outlet nodes of the pipeline have different values. Therefore, the compression state of the gas directly affects the amount of gas transported through each pipeline, so care must be taken when using equations based on average values.

On the other hand, even though the AFE representing the root mean of the NFI equations has the smallest deviation in results with respect to those obtained by using the GFE, this does not happen with the magnitude of the injections themselves, which have a growth in the deviation as the pressure drop increases. Note from Table 2.2 that for low pressure drops ($< 10\%$) the magnitude of the flows obtained with the NFI equations has similar values at both ends of the pipeline: the difference between the inlet and outlet flows tends to be zero ($\Delta q \approx 0$). This result is physically consistent because if the pressure drop along the pipeline is small, the loss of energy is also small, and, therefore, the frictional force has a weak impact on the transportation of gas. In addition, according to the linepack concept, if the pressure drop along the pipeline is small, the average pressure is higher such that the volume of gas stored in the pipeline is greater. Therefore the difference between the flow at both ends of the pipeline is smaller because no more gas can be contained.

From the results reported in Table 2.2, it is also observed that the greater the pressure drop the greater the difference between the gas flow injections computed by the NFI equations at the pipeline terminals. Hence, as the volume of gas injected at the inlet node increases, the amount of gas that reaches the other end decreases, which is of a different order of magnitude from the assumed average.

Based on the aforementioned analysis, it can be concluded that the assumption that the gas flows at both ends of a pipeline have similar magnitudes is only applicable in systems where the pressure drop is not that great, so the possibility of using gas flow

equations based on average magnitudes is restricted to such operating conditions.

Finally, an additional case study is presented for the case of extra high pressure where a 60 % of pressure drop is added. The results obtained are schematically shown in Figure 2.8, where with the exception of the NFI equations, all other equations obtain a gas flow profile that increases with the increment of the pressure drop. Note that these results would lead to the numerical conclusion that the flow will reach its maximum value when the pressure at the outlet node is equal to 0, which is physically impossible. An extreme case occurs when there is not enough pressure in the inlet node to make the gas circulate to the other end of the pipeline at that instant. In this case, the injected gas would only be stored in the pipeline and therefore the pressure in the outlet node would be 0. Under these extreme conditions, the pressure drop is maximum, and therefore the average pressure will be minimal. Consequently, the flow stored in the pipeline is minimal, and the difference between the inlet and outlet flow will be the maximum possible. This occurs, for example, in the process of filling the ducts, where gas is injected into the pipeline without being transmitted to other parts of the network until a certain operating pressure is reached. Once this operating condition is reached, the valves can be safely opened to start the transmission of gas through that network element.

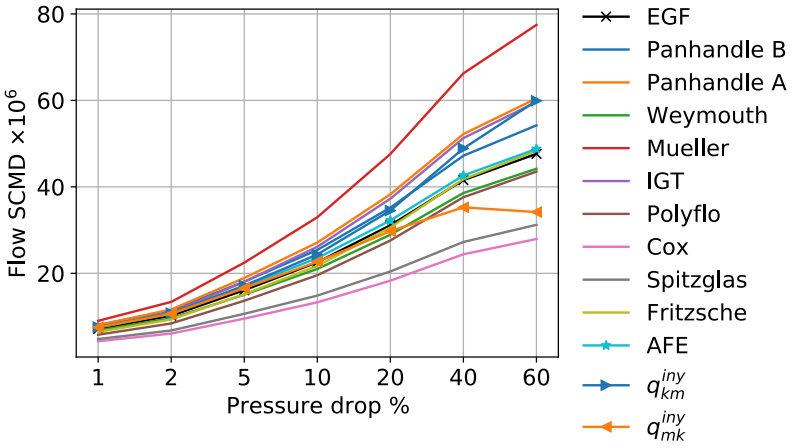

Figure 2.8: Comparison of flows.

Lastly, the importance of considering the compressibility factor as a function of the operating conditions is more significant as the nodal pressure and the pressure drop of the gas increase, which causes a greater difference between the pressure values at the inlet and outlet nodes of a pipeline. As the pressure drop increases, the compression state of the gas changes and produces the gas expansion along the pipeline. This phenomenon increases gas energy losses and reduces the amount of gas available at the other end of the pipeline. Hence, the applicability of the proposed NFI equations is very suitable in practice because the majority of natural gas networks commonly operate at high pressures with considerable pressure drops throughout the network, not to mention the great lengths that the gas must travel from the supply points to the consumption points, which is also a very important factor influencing the gas pressure drops.

2.5 Conclusions

A comprehensive mathematical model of nodal flow injection equations has been proposed in this chapter for assessing the steady-state operation status of a gas transmission network. These equations take into account the effect of gravity over non-horizontal pipelines, the way in which the compressibility factor is affected by the gas pressure, the temperature conditions to which the gas is subjected, the possible bidirectionality of the gas flow, and the existing difference in the amount of gas at the pipeline's inlet and outlet nodes.

The effectiveness of the proposed equations has been demonstrated by numerical examples. Within this context, it was demonstrated that the average-based gas flow equations currently used in practice have a limited region of validity that depends on the magnitude of gas pressure drop along a pipeline. On the other hand, the numerical results clearly show that the proposed NFI equations can be applied to different operating regimes, independently of the level of pressure drop at both ends of the pipeline.

Lastly, a new average-based gas flow equation has also been proposed that considers the effect of gravity on the pipeline inclination, the compressibility factor as a function of the

operating conditions, and the bidirectionality of the gas flow. The numerical results demonstrate that this new equation performs much better than all other equations based on an average model of gas flows.

Chapter 3

Modeling of natural gas and electricity networks

3.1 Introduction

In this chapter the modeling of natural gas and electricity transmission networks is presented. For the gas system, a network model developed from the nodal flow injection (NFI) equations is proposed, which is compared with the model based on the general flow equation (GFE). From this comparison, the implications and limitations of considering a model based on average flow magnitudes versus a model based on flow injections at the interconnection nodes of each pipeline are analyzed. On the other hand, the electricity transmission system is modeled considering the generator-governor characteristics as well as the voltage and frequency dependence of electric loads. This model is compared with the conventional AC power flow model, where all variations in demand are compensated by the slack generator.

3.2 Natural gas network

The transportation of natural gas is a fundamental activity for the gas industry in which the fuel must be moved from one place to another. Even though various means of transportation could be used for this purpose, pipelines represent the most economic

means of transporting large quantities of natural gas over long distances, so the mathematical modeling of gas flows through pipelines is a very important issue in the planning and operation of natural gas transportation networks.

The modeling of natural gas transportation networks becomes a complex problem because of the diversity of the phenomena that occur during the transportation and the variation in the properties of the gas [Narváez99]. Hence, the problem of natural gas flows in steady-state is formulated from the equations that relate the gas flow and nodal pressures at each device that composes the system. Based on these mathematical relationships, the nodal gas flow mismatch equations can be established to assess the operating equilibrium point of the natural gas system. For the proposed formulation, the system is assumed to be composed of pipelines, compressors, sources and demands. Note that storage reservoirs can be modeled as gas sources or gas demands according to their operating condition.

3.2.1 Pipeline

Even though several equations have been proposed to determine the isothermal gas flow through a pipeline in steady-state, the fundamental difference between these equations relies on how the friction factor is considered. In this sense, the GFE, given by (3.1), is the equation that has been universally adopted to relate the pressure drop to the average volumetric flow through a circular cross-sectional pipe [Menon05]. As demonstrated in Chapter 2, the GFE can be obtained as a particular case of the more general average flow equation (AFE) proposed in this work.

Based on the aforementioned, the AFE given by (3.2) will be used to derive the model of average gas flows, which will be compared with the one developed from the NFI equations (3.3) and (3.4). The purpose of this comparison is to analyze the repercussions and differences in considering both types of approaches in the modeling and simulation of the natural gas transportation system.

- General flow equation GFE

$$GFE = q_{km}^{avg} = \frac{\pi}{4}\left(\frac{T_0}{p_0}\right)\epsilon\sqrt{\frac{\left(p_k^2 - p_m^2\right)D_{km}^5 R_{air}}{GT_{km}L_{km}\lambda_{km}z}}. \tag{3.1}$$

- Average flow equation AFE

$$AFE = q_{km}^{avg} = \alpha\frac{\left(p_k^2\beta_k - p_m^2\beta_m + p_k p_m\beta_{km}\right)}{\left|p_k^2\beta_k - p_m^2\beta_m + p_k p_m\beta_{km}\right|^{\frac{1}{2}}}\epsilon. \tag{3.2}$$

- Nodal flow injection NFI equations

$$q_{km}^{iny} = \alpha^{\frac{1}{2}}\frac{\left(p_k^2\beta_{k1} - p_k p_m\beta_{k2}\right)}{\left|p_k^2\beta_{k1} - p_k p_m\beta_{k2}\right|^{\frac{1}{2}}}\epsilon, \tag{3.3}$$

$$q_{mk}^{iny} = \alpha^{\frac{1}{2}}\frac{\left(p_m^2\beta_{m1} - p_k p_m\beta_{m2}\right)}{\left|p_m^2\beta_{m1} - p_k p_m\beta_{m2}\right|^{\frac{1}{2}}}\epsilon. \tag{3.4}$$

3.2.2 Compressor stations

During the process of transporting gas through pipelines, the gas flow tends to lose part of its initial energy because of a pressure drop. This pressure drop results from friction between the gas flow and the inner wall of the pipeline. In order to compensate for this loss of energy and to be able to transport the gas from one place to another, compression stations are strategically installed at several points of the network [Mokhatab19]. A compressor station is a device designed to increase the pressure of gas in a node of the network. In this compensation process, the device consumes and transforms energy such that the analytical representation of a compressor is through its power consumption. This consumption depends on the amount of gas flowing through the station and the compression ratio (CR) given by the discharge pressure and the suction pressure, as shown in (3.5). On the other hand, the power consumption can be calculated by using the brake horsepower (BHP) equation given by (3.6) [Mokhatab19]:

$$CR = \frac{p_D}{p_S}, \tag{3.5}$$

$$BHP = \frac{p_0}{T_0}\frac{z_{comp}T_s}{E\eta}\left(\frac{\kappa}{\kappa - 1}\right)\left[(CR)^{\frac{\kappa-1}{\kappa}} - 1\right]q_{comp}, \tag{3.6}$$

where "κ" corresponds to the isentropic exponent, which can be calculated by the empirical correlation (3.7) if the specific gravity of the gas "G" does not exceed unity,

$$\kappa = 1.3 - 0.31 * (G - 0.55). \tag{3.7}$$

Grouping the independent terms of (3.6) into a constant $BHRC$, the BHP equation can be rewritten as:

$$BHP = BHRC q_{comp}. \tag{3.8}$$

On the other hand, based on [An03], the gas consumed by the compressor can be calculated by its specific consumption function (3.9):

$$\tau_{comp} = \alpha_c + \beta_c BHP + \gamma_c BHP^2. \tag{3.9}$$

Lastly, the expression (3.10) is obtained by replacing (3.8) into (3.9). Note that this resulting equation permits the calculation of the gas consumed by the compressor as a function of the amount of gas circulating through it:

$$\tau_{comp} = \alpha_c + \beta_c BHRC q_{comp} + \gamma_c (BHRC q_{comp})^2. \tag{3.10}$$

3.2.3 Network model

Based on the concept of nodal flow balance, it is possible to establish a general model to describe and analyze the behavior of a natural gas transportation system in steady-state operation state. In this sense, if "k" is a node of the transportation network, as shown in Figure 3.1, the principle of conservation of mass states that the sum of gas flows entering and leaving the node must equal 0, then the nodal mismatch equation can be established.

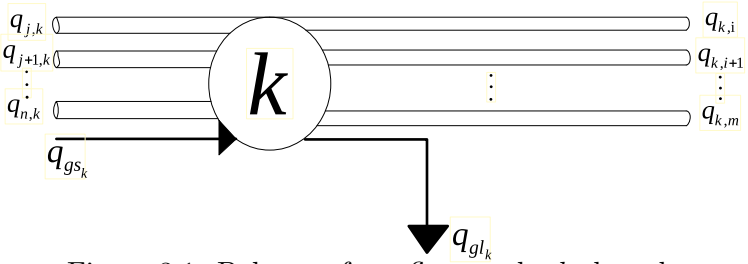

Figure 3.1: Balance of gas flow at the k-th node.

Based on the aforementioned, the gas flow balance for the k-th node of the gas network is given by (3.11), considering the average gas flow model

$$\Delta q_k = \sum_{m \in k} q_{km}^{avg} + \sum_{comp \in k} q_{comp_k} + \sum_{comp \in k} \tau_{comp_k} - \sum_{gs \in k} q_{gs_k} + \sum_{gl \in k} q_{gl_k} = 0, \tag{3.11}$$

where the first two terms of (3.11) correspond to the average gas flow contributed by the pipelines and compressors connected to the node "k", respectively. The third term is the total gas consumed by the compression stations, while the fourth and fifth terms correspond to the total gas injected and extracted in the node "k" through gas sources and gas demands, respectively.

On the other hand, Eq. (3.12) corresponds to the gas balance at the k-th node considering the nodal injection gas flow model:

$$\Delta q_k = \sum_{m \in k} q_{km}^{iny} + \sum_{comp \in k} q_{comp_k} + \sum_{comp \in k} \tau_{comp_k} - \sum_{gs \in k} q_{gs_k} + \sum_{gl \in k} q_{gl_k} = 0. \tag{3.12}$$

For this case, the first term corresponds to the gas flow injections leaving or reaching the node "k" through the pipelines connected to the node. Furthermore, the second and third terms represent the gas circulating through the compression stations connected to the node and the gas consumed by this set of compressors, respectively. Lastly, the fourth and fifth terms correspond to the total gas injected and extracted through the sources and demands embedded at the node, respectively.

On the other hand, the balance of nodal pressures for a compression station connected between the nodes "k" and "m" must be satisfied. This balance equation is directly derived from (3.5) and is given by

$$\Delta CR_{km} = -p_k CR_{km} + p_m = 0. \tag{3.13}$$

Lastly, the behavior of the steady-state gas flows in a transportation system is formulated by the nonlinear algebraic equations (3.11) and (3.13), or (3.12) and (3.13), which are iteratively solved by using the Newton-Raphson method.

Hence, the set of nonlinear algebraic equations that represent the equilibrium condition, which must be satisfied in each node of the network, is be given by

$$\Delta q_k = 0,\ \forall k \in (Ng-1)\,, \tag{3.14}$$

$$\text{and} \quad \Delta CR_{km} = -p_k CR_{km} + p_m = 0,\ \forall k, m \in Nc. \tag{3.15}$$

In general, for the entire natural gas transportation network,

$$\vec{f_{Ng}} = \begin{bmatrix} \Delta\vec{q_k} \\ \Delta\vec{CR}_{km} \end{bmatrix} = 0, \quad \begin{matrix} \forall k \in (Ng-1) \ \text{ and} \\ \forall k, m \in Nc, \end{matrix} \tag{3.16}$$

where (3.16) is defined for the Nc compression stations and for all Ng nodes in the gas network, except for the compensator node. Therefore, by solving for all state variables and assuming that the values of loads and sources in the system are known, the operating point of the system is obtained. In this sense, the set of balance equations (3.11) and (3.13), or (3.12) and (3.13), is solved for the set of state variables given by

$$\vec{x} = \begin{bmatrix} \vec{p_k} \\ \vec{q}_{comp_m} \end{bmatrix} \quad \begin{matrix} \forall k \in (Ng-1) \ \text{ and} \\ \forall m \in Nc. \end{matrix} \tag{3.17}$$

For this purpose (3.16) is approximated by its expansion into the first-order Taylor series, which results in the set of linearized algebraic equations (3.18):

$$\vec{f}_{Ng}\left(\vec{x}^0\right) + J\left(\vec{x}^0\right)\Delta\vec{x} = 0. \tag{3.18}$$

Solving (3.18) for $\Delta\vec{x}$ and generalizing the expression for the case of iteration (i) results in

$$\underbrace{\begin{bmatrix} \Delta\overrightarrow{p_k} \\ \Delta\vec{q}_{comp_m} \end{bmatrix}}_{\Delta\vec{x}^{(i)}} = -\underbrace{\begin{bmatrix} \frac{\partial\Delta\vec{q}}{\partial\vec{p}_k} & \frac{\partial\Delta\vec{q}}{\partial\vec{q}_{comp_m}} \\ \frac{\partial\Delta\overrightarrow{CR}}{\partial\vec{p}_k} & \frac{\partial\Delta\overrightarrow{CR}}{\partial\vec{q}_{comp_m}} \end{bmatrix}^{-1}}_{-J\left(\vec{x}^{(i-1)}\right)^{-1}} \underbrace{\begin{bmatrix} \Delta\vec{q_k} \\ \Delta\overrightarrow{CR}_m \end{bmatrix}}_{f_{Ng}\left(\vec{x}^{(i-1)}\right)} \quad \begin{matrix} \forall k \in (Ng-1) \text{ and} \\ \forall m \in Nc, \end{matrix} \tag{3.19}$$

so the new approximation of the value of the set of state variables will be given by

$$\vec{x}^{(i)} = \vec{x}^{(i-1)} + \Delta\vec{x}^{(i)}. \tag{3.20}$$

Furthermore, this process will be repeated until the n-th iteration, where a tolerance is fulfilled such that $\Delta\vec{x} < 10^{-6}$, or in case the maximum number of allowed iterations is exceeded.

3.2.4 Case studies

To validate and compare the proposed approach, the Belgian gas pipeline network shown in Figure 3.2 is analyzed [De Wolf00]. This network is composed of 20 nodes, 23 pipelines, 1 compression station, 6 gas sources and 9 gas loads. Details of the network are described in Appendix B.2.1.

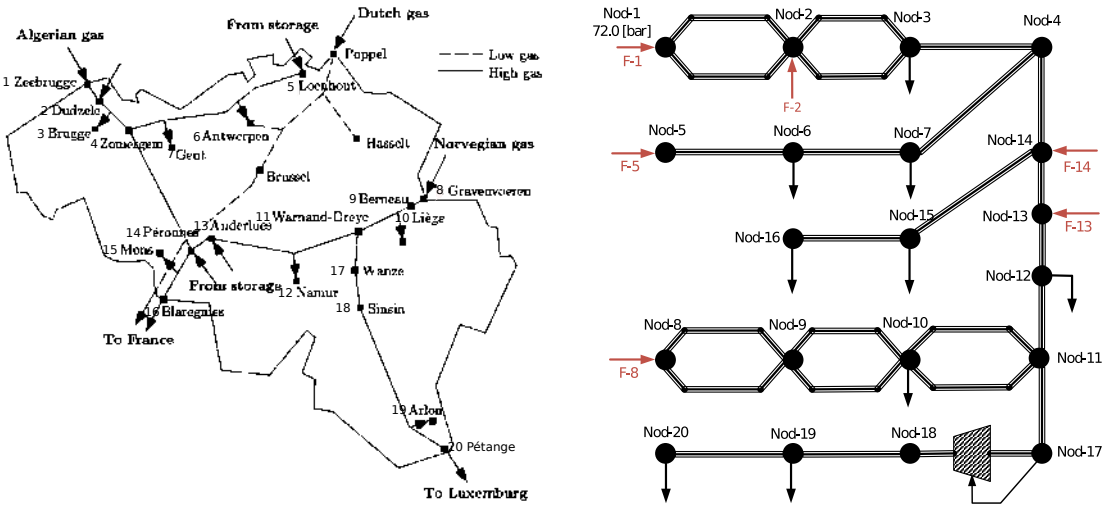

(a) Schematic gas network (b) Pipeline diagram of the gas network

Figure 3.2: Belgium natural gas network.

Considering the described test network, four case studies were carried out.

a.1) **Base case.** For this case, the compressibility factor has a constant value of 0.8 [De Wolf00], and all pipelines are at the same height: $\Delta h = 0$.

a.2) $\boldsymbol{z\,(p,T)}$. In this case, the compressibility factor is considered as a function of the nodal pressure and temperature magnitudes, and $\Delta h = 0$.

a.3) $\boldsymbol{\Delta h \neq 0}$. This case is similar to the a.2) case but considers that pipelines have different levels of height over the land.

a.4) $\boldsymbol{L_{18,22}}$. In this last case, the length of pipes 18 and 22 was changed from 15 to 25 $[km]$ and from 98 to 48 $[km]$, respectively, with $\Delta h = 0$ and $z\,(p,T)$.

The case studies described above were simulated considering both the AFE and NFI models. The results obtained were reported in Table 3.1 and Figures 3.3 and 3.4. From Table 3.1, it

is clear that the values of nodal gas flows at pipeline ends are different when using the NFI model. Note that the magnitude of this difference depends on the properties of the network and the conditions to which the gas is subjected. For example, the greatest difference between the inlet and outlet flows of the pipelines occurs in pipeline 22, which is physically consistent with the fact that it is the longest pipeline in the network (as seen in Appendix B.2.1), and, in the same way, this difference is significantly reduced in case a.4), where the length of the mentioned pipeline is reduced. On the other hand, as expected, the change in the pipeline length does not represent any change in the calculated gas flow magnitude when using the AFE model. This characteristic is numerically reported in Table 3.1, where the gas flows remain practically invariant for all case studies. Hence, the variations in the parameters of both the network and natural gas only have a direct impact on the magnitude of the nodal pressures, as schematically shown in Figure 3.3.

Table 3.1: Comparison of gas flows $[SCMH] \times 10^3$

Pipeline			a.1) **Base case**			a.2) $\boldsymbol{z\,(P,T)}$			a.3) $\boldsymbol{\Delta h \neq 0}$			a.4) $\boldsymbol{L_{18,22}}$ **modified**		
#	**From**	**to**	**AFE**	$\boldsymbol{q_{km}^{iny}}$	$\boldsymbol{q_{mk}^{iny}}$	**AFE**	$\boldsymbol{q_{km}^{iny}}$	$\boldsymbol{q_{mk}^{iny}}$	**AFE**	$\boldsymbol{q_{km}^{iny}}$	$\boldsymbol{q_{mk}^{iny}}$	**AFE**	$\boldsymbol{q_{km}^{iny}}$	$\boldsymbol{q_{mk}^{iny}}$
1	1	2	227.360	263.796	263.738	227.356	275.652	275.569	227.356	272.468	274.224	227.356	265.233	265.159
2	1	2	227.360	263.796	263.738	227.356	275.652	275.569	227.356	272.468	274.224	227.356	265.233	265.159
3	2	3	402.360	438.738	438.341	402.356	450.569	450.032	402.356	449.224	448.749	402.356	440.159	439.658
4	2	3	402.360	438.738	438.341	402.356	450.569	450.032	402.356	449.224	448.749	402.356	440.159	439.658
5	3	4	641.470	713.432	706.034	641.461	736.815	726.689	641.461	734.248	724.278	641.461	716.067	706.771
6	5	6	117.280	117.280	116.783	117.280	117.280	116.661	117.280	117.280	116.667	117.280	117.280	116.663
7	6	7	-50.804	-51.301	-51.330	-50.804	-51.422	-51.459	-50.804	-51.416	-51.166	-50.804	-51.421	-51.458
8	7	4	-269.804	-270.330	-272.992	-269.804	-270.459	-273.796	-269.804	-270.166	-273.485	-269.804	-270.457	-273.786
9	4	14	371.666	433.042	429.367	371.658	452.892	447.670	371.658	450.793	445.766	371.657	432.985	428.429
10	8	9	817.732	817.732	815.736	817.732	817.732	815.207	818.256	817.734	815.461	817.732	817.732	815.262
11	8	9	99.435	99.434	99.191	99.435	99.434	99.127	98.911	99.433	99.159	99.435	99.434	99.134
12	9	10	817.732	815.738	807.701	817.732	815.209	805.110	817.754	815.465	805.423	817.732	815.265	805.389
13	9	10	99.435	99.190	98.213	99.435	99.125	97.897	99.413	99.156	97.935	99.435	99.132	97.931
14	10	11	581.356	571.328	567.727	581.356	568.736	564.268	581.365	569.050	564.608	581.356	569.016	564.645
15	10	11	70.602	69.378	68.941	70.602	69.062	68.519	70.593	69.100	68.561	70.602	69.096	68.565
16	11	12	562.667	526.362	521.496	562.676	512.650	507.012	562.676	513.614	508.002	562.676	535.288	529.028
17	12	13	474.334	433.163	430.477	474.342	418.679	415.645	474.342	419.668	416.652	474.343	440.695	437.238
18	13	14	524.334	480.477	480.010	524.342	465.645	465.113	524.342	466.652	466.847	524.343	487.238	484.254
19	14	15	936.000	949.377	942.177	936.000	952.782	943.724	936.000	952.613	943.677	936.000	952.683	943.677
20	15	16	650.667	656.844	650.667	650.667	658.390	650.667	650.667	658.344	650.667	650.667	658.344	650.667
21	11	17	89.291	110.305	109.555	89.283	120.137	118.922	89.283	119.554	118.370	89.282	97.922	97.278
22	18	19	89.208	109.454	90.162	89.208	118.822	90.490	89.208	118.270	90.451	89.208	97.196	89.868
23	19	20	79.958	80.912	79.958	79.958	81.240	79.958	79.958	81.201	79.958	79.958	80.618	79.958

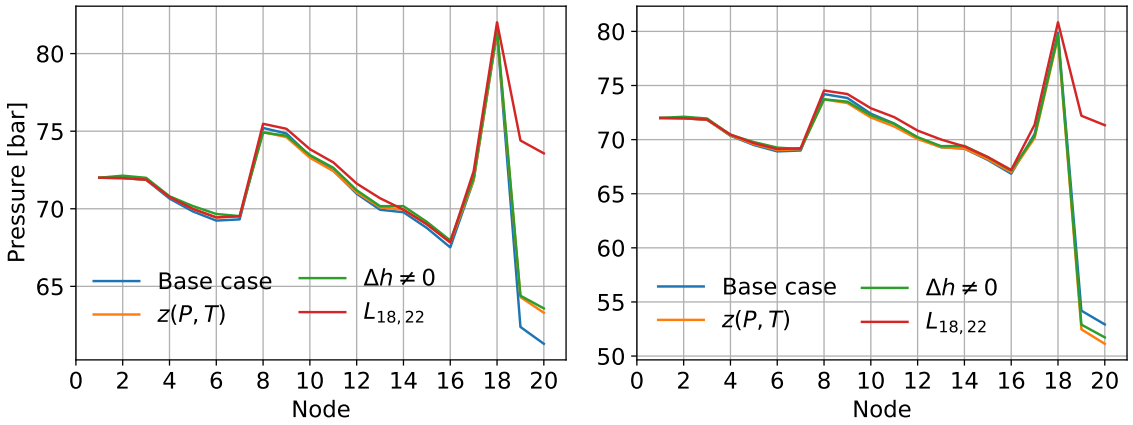

(a) AFE model (b) NFI model

Figure 3.3: Nodal pressure.

From Table 3.1, it is also clear that the inlet gas flow is of greater magnitude than the outlet gas flow for almost all cases when using the NFI model. This implies that an amount of the injected gas is being stored in the pipeline, and, consequently a greater quantity of gas must be supplied by the controlled pressure supply node. This statement is validated by the results reported in Table 3.2, where the gas supplied by the source node varies between 527,000 and 551,000 SCMH for the different case studies, while for the AFE model this magnitude remains constant.

Table 3.2: Gas supplied by node 1 $[SCMH] \times 10^3$

a.1) **Base case**		a.2) $\boldsymbol{z\,(P,T)}$		a.3) $\boldsymbol{\Delta h \neq 0}$		a.4) $\boldsymbol{L_{18,22}}$ **modified**	
AFE	**NFI**	**AFE**	**NFI**	**AFE**	**NFI**	**AFE**	**NFI**
454.7195	527.5915	454.7113	551.3037	454.7113	544.9368	454.7111	530.4654

The nodal compressibility factor values are shown in Figures 3.4a and 3.4b for the AFE and NFI models, respectively. Note that for both types of models, in most cases, these values are less than the 0.8 value assumed for the base case. This implies that under the operating conditions obtained in this study the gas actually occupies a smaller volume, and therefore there is a greater storage capacity.

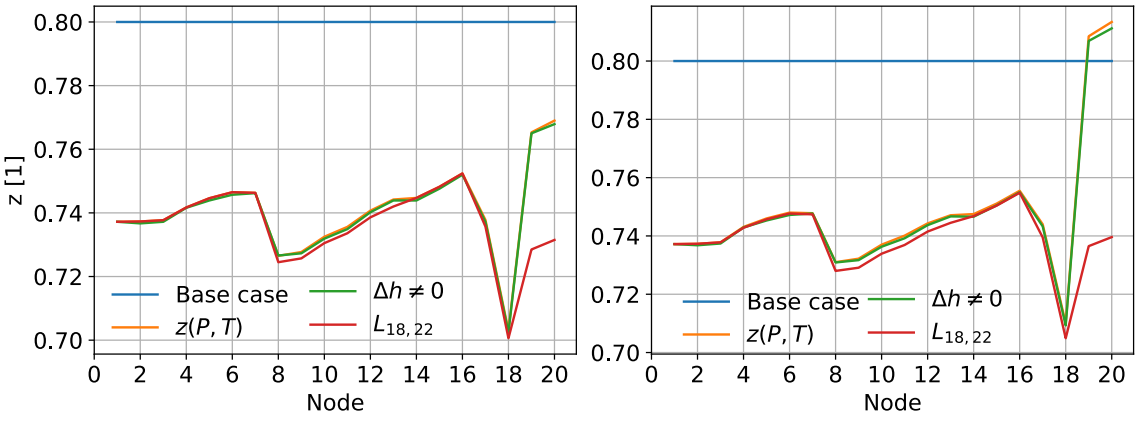

(a) AFE model (b) NFI model

Figure 3.4: Compressibility factor.

On the other hand, note that the difference between the inlet and outlet gas flows at the pipeline ends may be negative: the flow entering a pipeline may be less than the flow being extracted from it. Therefore the stored gas tends to decrease. An example of this occurs in pipelines 1, 2, 7 and 18 of case a.3), as reported in Table 3.1. In this case, the gas flow circulates from a point of lower pressure to another of higher pressure because of the gravity force acting on the pipeline's inclination. The aforementioned is illustrated in Figure 3.5.

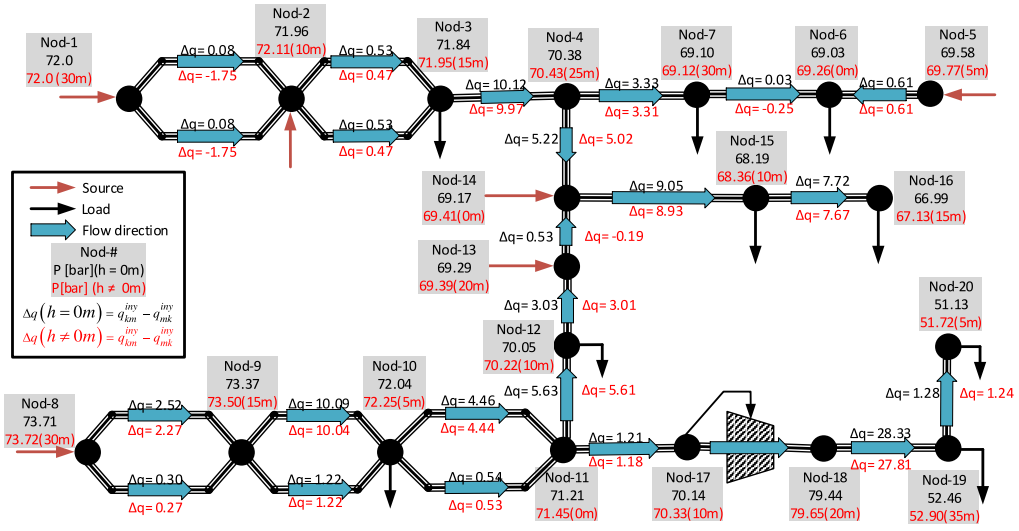

Figure 3.5: Gas flows a.2) and a.3) with the NFI model considering the elevation of nodes.

Table 3.3 reports the results of gas flows through compressors embedded in the network. When the AFE model is used, the gas flow remains almost invariant for all case studies, while the consumption and mechanical power only differ from the base case by the calculation of the compressibility factor. On the other hand, the magnitudes of the compressor gas flow vary according to the changes in the network, which is expected when using the NFI model. Note also that for the case where the length of duct 22 was reduced the amount of gas flow decreased with respect to the rest of the case studies such that the mechanical power of the compressor was also significantly reduced.

Table 3.3: Comparison of results in compressor stations

	a.1) **Base case**		a.2) $\boldsymbol{z\,(P,T)}$		a.3) $\boldsymbol{\Delta h \neq 0}$		a.4) $\boldsymbol{L_{18,22}}$ **modified**	
	AFE	**NFI**	**AFE**	**NFI**	**AFE**	**NFI**	**AFE**	**NFI**
$q_{comp}\,[SCMH] \times 10^3$	89.2083	109.4538	89.2083	118.8216	89.2083	118.2704	89.2083	97.1963
$\tau_{comp}\,[SCMH] \times 10^3$	0.0826	0.1013	0.0743	0.0999	0.0743	0.0993	0.0741	0.0812
$BHP\,[HP]$	350.0399	429.4800	315.0359	423.6936	315.0359	421.1480	314.1608	344.1987

Lastly, the difference between the inlet and outlet gas flow at pipeline ends modifies the pipeline capacity of storage and the amount of gas supplied through it. From this approach, the difference between the inlet and outlet gas flows Δq in each pipeline can be modeled as additional loads (resp. sources) to be considered in the AFE model. The above is schematically represented in Figure 3.6, where Δq is defined by Eq. (3.21) obtained in Chapter 2:

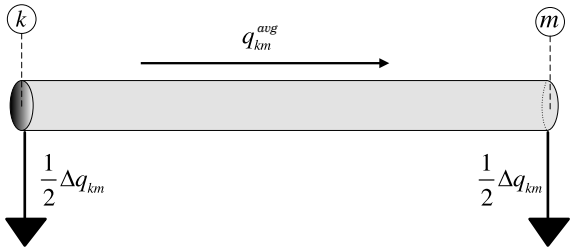

Figure 3.6: Distribution of Δq among the connection nodes of a pipeline.

$$\Delta_q^{pipe} = \Delta q_{km} = \frac{D_{km}^{2.5}\pi T_0}{p_0}\sqrt{\frac{R_{air}\left(p_k - p_m\right)}{8L_{km}\lambda_{km}GT_{km}z}}\left(p_k^{\frac{1}{2}} - p_m^{\frac{1}{2}}\right). \tag{3.21}$$

Equation (3.21) also depends only on nodal pressures, and, therefore, it can be easily included in the net flow balance equation (3.11) resulting in (3.22):

$$\Delta q_k = \sum_{m\in k} q_{km}^{avg} + \sum_{comp\in k} q_{comp_k} + \sum_{comp\in k} \tau_{comp_k} - \sum_{gs\in k} q_{gs_k} + \sum_{gl\in k} q_{gl_k} - \sum_{m\in k} \frac{1}{2}\Delta q_{km} = 0. \tag{3.22}$$

Case studies a.2) and a.4) have been newly simulated, but they consider the complemented AFE model (3.22), referred to as the AFE+Δq model, with the results presented in Figures 3.7 to 3.10. A comparison of results with those from the NFI model shows that the difference is significantly reduced. In addition to the fact that the results obtained with this adjustment in the AFE model were very close to those obtained with the NFI model, it was also achieved that the AFE model is sensitive to variations in the network and/or gas conditions, such as those presented in this study: in the length of the pipelines and the gas compressibility factor.

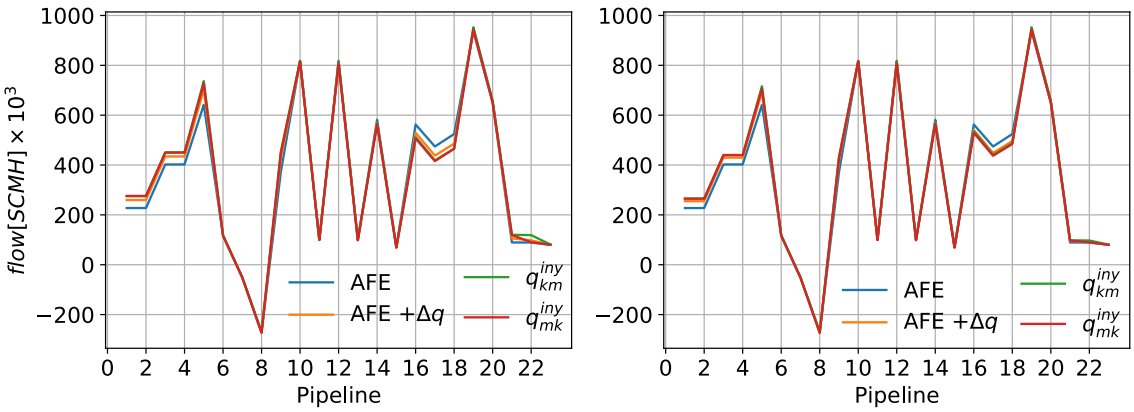

(a) case a.2) (b) case a.4)

Figure 3.7: Gas flows.

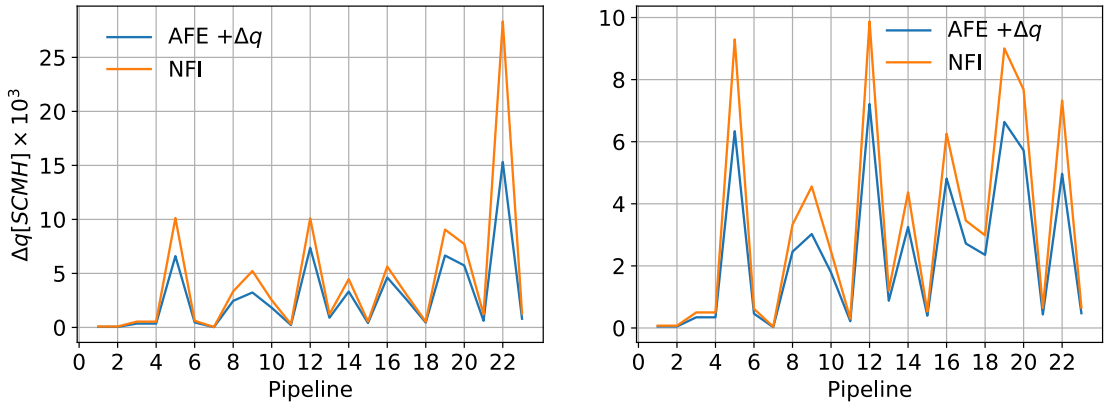

(a) case a.2) (b) case a.4)

Figure 3.8: Difference between the inlet and outlet gas flows.

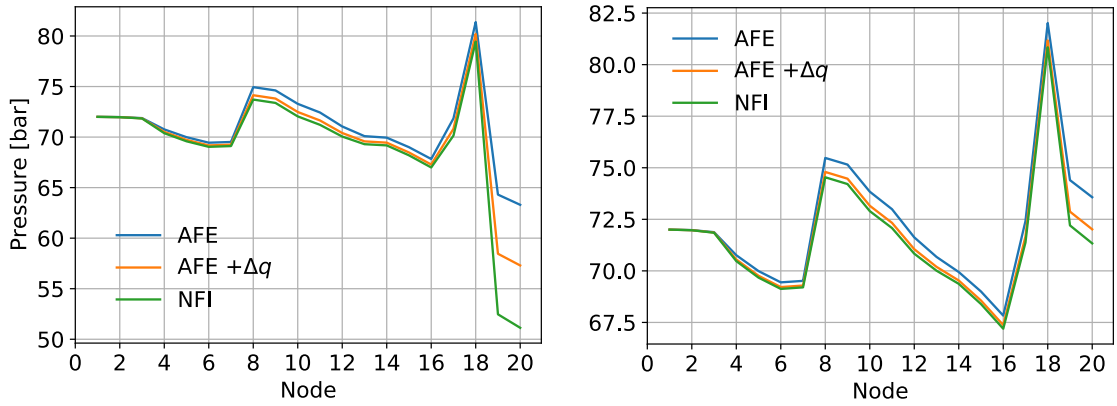

(a) case a.2) (b) case a.4)

Figure 3.9: Nodal pressures.

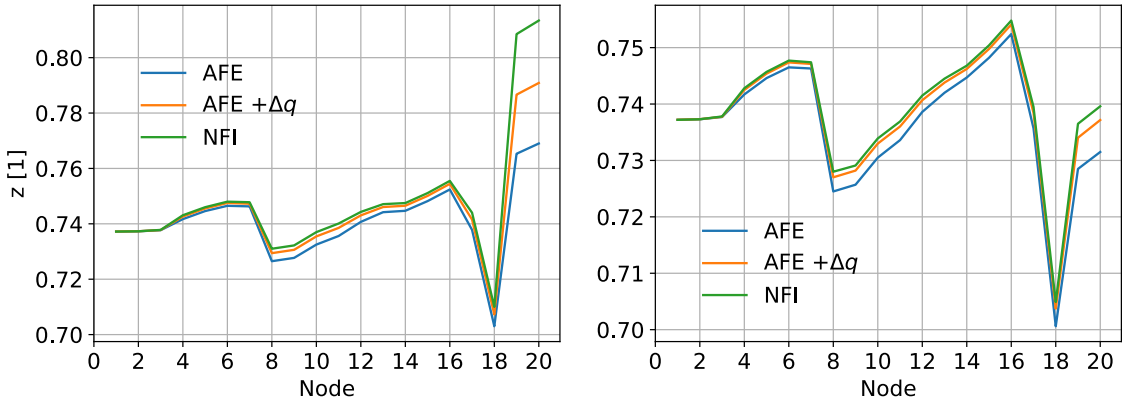

(a) case a.2) (b) case a.4)

Figure 3.10: Compressibility factor.

Despite the improvement of the results, there are more significant differences in the network's last nodes because of the compressor station connected between nodes 17 and 18. Note that a compressor station does not have the same behavior as a pipeline. Therefore, the AFE+Δq model presents more significant deviations in the pressures and flows in the subsequent nodes with respect to the NFI model.

Finally, and in order to expand the study and demonstrate the applicability of the proposed equations at any pressure level, the proposed model is applied to the low pressure system presented in the Figure 3.11 [Abeysekera16]. This system is composed of 11 nodes, 14 pipelines, 1 source and 10 charges as described in Appendix B.2.3. Tables 3.4 and 3.5 compare the results obtained from the NFI model with those presented in [Abeysekera16]. Note that the gas flows magnitudes are relatively similar, despite Lacey's equation (used in the reference case), turns out to be much more conservative, which results in more abrupt pressure drops than those obtained with the NFI model. The above is a consequence of the assumptions made for the deduction of Lacey's equation (2.48), which were described in Chapter 2.

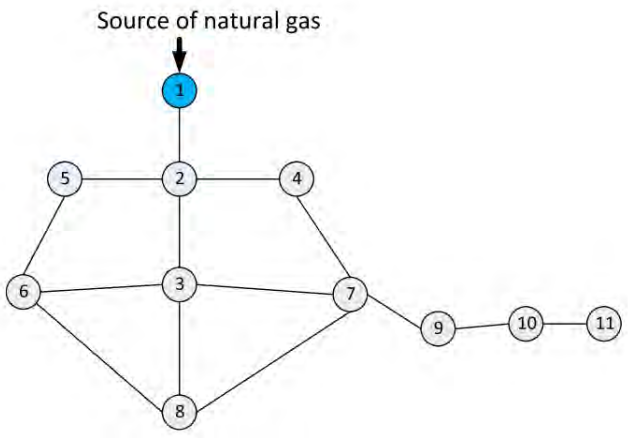

Figure 3.11: Low pressure gas network taken from [Abeysekera16].

Table 3.4: Comparison of gas flows [$SCMH$]

Pipeline			**Base case**	**Nodal injections**			**Pipeline**			**Base case**	**Nodal injections**		
#	from	to	**Lacey**	q_{km}^{iny}	q_{mk}^{iny}	Δq	#	from	to	**Lacey**	q_{km}^{iny}	q_{mk}^{iny}	Δq
1	1	2	1344.00	1356.35	1352.26	4.08	8	5	6	36.41	35.94	35.89	0.05
2	2	3	627.37	634.05	629.36	4.69	9	4	7	57.67	56.04	55.86	0.18
3	2	4	233.10	232.76	231.04	1.71	10	6	8	18.43	17.43	17.42	0.01
4	2	5	264.47	266.46	263.94	2.52	11	7	8	25.31	22.80	22.78	0.02
5	3	6	139.91	139.04	138.54	0.50	12	7	9	120.61	120.67	120.14	0.53
6	3	7	132.10	131.84	131.41	0.43	13	9	10	72.36	72.14	72.01	0.13
7	3	8	162.39	166.49	165.80	0.69	14	10	11	30.70	30.01	30.00	0.01

Table 3.5: Gas supplied, gas demanded and nodal pressures

Node	**Base case**		**Nodal injections**		**Load**
	Source	**Pressure**	**Source**	**Pressure**	
#	**SCMH**	**mbar**	**SCMH**	**mbar**	**SCMH**
1	1344.00	75.00	1356.29	75.00	0.00
2		66.09		68.48	219.00
3		46.68		52.61	192.00
4		46.95		52.66	175.00
5		41.45		48.21	228.00
6		38.40		45.05	157.00
7		39.30		45.74	43.80
8		37.39		43.89	206.00
9		28.15		36.49	48.00
10		24.14		32.81	42.00
11		23.40		32.04	30.00

3.3 Electricity network

The electric power system is modeled by using the AC nodal power flow mismatch equations [Acha04], including the models of generators with primary frequency regulation and loads dependent on the magnitudes of nodal voltage and frequency. This model is referred as frequency regulated power flows (FRPF), and the power equations associated with these two electric components are described below.

3.3.1 Electric generators

Two types of generators are considered in the proposed formulation.

- **Type 1 conventional** PV **generator.** This generator injects a specified active power, while its reactive power is independently adjusted within its limits to set its nodal voltage magnitude at a specified value. The power injected by the i-th generator is mathematically represented by

$$P_{G_i} = cte \tag{3.23}$$

$$Q_{G_i} = \sum_{j \in i} Q_{ij}^{cal} + Q_{L_i}. \tag{3.24}$$

If the generator operates within limits of Q_{G_i},

$$Q_{G_i}^{min} \leq Q_{G_i} \leq Q_{G_i}^{max} \Rightarrow v_i = v_{ref}; \tag{3.25}$$

otherwise,

$$Q_{G_i} = Q_{G_i}^{min} \;\; or \;\; Q_{G_i} = Q_{G_i}^{max} \Rightarrow v_i = v^{cal}. \tag{3.26}$$

To ensure that constraints (3.25) and (3.26) are explicitly satisfied during the iterative solution process of the power flow problem, the concepts of complementarity constraints and the Fischer-Burmeister merit function[Ferris97] are used. Hence, (3.25) and (3.26) are tranformed into a set of equality constrains given by

$$v_i - v_{ref} - v_a + v_b = 0 \tag{3.27}$$

$$\phi_{Q_G}^{min} = \sqrt{v_a^2 + \left(Q_{G_i} - Q_{G_i}^{min}\right)^2} - \left(v_a + \left(Q_{G_i} - Q_{G_i}^{min}\right)\right) = 0 \tag{3.28}$$

$$\phi_{Q_G}^{max} = \sqrt{v_b^2 + \left(Q_{G_i}^{max} - Q_{G_i}\right)^2} - \left(v_b + \left(Q_{G_i}^{max} - Q_{G_i}\right)\right) = 0. \tag{3.29}$$

- **Type 2 primary frequency regulation (PFR) generator .** In this case, the generated active and reactive powers are adjusted by the i-th generator's governor

according to the frequency variations [Okamura75]:

$$P_{G_i} = P_{G_i}^{sch} - \frac{P_{G_i}^{nom}}{K_{reg}} \frac{\Delta f}{f^{nom}} \tag{3.30}$$

$$Q_{G_i} = Q_{G_i}^{sch} + a_Q \Delta P_{G_i} + b_Q \Delta P_{G_i}^2, \tag{3.31}$$

where

$$\Delta P_{G_i} = -\frac{P_{G_i}^{nom}}{K_{reg}} \frac{\Delta f}{f^{nom}} \tag{3.32}$$

$$P_{G_i}^{min} \leq P_{G_i} \leq P_{G_i}^{max} \tag{3.33}$$

$$Q_{G_i}^{min} \leq Q_{G_i} \leq Q_{G_i}^{max}. \tag{3.34}$$

Based on the generator's capability curve, if the generation of active power varies, the reactive power limits cannot remain constant. Hence, a geometric-based approach is proposed to obtain a set of mathematical equations that consider the variability of the reactive power limits as a function of the known nominal value of $P_{G_i}^{nom}$ and the limitation imposed by the armature current. The three cases below were derived, depending on the magnitudes of the known nominal reactive power limits.

- If the limits are symmetric, i.e. $Q_{G_i}^{nom,max}$ == -$Q_{G_i}^{nom,min}$,

$$Q_{G_i}^{max} = \sqrt{\left(S_{G_i}^{nom}\right)^2 - P_{G_i}^2} \tag{3.35}$$

$$Q_{G_i}^{min} = -\sqrt{\left(S_{G_i}^{nom}\right)^2 - P_{G_i}^2}. \tag{3.36}$$

- If $Q_{G_i}^{nom,max} > -Q_{G_i}^{nom,min}$,

$$Q_{G_i}^{max} = \sqrt{\left(S_{G_i}^{nom}\right)^2 - P_{G_i}^2} \tag{3.37}$$

$$Q_{G_i}^{min} = -\sqrt{\frac{\left(Q_{G_i}^{nom,min}\right)^2}{\left(S_{G_i}^{nom} - P_{G_i}^{nom}\right)} \left(S_{G_i}^{nom} - P_{G_i}\right)}. \tag{3.38}$$

- Moreover, if $Q_{G_i}^{nom,max} < -Q_{G_i}^{nom,min}$,

$$Q_{G_i}^{max} = \sqrt{\frac{\left(Q_{G_i}^{nom,max}\right)^2}{\left(S_{G_i}^{nom} - P_{G_i}^{nom}\right)}\left(S_{G_i}^{nom} - P_{G_i}\right)} \tag{3.39}$$

$$Q_{G_i}^{min} = -\sqrt{\left(S_{G_i}^{nom}\right)^2 - P_{G_i}^2}. \tag{3.40}$$

Lastly, if the value of P_{G_i} is set at a violated limit, the generator is transformed to type 1. On the other hand, if Q_{G_i} violates one of its limits, Q_{G_i} is set at the violated limit, but the unit will continue to regulate the frequency as long as it can.

3.3.2 Electric loads

One of the main challenges in the modeling of electric components is associated with electric loads. For the purpose of this paper, two types of loads are considered below.

- **Type 1 constant power.** In this case, loads extract a constant electric power from the point of connection to a specific power factor. Hence, for the i-th load,

$$P_{L_i} = cte \quad and \quad Q_{L_i} = cte. \tag{3.41}$$

- **Type 2 nonlinear load.** In this case, the i-th load is a function of voltage magnitude and frequency variations [Okamura75]:

$$P_{L_i} = P_{L_i}^{sch}\left(1 + K_{pf}\Delta f\right) \times \left(K_{pp} + K_{pc}\left(\frac{v_i}{v_i^{nom}}\right)^{N1} + K_{pz}\left(\frac{v_i}{v_i^{nom}}\right)^2\right) \text{ and}$$

$$Q_{L_i} = Q_{L_i}^{sch}\left(1 + K_{qf}\Delta f\right) \times \left(K_{qp} + K_{qc}\left(\frac{v_i}{v_i^{nom}}\right)^{N2} + K_{qz}\left(\frac{v_i}{v_i^{nom}}\right)^2\right),$$

where K_{pf} and K_{qf} are the coefficients of the frequency characteristic. Typically, K_{pf} has values ranging from 0 to 3.0, while K_{qf} has a range of -2.0 to 0. On the other hand the factors K_{pp}, K_{pc}, K_{pz}, K_{qp}, K_{qc} and K_{qz}, correspond to the coefficients of the characteristic of voltage, and they must satisfy Eq. (3.42) and Eq. (3.43), respectively.

Lastly, $N1$ and $N2$ are factors that adjust the voltage characteristic, and for this work, they will be assumed to be equal to 1.

$$K_{pp} + K_{pc} + K_{pz} = 1 \tag{3.42}$$

$$K_{qp} + K_{qc} + K_{qz} = 1. \tag{3.43}$$

For the rest of the electric power system components, e.g., transmission lines, transformers and shunt compensators, among others, the conventional models reported in [Acha04] are considered.

3.3.3 Mismatch equations

The power flows problem is formulated by means of two equations associated with the electrical power balance at each network bus. Hence, the set of electric power flow mismatch equations at the "i" bus of the transmission network is given by (3.44) and (3.45):

$$\Delta P_i = \sum P_{G_i} - \sum P_{L_i} - \sum_{j \in i} P_{ij}^{cal} = 0, \ \ \forall i \in N_e, \tag{3.44}$$

$$\Delta Q_i = \sum Q_{G_i} - \sum Q_{L_i} - \sum_{j \in i} Q_{ij}^{cal} = 0, \ \ \forall i \in N_e, \tag{3.45}$$

where P_{ij}^{cal} and Q_{ij}^{cal} correspond to the active and reactive power injections, respectively, of the devices connected to bus "i". These devices can be transmission lines, conventional two-phase transformers, load tap-changing transformers or shunt compensators. The mathematical models of these devices are functions of nodal voltages and network impedances, and they can be consulted in [Acha04].

With Eq. (3.44) and Eq. (3.45), the system of nonlinear algebraic equations that govern the behavior of the steady-state power flows in a transmission system can be formulated, and the solution of this equation system results in the operating state of the electric power system.

Now to solve this set of equations, the Newton-Raphson method is applied. Therefore, Eq. (3.44) and Eq. (3.45) must be expressed from the expansion of the first-order Taylor series in the form of (3.46):

$$f_{Ne}\left(\vec{x}^{0}\right) + J\left(\vec{x}^{0}\right)\Delta\vec{x} = 0, \tag{3.46}$$

where $\vec{x}$ represents the set of state variables. The power mismatch equations ΔP and ΔQ are expanded around a initial condition $\left(\vec{x}^{0}\right)$, and, hence, isolating $\Delta\vec{x}$ from (3.46) and generalizing the expression for the case of iteration (i) result in

$$\underbrace{\begin{bmatrix} \Delta\theta \\ \Delta v \\ \Delta v_a \\ \Delta v_b \\ \Delta\left(\Delta f\right) \end{bmatrix}}_{\Delta\vec{x}^{(i)}} = -\underbrace{\begin{bmatrix} \frac{\partial\Delta P}{\partial\theta} & \frac{\partial\Delta P}{\partial v} & 0 & 0 & \frac{\partial\Delta P}{\partial\Delta f} \\ \frac{\partial\Delta Q}{\partial\theta} & \frac{\partial\Delta Q}{\partial v} & \frac{\partial\Delta Q}{\partial v_a} & \frac{\partial\Delta Q}{\partial v_b} & \frac{\partial\Delta Q}{\partial\Delta f} \\ \frac{\partial\phi^{min}_{Q_G}}{\partial\theta} & \frac{\partial\phi^{min}_{Q_G}}{\partial v} & \frac{\partial\phi^{min}_{Q_G}}{\partial v_a} & \frac{\partial\phi^{min}_{Q_G}}{\partial v_b} & 0 \\ \frac{\partial\phi^{\max}_{Q_G}}{\partial\theta} & \frac{\partial\phi^{\max}_{Q_G}}{\partial v} & \frac{\partial\phi^{\max}_{Q_G}}{\partial v_a} & \frac{\partial\phi^{\max}_{Q_G}}{\partial v_b} & 0 \\ \frac{\partial\Delta P_{G_{ref}}}{\partial\theta} & \frac{\partial\Delta P_{G_{ref}}}{\partial v} & 0 & 0 & \frac{\partial\Delta P_{G_{ref}}}{\partial\Delta f} \end{bmatrix}^{-1}}_{-J\left(\vec{x}^{(i-1)}\right)^{-1}} \underbrace{\begin{bmatrix} \Delta P \\ \Delta Q \\ \phi^{\min}_{Q_G} \\ \phi^{\max}_{Q_G} \\ \Delta P_{G_{ref}} \end{bmatrix}}_{f_{Ne}\left(\vec{x}^{(i-1)}\right)}, \tag{3.47}$$

where θ is defined for all Ne buses in the electrical network, except for the reference bus.

Lastly, the new approximation of the value of the set of state variables will be given by $\vec{x}^{(i)} = \vec{x}^{(i-1)} + \Delta\vec{x}^{(i)}$. This process will be repeated until the n-th iteration in which a tolerance of $\Delta\vec{x} < 10^{-12}$ is met, or the maximum number of iterations is exceeded.

3.3.4 Case study

The performance of the proposed approach is evaluated by using the 3-bus electricity network shown in Figure 3.12, which consists of 3 transmission lines, 3 generators, 3 loads and 1 shunt compensator. In this case, there are two power plants contributing to the primary frequency control, as shown in Table 3.6, and 2 loads are dependent on the system's frequency and nodal voltage magnitudes. The network parameters can be consulted in Appendix B.1.1.

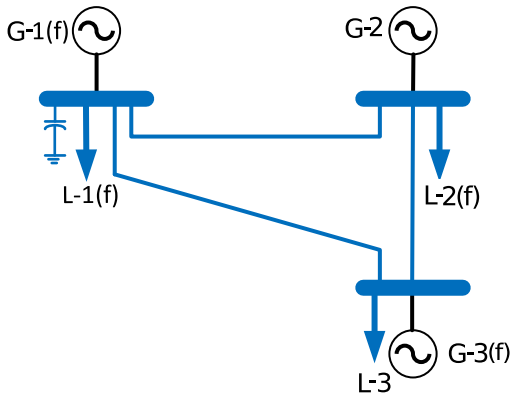

Figure 3.12: Three-bus network.

Table 3.6: Generators' description

Generator Bus	P_G^{sch} $[MW]$	Q_G^{sch} $[MVARs]$	P_G^{nom} $[MW]$	$Q_G^{nom,min}$ $[MVARs]$	$Q_G^{nom,max}$ $[MVARs]$	v_{ref} $[p.u.]$	K_{reg} %
1	486.55	-30.614	500	-150	160	1.02	4.5
2	350	87.278	350	-100	125	1.03	-
3	617.24	174.302	650	-300	160	1.05	3.2

Three different case studies where the electric system's loadability is changed from its nominal value are reported. The first case study, referred to as the base case, corresponds to the load values reported in Appendix B.1.1. The other two case studies correspond to an increment and decrement of 5% of the nominal power demanded by each load, respectively. All these load changes are performed while considering a constant power factor, and in order to illustrate the reliability of the FRPF model, the results obtained by the proposed approach in each case study are compared with those obtained when the electric power system is modeled in the conventional way. Note that in this last type of modeling, the slack generator is the one connected at node 1, while the rest of the generators inject a constant active power and control their voltage magnitudes by adjusting their generation of reactive power within limits.

Table 3.7 reports the results obtained for the base case by using the conventional and proposed power flow approaches, which practically provide the same results. This

is because the initial conditions considered for the frequency regulation analysis meet the balance of power between generation and demand, and with this the validity of the proposed approach is demonstrated. There is, however, a small difference between the results reported for this case study because of the variations in the loads depending on frequency and nodal voltage magnitudes, as reported in Table 3.10.

Table 3.7: Active power generated [MW]

Generator	**Base case**		**+5%**		**-5%**	
bus	**FRPF**	**Conv.**	**FRPF**	**Conv.**	**FRPF**	**Conv.**
1	486.7512	486.8951	512.6593	560.1074	460.5910	413.9301
2	350	350	350	350	350	350
3	617.6078	617.2400	664.9711	617.2400	569.7838	617.2400

The results associated with the system's frequency of operation for the two different ways of modeling the electric power system are reported in Table 3.8. As expected, the proposed and conventional approaches provide the same value of frequency for the base case. When the electric power demanded by the loads is changed from its nominal value, however, the equilibrium point of the electric system is achieved at a frequency value different from 60 Hz by the proposed approach. This is because of the steady-state error of the primary regulation of generators as well as the load dependency on voltage magnitudes and frequency. On the other hand, the frequency remains unaltered from its nominal value when considering conventional generators and load models. This is because the slack generator freely adjusts its active and reactive power injected into the network to whatever it needs to be able to achieve the nodal power balance at 60 Hz. Note that although there exists no slack generator as such in the physical system, its definition is necessary because the way in which the conventional electric power flow problem is formulated. This discrepancy between the real world and that conventional formulation is resolved by using the type 2 generator model.

Table 3.8: Frequency magnitudes

	Base case	**+5%**	**-5%**
Conventional	60	60	60
FR	59.998913	59.859009	60.140178

The results reported in Table 3.8 show that the frequency deviation is approximately ±0.14 Hz in cases where the level of the loadability of the system is increased or decreased, respectively, which leads the system to a new equilibrium point operating at a lower (resp. higher) frequency than nominal. This implies that the regulating generators must increase or decrease their electrical power output in response to the governor's action and their own statism, as reported in Tables 3.7 and 3.9. On the other hand, the variations in demand are completely compensated by the slack generator 1 in the conventional model.

As the active power of the frequency regulating generators increases (resp. decreases), the reactive power limits are reduced (resp. increased). For example, from Table 3.9 when the load is increased, generator 3 is set at its maximum limit of 140.654 MVARs, while a decrement of load results in the maximum reactive power of 238.25 MVARs for this generator. Similarly, generator 2 was set at its maximum value of 125 MVARs when the load is decreased, which did not change its value because of being considered a type 1 generator.

Table 3.9: Reactive power generated [MVARs] - FRPF model

Generator	**Base case**			**+5%**			**-5%**		
bus	Q_G	Q_G^{min}	Q_G^{max}	Q_G	Q_G^{min}	Q_G^{max}	Q_G	Q_G^{min}	Q_G^{max}
1	-30.4124	-185.5670	196.6550	2.3123	-105.3360	113.0500	-49.8343	-240.8360	251.9040
2	86.8263	-100.0000	125.0000	104.8880	-100.0000	125.0000	125.0000	-100.0000	125.0000
3	174.6712	-362.0230	195.4100	140.6540	-265.1670	140.6540	149.3667	-433.4120	238.2550

Lastly, from the Eq. (3.42) and Eq. (3.42), which define the behavior of type 2 load, it can be deduced that if the frequency deviation is negative the load will tend to decrease, and, conversely, if the frequency deviation is positive, the magnitude of the load will increase. Since the loads also depend on the voltage magnitude, however, the increasing (resp. decreasing) of voltage magnitudes produces an increment (resp. decrement) of load regarding the programmed demand values. Hence, the existing relation between variations in frequency and nodal voltage magnitudes will determine if the load demanded at a given node increases or decreases, as reported in Table 3.10.

Table 3.10: Electric power load

Gen.	Base case				+5%				-5%			
Bus	FRPF		Conv.		FRPF		Conv.		FRPF		Conv.	
	$P\,[MW]$	$Q\,[MVARs]$	$P\,[MW]$	$Q\,[MVARs]$	$P\,[MW]$	$Q\,[MVARs]$	$P\,[MW]$	$Q\,[MVARs]$	$P\,[MW]$	$Q\,[MVARs]$	$P\,[MW]$	$Q\,[MVARs]$
1	400.1553	31.0021	400.0000	30.9900	420.1407	32.5535	420.0000	32.5395	379.8462	29.4258	380.0000	29.4405
2	650.3899	105.4132	650.0000	105.3500	682.8935	110.6839	682.5000	110.6175	616.9228	99.9866	617.5000	100.0825
3	400.0000	123.9400	400.0000	123.9400	420.0000	130.1370	420.0000	130.1370	380.0000	117.7430	380.0000	117.7430

3.4 Conclusions

In this chapter, the network models for the steady-state calculation of gas flows and electric power flows were developed for the natural gas and electricity transmission systems. These models were implemented in digital computer programs developed in Python programming language and using object-oriented programming.

Regarding the natural gas system, a new model based on the NFI equations was proposed that unlike a model based on average gas flow magnitude equations implicitly considers the inherent difference between the inlet and outlet gas flow at the pipeline ends for a given instant of time. This difference is due to the physical and operating conditions associated with the natural gas and pipelines. In addition, the model implicitly considers the direction in which the gas circulates through the pipelines and allows knowing how the physical conditions of the gas and the pipelines system (e.g., compressibility, friction and length of the ducts) affect the amount of gas circulating through the gas transmission network. Note that these conditions are irrelevant when the gas flows are modeled by using the AFE model.

Lastly, the proposed model allows analyzing the effect of gravity force and inclination of pipelines on the inlet and outlet gas flows and on the amount of gas that can be stored in pipelines. In this sense, it was shown that the flow that leaves a pipeline can be of greater magnitude than that which enters a pipeline and that it can also circulate from a point of lower pressure to another of higher pressure.

On the other hand, the electricity network model no longer considers either the fixed active power injection into the electricity network or the constant power demands. Within this context, the dependency of electric loads with respect to frequency deviations and voltage magnitudes is fully considered. Furthermore, the primary frequency control of generators is also taken into account for relating frequency deviations to the power generated by those plants. The effect of considering the control characteristics of generators and the dependent modeling of loads on the operation of the electrical system is numerically demonstrated through the power flow analysis of different case studies.

Lastly, a new way to consider reactive power limits as a function of changes in active power delivered by regulating generators was proposed.

Chapter 4

Static power flow analysis of integrated natural gas and electricity networks

4.1 Introduction

Among the different types of primary energies that are used to generate electricity, the amount of natural gas used as an primary energy source for producing electricity has dramatically increased in the last decade. Hence, from the steady-state operational interdependence viewpoint, a natural gas and electric power flow program should offer a very useful tool for system planners and system operators for evaluating how these two energy infrastructures interact between each other.

In this chapter, a unified formulation suitable for the steady-state analysis of natural gas and electric power flows in a single frame of reference is proposed. Unlike other proposals, this approach considers the governor characteristics to perform the primary frequency regulation, the dependency of loads on voltage magnitudes and frequency as well as a gas flow model based on nodal gas flow injections. Lastly, a methodology to preserve frequency within its operational limits is proposed.

4.2 Coupling between natural gas and electricity networks

In order to carry out a unified study of the electricity and natural gas transportation systems, it is necessary to analyze the way in which these systems interact with each other. In this context, the interdependence between the natural gas and electricity networks is provided by the plants that operate with gas turbine-driven generators, where these plants act as energy converters. This coupling is mathematically formulated by the function associated with the fuel consumption rate, which is referred to as the "heat rate curve." This function defines the relationship between the active electrical power at the plant output and the amount of fuel required to supply the plant for producing that electrical power.

The heat rate curve implicitly considers the efficiency of the energy conversion process of natural gas that is demanded through the k-th node of the gas network to the electrical output power injected into the i-th bus of the electrical power system transmission network. This relationship is given by

$$q_{req_k/P_{G_i}} = \frac{F\left(P_{G_i}\right)}{GHV} = \frac{a + bP_{G_i} + cP_{g_i}^2}{GHV}. \tag{4.1}$$

On the other hand, the coupling of the gas system to the electrical system is provided by the electrical power demanded by the n-th compression station connected to the i-th bus of the electrical network. Assuming that the compressor station connected between nodes "k" and "m" is driven by electric motors, the conversion of mechanical energy to electrical power is given by [Menon05],

$$\mathrm{P}_{L_i/comp_{km}} = \mathrm{BHP}_{km} \frac{745.7}{P_{base} \times 10^6} \left[p.u.\right]. \tag{4.2}$$

Finally, the gas demanded by gas-fired generating units is limited to the amount of gas available and/or to the amount of gas that the gas system is capable of delivering at a given time. Therefore, the active power that the unit can deliver to the electrical system is also restricted by the availability of fuel. Therefore, to consider this feature within the global model proposed, the constraint (4.3) is added. This expression states that the sum of the independent gas load and the gas required by i-th generator connected to k-th node must be higher and lower, respectively, than a minimum and maximum gas flow limit imposed

by the gas network. Note that implicitly this constraint also limits the active power that can be delivered by the generator to the electric power system:

$$q_{gl_k}^{min} < q_{gl_k} + q_{req_k/P_{G_i}} < q_{gl_k}^{\max}. \tag{4.3}$$

4.3 Integrated natural gas and power flow methodology

The natural gas and electric power flows problem is formulated in a unified framework of solution by means of two sets of nodal mismatch equations associated with the gas and electricity networks, respectively, which are interrelated through Eq. (4.1), Eq. (4.2) and constraint (4.3). Hence, the set of electric power flow mismatch equations at i-th bus of the electrical network is given by (4.4) and (4.5):

$$\Delta P_i = \sum P_{G_i} - \sum P_{L_i} - \sum_{j \in i} P_{ij}^{cal} - \sum_{k \in i} \mathrm{P}_{L_i/comp_{km}} = 0, \quad \forall i \in N_e, \tag{4.4}$$

$$\Delta Q_i = \sum Q_{G_i} - \sum Q_{L_i} - \sum_{j \in i} Q_{ij}^{cal} = 0, \quad \forall i \in N_e. \tag{4.5}$$

On the other hand, from the NFI model developed in the previous chapter, the natural gas flow mismatch equations at the k-th node of the gas infrastructure are given by

$$\begin{aligned} \Delta q_k = & \sum_{m \in k} q_{km}^{iny} + \sum_{comp \in k} q_{comp_k} + \sum_{comp \in k} \tau_{comp_k} \\ & - \sum_{gs \in k} q_{gs_k} + \sum_{gl \in k} q_{gl_k} + \sum_{i \in k} q_{req_k/P_{G_i}} = 0, \quad \forall k \in (N_g - 1)\,, \text{ and} \end{aligned} \tag{4.6}$$

$$\Delta CR_{km} = -p_k CR_{km} + p_m = 0, \quad \forall k, m \in Nc. \tag{4.7}$$

Lastly, the set of nonlinear algebraic equations that govern the interdependent steady-state behavior of the natural gas and electric power systems are given by Eqs. (4.4), (4.5), (4.6) and (4.7). The solution of this set of equations results in the operating state of a multi-energy system, which is performed through the Newton-Raphson method to obtain the set of linearized algebraic equations given by (4.8). This system of equations is iteratively solved until a specified mismatch tolerance is satisfied or a maximum number of iterations is reached.

$$\begin{bmatrix} \Delta\theta \\ \Delta v \\ \Delta v_a \\ \Delta v_b \\ \Delta p \\ \Delta q_{comp} \\ \Delta\left(\Delta f\right) \end{bmatrix} = - \begin{bmatrix} \frac{\partial \Delta P}{\partial \theta} & \frac{\partial \Delta P}{\partial v} & 0 & 0 & 0 & \frac{\partial \Delta P}{\partial q_{comp}} & \frac{\partial \Delta P}{\partial \Delta f} \\ \frac{\partial \Delta Q}{\partial \theta} & \frac{\partial \Delta Q}{\partial v} & \frac{\partial \Delta Q}{\partial v_a} & \frac{\partial \Delta Q}{\partial v_b} & 0 & 0 & \frac{\partial \Delta Q}{\partial \Delta f} \\ \frac{\partial \phi_{Q_G}^{min}}{\partial \theta} & \frac{\partial \phi_{Q_G}^{min}}{\partial v} & \frac{\partial \phi_{Q_G}^{min}}{\partial v_a} & \frac{\partial \phi_{Q_G}^{min}}{\partial v_b} & 0 & 0 & 0 \\ \frac{\partial \phi_{Q_G}^{max}}{\partial \theta} & \frac{\partial \phi_{Q_G}^{max}}{\partial v} & \frac{\partial \phi_{Q_G}^{max}}{\partial v_a} & \frac{\partial \phi_{Q_G}^{max}}{\partial v_b} & 0 & 0 & 0 \\ 0 & 0 & 0 & 0 & \frac{\partial \Delta q}{\partial p} & \frac{\partial \Delta q}{\partial q_{comp}} & \frac{\partial \Delta q}{\partial \Delta f} \\ 0 & 0 & 0 & 0 & \frac{\partial \Delta RC}{\partial p} & \frac{\partial \Delta RC}{\partial q_{comp}} & 0 \\ \frac{\partial \Delta P_{G_{ref}}}{\partial \theta} & \frac{\partial \Delta P_{G_{ref}}}{\partial v} & 0 & 0 & 0 & 0 & \frac{\partial \Delta P_{G_{ref}}}{\partial \Delta f} \end{bmatrix}^{-1} \begin{bmatrix} \Delta P \\ \Delta Q \\ \phi_{Q_G}^{\min} \\ \phi_{Q_G}^{\max} \\ \Delta q \\ \Delta RC \\ \Delta P_{G_{ref}} \end{bmatrix} \tag{4.8}$$

Note that in the proposed formulation the generated and demanded electric powers are not constants because of their dependency on the system's frequency and nodal voltage magnitudes. This characteristic is taken into account by incorporating the frequency deviation Δf as a state variable. Similarly, note from (4.8) that the nodal gas flow mismatch equation is a function of the frequency deviation. This is due to the active power generation P_{G_i} of (4.1), which can be a type 1 or type 2 generator.

4.3.1 Case study

To validate the performance of the proposed modeling approach, the Belgian gas pipeline network was interconnected to a 3-bus electrical network, as shown in Figure 4.1. These systems were used and analyzed in the previous chapter.

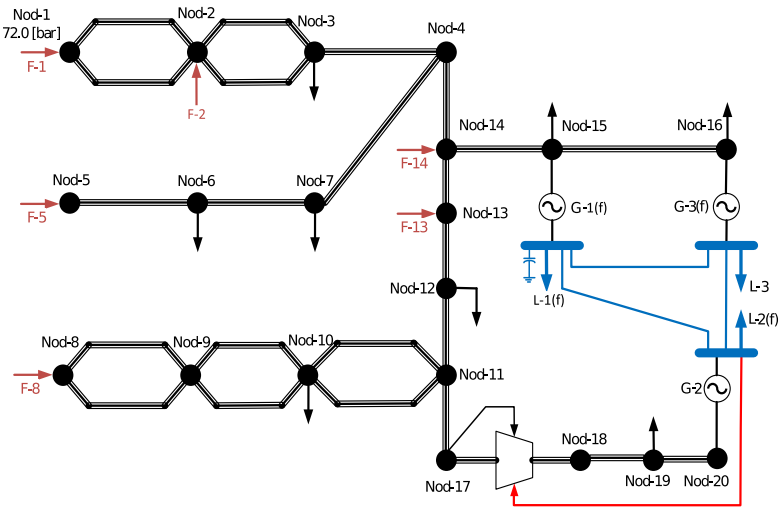

Figure 4.1: The 20-node gas network coupled with a 3-bus electrical network.

In the multi-energy system, the generators correspond to gas-fired generators connected to the natural gas network, but only two of them participate in the primary frequency regulation. Similarly, the compression station is connected to bus 2 of the electrical network. The multi-energy system's data correspond to those used in the previous chapter, which are reported in Appendix B. For practical purposes of this case study, however, the limit $Q_G^{nom,max}$ of generator 3 was changed from 160 MVARs to 360 MVARs.

All scenarios analyzed for the electrical system in the previous chapter are also considered for the analysis of the multi-energy system. In the first case, referred to as the base case, the electric system's loadability corresponds to the nominal values. On the other hand, a decrement and increment of 5% of the nominal power demanded by each load are considered for case studies 2 and 3, respectively. Note that these load changes are performed considering a constant power factor.

Results associated with the three case studies mentioned above are reported in Table 4.1. These results clearly show that for the base and third case studies the magnitudes of active and reactive power supplied by each generator are very similar to the values obtained for the same case studies reported in the previous chapter. In these cases, the magnitudes are only affected by the electrical power demanded by the compressor station.

On the other hand, in the results obtained for the second case study, where demand increases by 5%, the generated electric powers are completely different from those obtained when considering the electrical system uncoupled from the gas infrastructure. This is due to the limit imposed on the demand of natural gas in node 15, which has a maximum value of 407.8×10^3 SCMH. Since the independent gas load at this node has a value of 285×10^3 SCMH, there is only a gas availability of 122.8×10^3 SCMH to supply generator 1. Therefore, according to the generator's heat rate curve, its maximum active power capacity is limited to 492.6185 MW, as reported in Table 4.1. Within this context, when the electrical demand increases, the active power of generator 1 is set at its maximum value such that generator 3 must provide the rest of active power to satisfy the demand. Consequently,

generator 3 reduces its capacity to supply reactive power to the grid such that its maximum limit is violated, and the reactive power is set at 284,577 MVARs, as reported in Table 4.1.

Table 4.1: Results for electric generators

Generator	P_G $[MW]$	P_G^{max} $[MW]$	Q_G $[MVARs]$	Q_G^{min} $[MVARs]$	Q_G^{max} $[MVARs]$	**Gas consumed** $[SCMH] \times 10^3$	**Cost** $[\$/s]$
Base case:	$f = 59.99840\,[Hz]\,, \Delta f = -0.00159\,[Hz]$						
Gen_1	486.8448	492.6185	-30.3183	-185.3400	196.4230	121.3250	1147.062028
Gen_2	350.0000	350.0000	86.5878	-100.0000	125.0000	69.6278	804.5807
Gen_3	617.7789	728.1740	174.8438	-348.0950	412.8550	131.4685	1381.070201
Tot:	1454.6237		231.1133			322.4213	3332.7129
Case -5%	$f = 60.13967\,[Hz]\,, \Delta f = 0.13967\,[Hz]$						
Gen_1	460.6834	492.6185	-49.7898	-240.6630	251.7360	116.3197	1099.7399
Gen_2	350.0000	350.0000	125.0000	-100.0000	125.0000	69.6278	804.5807
Gen_3	569.9526	728.1740	149.3756	-409.1900	476.7120	120.0108	1260.7074
Tot:	1380.6360		224.5858			305.9583	3165.0281
Case +5%	$f = 59.79577\,[Hz]\,, \Delta f = -0.20422\,[Hz]$						
Gen_1	492.6185	492.6185	-141.4042	-170.7330	181.4580	122.4667	1157.8559
Gen_2	350.0000	350.0000	111.9033	-100.0000	125.0000	69.6278	804.5807
Gen_3	686.3788	728.1740	284.5770	-234.1100	284.5770	149.5071	1570.5653
Tot:	1528.9973		255.0760			341.6016	3533.0020

Table 4.2 reports the nodal voltages at generators' nodes. In the second case study, where the load is increased to +5%, there is a violation of gas consumption by generator 1. Hence, generators 1 and 2 are type 1 with the ability to regulate voltage magnitude at their terminals. Note that these voltage magnitudes are closer to the nominal ones. Since only one generator participates in the primary regulation, however, a greater frequency deviation occurs. The opposite occurs for the study case where the load is reduced by -5%. In this case, two of the three generators regulate frequency, and, therefore, there is a greater voltage drop but the frequency deviation is less significant.

Table 4.2: Nodal voltages

Bus	**Base case**		**-5%**		**+5%**	
	v	θ	v	θ	v	θ
1	1.0390	0.0000	0.9500	0.0000	1.0200	0.0000
2	1.0300	-3.1387	0.9519	-3.4589	1.0300	-3.5217
3	1.0517	0.4554	0.9647	0.3867	1.0616	0.5214

From Table 4.1, it is clear that although the gas consumed by generators is consistent with the decrease or increase in the electricity demand, this change is not proportional. Note that for the increment of load there is an increase of approximately 19000 SCMH in the natural gas consumption, while for the case study associated with the reduction in the electric load there is a decrease of approximately 16500 SCMH in the gas demanded by the gas-fired generators. This variation is due to the heat rate curve and the regulation conditions of each generator, as well as the violated gas demand limit. The information mentioned above can also be observed in the gas supplied by node 1 of the gas network, where the variation is approx +27900 SCMH for the +5% case and -23000 SCMH for the -5% case, as reported in Table 4.3.

Table 4.3: Gas supplied by node 1 $[SCMH] \times 10^3$

Base case	**-5%**	**+5%**
840.1744	817.1428	868.0364

Note also that for all case studies the values of gas supplied from node 1 do not have a direct proportional relationship with the total gas demanded by the generators in each case. This is because in the NFI equations the inlet and outlet gas flows in each pipeline depend on the operating conditions and physical properties of the gas and pipelines, unlike the average gas flow equations. Therefore, when demand conditions change, the entire gas transport system is affected, as shown in Tables 4.4 and 4.5.

Table 4.4: Results in the gas pipelines

Pipeline			Base case				+5%				-5%			
#	From	to	q_{km}^{iny}	q_{mk}^{iny}	Δq	LP	q_{km}^{iny}	q_{mk}^{iny}	Δq	LP	q_{km}^{iny}	q_{mk}^{iny}	Δq	LP
			$[SCMH] \times 10^3$	$[SCMH] \times 10^3$	$[SCMH] \times 10^3$	SCM	$[SCMH] \times 10^3$	$[SCMH] \times 10^3$	$[SCMH] \times 10^3$	SCM	$[SCMH] \times 10^3$	$[SCMH] \times 10^3$	$[SCMH] \times 10^3$	SCM
1	1	2	420.0872	419.7971	0.2901	0.2329	434.0182	433.6985	0.3197	0.2329	408.5714	408.3043	0.2670	0.2329
2	1	2	420.0872	419.7971	0.2901	0.2329	434.0182	433.6985	0.3197	0.2329	408.5714	408.3043	0.2670	0.2329
3	2	3	594.7971	593.5669	1.2302	0.3483	608.6985	607.3803	1.3182	0.3483	583.3043	582.1439	1.1604	0.3484
4	2	3	594.7971	593.5669	1.2302	0.3483	608.6985	607.3803	1.3182	0.3483	583.3043	582.1439	1.1604	0.3484
5	3	4	1023.8839	996.7077	27.1762	1.4670	1051.5106	1022.0695	29.4412	1.4645	1001.0378	975.6438	25.3940	1.4691
6	5	6	117.2797	116.6333	0.6464	1.0157	117.2797	116.6300	0.6497	1.0122	117.2797	116.6359	0.6438	1.0184
7	6	7	-51.4501	-51.4888	0.0388	0.6817	-51.4533	-51.4923	0.0390	0.6794	-51.4474	-51.4860	0.0386	0.6836
8	7	4	-270.4888	-273.9793	3.4905	0.4528	-270.4923	-274.0008	3.5085	0.4513	-270.4860	-273.9620	3.4760	0.4540
9	4	14	722.7285	700.7301	21.9984	2.9295	748.0686	723.5624	24.5062	2.9132	701.6819	681.6231	20.0588	2.9426
10	8	9	817.7325	814.9914	2.7411	0.2836	817.7325	814.9623	2.7702	0.2816	817.7325	815.0145	2.7181	0.2852
11	8	9	99.4341	99.1008	0.3333	0.0560	99.4341	99.0973	0.3369	0.0556	99.4341	99.1036	0.3305	0.0563
12	9	10	814.9938	804.0304	10.9634	1.1154	814.9647	803.8843	11.0804	1.1073	815.0169	804.1460	10.8708	1.1220
13	9	10	99.0984	97.7653	1.3331	0.2203	99.0949	97.7475	1.3473	0.2187	99.1013	97.7794	1.3218	0.2216
14	10	11	567.6574	562.8120	4.8454	1.3637	567.5113	562.6150	4.8963	1.3534	567.7729	562.9679	4.8051	1.3719
15	10	11	68.9301	68.3417	0.5884	0.2693	68.9122	68.3177	0.5945	0.2673	68.9442	68.3607	0.5835	0.2709
16	11	12	534.7800	527.7890	6.9910	2.2418	534.0784	527.0337	7.0447	2.2245	535.3198	528.3721	6.9477	2.2558
17	12	13	439.4557	435.5978	3.8579	2.0886	438.7004	434.8160	3.8844	2.0720	440.0388	436.2025	3.8363	2.1019
18	13	14	485.5978	484.9309	0.6669	0.2584	484.8160	484.1441	0.6719	0.2563	486.2025	485.5396	0.6629	0.2601
19	14	15	1225.6610	1204.3538	21.3072	0.5072	1247.7066	1224.9521	22.7545	0.5027	1207.1627	1187.0033	20.1594	0.5109
20	15	16	797.6954	782.1351	15.5603	1.2218	817.1521	800.1738	16.9783	1.2084	785.3503	770.6774	14.6728	1.2324
21	11	17	96.3737	95.6855	0.6881	0.1113	96.8543	96.1478	0.7065	0.1105	96.0088	95.3346	0.6741	0.1120
22	18	19	95.6039	79.5629	16.0410	0.6606	96.0656	79.5827	16.4829	0.6529	95.2535	79.5479	15.7057	0.6668
23	19	20	70.3129	69.6278	0.6851	0.0326	70.3327	69.6278	0.7049	0.0321	70.2979	69.6278	0.6701	0.0331
LP_{Tot}						18.1397055				18.0258138				18.231208

The results of gas flows reported in Table 4.4 clearly show that the gas flow through pipelines changes according to gas demanded by generators 1 and 3, from which the active power required to achieve the frequency regulation is generated. These changes in gas flows are more noticeable through the trajectory of pipelines 1-2, 2-3, 3-4, 4-14, 14-15 and 15-16, which contain three gas sources that supply the gas demanded by those generators, as shown in Figure 4.1.

On the other hand, from Table 4.4 it is clear that when the electrical load increases, not only the gas flows that circulate through the pipes increase but also the difference between the inlet and outlet gas flow at each pipeline's ends. Furthermore, because of the increased demand for natural gas, there is a higher pressure drop in the pipelines, and the compressibility state of gas decreases. Consequently the gas begins to expand slightly, so the pipeline linepack also decreases. On the other hand, when the electricity load is shed, the total gas demanded by generators, the magnitude of gas flows and the difference between the inlet and outlet gas flows at each pipeline also decrease. In this case, the pressure drop is smoother so that the compression state of the gas increases, and, therefore, the linepack in the ducts of the system also increases. The above is reported in Tables 4.4, 4.5 and Figures 4.2 and 4.3.

Table 4.5: Gas demanded $[SCMH] \times 10^3$

Node	**Base case**	**-5%**	**+5%**	$q_{gl_k}^{min}$	$q_{gl_k}^{max}$
15	406.6583	401.6531	407.8000	0.0	407.8
16	782.1351	770.6774	800.1738	0.0	1000.0
17	0.0816	0.0811	0.0821	0.0	1.0
20	69.6278	69.6278	69.6278	0.0	90.0

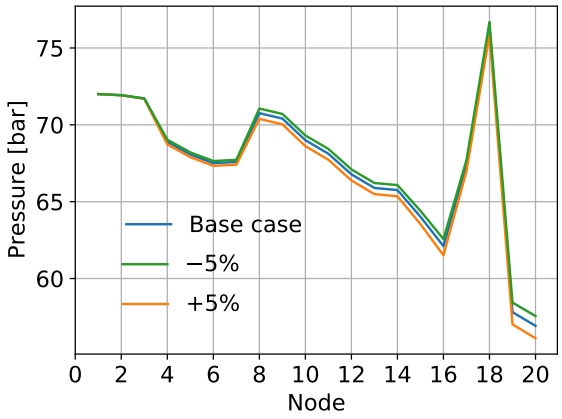

Figure 4.2: Nodal pressures.

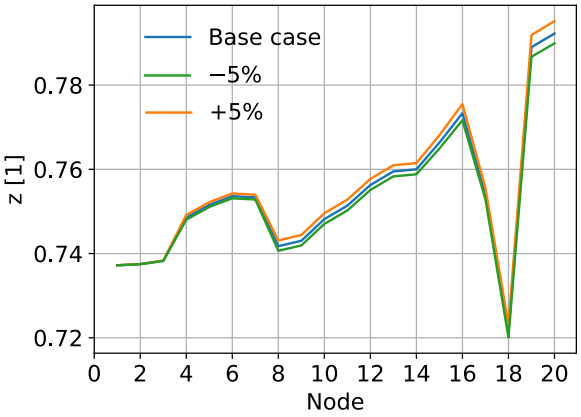

Figure 4.3: Compressibility factor.

Similarly, from Table 4.6, it is clear that the gas flow through the compressor station changes according to electrical demand. This leads to higher (resp. lower) gas consumption and higher (resp. lower) mechanical effort when there is a higher (resp. lower) electric power consumption.

Table 4.6: Results in the compressor station

	Base case	**-5%**	**+5%**
$q_{comp}\,[SCMH] \times 10^3$	95.6039	95.2535	96.0656
$\tau_{comp}\,[SCMH] \times 10^3$	0.0816	0.0811	0.0821
$BHP\,[HP]$	346.0622	343.8595	348.2047
$\mathrm{P}_{L_i/comp_{km}}\,[MW]$	0.2581	0.2564	0.2597

Lastly, note from Table 4.1 that the frequency deviation for the case where the electricity demand is increased by 5 % is 0.20422 Hz. This value is outside the range of operative frequency allowed in grid codes, such as the one associated with the Mexican interconnected power system where the system's frequency deviation from its nominal value must be ±2% Hz; otherwise, the safety and integrity of the electric power system could be compromised.

In this sense, from the operational point of view, setting the frequency value at the violated limit does not represent a feasible solution since any subsequent disturbance could lead the system back into an alert operating mode. Furthermore, the ability of the generators to regulate frequency would be impossible such that the supplied active power would be fixed at a constant value. In this operational scenario, the power imbalance would have to be adjusted by the rest of the variables, such as the voltage phase angle and magnitude, which could also lead to undesirable operating conditions of the electrical system.

4.3.2 Case study 2

A second case study is developed below to analyze and compare the performance of a gas network model based on nodal gas flow injections versus the model based on average gas flows in the event of disturbances or contingencies in the electrical power system.

For this study case, a multi-energy system composed of the IEEE 118-bus electricity network [University of Washington07] and a 15-node gas network [An03] is analyzed. The former consists of 177 transmission lines, 9 transformers, 15 electric motors, 20 synchronous capacitors, 19 generators and 91 loads. In this system, there are 11 power plants contributing to the primary frequency control, as reported in Table 4.7. Note that 8 of these generators are gas-fired power plants directly connected to the gas system, as reported in Figure 4.4 and Table 4.7. Furthermore, 7 electric loads depend on the system's frequency and nodal voltage magnitudes.

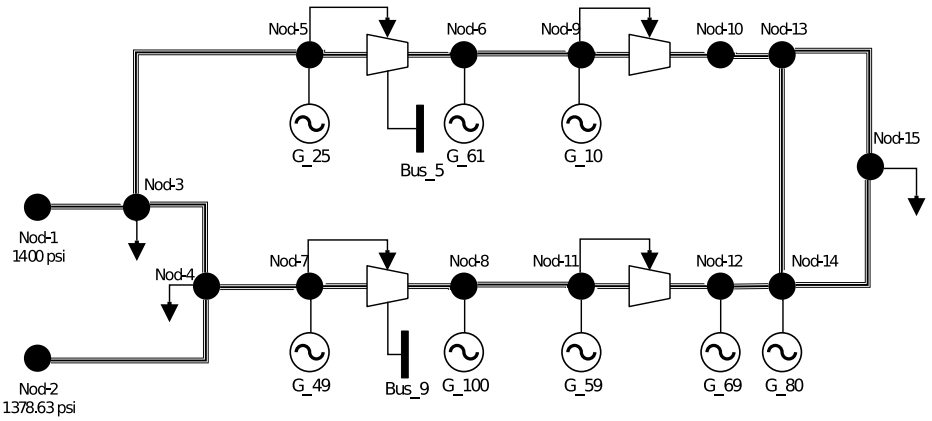

Figure 4.4: The 15-node gas network coupled with the IEEE-118 network.

Table 4.7: Generators in primary frequency regulation

Gen	P_G^{sch}	Q_G^{sch}	P_G^{nom}	$Q_G^{nom,min}$	$Q_G^{nom,max}$	v_{ref}	K_{reg}	**Gas**
	$[MW]$	$[MVARs]$	$[MW]$	$[MVARs]$	$[MVARs]$	$[pu]$	%	**node**
10	436.68	-53.41	450	-147	200	1.05	3.05	9
25	255	51.89	220	-47	140	1.05	2.72	5
26	158.57	-1.261	314	-500	500	1.015	2.42	0
49	286	58.26	204	-85	210	1.025	2.72	7
59	232	47.27	155	-60	180	0.985	3.34	11
61	182.01	-38.13	160	-100	300	0.995	2.34	6
65	262.01	75.79	391	-67	200	1.005	3.18	0
66	431.27	27.9	392	-67	200	1.05	2.18	0
69	585.27	-71.51	516.4	-300	300	1.035	3.05	12
80	403.35	129.24	477	-165	280	1.04	3.05	14
100	289.93	58.87	252	-50	155	1.017	2.72	8

On the other hand, the 15-node gas network is composed of 15 nodes, 12 pipelines, 2 sources, 3 independent loads, and 4 compressor stations driven by gas turbines. Note that two of these compressors are connected to the electrical system through buses 5 and 9, respectively, as shown in Figure 4.4. The network's data are presented in Appendix B.

Three different case studies are analyzed in which the electric system's loadability is changed from its nominal value. The first case study, referred to as the base case, corresponds to the load values reported in the database of the IEEE 118-bus system [University of Washington07].

The other two cases correspond to changes in the total load demanded by the electric system through load disturbances: i) the disconnection of electric loads embedded at nodes 15, 59 and 80, with the complex power demand of $S = 90 + j30$, $277 + j113$ and $130 + j26$, respectively, and ii) the sudden increase in electric loads connected to buses 14 and 85 by 90 and 30 units of power respectively, considering a constant power factor. The former case study is referred to as $\Delta P > 0$, while the latter is referred to as $\Delta P < 0$. The assumed parameters for the loads dependent on the frequency and voltage magnitudes are the following: $K_{pf} = 0.8$, $K_{pp} = 0.5$, $K_{pc} = 0.3$, $K_{pz} = 0.2$,$K_{qf} = 0$, $K_{qp} = 0.5$, $K_{qc} = 0.3$ and $K_{qz} = 0.2$.

The results reported in Table 4.8 show that the difference between the system's frequency obtained by using the AFE and NFI models, respectively, for the three case studies is very small. Note, however, that the system's frequency is slightly smaller when using the NFI model. This is due to the fact that, as reported in Table 4.9, the flow that circulates through the compression stations connected to the electrical network is higher in the NFI model compared with the AFE model, which requires a greater mechanical effort, and therefore increases the demand for electrical energy.

Table 4.8: Frequency magnitudes

	Base case		**$\Delta P > 0$**		**$\Delta P < 0$**	
	f	Δf	f	Δf	f	Δf
AFE	59.997306	-0.002694	60.236408	0.236408	59.872592	-0.127408
NFI	59.997244	-0.002756	60.236391	0.236391	59.872459	-0.127541

The gas demanded by each thermal generator connected to the natural gas network is reported in Table 4.10. As expected, these results change with the operating conditions because of the different gas consumption by compression stations and changes in the active power generated by generators to supply all electric loads and compressors, which is reported in Tables 4.9 and 4.11, respectively.

Table 4.9: Compressor stations' results

From	to	q_{comp} $[SCFH]\times10^6$		τ_{comp} $[SCFH]\times10^6$		BHP $[HP]$		$P_{L_i/comp_{km}}$ $[MW]$	
		AFE	NFI	AFE	NFI	AFE	NFI	AFE	NFI
Base case									
5	6	4.4966	4.7029	0.0063	0.0067	753.8943	807.5922	0.5622	0.6022
7	8	4.5239	4.6441	0.0089	0.0094	1069.5560	1125.0310	0.7976	0.8389
9	10	1.1794	1.2908	0.0003	0.0003	35.6849	40.2672	-	-
11	12	2.9798	2.8911	0.0000	0.0000	0.0000	0.0000	-	-
$\Delta P > 0$									
5	6	3.4737	3.5807	0.0047	0.0049	568.3048	590.9332	0.4238	0.4407
7	8	3.9510	3.9974	0.0076	0.0078	913.8035	934.1235	0.6814	0.6966
9	10	0.8327	0.9063	0.0002	0.0002	24.3410	26.8151	-	-
11	12	2.5666	2.5034	0.0000	0.0000	0.0000	0.0000	-	-
$\Delta P < 0$									
5	6	4.9630	5.2520	0.0070	0.0077	842.7632	925.7160	0.6284	0.6903
7	8	4.7444	4.9362	0.0094	0.0102	1133.0551	1224.5261	0.8449	0.9131
9	10	1.2535	1.3902	0.0003	0.0004	38.5992	44.9197	-	-
11	12	3.1974	3.0982	0.0000	0.0000	0.0000	0.0000	-	-

Table 4.10: Gas demanded $[SCFH]\times10^6$

Node	Base case		$\Delta P > 0$		$\Delta P < 0$		Gen	$q_{gl_k}^{min}$	$q_{gl_k}^{max}$
	AFE	NFI	AFE	NFI	AFE	NFI			
3	3.8380	3.8380	3.8380	3.8380	3.8380	3.8380	-	0	4
4	1.2180	1.2180	1.2180	1.2180	1.2180	1.2180	-	0	2
5	0.6864	0.6868	0.6294	0.6296	0.6874	0.6881	25	0	2
6	0.8468	0.8468	0.6824	0.6824	0.9430	0.9431	61	0	2
7	0.6959	0.6964	0.6365	0.6366	0.6977	0.6984	49	0	2
8	0.7299	0.7299	0.6588	0.6588	0.7299	0.7299	100	0	2
9	2.4704	2.4706	1.9586	1.9587	2.7665	2.7669	10	0	3
11	0.8142	0.8142	0.7256	0.7256	0.8171	0.8171	59	0	2
12	1.4840	1.4840	1.2204	1.2204	1.4840	1.4840	69	0	2
14	2.1742	2.1744	1.6779	1.6779	2.4659	2.4662	80	0	2.5
15	0.5010	0.5010	0.5010	0.5010	0.5010	0.5010	-	0	2

Table 4.11: Total network values

	Base case				**$\Delta P > 0$**				**$\Delta P < 0$**			
	AFE		**NFI**		**AFE**		**NFI**		**AFE**		**NFI**	
	P [MW]	Q [MVARs]	P [MW]	Q [MVARs]	P [MW]	Q [MVARs]	P [MW]	Q [MVARs]	P [MW]	Q [MVARs]	P [MW]	Q [MVARs]
Generation	3797.815	777.027	3797.900	777.051	3294.055	544.962	3294.090	544.979	3929.080	973.577	3929.218	973.629
Load	3665.267	1436.961	3665.348	1436.961	3168.449	1267.752	3168.481	1267.752	3784.604	1556.870	3784.734	1556.870
Losses	132.547	-659.934	132.552	-659.910	125.606	-722.790	125.608	-722.772	144.475	-583.293	144.484	-583.241
LP [MSCF]	1274.1129		1179.9604		1377.5620		1337.1871		1226.0729		1083.0377	
q_{gs} [MSCFH]	15.4588		18.4339		13.7467		15.3721		16.1485		20.1669	
q_{gl} [MSCFH]	15.4588		15.4601		13.7467		13.7471		16.1485		16.1507	

From the results reported in Table 4.12 regarding the gas supplied from the gas sources, it is clear that there is a direct but not proportional relationship between the decrease (resp. increase) in electricity demand and the amount of gas supplied from those sources of natural gas. Furthermore, from Table 4.11 is clear that with the AFE model the balance between the total gas supplied by sources and demanded by loads is completely satisfied, which does not occur with the NFI model. This is because in the latter the gas flows respond to variations in demand in terms of the pressure conditions, compressibility, and the amount of gas stored inside pipelines.

Table 4.12: Gas supplied by sources $[SCFH] \times 10^6$

Source	**Base case**		**$\Delta P > 0$**		**$\Delta P < 0$**	
	AFE	NFI	AFE	NFI	AFE	NFI
1	8.0369	9.5347	7.2087	8.0325	8.3743	10.3932
2	7.4219	8.8993	6.5380	7.3397	7.7741	9.7737

In this context, Figures 4.5, 4.6, 4.7 and 4.8 show that when the electrical load is disconnected, the gas demanded decreases. Therefore, the pressure drop is attenuated, and the state of the compression of gas increases, which in turn increases the linepack. The result of everything mentioned above is that the difference between the inlet and outlet gas flow of each pipeline is reduced. On the other hand, when the electricity demand increases, the gas demand increases so that part of the stored gas emerges, and the gas expands within the pipeline. The above increases the difference between the inlet and outlet gas flow at each duct, and therefore the pressure drop is greater.

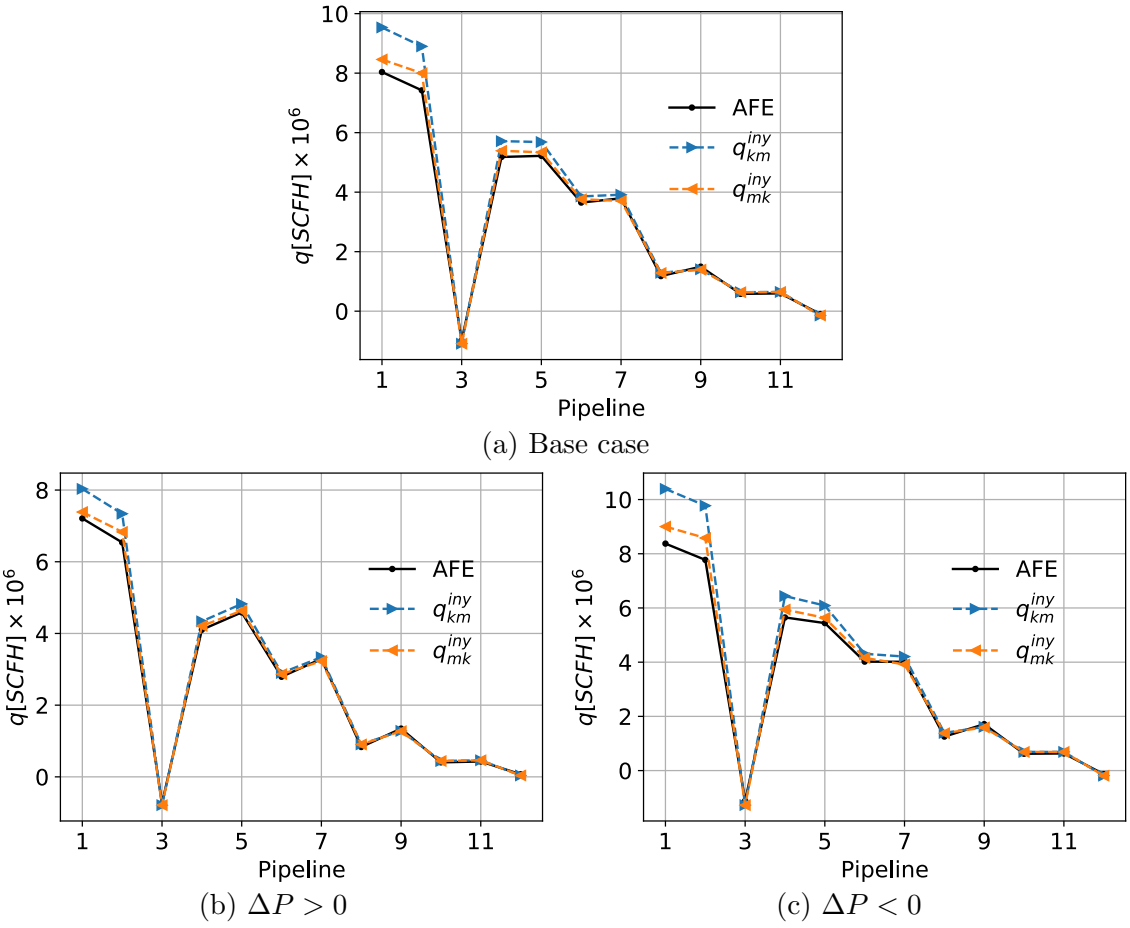

(a) Base case

(b) $\Delta P > 0$

(c) $\Delta P < 0$

Figure 4.5: Gas flows in the pipelines.

From the results associated with all the case studies, note that as the gas demand increases, the magnitudes of nodal pressures, linepack, compressibility and gas flows obtained with the AFE and NFI models are increasingly different from each other. The opposite applies, when the gas demand is low. Therefore, it can be concluded that the smaller the pressure drops are, the smaller the difference between the inlet and outlet gas flows in the pipelines, with the use of a model based on average gas flow magnitudes only justifiable under this condition.

Lastly, small pressure drops are achieved by operating the natural gas transportation system at excessively high pressures or at low demands in proportion to the system gas flow, which is not necessarily a feasible solution from an operational and/or economic point of view.

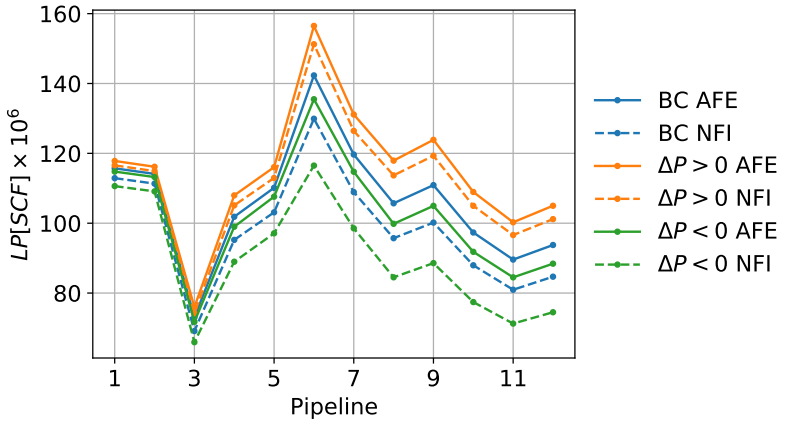

Figure 4.6: Linepack in the pipelines.

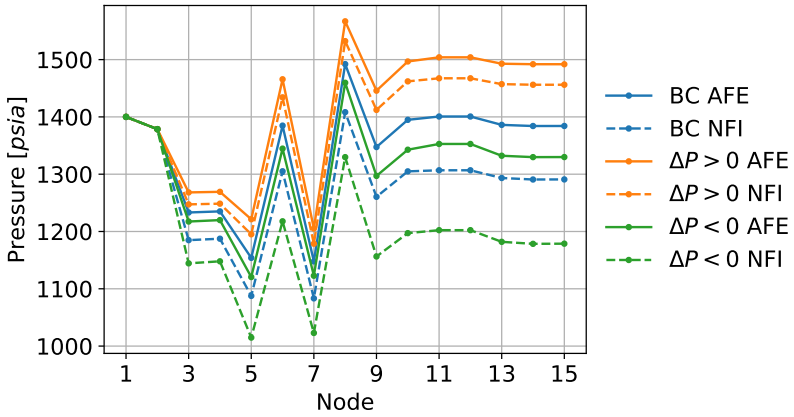

Figure 4.7: Nodal pressures.

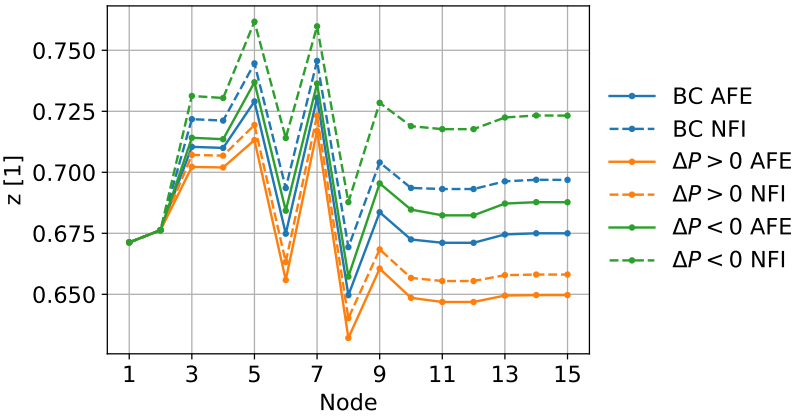

Figure 4.8: Nodal compressibility factor.

4.4 Preventive control of electric frequency methodology

In practice, from the steady-state operational interdependence viewpoint, the demand for electrical energy fluctuates over time; therefore, several generators must continuously modify their active power outputs to reduce frequency deviations caused by imbalances between generation and demand. In other words, the generators must adjust the active power output according to the static response of their prime motors and the frequency deviation when demand variations occur in the electrical system.

Hence, the consideration of these characteristics permits a better representation of the interdependencies between interconnected natural gas and electricity networks, which was demonstrated in the previous section. In the event of a critical disturbance, however, the primary regulation of active power starting from a specified dispatch of generation may not be sufficient for keeping the system frequency within its operating range, and, therefore, a feasible solution cannot be obtained.

To overcome this drawback, a control action to obtain a gas and power flow solution where the electrical frequency is within limits is proposed below. The proposal consists of sequentially solving two interconnected subproblems: a gas and power flow problem as well as an economic dispatch problem. First, the natural gas and power flow problem is solved considering the primary regulation of generators. If the equilibrium point of the multi-energy system is declared unfeasible because the steady-state error of the frequency deviation is outside its normal operating range, an economic dispatch study is carried out to obtain a new dispatch of active powers $P_{G_i}^{sch}$ in those generators that participate in frequency regulation. With the new set of $P_{G_i}^{sch}$ a study of conventional power flows is performed to obtain the new scheduling reactive powers $Q_{G_i}^{sch}$ of these generators. Lastly, from this new set of $P_{G_i}^{sch}$ and $Q_{G_i}^{sch}$, as well as the corresponding adjustment to its operating limits, the gas and power flow problem with primary regulation is newly solved for obtaining a feasible equilibrium point for the critical disturbance. The connection between both problems is given by the active power balance equation in the electricity system.

The proposed control scheme is reported in Figure 4.9 and Algorithm 1.

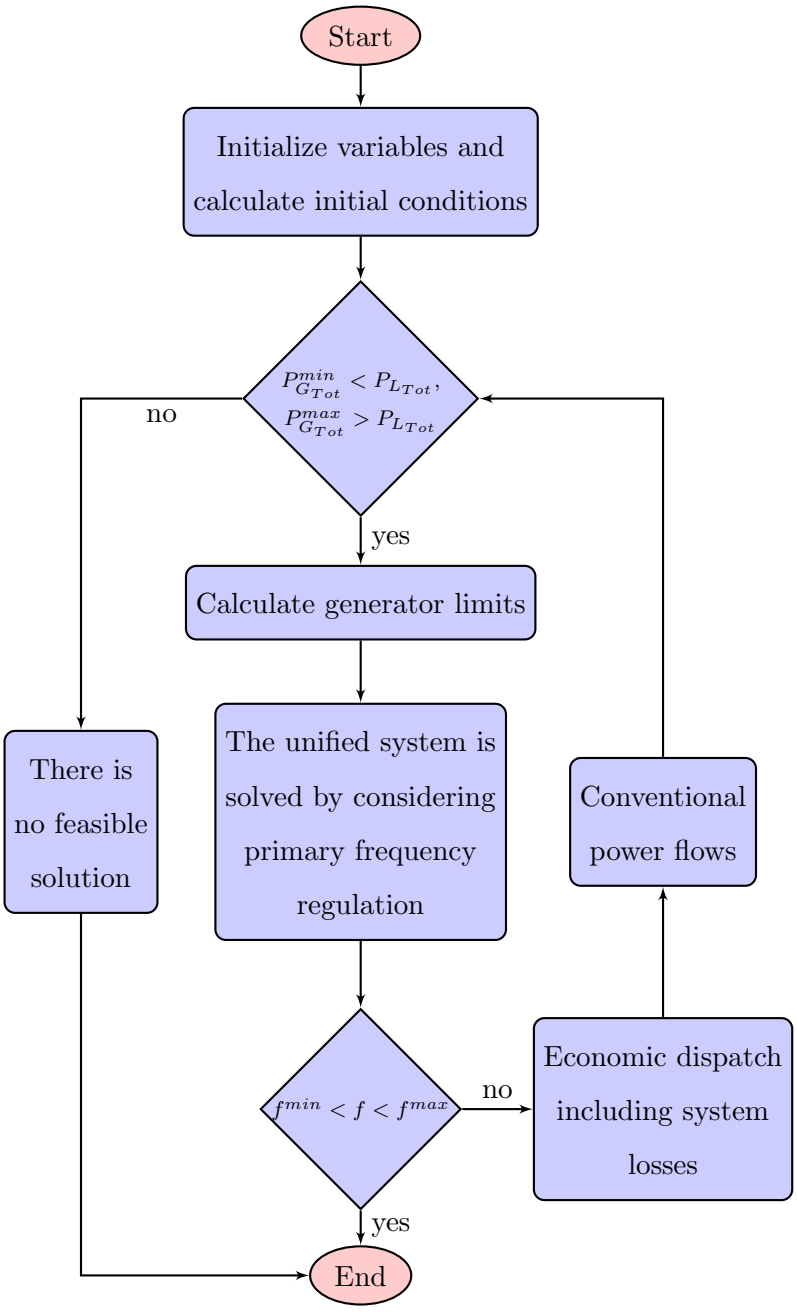

Figure 4.9: Flow chart of the implemented algorithm.

Algorithm 1 Proposed control action to limit frequency deviation.

Initialize state variables $p, q, q_{comp}, v, \theta$.
Initialize $P_{G_i} = P_{G_i}^{sch}$.
Calculate $P_{G_i}^{max}$.
Calculate $P_{G_{Tot}}^{max} = \sum P_{G_i}^{max}, P_{G_{Tot}}^{min} = \sum P_{G_i}^{min}$ and
$P_{L_{Tot}} = \sum P_{L_i}$.
if $\left(P_{G_{Tot}}^{min} < P_{L_{Tot}} < P_{G_{Tot}}^{max}\right)$ **then**
  $flag = 0, it = 0$
  while $(it < it_{max}$ & flag$== 0)$ **do**
    Solve gas-electric flows (4.8).
    if $\left(P_{G_i}^{new} < P_{G_i}^{min} \| P_{G_i}^{new} > P_{G_i}^{max}\right)$ **then**
      $P_{G_i}^{new} = P_G^{lim} \rightarrow \text{Gen}_i$ stops regulating frequency.
    end if
    Calculate $Q_{G_i}^{min}\left(P_{G_i}^{new}\right), Q_{G_i}^{max}\left(P_{G_i}^{new}\right)$
    if $error > tol$ **then**
      $it+ = 1$
      $flag1 = 0$
    else
      $flag1 = 1$
      if $f^{min} < f_{sist} < f^{max}$ **then**
        $flag2 = 1$
      else
        Calculate $P_{L_{Tot}} = \sum P_{G_i}(f)$
        Economic dispatch of the generators that regulate f to satisfy $P_{L_{Tot}}$
        return new $P_{G_i}^{sch}$.
        Conventional power flows with new $P_{G_i}^{sch}$.
        return new $Q_{G_i}^{sch}$.
        $flag2 = 0$
      end if
    end if
    $flag = flag1 * flag2$
  end while
  print Solution
else
  The problem has no feasible solution.
end if

An "unfeasible solution" is possible in the context of the algorithm described when the total system demand is less than the minimum condition of power generated by all the units or greater to the sum of the maximum power that each generator can contribute to the system. Hence, under these two operational conditions it is impossible to satisfy the power balance. These scenarios, however, are outside the scope of this work.

On the other hand, if the solution of the integrated gas and power flow problem indicates that $f^{min} < f < f^{max}$, the results correspond to the feasible operation of the multi-energy system. If the frequency deviation Δf is outside the established limits (for this work $\pm 0.2Hz$), however, the economic dispatch of the generators participating in the frequency regulation is performed by solving the Lagrangian function (4.9) for $P_{G_i}^{sch}$:

$$C = \sum_{i=1}^{nG_{Type2}} \left(a + bP_{G_i}^{sch} + c\left(P_{G_i}^{sch}\right)^2\right) + \mu \left[\sum_{i=1}^{nG_{Type2}} P_{G_i}^{sch} + \sum_{i=1}^{nG_{Type1}} P_{G_i} - \sum_{i=1}^{nL} P_{L_i} - P_{loss_{Tot}}\right]. \quad (4.9)$$

In this case, $P_{loss_{Tot}}$ corresponds to the total electric losses obtained from the solution of gas-electricity flows with frequency regulation. Based on the new values of $P_{G_i}^{sch}$, a conventional electric power flow study is carried out to obtain the new value of $Q_{G_i}^{sch}$. Lastly, the new set of $P_{G_i}^{sch}$ and $Q_{G_i}^{sch}$ is used to solve the gas and power flow problem with frequency regulation to obtain a new operating state of the multi-energy system. This process can be done as many times as necessary to bring the frequency as close to 60 Hz as desired.

4.4.1 Case study

The performance of the proposed control scheme is evaluated, taking up the case study with the 5% increase in electrical demand from Section 4.3.1. In this case, the resulting system's frequency has a deviation greater than 0.2 Hz. These results are then compared with those obtained from the model that includes the frequency control action referred to as case +5% with FC. In this case, the solution of the economic dispatch and the conventional power flows reported in Table 4.13 shows that generator 1 is rescheduled at its maximum value, so generator 3 is rescheduled at a value of 686.379 MW. Based on these new operating conditions, the reactive powers scheduling their limits are calculated.

Table 4.13: Economic dispatch and conventional flows' results

Generator	P_G^{sch} $[MW]$	$P_G^{sch,new}$ $[MW]$	P_G^{max} $[MVARs]$	Q_G^{sch} $[MVARs]$	$Q_G^{sch,new}$ $[MVARs]$	Q_G^{min} $[MVARs]$	Q_G^{max} $[MVARs]$	**Cost** $[\$/s]$	$P_{L_{Tot}}$ $[MW]$
Gen_1	486.550	492.619	492.619	-30.614	-101.117	-170.733	181.458	1157.856	
Gen_2	350.000	350.000	350.000	87.278	125.000	-100.000	125.000	804.581	
Gen_3	617.240	686.379	728.174	174.302	228.849	-234.110	284.577	1570.565	
Totales	1453.790	1528.997	1570.793	230.966	252.732	-504.843	591.035	3533.002	1528.997

The problem of gas and electricity flows with frequency regulation is solved considering the new power schedules, with the results of electricity generation reported in Table 4.14. Note that the gas consumption by generators was reduced, which results in a reduction of the gas demanded to the gas network and, therefore, in the gas supplied by the source node; see Tables 4.15 and 4.16. Similarly, the generation costs were reduced. Lastly, generator 1 no longer violates its maximum active power limit, and, therefore, the gas system can fully meet the gas demand, as reported in Table 4.15.

Table 4.14: Results for electric generators

Generator	P_G $[MW]$	P_G^{max} $[MW]$	Q_G $[MVARs]$	Q_G^{min} $[MVARs]$	Q_G^{max} $[MVARs]$	**Gas consumed** $[SCMH] \times 10^3$	**Cost** $[\$/s]$
Case +5%	$f = 59.79577\,[Hz]\,, \Delta f = -0.20422\,[Hz]$						
Gen_1	492.6185	492.6185	-141.4042	-170.7330	181.4580	122.4667	1157.8559
Gen_2	350.0000	350.0000	111.9033	-100.0000	125.0000	69.6278	804.5807
Gen_3	686.3788	728.1740	284.5770	-234.1100	284.5770	149.5071	1570.5653
Tot:	1528.9973		255.0760			341.6016	3533.0020
Case +5% with FC	$f = 60.00089\,[Hz]\,, \Delta f = 0.00089\,[Hz]$						
Gen_1	492.4532	492.6185	-101.2817	-171.1680	181.9060	122.4337986	1157.545145
Gen_2	350.0000	350.0000	125.0000	-100.0000	125.0000	69.6278237	804.5807
Gen_3	686.0766	728.1740	228.5478	-234.7340	285.3050	149.4235245	1569.687069
Tot:	1528.5298		252.2661			341.4851	3531.8129

Table 4.15: Gas demanded $[SCMH] \times 10^3$

Node	**+5%**	**+5% with FC**
15	407.8000	407.7671
16	800.1738	800.0902
17	0.0821	0.0821
20	69.6278	69.6278

Table 4.16: Gas supplied by node 1 $[SCMH] \times 10^3$

+5%	**+5% with FC**
868.0364	867.8672

Note that the values reported in Table 4.14 are not equal to those obtained with the economic dispatch and conventional power flows, which are reported in Table 4.13. Note, however, that the new power rescheduling of the units obtained by the multi-energy gas and power flow analysis considering frequency regulation is sufficient for reducing the frequency deviation from 0.20422 to 0.00089 Hz, as reported in the Table 4.14.

Lastly, the frequency control produces a new operating condition in which the nodal voltage magnitudes remain close to their nominal values: 1.02, 1.03, and 1.05, respectively, and keeping the magnitudes of the electrical loads nearly constant. The information mentioned above is numerically reported in Tables 4.17 and 4.18.

Table 4.17: Nodal voltages

Bus	**+5%**		**+5% with FC**	
	v	θ	v	θ
1	1.0200	0.0000	1.0234	0.0000
2	1.0300	-3.5217	1.0293	-3.4835
3	1.0616	0.5214	1.0533	0.6672

Table 4.18: Electric power demands

Bus	**+5%**		**+5% with FC**	
	$P\,[MW]$	$Q\,[MVARs]$	$P\,[MW]$	$Q\,[MVARs]$
1	420.0268	32.5460	420.0986	32.5471
2	683.1459	110.6839	683.1596	110.6823
3	420.0000	130.1370	420.0000	130.1370

In Table 4.19 a comparison of gas flows is reported, where it is clear that the gas flows and the difference between the inlet and outlet gas flows in each pipeline were reduced.

Table 4.19: Results in the gas pipelines

Pipeline			**+5%**				**+5% with FC**			
#	**From**	**to**	$\boldsymbol{q_{km}^{iny}}$	$\boldsymbol{q_{mk}^{iny}}$	$\boldsymbol{\Delta q}$	$\boldsymbol{LP}$	$\boldsymbol{q_{km}^{iny}}$	$\boldsymbol{q_{mk}^{iny}}$	$\boldsymbol{\Delta q}$	$\boldsymbol{LP}$
			$[SCMH]\times10^3$	$[SCMH]\times10^3$	$[SCMH]\times10^3$	SCM	$[SCMH]\times10^3$	$[SCMH]\times10^3$	$[SCMH]\times10^3$	SCM
1	2	1	434.0182	433.6985	0.3197	0.2329	433.9336	433.6141	0.3195	0.2329
1	2	2	434.0182	433.6985	0.3197	0.2329	433.9336	433.6141	0.3195	0.2329
2	3	3	608.6985	607.3803	1.3182	0.3483	608.6141	607.2965	1.3176	0.3483
2	3	4	608.6985	607.3803	1.3182	0.3483	608.6141	607.2965	1.3176	0.3483
3	4	5	1051.5106	1022.0695	29.4412	1.4645	1051.3430	1021.9159	29.4271	1.4645
5	6	6	117.2797	116.6300	0.6497	1.0122	117.2797	116.6300	0.6497	1.0122
6	7	7	-51.4533	-51.4923	0.0390	0.6794	-51.4533	-51.4923	0.0390	0.6794
7	4	8	-270.4923	-274.0008	3.5085	0.4513	-270.4923	-274.0007	3.5084	0.4513
4	14	9	748.0686	723.5624	24.5062	2.9132	747.9152	723.4248	24.4904	2.9133
8	9	10	817.7325	814.9623	2.7702	0.2816	817.7325	814.9625	2.7700	0.2816
8	9	11	99.4341	99.0973	0.3369	0.0556	99.4341	99.0973	0.3368	0.0556
9	10	12	814.9647	803.8843	11.0804	1.1073	814.9649	803.8852	11.0797	1.1073
9	10	13	99.0949	97.7475	1.3473	0.2187	99.0949	97.7477	1.3472	0.2187
10	11	14	567.5113	562.6150	4.8963	1.3534	567.5122	562.6162	4.8960	1.3534
10	11	15	68.9122	68.3177	0.5945	0.2673	68.9123	68.3178	0.5945	0.2673
11	12	16	534.0784	527.0337	7.0447	2.2245	534.0829	527.0385	7.0443	2.2246
12	13	17	438.7004	434.8160	3.8844	2.0720	438.7052	434.8209	3.8843	2.0721
13	14	18	484.8160	484.1441	0.6719	0.2563	484.8209	484.1491	0.6719	0.2563
14	15	19	1247.7066	1224.9521	22.7545	0.5027	1247.5739	1224.8284	22.7455	0.5028
15	16	20	817.1521	800.1738	16.9783	1.2084	817.0613	800.0902	16.9711	1.2084
11	17	21	96.8543	96.1478	0.7065	0.1105	96.8512	96.1448	0.7064	0.1105
18	19	22	96.0656	79.5827	16.4829	0.6529	96.0627	79.5826	16.4801	0.6530
19	20	23	70.3327	69.6278	0.7049	0.0321	70.3326	69.6278	0.7048	0.0321
LP_{Tot}						18.0258138				18.0265135

Additionally, from the results reported in Table 4.19, it is observed that when generators are rescheduled by using the proposed approach the linepack has its greater magnitude compared with the case where the primary regulation is performed without

enforcing frequency limits. Similarly, by reducing the demand for gas, the mechanical power of the compressor was also slightly reduced and thus the demand for electricity, as shown in Table 4.20. Hence, when applying the proposed preventive control action to enforce the steady-state error of frequency deviation within the established limits, there is a more efficient use of the gas demanded by generators. This also produces a lower cost of operation, as reported in the Table 4.14.

Table 4.20: Compressor stations' results

	+5%	**+5% with FC**
$q_{comp}\,[SCMH] \times 10^3$	96.0656	96.0627
$\tau_{comp}\,[SCMH] \times 10^3$	0.0821	0.0821
$BHP\,[HP]$	348.2047	348.1941
$\mathrm{P}_{L_i/comp_{km}}\,[MW]$	0.2597	0.2596

4.4.2 Case study 2

As a second case study, the multi-energy system used in case study 4.3.2 composed of the IEEE 118-bus electricity network and the 15-node gas network is used. The data of 11 power plants that contribute to the primary frequency regulation are reported in Table 4.21, where 8 of these generators are gas-fired power plants connected to the gas system as reported in Figure 4.10. For the purposes of this case study, the pressures at the source nodes of the gas transport system were reduced by 100 psia, as reported in Figure 4.10. Furthermore, the maximum gas availability in nodes 9 and 14 were reduced to 2.5 and 2.2 MSCFH, respectively.

The same three case studies are reported in which the electric system's loadability is changed from its nominal value. Consider that the initial condition of active and reactive power P_G^{sch} and Q_G^{sch} reported in Table 4.21 for each generator correspond to the economic solution obtained from an economic pre-dispatch that satisfies the nominal load values reported in the IEEE 118-bus system database [University of Washington07]. Hence, for the base case, the frequency deviation $\Delta f \approx 0$, as reported in Table 4.22.

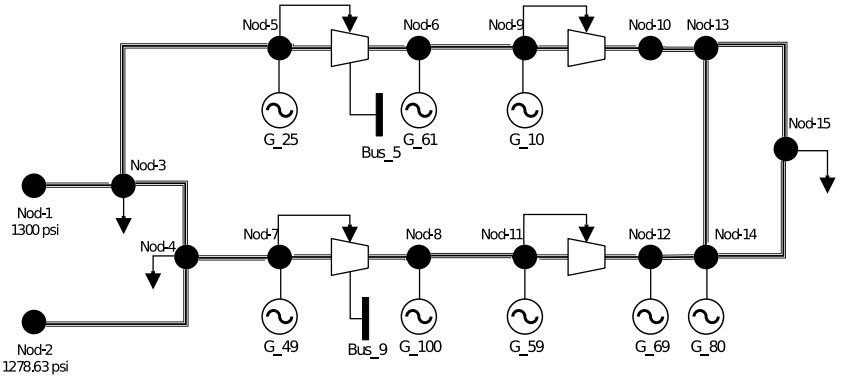

Figure 4.10: The 15-node gas network coupled with the IEEE-118 network.

Table 4.21: Generators in primary frequency regulation

Gen	P_G^{sch}	Q_G^{sch}	P_G^{nom}	$Q_G^{nom,min}$	$Q_G^{nom,max}$	v_{ref}	K_{reg}	**Gas**	**Heat rate**			C
	$[MW]$	$[MVARs]$	$[MW]$	$[MVARs]$	$[MVARs]$	$[pu]$	%	**node**	a	b	c	\$/BTU
10	436.68	-53.41	450	-147	200	1.05	3.05	9	120000	6	3	1
25	255	51.89	220	-47	140	1.05	2.72	5	125000	6	1	1
26	158.57	-1.261	314	-500	500	1.015	2.42	0	125000	10	7	1
49	286	58.26	204	-85	210	1.025	2.72	7	110000	6	1	1
59	232	47.27	155	-60	180	0.985	3.34	11	65000	12	3	1
61	182.01	-38.13	160	-100	300	0.995	2.34	6	70000	14	5	1
65	262.01	75.79	391	-67	200	1.005	3.18	0	225000	6	5	1
66	431.27	27.9	392	-67	200	1.05	2.18	0	255000	8	1	1
69	585.27	-71.51	516.4	-300	300	1.035	3.05	12	70000	10	1	1
80	403.35	129.24	477	-165	280	1.04	3.05	14	120000	8	3	1
100	289.93	58.87	252	-50	155	1.017	2.72	8	120000	6	1	1

Table 4.22: Frequency magnitudes

	$\Delta P \approx 0$		$\Delta P > 0$		$\Delta P < 0$	
	f	Δf	f	Δf	f	Δf
FRPF	59.997145	-0.002854	60.236361	0.236361	59.767402	-0.232597
FRPF with FC	-	-	59.996526	-0.003473	59.995589	-0.004410

Regarding the electric power system, the results reported in Table 4.22 show that in the base case the equilibrium point of the integrated energy system is achieved at a value of frequency very close to its nominal value. For the other two case studies, the system's frequency is outside its operating ranges, however, when the primary regulation is applied without using the proposed control scheme. On the other hand, when applying the proposed

approach, the nominal active power is rescheduled to perform a primary regulation that steers the system's frequency within limits. The results of this rescheduling are reported in Tables 4.23 and 4.24 for the case studies $\Delta P > 0$ and $\Delta P < 0$, respectively.

Table 4.23: Economic dispatch and conventional flows results for the $\Delta P > 0$ case

Generator	$\boldsymbol{P_G^{sch}}$	$\boldsymbol{P_G^{sch,new}}$	$\boldsymbol{P_G^{max}}$	$\boldsymbol{Q_G^{sch}}$	$\boldsymbol{Q_G^{sch,new}}$	$\boldsymbol{Q_G^{min}}$	$\boldsymbol{Q_G^{max}}$	**Cost**
	$[MW]$	$[MW]$	$[MVARs]$	$[MVARs]$	$[MVARs]$	$[MVARs]$	$[MVARs]$	$[\$/s]$
Gen_10	436.68	305.73	440.54	-53.41	-71.13	-308.32	386.04	402252.94
Gen_25	255.00	255.55	255.55	51.89	51.89	-16.81	51.89	191840.65
Gen_26	158.57	102.46	578.61	-1.26	-1.92	-581.46	581.46	199506.81
Gen_49	286.00	286.92	286.92	58.26	58.26	-21.83	58.26	194042.87
Gen_59	232.00	205.73	232.79	47.27	-37.25	-37.25	118.74	194447.36
Gen_61	182.01	103.44	312.89	-38.13	-59.50	-114.64	323.88	124947.30
Gen_65	262.01	183.44	430.40	75.79	80.22	-154.36	399.04	394351.76
Gen_66	431.27	431.27	431.27	27.90	33.92	-28.67	87.58	444444.84
Gen_69	585.27	585.27	585.27	-71.51	-71.31	-118.85	118.85	418397.21
Gen_80	403.35	272.40	407.03	129.24	102.53	-316.88	481.38	344784.41
Gen_100	289.93	289.94	289.94	58.87	58.87	-18.37	58.87	205802.50

Table 4.24: Economic dispatch and conventional flows results for the $\Delta P < 0$ case

Generator	$\boldsymbol{P_G^{sch}}$	$\boldsymbol{P_G^{sch,new}}$	$\boldsymbol{P_G^{max}}$	$\boldsymbol{Q_G^{sch}}$	$\boldsymbol{Q_G^{sch,new}}$	$\boldsymbol{Q_G^{min}}$	$\boldsymbol{Q_G^{max}}$	**Cost**
	$[MW]$	$[MW]$	$[MVARs]$	$[MVARs]$	$[MVARs]$	$[MVARs]$	$[MVARs]$	$[\$/s]$
Gen_10	436.68	440.54	440.54	-53.41	-52.74	-162.56	220.06	704861.11
Gen_25	255.00	255.55	255.55	51.89	51.89	-16.81	51.89	191840.65
Gen_26	158.57	191.33	578.61	-1.26	3.10	-558.56	558.56	383169.32
Gen_49	286.00	286.92	286.92	58.26	58.26	-21.83	58.26	194042.87
Gen_59	232.00	232.79	232.79	47.27	47.27	-14.39	47.27	230365.62
Gen_61	182.01	227.87	312.89	-38.13	-42.51	-78.93	252.34	332802.50
Gen_65	262.01	307.87	430.40	75.79	84.26	-110.61	313.21	700751.61
Gen_66	431.27	431.27	431.27	27.90	30.10	-28.67	87.58	444444.84
Gen_69	585.27	585.27	585.27	-71.51	-73.85	-118.85	118.85	418397.21
Gen_80	403.35	407.03	407.03	129.24	124.82	-228.59	374.51	620277.78
Gen_100	289.93	289.94	289.94	58.87	58.87	-18.37	58.87	205802.50

The solution of the gas and power flows problem with primary frequency regulation, which was obtained by the aforementioned rescheduling of P_G^{sch} and Q_G^{sch}, is reported in Tables 4.25 to 4.30 and Figures 4.11 to 4.15.

The results of active and reactive powers delivered by the generators that are reported in Tables 4.25 and 4.26, respectively, are different from the solution of the economic dispatches and conventional power flows reported in Tables 4.23 and 4.24. On the other hand, when the disconnection of electric loads takes place, the power dispatched is lower than that delivered to the system in the final solution of the multi-energy system. Note that for the case where the demand increases these results are slightly higher. Note also that although generators 25, 49, 66, 69 and 100 have the ability to regulate, they do not contribute to the frequency regulation in all case studies because they have the cheapest cost of power production, as shown in Table 4.21. Therefore, the active power of these generators is set at their maximum capacity, as reported in Table 4.25.

Table 4.25: Active power generated

	$\Delta P \approx 0$		$\Delta P > 0$		$\Delta P < 0$		
Generator	P_G	**Gas consumed**	P_G	**Gas consumed**	P_G	**Gas consumed**	P_G^{max}
	$[MW]$	$[SCFH] \times 10^6$	$[MW]$	$[SCFH] \times 10^6$	$[MW]$	$[SCFH] \times 10^6$	$[MW]$
Gen_10	437.38	2.47	306.59	1.43	440.54	2.50	440.54
Gen_25	255.38	0.68	255.55	0.68	255.55	0.68	255.55
Gen_26	159.19	0.00	103.21	0.00	192.29	0.00	578.61
Gen_49	286.36	0.69	286.92	0.69	286.92	0.69	286.92
Gen_59	232.22	0.81	206.00	0.69	232.79	0.82	232.79
Gen_61	182.34	0.85	103.84	0.44	228.37	1.18	312.89
Gen_65	262.60	0.00	184.15	0.00	308.77	0.00	430.40
Gen_66	431.27	0.00	431.27	0.00	431.27	0.00	431.27
Gen_69	585.27	1.48	585.27	1.48	585.27	1.48	585.27
Gen_80	404.09	2.17	273.31	1.23	407.03	2.20	407.03
Gen_100	289.94	0.73	289.94	0.73	289.94	0.73	289.94

On the other hand, the effect of considering the capability curve to compute the reactive power limits as a function of the active power generation is numerically shown in Table 4.26 and Figure 4.11. Based on the reactive power limits reported in Table 4.21 for the nominal active powers of generators, the results reported in Table 4.26 numerically demonstrate how reactive power limits change according to the active power that is being generated.

Table 4.26: Reactive power generated

Generator	$\Delta P \approx 0$			$\Delta P > 0$			$\Delta P < 0$		
	Q_G	Q_G^{min}	Q_G^{max}	Q_G	Q_G^{min}	Q_G^{max}	Q_G	Q_G^{min}	Q_G^{max}
	$[MVARs]$	$[MVARs]$	$[MVARs]$	$[MVARs]$	$[MVARs]$	$[MVARs]$	$[MVARs]$	$[MVARs]$	$[MVARs]$
Gen_10	-52.70	-167.43	226.27	-70.27	-307.61	385.36	-52.76	-162.56	220.06
Gen_25	52.28	-17.08	52.71	51.89	-16.81	51.89	51.89	-16.81	51.89
Gen_26	-0.64	-568.56	568.56	-1.16	-581.33	581.33	4.07	-558.23	558.23
Gen_49	58.62	-22.85	60.96	58.26	-21.83	58.26	58.26	-21.83	58.26
Gen_59	47.49	-15.23	49.99	-36.98	-37.09	118.27	47.27	-14.39	47.27
Gen_61	-37.80	-93.59	286.97	-59.10	-114.54	323.76	-42.00	-78.75	251.89
Gen_65	76.38	-128.27	352.03	80.93	-154.14	398.71	85.17	-110.23	312.32
Gen_66	27.62	-28.67	87.58	33.70	-28.67	87.58	29.91	-28.67	87.58
Gen_69	-71.56	-118.85	118.85	-71.19	-118.85	118.85	-73.92	-118.85	118.85
Gen_80	129.99	-230.88	377.67	103.44	-316.37	480.87	124.80	-228.59	374.51
Gen_100	58.87	-18.37	58.87	58.87	-18.37	58.87	58.87	-18.37	58.87

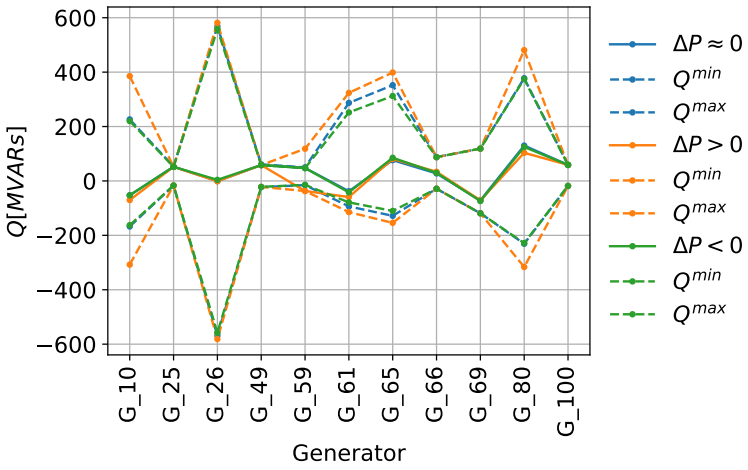

Figure 4.11: Reactive power generated.

A comparative analysis of the results reported in Tables 4.25 and 4.26 shows how the reactive power limits change in relation to the variations of active power delivered by the generators. Within this context, if the active power increases (resp. decreases), the margin for supply Q_{G_i} decreases (resp. increases), which in turn is directly linked to the ability of generators to regulate voltage. For example, in the base case, the active power of generator 25 is slightly less than its maximum power limit ,i.e., 255.55 MW, while the reactive power delivered is 52.28 MVARs, which is also less than its upper limit of 52.71 MVARs. For the other two case studies, however, the active power is set at its maximum limit, thus reducing its ability to provide reactive power to the network. Consequently, the generator violates its maximum reactive power limit and is set in both cases at a magnitude of 51.89 MVARs. The same scenario occurs with generator 49.

In this context, observe the case of generator 59, which in the base case provides a power of $232.22 + j47.49$ with reactive power limits of -15.23 and 49.99, respectively. For the case where the load is disconnected, however, the active power generated decreases to 206 MW, increasing its reactive power limits such that the generator is absorbing -36.98 MVARs, a value that is very close to its new limit of, $Q_G^{min} = -37.09$ MVARs. Furthermore, when the electrical load increases, the generator 59 is set at its maximum active power value $P_G^{max} = 232.79$MW, which converts the generator from type 2 to 1 and also reduces its reactive power limits; therefore, its output is set at its maximum value of $Q_G^{max} = 47.27$ MVARs.

Similarly, generators 10 and 80 reach their maximum active power capacity in the case where demand increases; however, this limitation is imposed by the gas system because generators 10 and 18 have a gas demands of 2.5 and 2.2 MSCFH, respectively, which correspond to the limits in the gas demand, as reported in Table 4.27.

Table 4.27: Gas demanded $[SCFH] \times 10^6$

Node	$\Delta P \approx 0$	$\Delta P > 0$	$\Delta P < 0$	Gen	$q_{gl_k}^{min}$	$q_{gl_k}^{max}$
3	3.8380	3.8380	3.8380	-	0	4
4	1.2180	1.2180	1.2180	-	0	2
5	0.6876	0.6847	0.6889	25	0	2
6	0.8469	0.4446	1.1845	61	0	2
7	0.6971	0.6956	0.6990	49	0	2
8	0.7299	0.7299	0.7299	100	0	2
9	2.4709	1.4326	2.5004	10	0	2.5
11	0.8142	0.6909	0.8171	59	0	2
12	1.4840	1.4840	1.4840	69	0	2
14	2.1746	1.2282	2.2000	80	0	2.2
15	0.5010	0.5010	0.5010	-	0	2

On the other hand, the regulation of active power in generators is achieved by opening (resp. closing) the fuel inlet valve of the combustion chamber, where gases are generated to drive the turbine that delivers a mechanical torque to the generator shaft. This implies a higher (resp. lower) fuel consumption as shown in Tables 4.25 and 4.27, which must be provided by the system sources as reported in Table 4.28. As expected, the fuel demanded by regulating generators varies in the same way that the electrical load changes. This variation in fuel demand in turn manifests itself in changes in gas flows through the natural gas system. Therefore, the behavior of the gas flows is proportional to the disturbance: if the electricity demand increases, the gas flows that circulate through the gas pipeline network also increase. Consequently, the pressure drop increases, and the stored gas tends to flow out to satisfy the requested demand, as can be seen in Figures 4.12 to 4.15.

Table 4.28: Gas supplied by sources $[SCFH] \times 10^6$

Source	$\Delta P \approx 0$	$\Delta P > 0$	$\Delta P < 0$
1	10.2514	7.5654	11.3903
2	9.6658	6.9101	10.8088

Note from Table 4.29 that there is an important difference between the total gas demand and total gas supplied by sources. Because of the behavior of the natural gas transportation system, factors such as circulation speed, changes in the state of the compression of gas, and friction, among others, have a direct impact on the gas flow that is extracted in the load nodes such that the demand of gas is completely different to the gas that must be supplied by the source nodes. Therefore, the amount of gas supplied to the system must be readjusted to satisfy the variations in demand and to keep the system under pressure conditions that guarantee this supply. The foregoing can only be observed and analyzed thanks to the implementation of a model based on the NFI equations proposed in this work.

Table 4.29: Total network values

	$\boldsymbol{\Delta P \approx 0}$		$\boldsymbol{\Delta P > 0}$		$\boldsymbol{\Delta P < 0}$	
	$P[MW]$	$Q[MVARs]$	$P[MW]$	$Q[MVARs]$	$P[MW]$	$Q[MVARs]$
Generation	3798.0362	777.0921	3298.0408	549.0732	3930.7289	980.5302
Load	3665.4777	1436.9609	3167.9330	1267.9588	3785.3325	1556.8610
Losses	132.5584	-659.8688	130.1078	-718.8855	145.3964	-576.3308
Frequency $[Hz]$	59.9971		59.9965		59.9955	
Cost $[M\$/s]$	4.582176		3.595770		4.908008	
LP [MSCF]	908.5531		1189.4124		783.9113	
q_{gs} [MSCFH]	19.9172		15.4755		22.1991	
q_{gl}[MSCFH]	15.4622		12.9475		15.8608	

Note from Figure 4.12 that variations in electricity demand inherently produce changes in the nodal pressures of the natural gas system. When the electrical load is disconnected, the pressure drop is smoother, while with the increase in electrical demand the pressure drop is deeper, reaching almost 850 psia. Note also that there is an inverse proportional relationship between nodal pressures and the gas compressibility factor, so considering a constant magnitude for this factor does not correctly describe the operating state of natural gas. To validate this statement, note from Figure 4.12 that the lower the pressure magnitude is the higher the compressibility factor, which physically implies that the gas is less compressed or even expanding, and, therefore, there is less gas availability.

The aforementioned can lead to limited gas consumption for an electric generator.

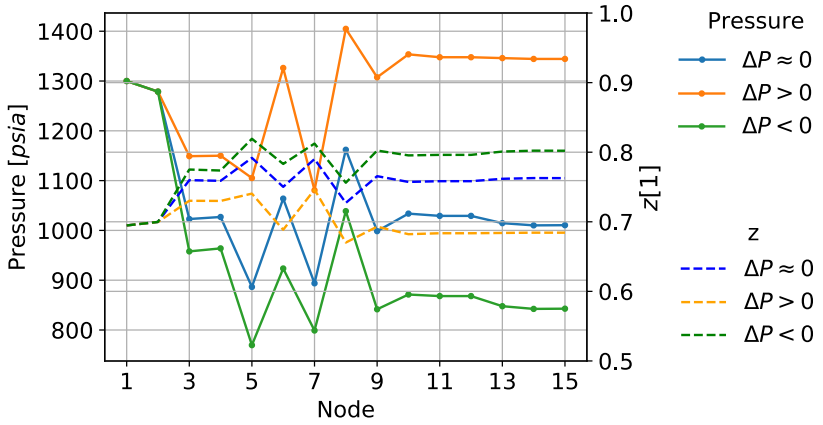

Figure 4.12: Nodal pressure.

On the other hand, from Figure 4.13 it is observed that the flows in the pipelines change as a function of the changes in electricity demand, which implies that the difference between the inlet and outlet gas flow in each duct also changes. Taking the base case as a reference, note that as electricity demand decreases the difference between the inlet and outlet gas flows is also reduced, which implies that the stored gas has increased. On the contrary, in response to the increase in electricity demand, the gas flows that leave the pipelines are of greater magnitude than those that enter each duct, so the difference between the inlet and outlet gas flows is increases, and the linepack in each pipeline is reduced. These phenomena are shown in Figures 4.14 and 4.15, respectively.

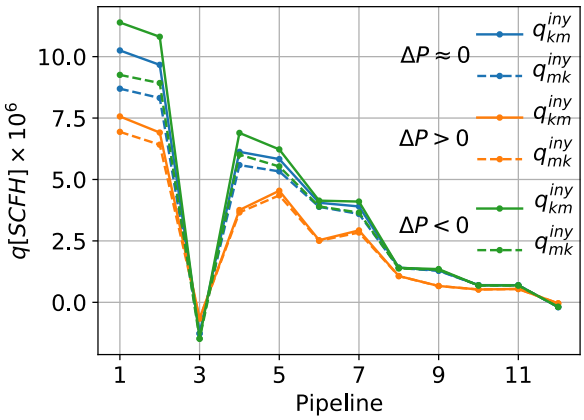

Figure 4.13: Gas flows in the pipelines.

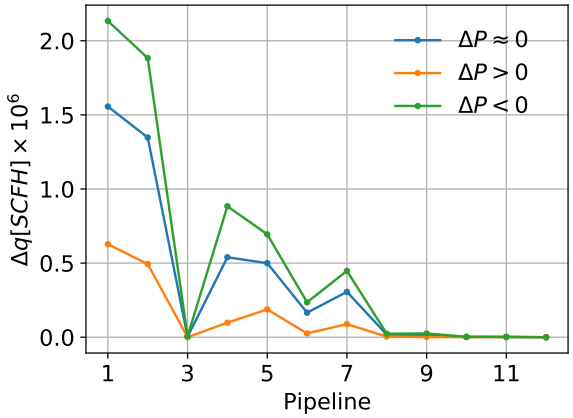

Figure 4.14: Difference between inlet and outlet gas flows in the pipelines.

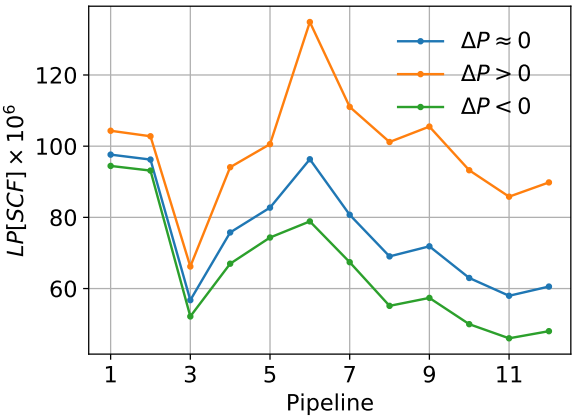

Figure 4.15: Linepack in the pipelines.

As expected, and similar to the behavior of gas through the pipelines, when the electrical demand is disconnected, the gas flow through the compression stations decreases and therefore the gas consumption. Since there is a lower pressure drop in the network, less effort is required by the compressor station to raise the pressure, so its mechanical power is lower. Consequently, the electricity demanded by compression stations from the electrical network is reduced by almost half. The opposite occurs for the case in which the demand for electricity increases suddenly, as reported in Table 4.30.

Table 4.30: Compressor stations' results

From	**to**	q_{comp} $[SCFH] \times 10^6$	τ_{comp} $[SCFH] \times 10^6$	BHP $[HP]$	$P_{L_i/comp_{km}}$ $[MW]$
			Base case		
5	6	4.8979	0.0075	901.8996	0.6725
7	8	4.6324	0.0100	1204.7143	0.8984
9	10	1.4144	0.0004	48.0342	-
11	12	2.7822	0.0000	0.0000	-
			$\Delta P > 0$		
5	6	2.9737	0.0042	507.8106	0.3787
7	8	3.6581	0.0074	887.4180	0.6617
9	10	1.0706	0.0003	32.8723	-
11	12	2.1491	0.0000	0.0000	-
			$\Delta P < 0$		
5	6	5.3228	0.0085	1018.2718	0.7593
7	8	4.8313	0.0108	1297.8287	0.9678
9	10	1.4024	0.0004	50.0072	-
11	12	2.8369	0.0000	0.0000	-

Finally, it is important to mention that in the case study $\Delta P < 0$, where the demand for electricity increases, if the limits of available gas are increased, the electrical system operates with a frequency deviation of $\Delta f = -0.127541$ Hz from the nominal value, which is within the allowed limits. In this case, generators 10 and 80 require 2.766 and 2.5549 MSCFH of fuel from the natural gas system, respectively. Under the pressure conditions established for the gas system, however, this system is not capable of supplying the gas demanded by generators, so the multi-energy system does not converge to a feasible solution.

Based on the information mentioned above, the gas availability at nodes 9 and 14 was limited to a maximum available demand values of 2.5 and 2.2 MSCFH, respectively, which correspond to magnitudes of gas that the system is capable of supplying. As a result of this action, however, the active power capacity that the generators can deliver to the system is restricted, and, therefore, the capacity of frequency regulation is reduced. This leads the electrical system to violate the maximum level of frequency deviation, and, therefore, the frequency control scheme proposed in this work is applied.

4.5 Conclusions

This chapter has proposed a comprehensive solution to the problem of gas and electricity flows from a centralized operation point of view, where the interdependence between natural gas and electricity infrastructures is better represented. Since the quantity of gas demanded from gas-fired power plants to satisfy the demand for electrical energy is of utmost importance, the dependence of electrical loads on frequency deviations and voltage magnitudes is fully considered. In addition, the primary frequency control of the generators is also taken into account to relate the frequency deviations with the power generated and, in turn, with the natural gas demanded by these plants. The effect of considering the control characteristics of the generators and the load-dependent modeling on the operation of the entire multi-energy system is demonstrated numerically in the cases studied. These numerical results clearly show that the consideration of the frequency deviations has a direct effect on the operational state of both energy infrastructures; therefore, this must be taken into account for more realistic studies of energy interdependence.

Furthermore, the results reported in this chapter show numerically that the primary frequency regulation performed from a previous dispatch of active power generation may not be sufficient for obtaining a viable steady-state operation of a multi-energy system, in terms of deviation of frequency. Therefore, a control action approach has been proposed to prevent this unfeasible operation in a multi-energy system.

Likewise, the importance of considering the maximum amount of gas available within the formulation of the multi-energy problem was demonstrated, which is a very common problem in practice, and with its prior consideration could help to take better decisions in programming and the control of multi-energy system.

Finally, it was possible to determine a feasible stable state operating condition of a multi-energy system, guaranteeing that the system operates within the established frequency band and that the reactive power limits of the generators are consistent with their corresponding active power generation. In addition, the maximum availability of gas was considered in such a way that a more efficient use of the gas demanded by the generators also produces a safer and more reliable operation of the multi-energy system and thus at a lower operating cost.

Chapter 5

Multi-period power flow analysis of integrated natural gas and electricity networks

5.1 Introduction

A multi-period mathematical model that efficiently represents the operational interdependence between electricity and natural gas systems is proposed in this chapter. This model is developed within a unified frame of reference for a short-term study period, where boundary conditions such as electrical load, gas demand, and linepack, among others, change over time.

Since electricity travels at the speed of light, a steady-state model is sufficient for modeling the electrical infrastructure. On the other hand, the transient behavior of the natural gas infrastructure must be modeled in detail: the natural gas flow's transient behavior is mathematically represented by two new nonlinear algebraic equations derived from the nodal flow injection equations. Unlike other works, the proposed approach considers the effect of primary frequency regulation on the electric power generation, which occurs in response to temporary changes in the electric demand conditions. Lastly, the proposed

methodology to maintain the electrical frequency value within its operating limits is also implemented in the unified multi-period gas and electricity model.

5.2 Transient natural gas flow modeling

Compared to the electric power system, the natural gas dynamics evolve over long time scales because of greater inertia. Factors such as the speed at which the gas travels (60 to 90 km/hr), the friction force, the gas's compression state and the amount of gas stored and transported through the pipelines cause gas flows to react more slowly to disturbances in the system.

The dynamics acting on a natural gas transportation system are predominantly determined by the gas flow that circulates through the pipelines and the variations in the linepack. Furthermore, in the case of transients caused by fluctuations in demand, the gas in the pipeline has enough time to reach thermal equilibrium with its surroundings. Hence, the transient flow of natural gas in the pipes can be adequately described using a one-dimensional isothermal approach. Within this context, the energy balance establishes that the sum of all forces acting on a gas particle within a pipeline is equal to 0, as given by the momentum (or motion) equation (5.1):

$$\frac{\partial p}{\partial x} + g\rho\frac{\partial h}{\partial x} + \frac{\lambda\left|\upsilon\right|\upsilon}{2D}\rho + \frac{1}{A}\frac{\partial \dot{m}}{\partial t} + \frac{\partial\left(\rho\upsilon^2\right)}{\partial x} = 0. \tag{5.1}$$

If the gas mass flow rate "$\dot{m}$" and the fluid velocity "υ" are expressed in terms of the fluid density

$$\dot{m} = \rho_0 q_{st} = \rho\upsilon A \quad \text{and} \quad \upsilon = \frac{\rho_0 q_{st}}{\rho A}, \tag{5.2}$$

then Eq. (5.1) can be expressed as

$$\frac{A}{\rho_0}\frac{\partial p}{\partial x} + \frac{A}{\rho_0}g\rho\frac{\partial h}{\partial x} + \frac{\lambda\rho_0}{2D\rho A}\left|q_{st}\right|q_{st} + \frac{\partial q_{st}}{\partial t} + \frac{\rho_0}{\rho A}\frac{\partial\left(q_{st}^2\right)}{\partial x} = 0. \tag{5.3}$$

In Chapter 2 two new expressions for modeling the gas flow in steady-state were derived based on the concept of nodal injections and by neglecting the temporal term of Eq. (5.3). These expressions were referred to as nodal flow injection (NFI) equations.

On the other hand, the principle of conservation of mass states that the mass contained in a certain volume will remain constant unless some gas is added to or removed from the container. For a pipeline, this principle is modeled by the continuity equation:

$$\frac{\partial \dot{m}}{\partial x} + A\frac{\partial \rho}{\partial t} = 0. \tag{5.4}$$

By replacing the variable $\dot{m}$ in (5.4) with the relationships reported in (5.2),

$$\frac{\partial q_{st}}{\partial x} + \frac{A}{\rho_0}\frac{\partial \rho}{\partial t} = 0. \tag{5.5}$$

Furthermore, from the equation of state of gases, the relationships given by (5.6) can be obtained:

$$\rho = \frac{p}{zR_{gas}T} \qquad \text{and} \qquad \rho_0 = \frac{p_0}{z_0 R_{gas} T_0}. \tag{5.6}$$

Lastly, replacing (5.6) into (5.4) results in the continuity equation expressed in terms of magnitudes of volumetric gas flow and pressure:

$$\frac{\partial q_{st}}{\partial x} + A\frac{z_0 T_0}{p_0}\frac{\partial}{\partial t}\left(\frac{p}{zT}\right) = 0. \tag{5.7}$$

Equation (5.7) and the momentum equation (5.3) are used to describe the transient behavior of gas flows inside a pipeline or a natural gas transportation system. Conventional methods for pipe network transient analysis are generally performed through the numerical solution of two partial differential equations, which are complex and cumbersome. From these two equations and the nodal injection theory proposed in this work, however, it is possible to derive two new nonlinear algebraic equations suitable for describing the transient gas flow through the pipeline.

Eq. (5.8) is obtained by discretizing Eq. (5.7) temporally and spatially through the implicit Euler scheme. This discretization assumes that $\partial x = L_{km}$ and that $t^* = t - \Delta t$ correspond to the current and previous time period of study, respectively:

$$\Delta q_{st} + AL_{km}\frac{z_0 T_0}{p_0 \Delta t}\left(\frac{p\,(t)}{z\,(t)\,T\,(t)} - \frac{p\,(t^*)}{z\,(t^*)\,T\,(t^*)}\right) = 0. \tag{5.8}$$

Since the linepack in each pipeline is given by (5.9), the continuity equation (5.8) can finally be expressed by Eq (5.10):

$$LP_{km}^{avg} = \frac{\pi}{4}D_{km}^2 L_{km}\frac{z_0 T_0}{p_0}\frac{p_{km}^{avg}}{z_{km}^{avg}T_{km}^{avg}} = AL_{km}\frac{z_0 T_0}{p_0}\frac{p_{km}^{avg}}{z_{km}^{avg}T_{km}^{avg}}, \tag{5.9}$$

$$\Delta q_{st} + \left(\frac{LP\,(t)}{\Delta t} - \frac{LP\,(t^*)}{\Delta t} \right) = 0. \tag{5.10}$$

Note that the term $\frac{LP(t^*)}{\Delta t}$ can be assumed known and constant since it is obtained from the previous operation state. Furthermore, the initial state of storage can be obtained from the solution of the steady-state gas flows.

5.2.1 Multi-period AFE model

In order to have a reference point for validating and comparing the performance of the proposed model, first a model will be derived based on average magnitudes of the gas flow that circulates through each pipeline. To achieve this goal and have a better point of comparison, the model developed below will be based on average flow equation (AFE) proposed in this work.

Considering the gas flow behavior described in Figure 5.1 for a general pipeline connected between nodes "k" and "m", Eq. (5.10) is obtained by applying the mass balance Eq. (5.11):

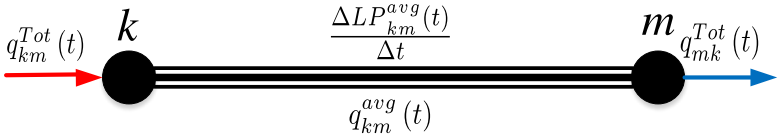

Figure 5.1: AFE multi-period model.

$$\Delta q^{Tot} = q_{mk}^{Tot}\,(t) - q_{km}^{Tot}\,(t) = -\left(\frac{LP_{km}^{avg}\,(t) - LP_{km}^{avg}\,(t^*)}{\Delta t} \right) = 0. \tag{5.11}$$

The average gas flow through the pipeline can be approximated by the arithmetic mean as

$$q_{km}^{avg}\,(t) = \frac{q_{km}^{Tot}\,(t) + q_{mk}^{Tot}\,(t)}{2}, \tag{5.12}$$

so the gas flow from nodes "k" to "m" can be expressed as

$$q_{mk}^{Tot}\,(t) = 2q_{km}^{avg}\,(t) - q_{km}^{Tot}\,(t)\,. \tag{5.13}$$

Replacing $q_{mk}^{Tot}\,(t)$ given by (5.13) in (5.11),

$$q_{km}^{Tot}\,(t) = q_{km}^{avg}\,(t) + \left(\frac{LP_{km}^{avg}\,(t) - LP_{km}^{avg}\,(t^*)}{2\Delta t} \right) = 0. \tag{5.14}$$

By applying a similar analysis but for the gas flow that circulates from node "m" to node "k," the resulting equation is given by

$$q_{mk}^{Tot}(t) = q_{km}^{avg}(t) - \left(\frac{LP_{km}^{avg}(t) - LP_{km}^{avg}(t^*)}{2\Delta t}\right) = 0. \tag{5.15}$$

Note that (5.14) and (5.15) depend on the magnitude of the average gas flow that circulates through the pipeline connected between nodes "k" and "m." Therefore, by replacing $q_{km}^{avg}(t)$ with the average flow equation (AFE) proposed in Chapter 2, Eq. (5.16) and Eq. (5.17) are obtained:

$$q_{km}^{Tot}(t) = \alpha \frac{\left(p_k^2(t)\beta_k - p_m^2(t)\beta_m + p_k(t)p_m(t)\beta_{km}\right)}{\left|p_k^2(t)\beta_k - p_m^2(t)\beta_m + p_k(t)p_m(t)\beta_{km}\right|^{\frac{1}{2}}}\epsilon + \left(\frac{LP_{km}^{avg}(t) - LP_{km}^{avg}(t^*)}{2\Delta t}\right) = 0 \tag{5.16}$$

$$q_{mk}^{Tot}(t) = \alpha \frac{\left(p_k^2(t)\beta_k - p_m^2(t)\beta_m + p_k(t)p_m(t)\beta_{km}\right)}{\left|p_k^2(t)\beta_k - p_m^2(t)\beta_m + p_k(t)p_m(t)\beta_{km}\right|^{\frac{1}{2}}}\epsilon - \left(\frac{LP_{km}^{avg}(t) - LP_{km}^{avg}(t^*)}{2\Delta t}\right) = 0. \tag{5.17}$$

The multi-period average flow equations (5.16) and (5.17) (referred to as MP-AFE) represent a new way to approximate the transitory behavior of gas flow in a pipe considering only two time-variant nonlinear algebraic equations. Note that these equations only depend on nodal pressures, so there is no need to add equations or state variables to the formulation of the multi-period gas flow problem.

Similarly, the direction of gas flow inside the pipe is implicitly considered in these equations. Finally, note that the arithmetic mean of (5.16) and (5.17) corresponds to the average gas flow magnitude given by the AFE equation, while the difference between (5.16) and (5.17) corresponds to the continuity equation given by (5.10).

5.2.2 Multi-period NFI model

Considering that the gas flow through a pipeline can be modeled as injections of gas flow at the pipe ends, as shown in Figure 5.2, the law of mass conservation given by (5.10) can be applied to obtain the gas flow balance at each end of the pipe:

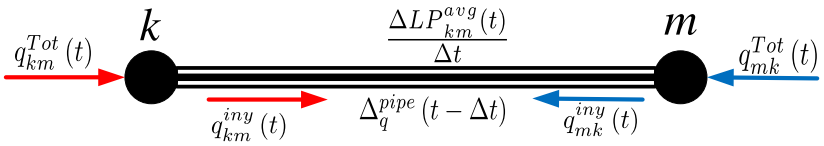

Figure 5.2: NFI multi-period model.

$$q_{km}^{Tot}(t) = q_{km}^{iny}(t) + \left(\frac{LP_{km}^{avg}(t) - LP_{km}^{avg}(t^*)}{2\Delta t}\right) - \frac{q_{km}^{iny}(t^*) + q_{mk}^{iny}(t^*)}{2} \quad \text{and} \tag{5.18}$$

$$q_{mk}^{Tot}(t) = q_{mk}^{iny}(t) + \left(\frac{LP_{km}^{avg}(t) - LP_{km}^{avg}(t^*)}{2\Delta t}\right) - \frac{q_{mk}^{iny}(t^*) + q_{km}^{iny}(t^*)}{2}. \tag{5.19}$$

In this case, the first term of (5.18) and (5.19) correspond to the nodal gas flow injection for nodes "k" and "m", respectively. The second term, as in expressions (5.16) and (5.17), corresponds to the variation in the nodal gas flows due to changes in the linepack during the time interval. Lastly, the third term corresponds to the difference between the inlet and outlet gas flows in the pipeline during the previous time period.

Based on the information mentioned above, the multi-period nodal flow injection (MP-NFI) equations are obtained by substituting in (5.18) and (5.19) the steady-state nodal flow injection (NFI) equations previously derived. The resulting equations are given by (5.20) and (5.21), which indicate that the gas flow transient state can be modeled by two new nonlinear algebraic equations. Note that these equations implicitly consider the nodal flow injections the direction in which the gas flows inside the pipe and the temporal changes in the pipeline linepack and in the difference between the inlet and outlet gas flows:

$$q_{km}^{Tot}(t) = \alpha^{\frac{1}{2}} \frac{\left(p_k^2(t)\,\beta_{k1} - p_k(t)p_m(t)\beta_{k2}\right)}{\left|p_k^2(t)\,\beta_{k1} - p_k(t)p_m(t)\beta_{k2}\right|^{\frac{1}{2}}}\epsilon + \left(\frac{LP_{km}^{avg}(t) - LP_{km}^{avg}(t^*)}{2\Delta t}\right) - \frac{q_{km}^{iny}(t^*) + q_{mk}^{iny}(t^*)}{2} \tag{5.20}$$

$$q_{mk}^{Tot}(t) = \alpha^{\frac{1}{2}} \frac{\left(p_m^2(t)\,\beta_{m1} - p_k(t)p_m(t)\beta_{m2}\right)}{\left|p_m^2(t)\,\beta_{m1} - p_k(t)p_m(t)\beta_{m2}\right|^{\frac{1}{2}}}\epsilon + \left(\frac{LP_{km}^{avg}(t) - LP_{km}^{avg}(t^*)}{2\Delta t}\right) - \frac{q_{mk}^{iny}(t^*) + q_{km}^{iny}(t^*)}{2}. \tag{5.21}$$

Furthermore, because (5.20) and (5.21) implicitly consider the possible bidirectionality of the gas flow in their formulation, they will always circulate in opposite directions: if $q_{km}^{iny}\left|q_{km}^{iny}\right| > 0$, then $q_{mk}^{iny}\left|q_{mk}^{iny}\right| < 0$, and conversely if $q_{km}^{iny}\left|q_{km}^{iny}\right| < 0$, then $q_{mk}^{iny}\left|q_{mk}^{iny}\right| > 0$.

On the other hand, the difference between the inlet and outlet gas flow at the pipeline

ends can be directly computed from the MP-NFI equations, which results in Eq. (5.22):

$$\Delta_q^{pipe}(t) = q_{km}^{Tot}(t) + q_{mk}^{Tot}(t) = \left(q_{km}^{iny}(t) - q_{km}^{iny}(t^*)\right) + \left(q_{mk}^{iny}(t) - q_{mk}^{iny}(t^*)\right) + \left(\frac{LP_{km}^{avg}(t) - LP_{km}^{avg}(t^*)}{\Delta t}\right). \tag{5.22}$$

Note that if the magnitude of the nodal gas flow injections remains unchanged over time Eq.(5.22) reduces to

$$\Delta_q^{pipe}(t) = q_{km}^{Tot}(t) + q_{mk}^{Tot}(t) = \left(\frac{LP_{km}^{avg}(t) - LP_{km}^{avg}(t^*)}{\Delta t}\right). \tag{5.23}$$

Therefore, the following two possible directions of gas flow are obtained by writing Eq. (5.23) in terms of absolute values:

$$\left|q_{mk}^{Tot}(t)\right| - \left|q_{km}^{Tot}(t)\right| + \left(\frac{LP_{km}^{avg}(t) - LP_{km}^{avg}(t^*)}{\Delta t}\right) = 0 \quad \text{if: } q_{mk}^{iny}\left|q_{km}^{iny}\right| < 0, \tag{5.24}$$

$$\left|q_{km}^{Tot}(t)\right| - \left|q_{mk}^{Tot}(t)\right| - \left(\frac{LP_{km}^{avg}(t) - LP_{km}^{avg}(t^*)}{\Delta t}\right) = 0 \quad \text{if: } q_{mk}^{iny}\left|q_{km}^{iny}\right| > 0. \tag{5.25}$$

Equations (5.25) and (5.24) correspond to the continuity equation (5.10), which implies that the law of conservation of mass is fulfilled for the two possible directions of gas flow.

Similarly, note that the differences $\left(q_{km}^{iny}(t) - q_{km}^{iny}(t^*)\right)$ and $\left(q_{mk}^{iny}(t) - q_{mk}^{iny}(t^*)\right)$ agree with the term $\frac{\partial q_{st}}{\partial t}$ of the moment equation (5.3), which was neglected in the deduction of the steady-state model and represents the change in the magnitude of the nodal gas flow injections at the pipeline's ends with respect to time.

Finally, observe from Eq. (5.26) that the sum of absolute values associated with total gas flows corresponds to the sum of absolute values of nodal injections given by the NFI equations:

$$\left|q_{km}^{Tot}(t)\right| + \left|q_{mk}^{Tot}(t)\right| = \left|q_{km}^{iny}(t)\right| + \left|q_{mk}^{iny}(t)\right|. \tag{5.26}$$

5.2.3 Compressor stations

As described in previous chapters, the gas flow tends to lose part of its initial energy because of a pressure drop during the process of transporting gas through pipelines.

To compensate this loss of energy, compression stations are strategically installed at several points of the network to increase the pressure of gas. For multi-period studies, the compression ratio (CR) is given by the discharge pressure and the suction pressure, as shown in (5.27). On the other hand, the power consumption is calculated by using the brake horsepower (BHP) equation given by (5.28):

$$CR\left(t\right) = \frac{p_D\left(t\right)}{p_S\left(t\right)}, \tag{5.27}$$

$$BHP\left(t\right) = \frac{p_0}{T_0}\frac{z_{comp}\left(t\right)T_s}{E\eta}\left(\frac{\kappa}{\kappa-1}\right)\left[\left(CR\left(t\right)\right)^{\frac{\kappa-1}{\kappa}} - 1\right]q_{comp}\left(t\right). \tag{5.28}$$

By grouping the independent terms of (5.28) into a constant $BHRC$, the BHP equation can be rewritten as

$$BHP\left(t\right) = BHRCq_{comp}\left(t\right). \tag{5.29}$$

Therefore, the compressor gas consumption can be calculated by its specific consumption function (5.30), which permits the calculation of gas consumed in the period "t" to be a function of the amount of gas circulating through the compressor at that time instant:

$$\tau_{comp}\left(t\right) = \alpha_c + \beta_c BHRCq_{comp}\left(t\right) + \gamma_c(BHRCq_{comp}\left(t\right))^2. \tag{5.30}$$

5.2.4 Network model

Based on the multi-period equations of the elements making up the natural gas transportation system and the concept of nodal flow balance, it is possible to develop a general model to describe and analyze the behavior of a natural gas transportation system in a transient-state operation state. Hence, the gas flow balance at the k-th node of the gas network is given by

$$\Delta q_k\left(t\right) = \sum_{m\in k} q_{km}^{Tot}\left(t\right) + \sum_{comp\in k} q_{comp_k}\left(t\right) + \sum_{comp\in k} \tau_{comp_k}\left(t\right) - \sum_{gs\in k} q_{gs_k}\left(t\right) + \sum_{gl\in k} q_{gl_k}\left(t\right) = 0. \tag{5.31}$$

From Eq. (5.31), the first term corresponds to the gas flow leaving or reaching the k-th node through the pipelines connected to the node. This term is replaced by Eqs. (5.16) and (5.17) or by Eqs. (5.20) and (5.21) for the MP-AFE or MP-NFI model, respectively. Similarly, note that this term depends on the previous operational state. The second and

third terms represent the gas circulating through the compression stations connected to the k-th node and the gas consumed by this set of compressors, respectively. Lastly, the fourth and fifth terms correspond to the total gas injected and extracted through the sources and demands embedded at the k-th node, respectively.

On the other hand, the balance of nodal pressures for a compression station connected between nodes "k" and "m" is directly derived from (5.27), which results in

$$\Delta CR_{km}(t) = -p_k(t) CR_{km}(t) + p_m(t) = 0. \tag{5.32}$$

Lastly, the transient behavior of gas flows is formulated by the nonlinear algebraic equations (5.31) and (5.32), which are iteratively solved using the Newton-Raphson method. Hence, the set of nonlinear algebraic equations that represent the equilibrium condition at each node of the natural gas transportation network is given by

$$\vec{f_{Ng}}(t) = \begin{bmatrix} \Delta\vec{q_k}(t) \\ \Delta\vec{CR}_{km}(t) \end{bmatrix} = 0, \quad \begin{matrix} \forall k \in (Ng-1) \text{ and} \\ \forall k, m \in Nc, \end{matrix} \tag{5.33}$$

where (5.33) is defined for the Nc compression stations and for all Ng nodes in the gas network, except for the compensator node. Therefore, the system's operating point is obtained by solving (5.33) for all state variables under the assumption that the gas demanded by loads and injected by sources is known.

Lastly, the linearization of (5.33) by its expansion into the first-order Taylor series results in

$$\underbrace{\begin{bmatrix} \Delta\overrightarrow{p_k}(t) \\ \Delta\vec{q}_{comp_m}(t) \end{bmatrix}}_{\Delta\vec{x}(t)^{(i)}} = -\underbrace{\begin{bmatrix} \frac{\partial\Delta\vec{q}(t)}{\partial\vec{p}_k(t)} & \frac{\partial\Delta\vec{q}(t)}{\partial\vec{q}_{comp_m}(t)} \\ \frac{\partial\Delta\vec{CR}(t)}{\partial\vec{p}_k(t)} & \frac{\partial\Delta\vec{CR}(t)}{\partial\vec{q}_{comp_m}(t)} \end{bmatrix}^{-1}}_{-J\left(\vec{x}(t)^{(i-1)}\right)^{-1}} \underbrace{\begin{bmatrix} \Delta\vec{q_k}(t) \\ \Delta\overrightarrow{CR}_m(t) \end{bmatrix}}_{f_{Ng}\left(\vec{x}(t)^{(i-1)}\right)} \quad \begin{matrix} \forall k \in (Ng-1) \text{ and} \\ \forall m \in Nc, \end{matrix} \tag{5.34}$$

where the superindex "i" denotes the number of iteration.

Lastly, (5.34) is iteratively solved for $\Delta\vec{x}$, and the set of algebraic state variables x are updated by (5.35) until a specified tolerance of $\Delta\vec{x} < 10^{-6}$ is satisfied, or the maximum number of allowed iterations is exceeded:

$$\vec{x}\,(t)^{(i)} = \vec{x}\,(t)^{(i-1)} + \Delta\vec{x}\,(t)^{(i)}\,. \tag{5.35}$$

5.2.5 Case study

The Belgian gas pipeline network shown in Figure 5.3 is used in this section to validate the proposed transient-state model of natural gas flows, referred to as the MP-NFI model. The multi-period gas flow analysis is performed one day in advance, divided into sub periods of 1 hour according to the demand characteristic presented in Figure 5.4. Note that the gas loads connected to nodes 3, 6, 7, and 10 present variations in their magnitudes in between the 11th and 21st hour; after that, these loads return to their initial condition. The rest of the gas loads remain invariant during the entire period of study. Similarly, it was assumed that only the source connected to node 1 can adjust its supply of natural gas to the network according to the demand variability. In contrast, the rest of the sources remain constant.

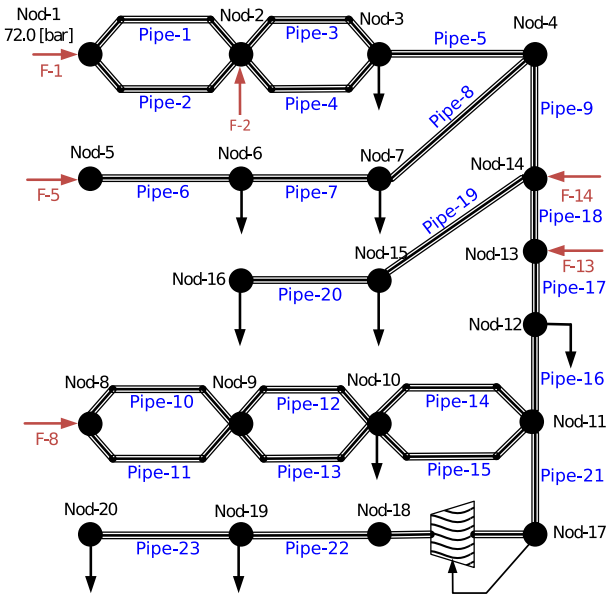

Figure 5.3: Pipeline diagram of the Belgium gas network.

The results obtained using the MP-NFI model are compared with those obtained by the model based on the average flow equation, referred to as the MP-AFE model.

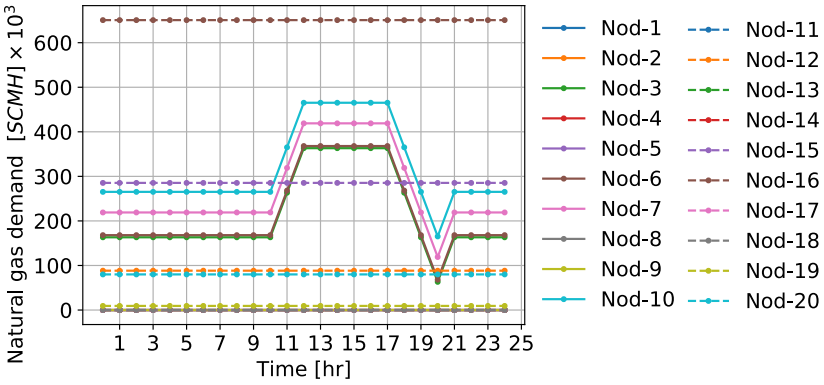

Figure 5.4: Natural gas demand characteristic for a 24-hour period.

The gas flows obtained by the MP-AFE and MP-NFI models at the inlet and outlet ends of each pipeline are shown in Figures 5.5 and 5.6. A comparison of these results clearly shows that both models obtain very similar magnitudes of gas injections. As expected, when gas demand begins to increase at the 11th hour, the gas flows at the inlet and outlet ends of each pipeline tend to increase, especially in ducts 1, 2, 3, 4, 7, and 8 closer to nodes with varying demand. Even though the demands are invariant between the 12th and 17th hour, the gas flows have their maximum values at the 17th hour, where the transient is damped out because of the system's inertia. After this time, the gas demand decreases for the next 3 hours such that the flows through the ducts decrease. Lastly, when the demand returns to its initial conditions, the system operating state tends to return to its initial equilibrium point, as do the gas flows.

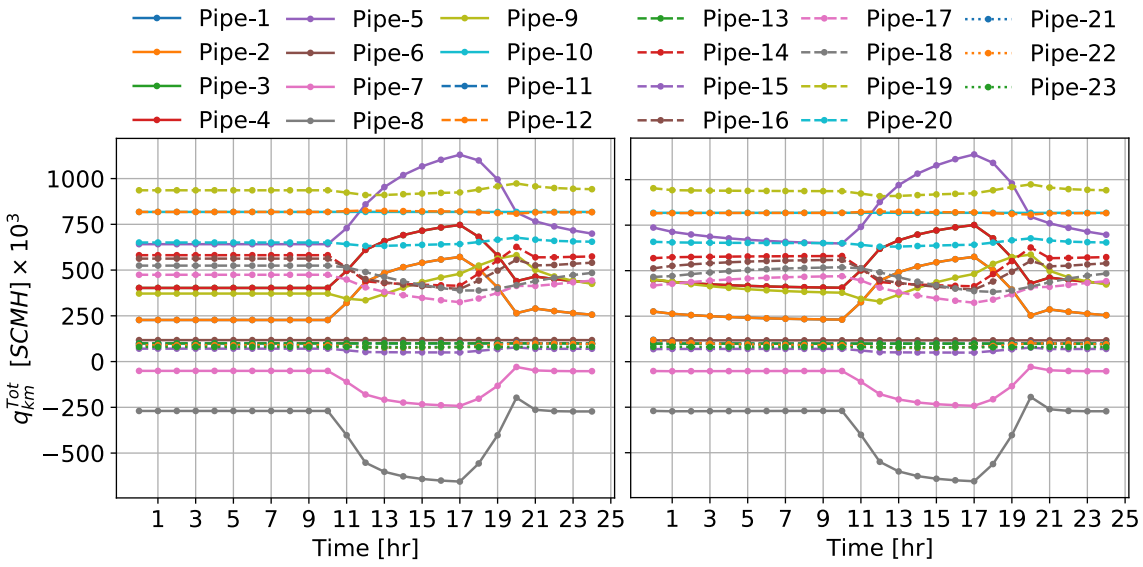

(a) MP-AFE model (b) MP-NFI model

Figure 5.5: Natural gas flows from node "k" to node "m".

On the other hand, from Figures 5.5 and 5.6 it is observed the magnitude of gas flow through pipelines 14 to 18 changes in an opposite direction with respect to the variation of gas demand. This is because one of the largest system's sources is connected to node 8, and gas demanded at node 10 varies over time. Therefore, as the demand for gas increases (resp. decreases) at node 10, a greater (or lesser) amount of gas is supplied from the source at node 8, which implies a redistribution of gas flows through the network that results in a decrease (resp. increase) of mass flow through the pipelines mentioned above.

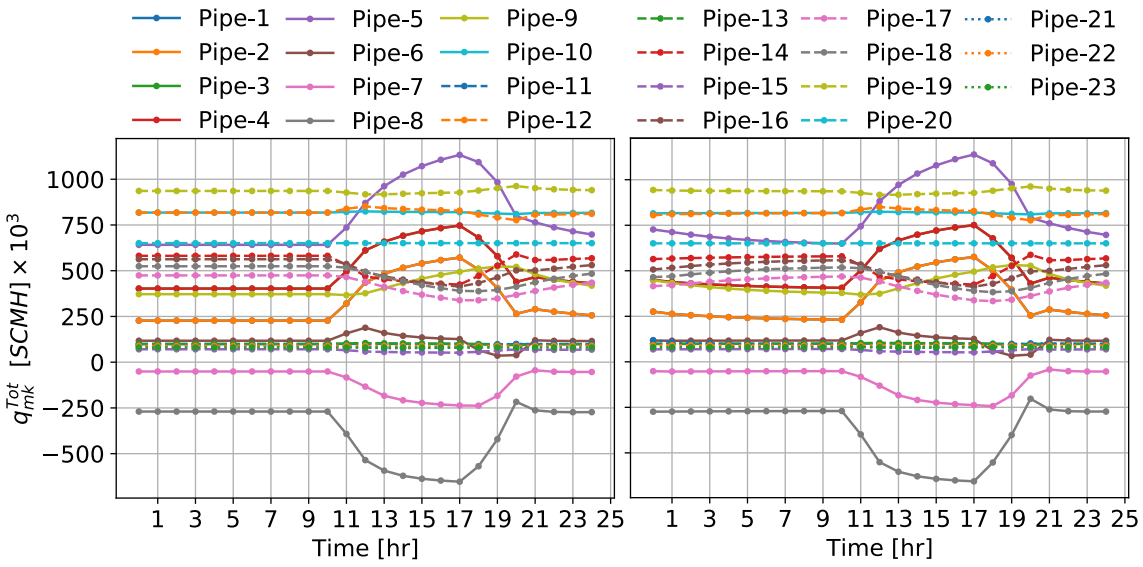

(a) MP-AFE model (b) MP-NFI model

Figure 5.6: Natural gas flows from node "m" to node "k".

Note also from Figures 5.5 and 5.6 that between 0 and 10th hour, where gas demand remains constant, the gas flows through the pipes are completely invariant in the MP-AFE model. When the MP-NFI model is used, however, the gas that flows through some pipelines, e.g., 2, 4, 5, and 9, has a decreasing temporal trend until reaching its steady-state value at the 10th hour. These values are very similar to the ones associated with the constant state of the MP-AFE model. The operating condition mentioned above is due to the transient gas behavior inside each pipeline produced by the difference of gas injections at the pipeline's inlet and outlet ends, as shown in Figure 5.7. Note also that the difference between the inlet and outlet gas flows has a similar behavior after the 10th hour when the gas demand begins to change over time. If the gas demand increases, the gas flow in the pipeline is greater in the outlet end than in the inlet end. The opposite takes place if gas demand decreases. This difference between gas injections decreases between the 12th and 17th hour because the gas demand remains constant, and the transient behavior is damped out. Similar behavior is observed after the 21ts hour. Lastly, the transients of gas flow through pipelines are dictated by the system's inertial response, which modifies the nodal pressure conditions and, therefore, the magnitude of the nodal gas flow injections. Hence, the inlet gas flow is greater than the outlet gas flow in most of the pipelines, but the opposite

operational condition is observed in few pipelines, e.g., pipeline 8.

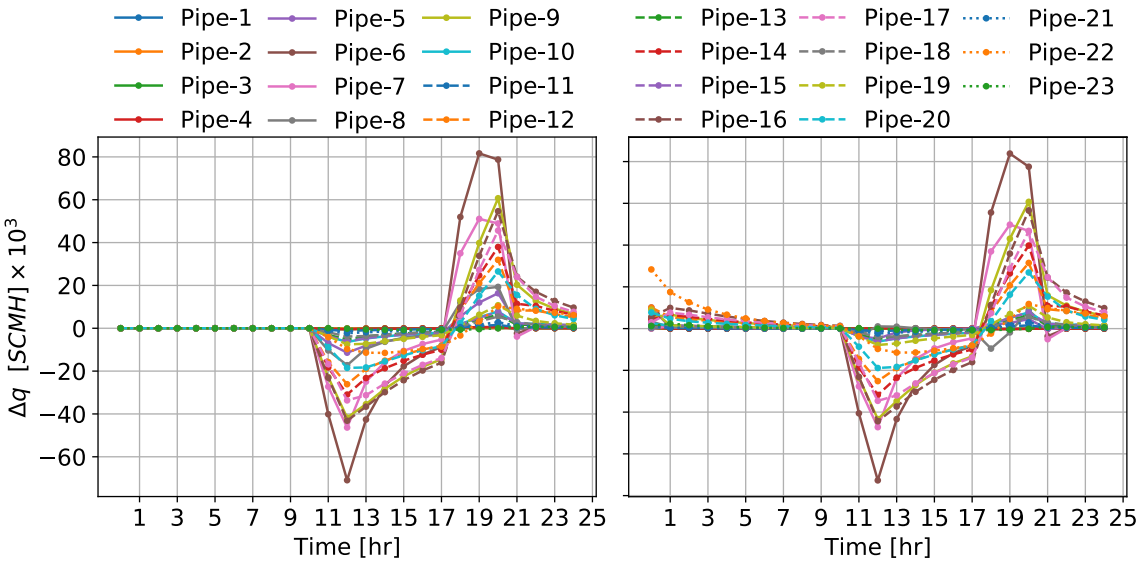

(a) MP-AFE model (b) MP-NFI model

Figure 5.7: Difference between inlet and outlet gas flows by pipeline.

On the other hand, the nodal gas pressures change in an opposite direction to the gas demand behavior. Figure 5.8 shows that the nodal pressures begin to drop abruptly because of the increase in gas demand at the 11th hour; however, the pressures drop is smoother in between 13rd and 17th hour, and it tends to stabilize because the gas demand remains constant during this time period. Note also that the decrease in gas demand between the 18th and 20th hour produces an increment of nodal pressures along the network to bring the system to a new equilibrium point that satisfies the new demand conditions. In this case, however, the transient response of gas pressures at nodes 19 and 20 has a significant time delay because they reach their maximum pressure drop at the 20th hour, the hour at which the system presents the minimum gas demand of the entire study period. This is because these nodes are at the end of the radial network, as can be seen in Figure 5.3, and also because nodes 18 and 19 interconnect the longest pipeline in the entire network with a length of 98 km. Hence, the dynamics occurring in these nodes and their corresponding pipelines are much slower than in the rest of the network.

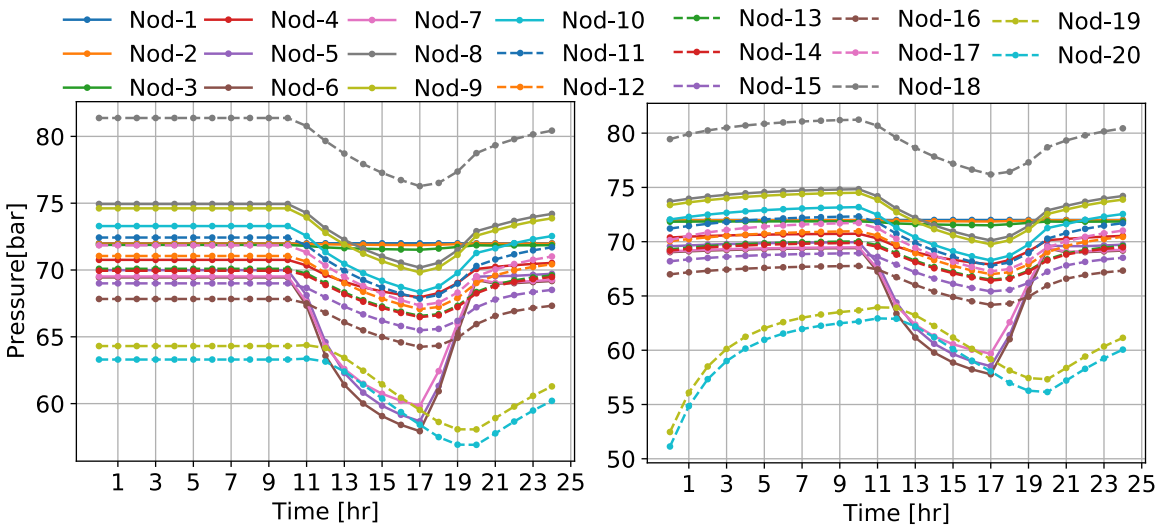

(a) MP-AFE model

(b) MP-NFI model

Figure 5.8: Nodal pressures.

On the other hand, the compressibility factor varies according to changes in demand and is inversely proportional to pressure, as shown in Figure 5.9. This is because the temperature remains constant such that this factor only depends on the gas pressure conditions. Furthermore, the compressibility factor defines the state of gas compression: an increment (resp. decrement) of the compressibility factor produces a decrement (resp. increment) in the gas compression. From a physical viewpoint, a decrement in the gas compression means an expansion of gas such that the gas flow at the outlet end is higher than at the inlet end of the pipeline. In this case, the gas flow occupies a larger volume, and the gas storage is reduced: the linepack decreases. Even though the compressibility factor remains invariant during the first 10 hours when using the MP-AFE model, this factor decreases with time in the MP-NFI model. This also implies that the linepack increases until reaching a state of equilibrium compression. At this equilibrium point, the compressibility factor has similar values for both the MP-AFE and MP-NFI models.

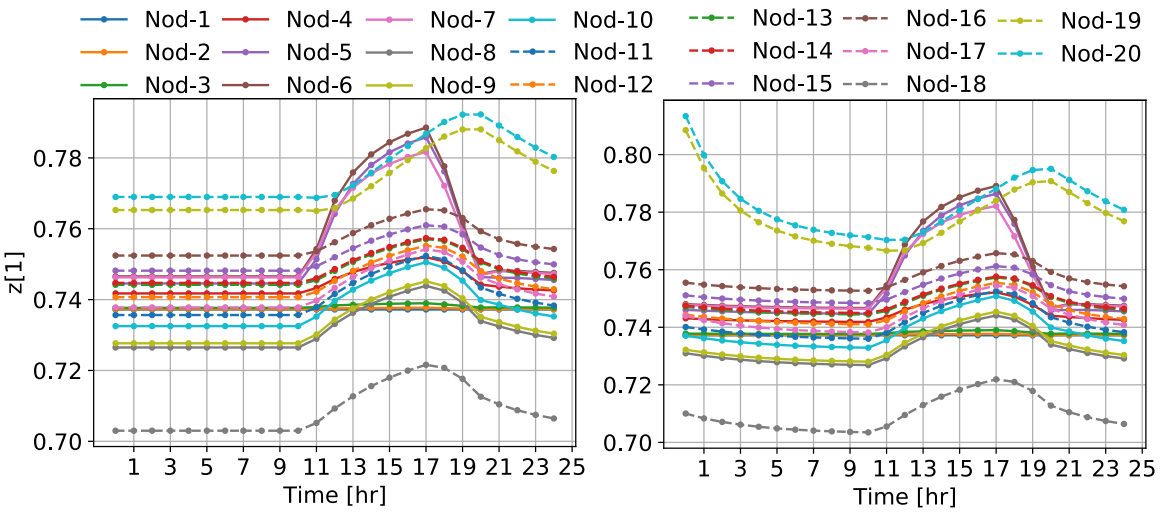

(a) MP-AFE model (b) MP-NFI model

Figure 5.9: Compressibility factor by node.

The information mentioned above regarding the linepack behavior is schematically shown in Figure 5.10. Considering the MP-NFI model, the transient linepack behavior during the first 10 hours is mainly caused by the gas flow in pipes and nodes at the end of the radial network. This transient is commonly known as a period of dynamic stabilization or "*pipe filling*" (from a physical point of view), which occurs until reaching a point of equilibrium. Strictly speaking, this equilibrium point can only be reached when the difference between the gas flows at both ends of a pipeline is precisely 0, which is a condition that is always assumed in models based on average gas flow equations.

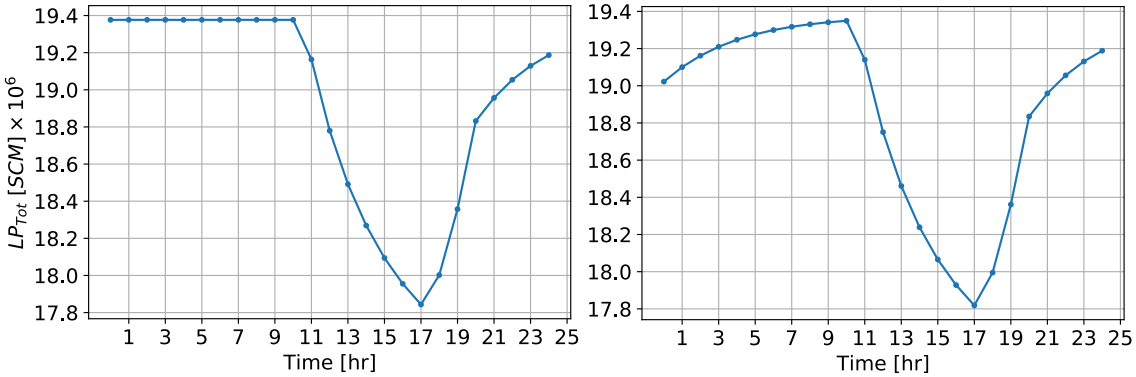

(a) MP-AFE model (b) MP-NFI model

Figure 5.10: Total linepack in the network.

5.2.6 Case study 2

Case study 1, which was reported in the previous section, is newly analyzed in this section by adding the disconnection of pipeline 10, which is connected between nodes 8 and 9, for a period of time in between the 7th and 13th hour.

The results of the gas flow through the system's pipelines are shown in Figures 5.11 and 5.12. The failure of the pipeline causes all the gas supplied by the source connected to node 8 to be transported through pipeline 11, which does not affect the operating condition of the rest of the pipelines when using the MP-AFE model. In contrast, a small transient that reduces the outlet gas flow in adjacent pipelines is produced when using the MP-NFI model. This is because at the fault inception there is a momentary reduction of gas that flows through the other pipelines comprising the radial trajectory at which pipeline 11 is connected: pipelines 12, 13, 14 and 15.

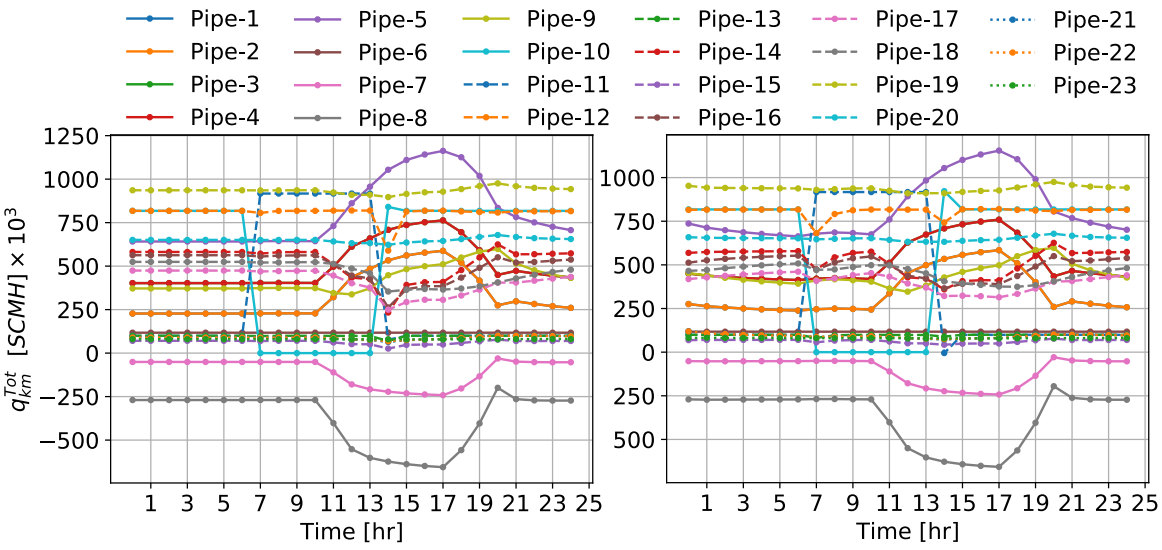

(a) MP-AFE model (b) MP-NFI model

Figure 5.11: Natural gas flows from node "k" to node "m".

Figure 5.12 clearly shows that the gas flow response at the outlet end of pipeline 11 (q_{mk}^{Tot}) is almost instantaneous when using the MP-AFE model, while when using the other model, the transient response takes approximately 3 hours to stabilize.

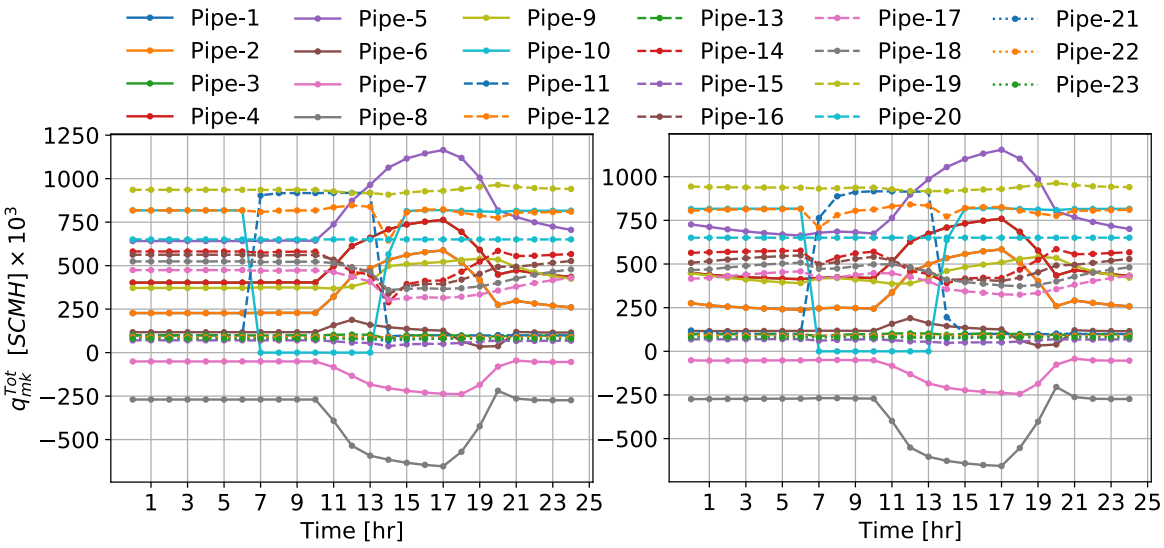

(a) MP-AFE model. (b) MP-NFI model.

Figure 5.12: Natural gas flows from node "m" to node "k".

After increasing the gas demand at the 11th hour, the fault is cleared by reconnecting the pipeline at the 14th hour, which causes a transient gas flow through pipeline 10 and other adjacent pipelines. This transient response is due to the process of *pipe filling*: $q_{km}^{Tot} > q_{mk}Tot$. On the other hand, the gas flow in pipe 11 tends to return to a value close to its initial condition because the source embedded at node 8 is constant. Unlike the almost instantaneous transient response when using the MP-AFE model, a small transient occurs when using the injection model because of the drastic reduction of gas injected into pipeline 11: $q_{8,9}^{Tot,11} < q_{9,8}^{Tot,11}$. The opposite occurs in pipeline 10: $q_{8,9}^{Tot,10} > q_{9,8}^{Tot,10}$. The information mentioned above is schematically shown in Figure 5.13, where the difference between the inlet and outlet gas flows of each pipeline is reported.

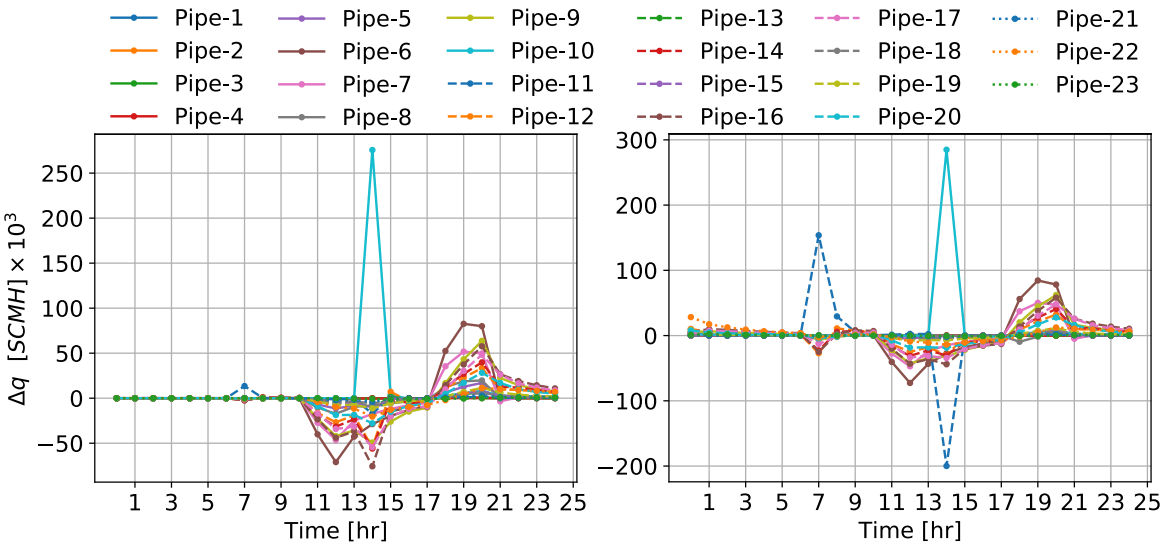

(a) MP-AFE model (b) MP-NFI model

Figure 5.13: Difference between inlet and outlet gas flows by pipeline.

Note also from Figure 5.13 that the pipeline fault generates only a small transient in pipe 11 when using the MP-AFE model, while the difference between the inlet and outlet gas flow in pipe 11 is just over 150,000 SCMH for the MP-NFI model. This is because the gas flow through pipe 10 is now injected into pipe 11. When the fault is cleared, it can be observed in both models that $q_{89}^{Tot,10} > q_{98}^{Tot,10}$, which is consistent with the fact that pipe 10 was empty when it was reconnected. Another consequence of the pipeline's reconnection is that $q_{89}^{Tot,11} < q_{98}^{Tot,11}$. This is because of the system's inertia and because ducts 10 and 11 are parallel connected. Note that this transient is unobservable with the MP-AFE model.

Regarding the magnitudes of the nodal gas pressures, it is shown in Figure 5.14 that the fault has a substantial impact on the gas pressure at node 8, which rises considerably to inject the same amount of gas but through a single pipeline and in less time. This involves raising the pressure and compression of gas to increase the speed and thus satisfy the demand. Unlike the MP-AFE model where only the gas pressure at node 8 is affected, the sudden increase of gas pressure at node 8 causes a slight pressure drop at various nodes in the network, especially those close to the fault: nodes 9 and 10. Furthermore, while in

the MP-AFE model the pressure at node 8 stabilizes almost immediately to a new operating condition, the transient response associated with the MP-NFI model tends to stabilize at the 10th hour: it has a delay of 3 hours.

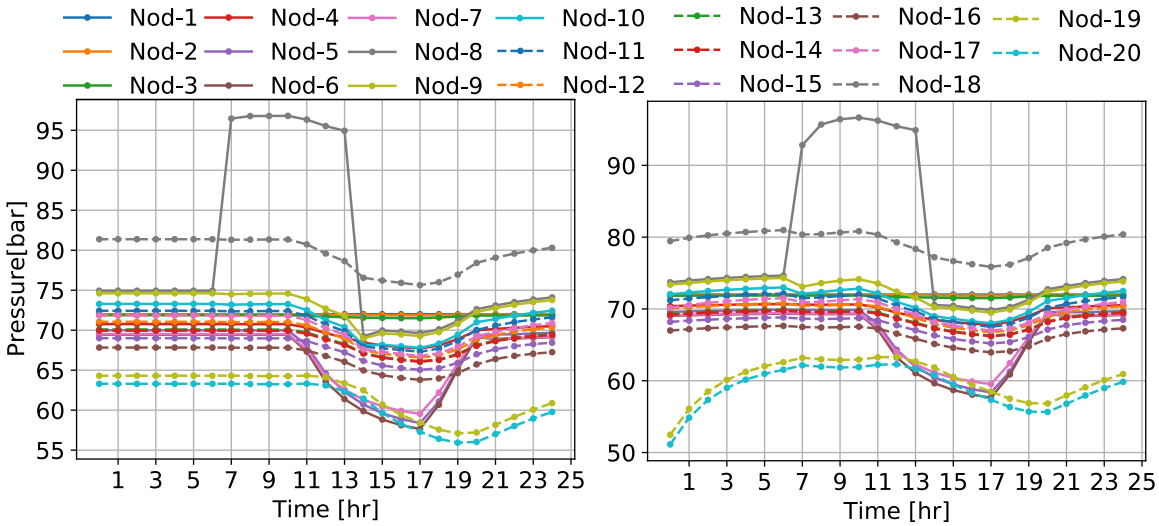

(a) MP-AFE model

(b) MP-NFI model

Figure 5.14: Nodal pressures.

On the other hand, the compressibility factor at node 8 is significantly reduced because of the fault occurrence, as shown in Figure 5.15. This implies that the gas is in a state of greater compression because the same amount of gas that circulated through two pipes must now circulate through only one. On the contrary, when the pipeline is reconnected at the 14th hour, the compressibility factor at node 8 increases such that the gas is in a lower state of compression because the amount of gas supplied by the source is distributed through two pipes again. Lastly, the state of gas compression at node 8 changes almost instantaneously in the MP-AFE model, while this state has a small transient that affects the gas compression at several nodes of the network when using the MP-NFI model.

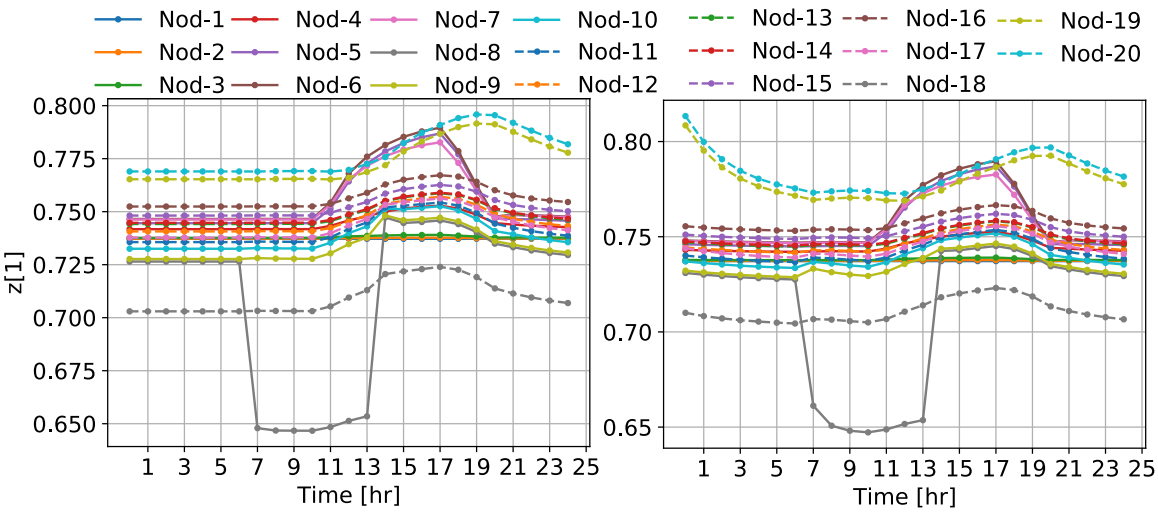

(a) MP-AFE model (b) MP-NFI model

Figure 5.15: Compressibility factor by node.

Figure 5.16 shows the transient behavior of the total system's linepack. When the MP-NFI model is used, the linepack has an initial transient behavior with a tendency to stabilize at a value close to 19.4 MSCM. The fault occurrence produces a total linepack's reduction, which tends to stabilize in the next 3 hours to a value close to 19 MSCM. As a consequence of the increase in gas demand, the system's total storage is further reduced until the 13th hour. The strong trend in decreasing storage is interrupted at the 14th hour when the fault is cleared. On the other hand, the MP-AFE model cannot observe this transient behavior: the total linepack goes from one stable operating condition to another at the fault inception.

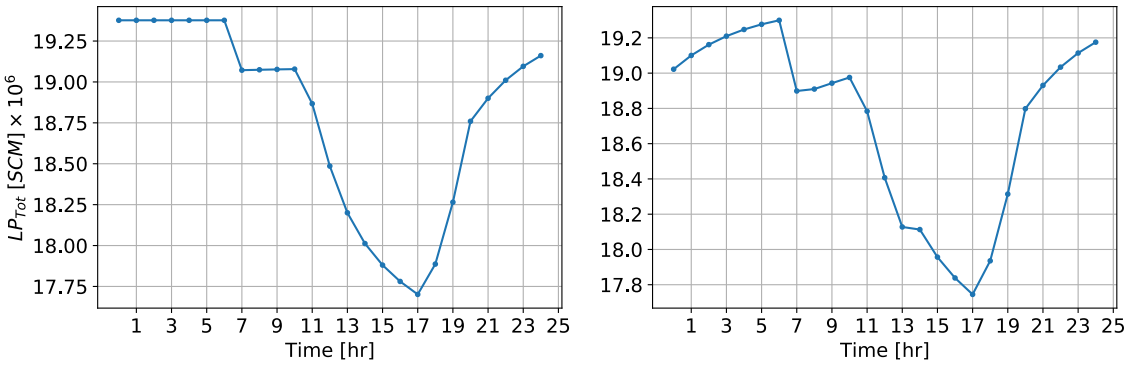

(a) MP-AFE model (b) MP-NFI model

Figure 5.16: Total linepack in the network.

Finally, the gas supplied by the source connected to node 1 during the entire period of study is reported in Figure 5.17 for both MP-AFE and MP-NFI models. Regarding the latter model, observe that as the system stabilizes the gas source varies in the period of constant demand, and, after the disconnection of pipeline 10, the gas injection provided by the source increases to satisfy the transitory effect. Meanwhile, the gas supplied by the source remains constant in the MP-AFE model during this study period.

When the increase in demand occurs, the gas supplied by the source in the MP-AFE model is less than the gas supplied in the MP-NFI model. When pipeline 10 is reconnected, however, the gas source in the MP-NFI model is reduced to a lower value than that provided in the MP-AFE model. This occurs because during the post-fault period the gas pressure decreases and causes a gas decompression, which demands less gas from the source.

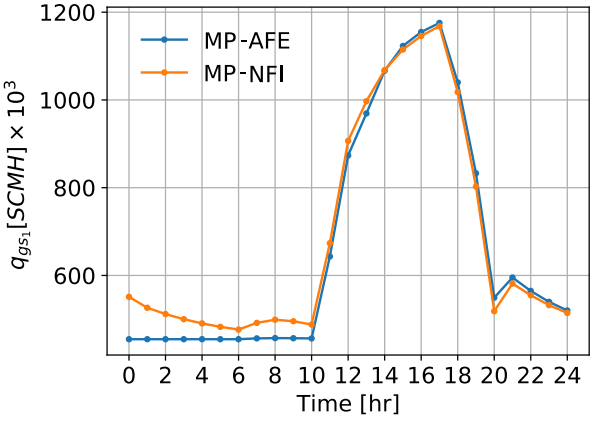

Figure 5.17: Natural gas source in node 1.

5.3 Integrated natural gas and power flow methodology

The equilibrium equations that must be fulfilled at each discrete time to describe the multi-period behavior of the gas and electricity systems, as well as the integration and solution of these equations in a unified framework of analysis, are summarized in this section.

5.3.1 Natural gas network

For the proposed formulation, the system is assumed to be composed of pipelines, compressors, sources and demands. The storage reservoirs can be modeled as gas sources or gas demands according to their operating condition.

Pipeline

- Multi-period average flow equation (MP-AFE) model

$$q_{km}^{Tot}(t) = \alpha \frac{\left(p_k^2(t)\beta_k - p_m^2(t)\beta_m + p_k(t)p_m(t)\beta_{km}\right)}{\left|p_k^2(t)\beta_k - p_m^2(t)\beta_m + p_k(t)p_m(t)\beta_{km}\right|^{\frac{1}{2}}}\epsilon + \left(\frac{LP_{km}^{avg}(t) - LP_{km}^{avg}(t^*)}{2\Delta t}\right) = 0 \quad (5.36)$$

$$q_{mk}^{Tot}(t) = \alpha \frac{\left(p_k^2(t)\beta_k - p_m^2(t)\beta_m + p_k(t)p_m(t)\beta_{km}\right)}{\left|p_k^2(t)\beta_k - p_m^2(t)\beta_m + p_k(t)p_m(t)\beta_{km}\right|^{\frac{1}{2}}}\epsilon - \left(\frac{LP_{km}^{avg}(t) - LP_{km}^{avg}(t^*)}{2\Delta t}\right) = 0 \quad (5.37)$$

- Multi-period nodal flow injection (MP-NFI) model

$$q_{km}^{Tot}(t) = \alpha \frac{\left(p_k^2(t)\beta_k - p_m^2(t)\beta_m + p_k(t)p_m(t)\beta_{km}\right)}{\left|p_k^2(t)\beta_k - p_m^2(t)\beta_m + p_k(t)p_m(t)\beta_{km}\right|^{\frac{1}{2}}}\epsilon + \left(\frac{LP_{km}^{avg}(t) - LP_{km}^{avg}(t^*)}{2\Delta t}\right) = 0 \quad (5.38)$$

$$q_{mk}^{Tot}(t) = \alpha \frac{\left(p_k^2(t)\beta_k - p_m^2(t)\beta_m + p_k(t)p_m(t)\beta_{km}\right)}{\left|p_k^2(t)\beta_k - p_m^2(t)\beta_m + p_k(t)p_m(t)\beta_{km}\right|^{\frac{1}{2}}}\epsilon - \left(\frac{LP_{km}^{avg}(t) - LP_{km}^{avg}(t^*)}{2\Delta t}\right) = 0 \quad (5.39)$$

Compressor stations

- Compression ratio (CR)

$$CR(t) = \frac{p_D(t)}{p_S(t)} \quad (5.40)$$

- Brake horsepower (BHP)

$$BHP(t) = \frac{p_0}{T_0}\frac{z_{comp}(t)T_s}{E\eta}\left(\frac{\kappa}{\kappa-1}\right)\left[\left(CR(t)\right)^{\frac{\kappa-1}{\kappa}} - 1\right]q_{comp}(t) = BHRCq_{comp}(t) \quad (5.41)$$

- Specific consumption function (gas consumed by the compressor)

$$\tau_{comp}(t) = \alpha_c + \beta_c BHRCq_{comp}(t) + \gamma_c\left(BHRCq_{comp}(t)\right)^2 \quad (5.42)$$

5.3.2 Electricity network

Considering that the dynamics of natural gas in pipelines evolve slowly, the time period of study has been divided into periods of 1 hour. On the other hand, the steady-state model is used for the electrical infrastructure under the assumption that electricity

travels at the speed of light. In this context, the electric power system is modeled by using the AC nodal power flow formulation but including the generators' model with primary frequency regulation and loads dependent on the nodal voltage magnitude and frequency. Furthermore, a control scheme to maintain the system frequency within its operating limits during the entire period of study is included in the formulation. This formulation is referred to as frequency regulated power flows with frequency control (FRPF with FC). The proposed frequency control scheme and the power equations associated with these two electrical components were described in Section 3.3 of Chapter 3.

5.3.3 Coupling between natural gas and electricity networks

The interdependence between the natural gas and electricity networks is provided by the plants operating with gas turbine-driven generators. This interdependence is mathematically formulated at the coupling point by the heat rate curve expressed by the energy conversion process's efficiency of the power plant. Hence, the efficiency for the time period "t" is given by the ratio of the active power injected into the i-th bus of the electrical network and the natural gas demanded from the k-th node of the gas network:

$$q_{req_k/P_{G_i}}(t) = \frac{F\left(P_{G_i}(t)\right)}{GHV} = \frac{a + bP_{G_i}(t) + cP_{g_i}^2(t)}{GHV}. \tag{5.43}$$

On the other hand, the coupling of the gas system to the electrical system is provided by the active power demanded by the n-th compression station connected to the i-th bus of the electrical network. Assuming that the compressor station connected between nodes "k" and "m" is driven by electric motors, the conversion of mechanical energy to electrical power for the time period "t" is given by [Menon05]:

$$\mathrm{P}_{L_i/comp_{km}}(t) = BHP_{km}(t)\,\frac{745.7}{P_{base}\times 10^6}\,[p.u.]\,. \tag{5.44}$$

Finally, the gas demanded by gas-fired generating units is limited to the amount of gas available and/or to the amount of gas that the system is capable of delivering at a given time. This operational constraint is considered in the proposed approach by adding the inequality constraint (5.45), which implicitly limits the active power that can be delivered

by the generator to the electric power system:

$$q_{gl_k}^{min} < q_{gl_k}(t) + q_{req_k/P_{G_i}}(t) < q_{gl_k}^{\max}. \tag{5.45}$$

5.3.4 Unified multi-period electricity and natural gas network model

The natural gas and electric power flows' multi-period problem is formulated in a unified solution framework through two sets of nodal mismatch equations associated with gas and electricity networks, respectively, which are interrelated through (5.43), (5.44) and constraint (5.45). Hence, the set of electric power flow mismatch equations at the i-th bus of the electrical network for the time period "t" is given by (5.46) and (5.47):

$$\Delta P_i(t) = \sum P_{G_i}(t) - \sum P_{L_i}(t) - \sum_{j\in i} P_{ij}^{cal}(t) - \sum_{k\in i} \mathrm{P}_{L_i/comp_{km}}(t) = 0, \quad \forall i \in N_e, \tag{5.46}$$

$$\Delta Q_i(t) = \sum Q_{G_i}(t) - \sum Q_{L_i}(t) - \sum_{j\in i} Q_{ij}^{cal}(t) = 0, \quad \forall i \in N_e. \tag{5.47}$$

Similarly, the natural gas flow mismatch equations at the k-th node of the gas infrastructure are given by (5.48) and (5.49) for the time period "t":

$$\begin{aligned}\Delta q_k(t) = &\sum_{m\in k} q_{km}^{Tot}(t) + \sum_{comp\in k} q_{comp_k}(t) + \sum_{comp\in k} \tau_{comp_k}(t) \\ &- \sum_{gs\in k} q_{gs_k}(t) + \sum_{gl\in k} q_{gl_k}(t) \sum_{i\in k} q_{req_k/P_{G_i}}(t) = 0, \quad \forall k \in (N_g - 1), \text{ and}\end{aligned} \tag{5.48}$$

$$\Delta CR_{km}(t) = -p_k(t) CR_{km} + p_m(t) = 0, \quad \forall k, m \in Nc, \tag{5.49}$$

where the first term of Eq. (5.48) corresponds to the gas flow leaving or reaching the k-th node through the pipelines connected to the node. According to the type of model used for representing the gas flow (the MP-AFE or MP-NFI model), this term is replaced by Eq. (5.16) or by Eq. (5.20), respectively.

Lastly, the set of nonlinear algebraic equations composed of (5.46), (5.47), (5.48) and (5.49) is linearized through the Newton-Raphson method to obtain the set of linearized algebraic equations (5.50). This system of equations is iteratively solved for each time period "t" until a specified mismatch tolerance is satisfied or a maximum number of iterations is reached:

$$\begin{bmatrix} \Delta\theta \\ \Delta v \\ \Delta v_a \\ \Delta v_b \\ \Delta p \\ \Delta q_{comp} \\ \Delta(\Delta f) \end{bmatrix} = - \begin{bmatrix} \frac{\partial \Delta P}{\partial \theta} & \frac{\partial \Delta P}{\partial v} & 0 & 0 & 0 & \frac{\partial \Delta P}{\partial q_{comp}} & \frac{\partial \Delta P}{\partial \Delta f} \\ \frac{\partial \Delta Q}{\partial \theta} & \frac{\partial \Delta Q}{\partial v} & \frac{\partial \Delta Q}{\partial v_a} & \frac{\partial \Delta Q}{\partial v_b} & 0 & 0 & \frac{\partial \Delta Q}{\partial \Delta f} \\ \frac{\partial \phi_{Q_G}^{min}}{\partial \theta} & \frac{\partial \phi_{Q_G}^{min}}{\partial v} & \frac{\partial \phi_{Q_G}^{min}}{\partial v_a} & \frac{\partial \phi_{Q_G}^{min}}{\partial v_b} & 0 & 0 & 0 \\ \frac{\partial \phi_{Q_G}^{max}}{\partial \theta} & \frac{\partial \phi_{Q_G}^{max}}{\partial v} & \frac{\partial \phi_{Q_G}^{max}}{\partial v_a} & \frac{\partial \phi_{Q_G}^{max}}{\partial v_b} & 0 & 0 & 0 \\ 0 & 0 & 0 & 0 & \frac{\partial \Delta q}{\partial p} & \frac{\partial \Delta q}{\partial q_{comp}} & \frac{\partial \Delta q}{\partial \Delta f} \\ 0 & 0 & 0 & 0 & \frac{\partial \Delta RC}{\partial p} & \frac{\partial \Delta RC}{\partial q_{comp}} & 0 \\ \frac{\partial \Delta P_{G_{ref}}}{\partial \theta} & \frac{\partial \Delta P_{G_{ref}}}{\partial v} & 0 & 0 & 0 & 0 & \frac{\partial \Delta P_{G_{ref}}}{\partial \Delta f} \end{bmatrix}^{-1} \begin{bmatrix} \Delta P \\ \Delta Q \\ \phi_{Q_G}^{\min} \\ \phi_{Q_G}^{\max} \\ \Delta q \\ \Delta RC \\ \Delta P_{G_{ref}} \end{bmatrix}. \tag{5.50}$$

Case study

The performance of the proposed multi-period unified model is numerically demonstrated by analyzing the multi-energy system composed of the 15-node gas network and the IEEE 118-bus electricity network. These two systems are interconnected as shown in Figure 5.18.

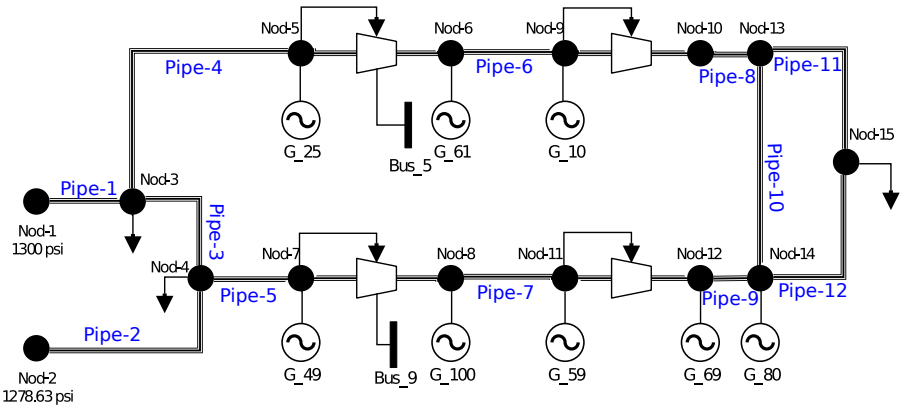

Figure 5.18: The 15-node gas network coupled with the IEEE 118-bus network.

For this case study, it is considered that the typical hourly variation of the total electricity load is as shown in Figure 5.19, where the nodal loads change at a constant power factor.

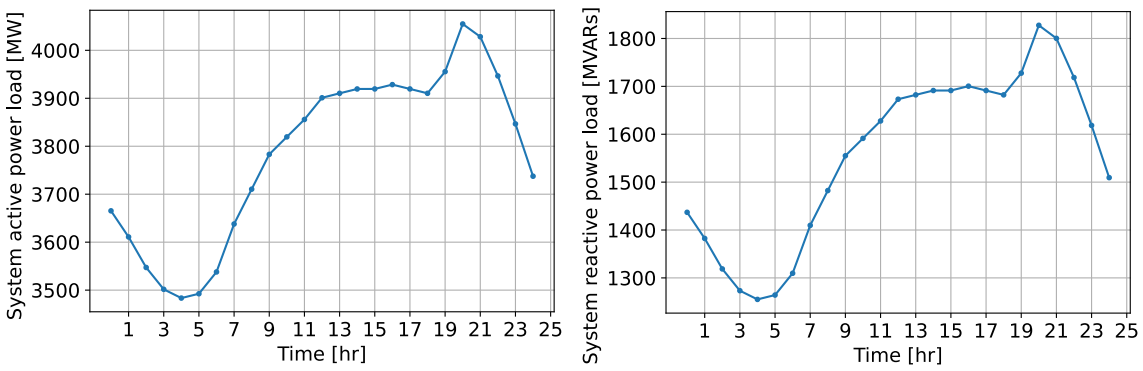

(a) Active power load. (b) Reactive power load.

Figure 5.19: Electric power load characteristic for a 24-hour period.

To compare the performance of both transient gas flow models, gas demand variations are considered solely a function of the fuel demanded by gas-fired generators. Other types of gas loads are considered constant throughout the entire study period. Similarly, it is assumed that the gas system can supply all gas demanded by the electric generators: the limitation imposed by the restriction (5.45) does not affect the multi-energy system's performance for this case study. Furthermore, since the electrical system is only affected by the gas system through variations in the electric power consumption of the compression stations, only the electric power system's behavior is reported for the studies performed with the MP-AFE and MP-NFI models. Lastly, the initial conditions for the multi-period study correspond to the base case data and solution reported in Section 4.4.2 of Chapter 4.

Figure 5.20 shows the system's frequency profile for the entire period of study. As expected, the frequency changes in the opposite direction to load changes. When the load is decreasing (resp. increasing), the generators speed up (resp. slow down), and the system's frequency value increases (resp. decreases) to a value defined by the steady-state error associated with the primary frequency control. Note that the load changes abruptly in between the 19th and 20th hour, which produces the largest frequency excursion with respect to its nominal value.

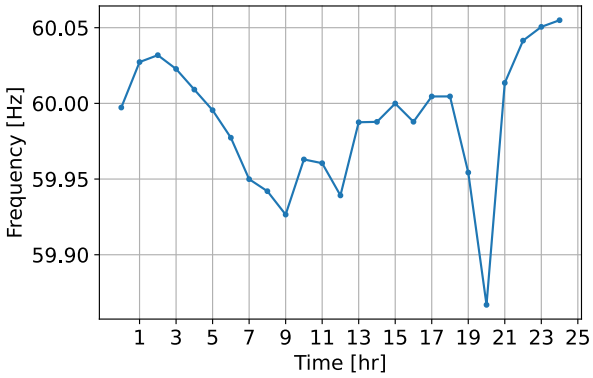

Figure 5.20: Electrical system frequency.

The profiles of active power generation are reported in Figure 5.21, where Figure 5.21a shows the generation of all units connected to the system and Figure 5.21b only shows the active power of those generators participating in the frequency regulation. Figure 5.21a shows that the active power of all generators that do not participate in frequency regulation remains constant during the entire study period. On the other hand, the regulated generators follow up the load demand changes, as shown in Figure 5.21b. Note, however, that the equilibrium point associated with the unified multi-period electricity and natural gas network model is achieved at a frequency value different than 60 Hz, as reported in Figure 5.20. Lastly, some generators such as 25, 49, 66, 69, and 100 always operate near their maximum limits. Hence, when an increase in electricity load occurs, these generators are set at their maximum limit, and they are unable to regulate frequency. Therefore, generators like 26, 65, and 80 have more abrupt variations in their active power to satisfy the electrical load.

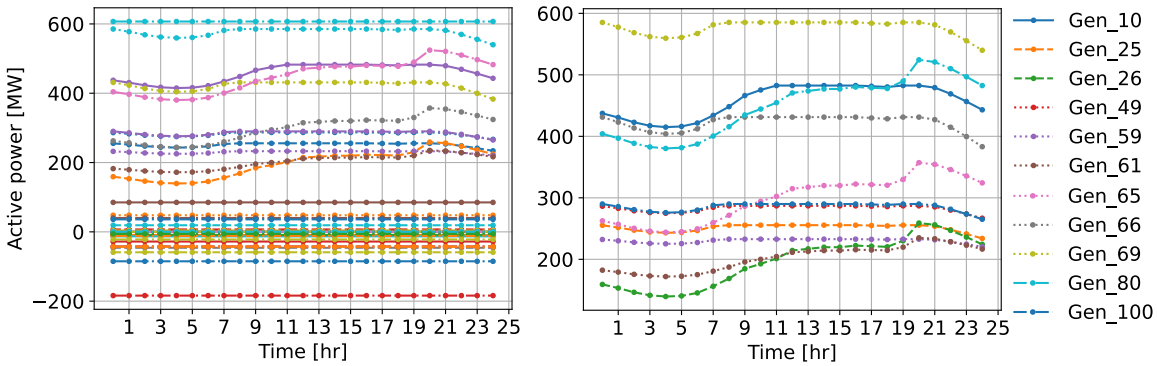

(a) All units of the electrical system (b) Generators in primary frequency regulation

Figure 5.21: Active power supplied by system units.

Similarly, Figures 5.22a and 5.22b show the reactive power generated by all synchronous machines connected to the system and by those only providing primary frequency regulation, respectively. As expected, the generators with frequency regulation present the more significant variation of reactive power, with generators 26, 65, and 80 providing the greatest support of reactive power. When generators reach their maximum active power limit (e.g., 10, 66, and 69), they maintain their reactive power support to regulate voltage magnitude instead of the system's frequency: these generators become type 1 during the gas and power flows solution process.

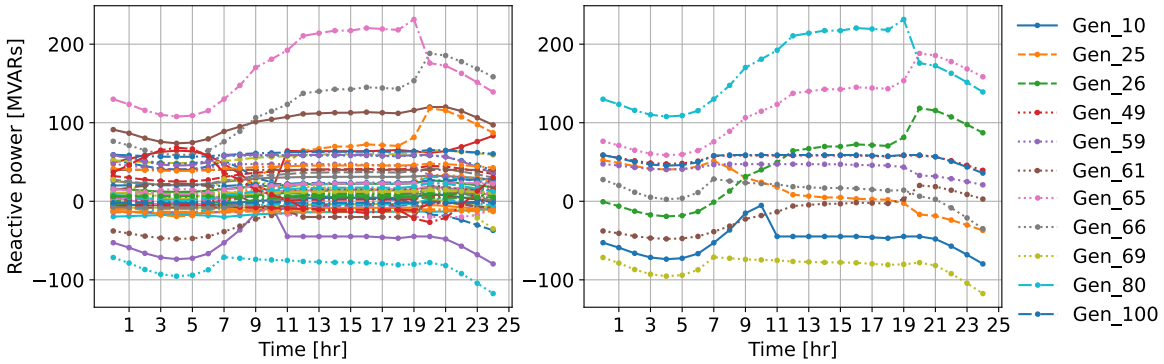

(a) All units of the electrical system (b) Generators in primary frequency regulation

Figure 5.22: Reactive power supplied by system units.

The consumption of natural gas by generators with primary frequency control is reported in Figure 5.23. Since these generators' active power changes according to variations in power demand, the gas consumption is changing in the same proportion. Note that only generators 61 and 80 follow up the load changes during the entire study period because the rest of the generators violate their active power limit at some time. In this case, the constrained generators maintain a constant demand for gas over time until they are back within their active power operational limits.

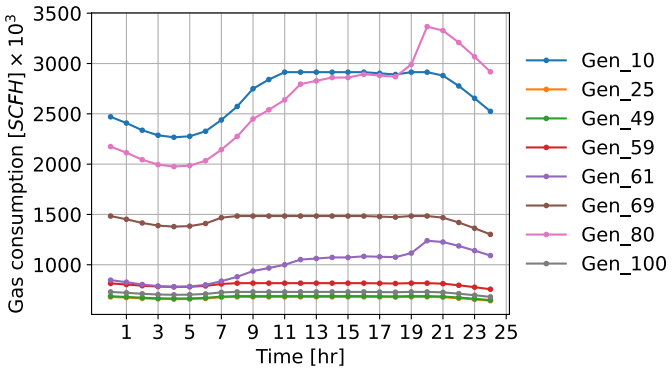

Figure 5.23: Gas consumption by gas-fired generators.

The differences between using MP-AFE and NFI -MP models in the proposed formulation can be deduced by analyzing the gas that flows through pipelines, which is reported in Figures 5.24 and 5.25. The gas flows remain almost invariant during the first 6 hours when using the MP-AFE model, while transient flows are observed in the same period of time in all pipelines when the analysis is performed using the MP-NFI model. This is because the MP-AFE model starts from a complete balance between the inlet and outlet gas flows in each pipeline. In contrast, the MP-NFI model starts from an initial state ruled by the pressure and compressibility conditions to which the gas is subjected, as well as the difference between each pipeline's inlet and outlet gas flows.

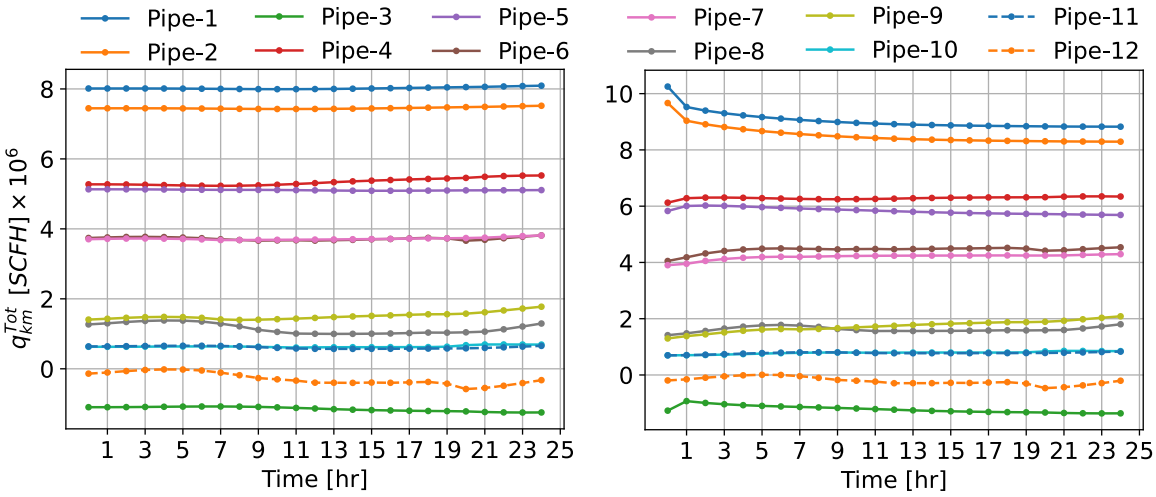

(a) MP-AFE model (b) MP-NFI model

Figure 5.24: Natural gas flows from node "k" to node "m".

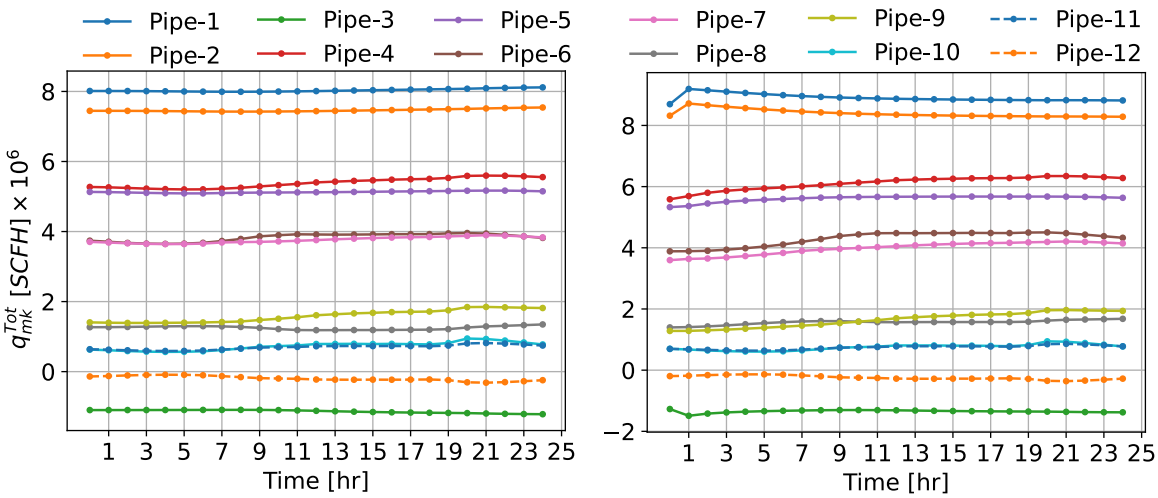

(a) MP-AFE model (b) MP-NFI model

Figure 5.25: Natural gas flows from node "m" to node "k".

Although the difference between the inlet and outlet gas flows of both models responds to changes in electrical load, this factor is lower with the MP-AFE model, as shown in Figure 5.26, because the electricity load effects occur in an initial state of zero difference between the gas flows of the pipelines. When there is a decrease (resp. increase) in the electrical load, the inlet gas flow is greater (resp. lower) than the outlet gas flow.

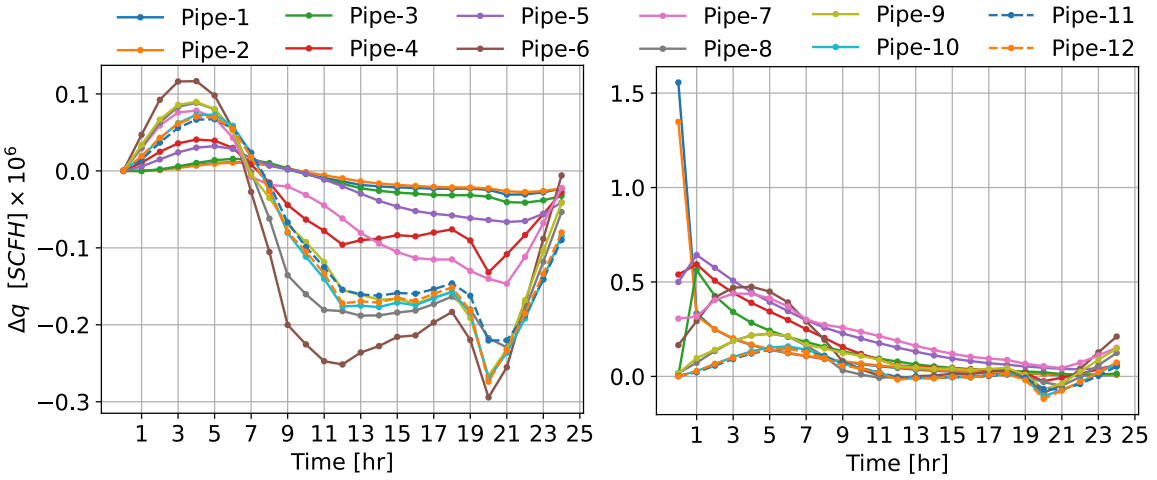

(a) MP-AFE model (b) MP-NFI model

Figure 5.26: Difference between inlet and outlet gas flows by pipeline.

The nodal pressures profiles are reported in Figure 5.27, where almost constant nodal pressures are observed during the first 9 hours for the MP-AFE model. The pressures begin to decrease from the 10th hour as a consequence of the increment in electric power demand, which in turn increases the generation of electric power and the amount of gas demanded by these generators. On the other hand, there is an increasing profile in the nodal pressures during the first 9 hours for the MP-NFI model, which is interrupted from the 10th hour because of the electric demand increase.

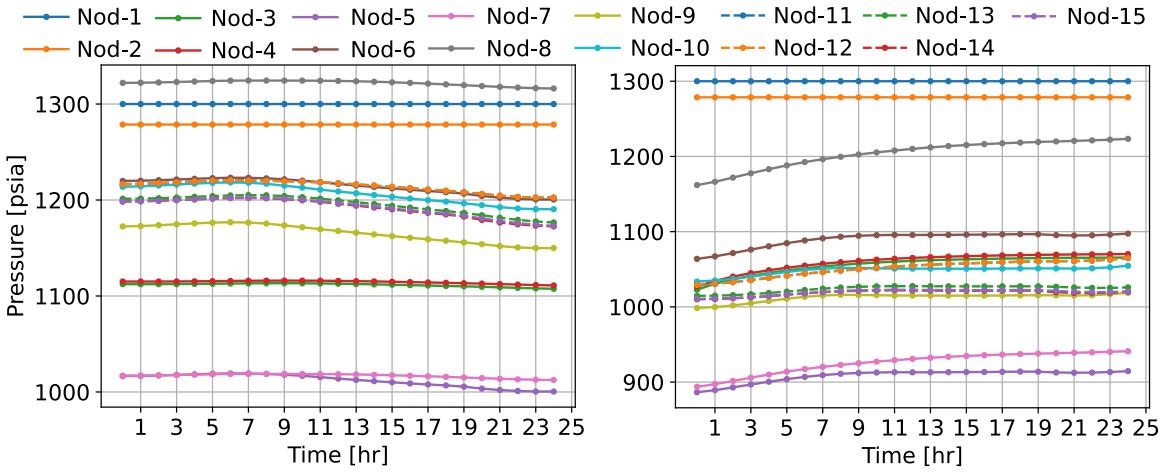

(a) MP-AFE model

(b) MP-NFI model

Figure 5.27: Nodal pressures.

Finally, the linepack transient behavior is reported in Figure 5.28a for both models of transient gas flow. For the MP-AFE model, the linepack starts from an initial value close to 1070 MSCF at which the equilibrium state is satisfied. As a consequence of the decrease in electric power demand in the first 4 hours, the gas flow at the inlet ends of pipelines is bigger than at their corresponding outlet ends such that the system's linepack increases. Even though the load starts increasing from the 5th hour, the linepack has its maximum value at the 7th hour because of the inertial response of the gas system. In between the 8th and 24th hour, the system's linepack has a clear decreasing trend, which is more pronounced during peak demand hours.

When the MP-NFI model is used to represent the gas flow transient behavior, the system's linepack starts from an initial state close to 910 MSCF, and it has an increasing linear trend for the first 5 hours, even when the electric demand is decreasing during the first 4 hours. The linepack's growth rate is reduced with the increment of electric demand at the 5th hour, and there is a small transitory decrease during the peak load hours. This transient response reaches its minimum value at the 21st hour, 1 hour after the peak electricity load, because of the gas system's inertial response.

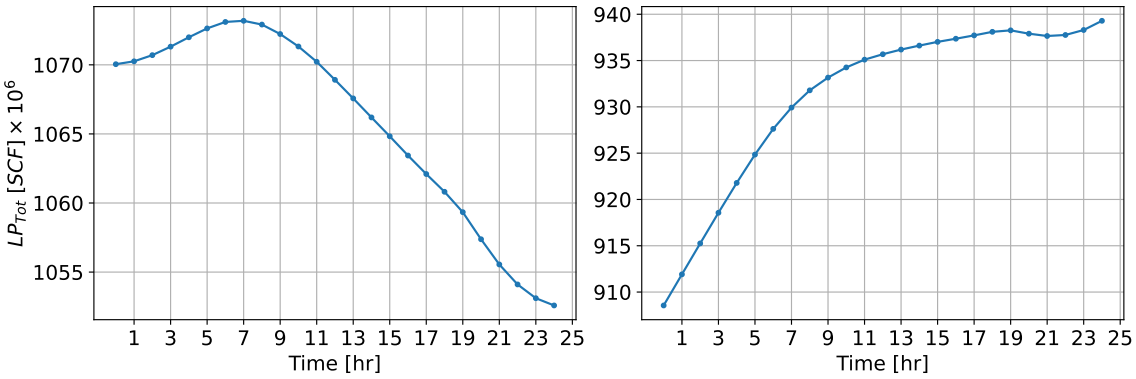

(a) MP-AFE model (b) MP-NFI model

Figure 5.28: Total linepack in the network.

Case study 2

The case study previously reported is newly analyzed in this section but considers load shedding and load connections in different nodes. Furthermore, the transient of gas flows is represented by the MP-NFI model. A load shedding of $89.7+j29.7$ and $276.7+j112.7$ is performed at the 7th hour in nodes 15 and 59, respectively, with a reconnection at the 8th hour. Electric loads connected to 14 and 85 are suddenly increased at 15th hour from $16.8 + j3.8$ and $26.8 + j17.8$ to $104 + j91$ and $55 + j45$, respectively. Finally, the loads connected to nodes 2 and 4, which correspond to $24.3 + j13.3$ and $34.3 + j16.3$, respectively, are completely disconnected from the system in between the 20th and 21st hour. The resulting profile for the active and reactive power system load is shown in Figure 5.29.

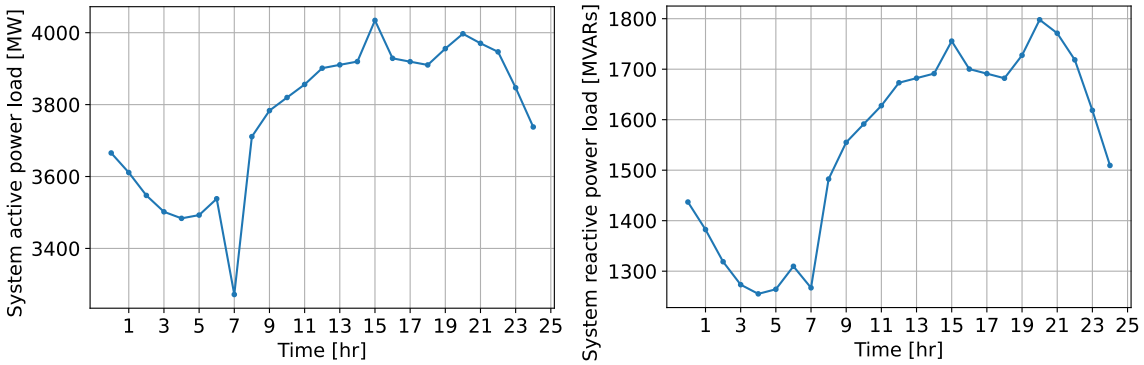

(a) Active power load (b) Reactive power load

Figure 5.29: Electric power load characteristic for a 24-hour period.

In addition, for this case study two operating scenarios are considered. First, the gas system can supply all the gas required by gas-fired generators. Second, the gas supplied to the electric system from gas nodes 6, 9 and 14 is limited to 1.8, 2.5 and 2.2 MSCFH, respectively.

The hourly frequency profile for those two scenarios is presented in Figure 5.30, where the same behavior is observed up to the 8th hour, 1 hour after the load shedding at nodes 15 and 59, where the frequency has its maximum excursion of 60.12 Hz. The load is reconnected at the 8th hour, producing a decrement in frequency to 59.76 Hz and 59.735 Hz for the unrestricted and restricted cases, respectively. At this operating point, generators are re-dispatched to bring the frequency to a value close to 60 Hz in both scenarios.

After the re-dispatch of active power, the electric load increases, and, because of the limitations imposed on the gas system, the frequency deviation at the 9th hour is considerably more significant with respect to the unrestricted case. Lastly, at the 15th hour, where the sudden increase in loads 14 and 85 occurs, a critical frequency drop is observed in the system. For the unrestricted case, the frequency drop is within its operating limits. In contrast, this contingency takes the frequency value to 59.762 Hz for the restricted case, which causes a new re-dispatch that modifies the programmed values of the active powers delivered by the generators to bring the frequency to a value close to the nominal. Finally, the frequency profile is very similar for the last study period for both scenarios.

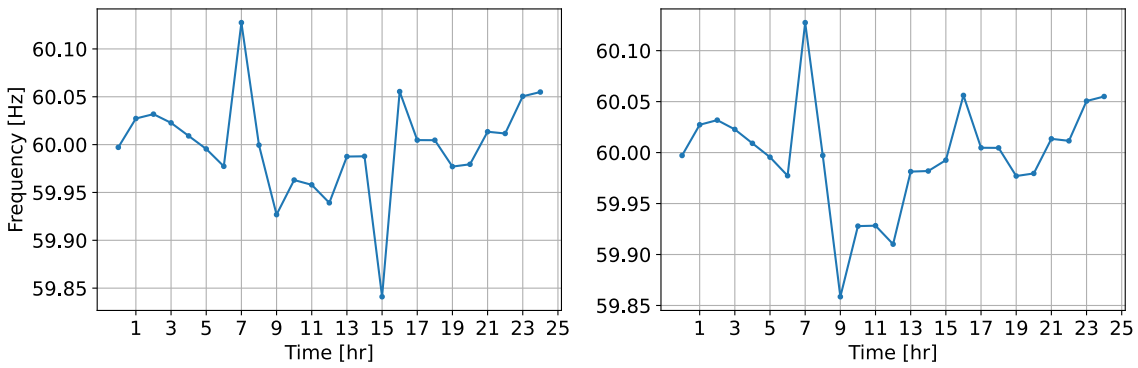

(a) Gas unrestricted unified model (b) Gas restricted unified model

Figure 5.30: Electrical system frequency.

Figure 5.31 shows the active power delivered by generators participating in the frequency regulation. Note that the active power profile is identical for the first 7 hours for both scenarios. From the 8th hour in the unrestricted case and with the continuous increase of electric demand, generators 49, 59, 66, 69, and 100 are set at their maximum active power limit, while generators 10, 26, 61, 65, and 80 are the only ones that follow up the electrical load. On the other hand, when fuel supply limits are considered, generators 10 and 80 are also set to their maximum deliverable active power capacity, which also occurs with generator 61 at the 15th hour. Therefore, generators 26, 61, and 65 are the only ones responding to variations in electrical load.

Lastly, Figure 5.31 clearly shows the sudden changes in active power associated with the load disturbances taking place at different times and generation re-dispatches to include the system's frequency value in its operating limits. Note also that after the 15th hour the generation profile of both models is not the same in terms of magnitude, but they have a similar trend behavior.

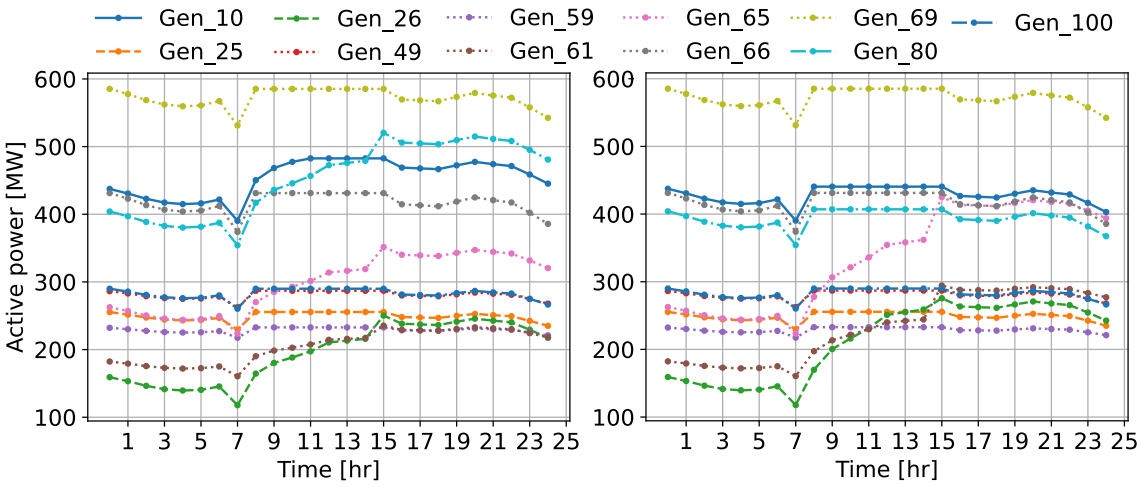

(a) Gas unrestricted unified model (b) Gas restricted unified model

Figure 5.31: Active power supplied by generators in primary frequency regulation.

Similar to the active power behavior, the reactive power generated in the first 7 hours is the same for both operating scenarios, as shown in Figure 5.32. Note, however, that the limitations imposed on the generation of active power also affect the ability to supply or absorb reactive power during periods where the electrical load is increasing. In this context, the generators set at their maximum active power limit show little variation in their reactive power delivery; hence, most of the reactive power demand is supplied by generators 26, 61, and 80 for the restricted case. Generators 10 and 80 supply a constant reactive power in between the 8th and 15th hour, which causes a significant increase in the reactive power generated by unit 61 to compensate the variations in the reactive power demand. This sudden change of generation in unit 61 is not proportional to the rate of change in reactive loads because of the following: i) other generators not using gas as primary energy also provide reactive power support (e.g., unit 26, 65 and 66), and ii) the heat rate curve is different for each generating unit. Even though some generators' reactive power support is limited by the availability of gas (e.g. units 10 and 80), other gas-fired generators are limited by their electrical capacity (e.g., unit 69) and not by the gas supply. Lastly, reactive power generation is proportional to changes in the reactive loads for the unrestricted case.

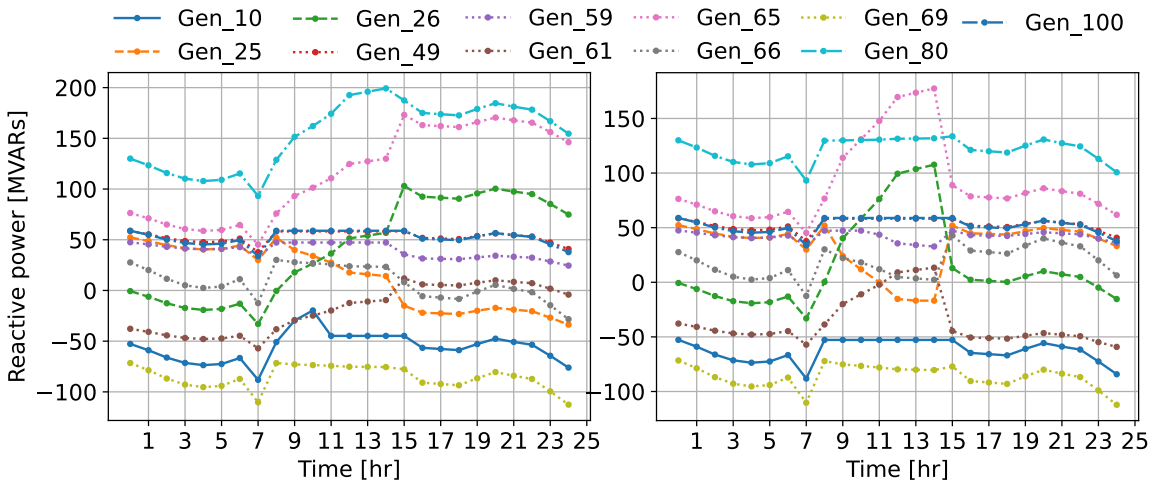

(a) Gas unrestricted unified model (b) Gas restricted unified model

Figure 5.32: Reactive power supplied by generators in primary frequency regulation.

The gas flow dynamics at the inlet and outlet ends of pipelines are shown in Figures 5.33 and 5.34, respectively. These results indicate that depending on the load disturbance the inlet or outlet gas flow is more affected. After the 7th hour, the gas flow results through pipes 4, 6, 8, 9 and 12 are different for both operating scenarios under study. This is because these pipelines supply a limited amount of gas to electric generators 10, 61 and 80 for the restricted case. Figure 5.33 shows that the inlet gas flows present sudden changes at the 7th and 15th hour because of the load shedding and load connections occurring at each of those hours, respectively. For the unrestricted case, the gas flow through pipeline 12 is the most affected by the increment of power demand because it is the one that supplies gas to generator 80, which has the most significant gas consumption in response to the sharp increase in electricity load. Note that this transient response is almost imperceptible in the restricted case. On the other hand, the same load increment does not significantly affect the inlet gas flow of pipe 4; however, the outlet gas flow rises in this pipe to satisfy the sudden increase in the gas demand from generator 61.

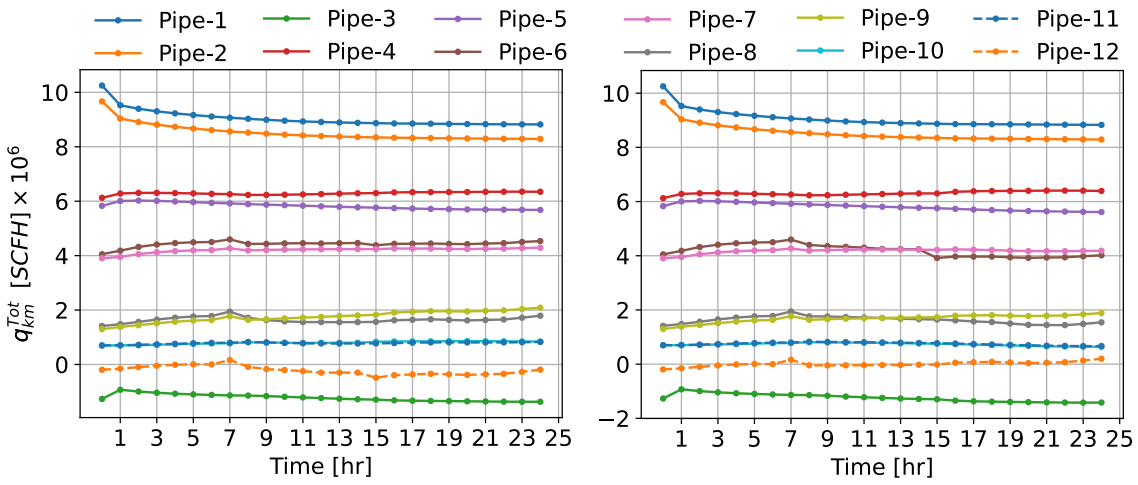

(a) Gas unrestricted unified model (b) Gas restricted unified model

Figure 5.33: Natural gas flows from node "k" to node "m".

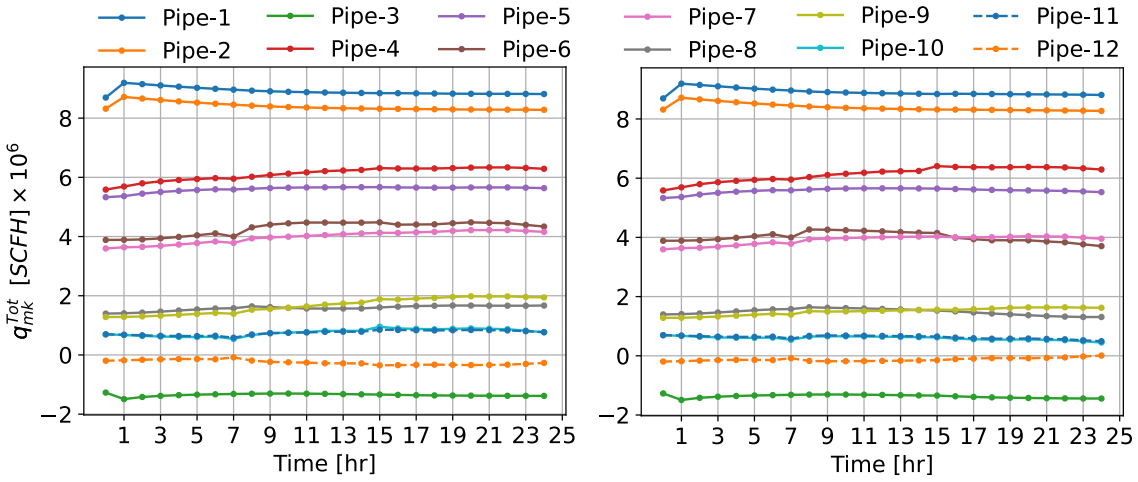

(a) Gas unrestricted unified model (b) Gas restricted unified model

Figure 5.34: Natural gas flows from node "m" to node "k".

The difference between the inlet and outlet gas flows of each pipe is shown in Figure 5.35 for both operating scenarios. As expected, this difference behaves as described above with respect to load variations. When a sudden decrease (resp. increase) in electrical load occurs, each pipe's inlet gas flow is greater (resp. lower) than the outlet gas flow. After a load disturbance, the system has a slower stabilization time when gas availability

is limited in some nodes. This limitation causes the corresponding generators to produce a constant active power, and only a small number of other generators will participate in the frequency regulation. Hence, when a disturbance occurs, the change of generation in those units will be larger, as will be their transitory behaviors.

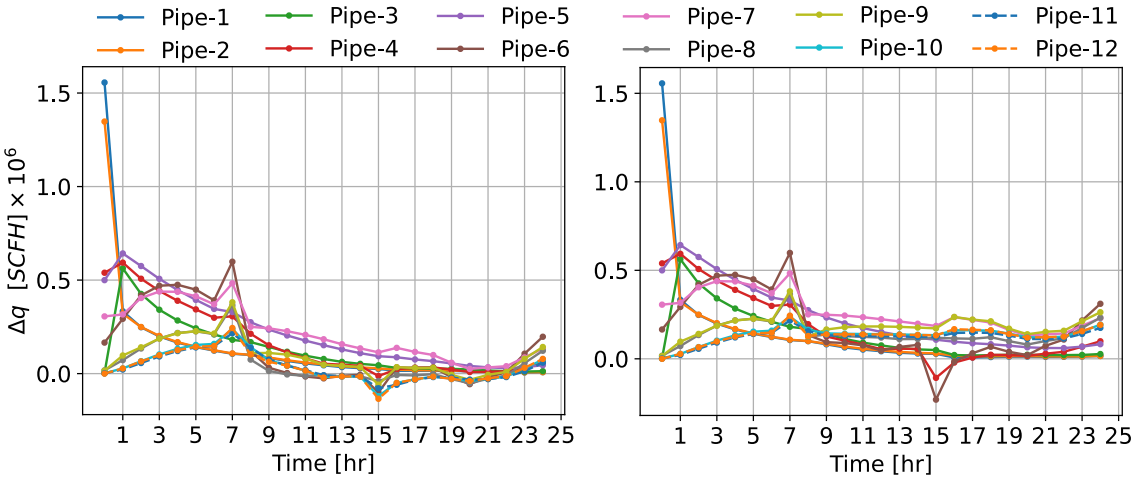

(a) Gas unrestricted unified model (b) Gas restricted unified model

Figure 5.35: Difference between inlet and outlet gas flows by pipeline.

The information mentioned above regarding the stabilization process after a load disturbance is also validated by the transient behavior of nodal pressures and the system's linepack shown in Figures 5.36 and 5.37, respectively.

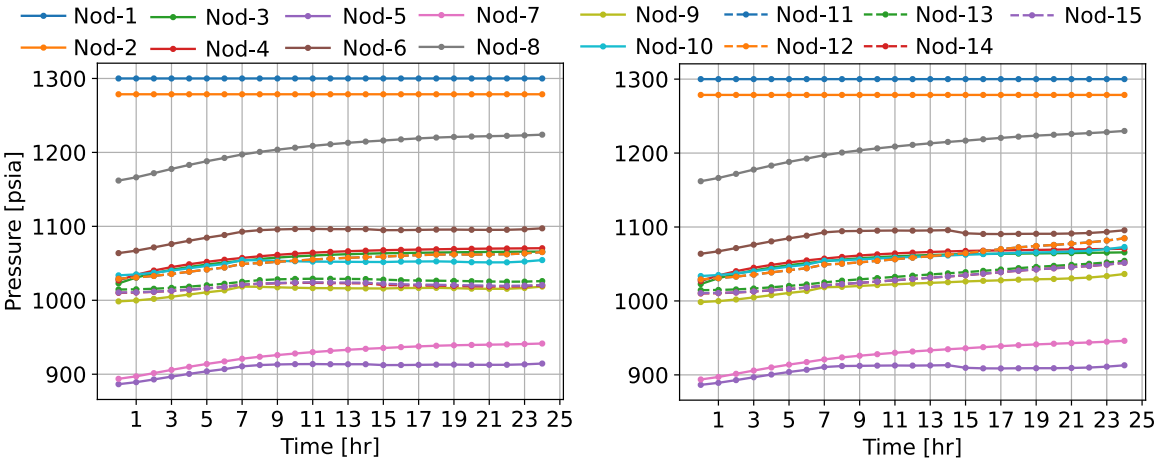

(a) Gas unrestricted unified model (b) Gas restricted unified model

Figure 5.36: Nodal pressures.

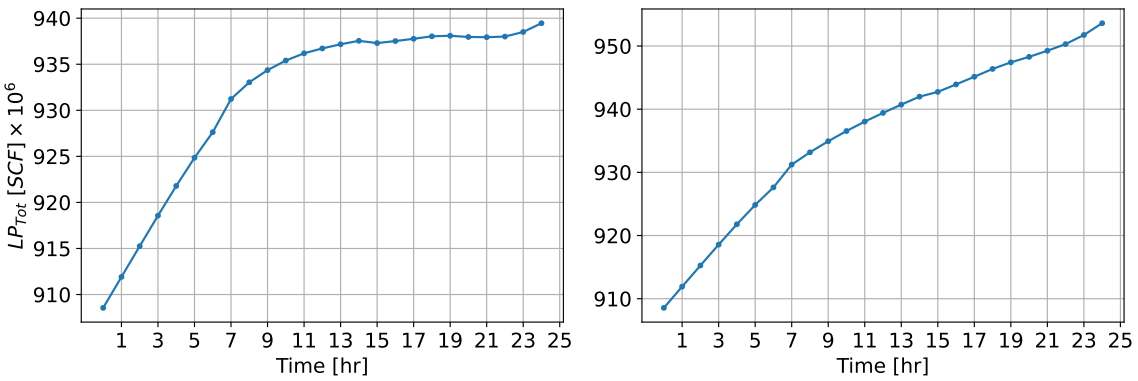

(a) Gas unrestricted unified model (b) Gas restricted unified model

Figure 5.37: Total linepack in the network.

5.4 Conclusions

A suitable multi-period formulation has been proposed in this chapter for solving the natural gas and electricity flows problem from a unified operation point of view.

A new mathematical model was developed regarding the natural gas network to describe the transient state of the natural gas transportation system. The model is based on three main aspects: i) the magnitude of the nodal gas flow injections q_{km}^{iny} and q_{mk}^{iny}, ii) the previous temporal state of the difference between the nodal gas flow injections $\Delta q\,(t-\Delta t)$, and iii) the temporal changes in gas storage contained in each pipeline $\Delta LP\,(t)$. Unlike other proposals where a set of nonlinear temporal/spatial partial differential equations is solved, or a set of equations and/or state variables are added to the problem formulation, the proposed model is formulated through two nonlinear algebraic equations that satisfy the moment and continuity equations. These equations depend solely on the nodal pressures, and they implicitly consider the direction of gas flows in pipelines as well as the difference between the inlet and outlet gas flows.

It has been numerically demonstrated that the transient gas model based on the NFI equations is more sensitive to disturbances associated with gas demand variations, the state of gas compression, and topological changes in the pipeline network, among others. On

the other hand, it has been also demonstrated that the model based on average gas flow magnitudes is only applicable when the system is operating in a state of equilibrium.

The proposed transient-state gas flow model was integrated into the power flow model with primary frequency regulation developed in the previous chapter. Based on this unified model, it was possible to assess the multi-energy system's interdependent transitory behavior when the boundary conditions change over time. In this context, the importance of considering the availability or limitation of gas demanded by generators participating in frequency regulation was highlighted, which could help make better decisions in the operation and control of multi-energy systems.

Chapter 6

General conclusions and future work

6.1 General conclusions

To help find solutions that more efficiently and realistically describe the operational interdependence between the electric power system and the infrastructure that provides the primary energy source, new ways of performing an integrated analysis of multi-energy systems must be proposed. In this context, an electricity and natural gas flow program results in a handy tool for evaluating how these two energy infrastructures interact with each other. This can help to operational and control decision-making from a global vision and achieve a more efficient, safe, and reliable use of the multi-energy system. Hence, a new approach for modeling and analyzing electricity and natural gas flows in a unified reference framework is proposed in this thesis.

Regarding the gas system model, a new mathematical approach was proposed to represent the natural gas transportation system more realistically. For the steady state, a new mathematical derivation based on the concept of "nodal flow injections" was developed, resulting in two equations to evaluate the operating state of a natural gas transportation network were obtained. The equations are referred to as nodal flow injection (NFI) equa-

tions, and they represent a new way of relating pressure drop and isothermal gas flows through pipelines. Unlike the gas flow equations currently developed and used in practice, which are based on average flow magnitudes and have a limited region of validity, the NFI equations consider the friction factor as a function of the gas operating regime. Furthermore, these equations are sensitive to the gas operating conditions and the gas pipeline network's physical properties. Similarly, these equations implicitly consider the possible bidirectionality of the gas flow and the inherent difference between each pipeline's inlet and outlet gas flow. The proposed NFI equations are also equally applicable to different operating regimes, pressure drop levels, and both low- as high-pressure systems.

Lastly, a new gas flow equation based on average magnitudes was also proposed, called the average flow equation (AFE), which proved to have better performance than the rest of the average gas flow equations developed so far.

On the other hand, the electricity network model no longer considers either the fixed active power injection into the electricity network or the constant power demands in the proposed approach. In this case, the dependency of electric loads with respect to frequency deviations and voltage magnitudes is fully considered. Furthermore, generators' primary frequency control is also taken into account by considering the generator-governor characteristics to perform the primary regulation of frequency. Lastly, a new way to consider reactive power limits as a function of changes in active power supplied by regulating generators was proposed.

A comprehensive solution for the steady-state gas and electric power flow problem was proposed from a centralized operation point of view. The interdependence between natural gas and electricity infrastructures is represented through the electricity demanded by compressor stations and the gas required by gas-fired plants to satisfy the electricity demand. In the latter case, the gas availability to generate electric power is also considered. In this context, the regulated generation of active power by gas-fired plants causes variations in the natural gas system's operating conditions, which are directly evaluated under the same

comprehensive study without the need for sequential simulations between electricity and natural gas networks

The case studies numerically demonstrate that considering frequency deviations directly affects the operational status of both energy infrastructures. The primary frequency regulation performed from an active power generation dispatch may not be sufficient to obtaining a viable multi-energy system operation. Hence, a control action approach was proposed to avoid the multi-energy system's unfeasible operation by maintaining the system's frequency within an established frequency band.

A suitable formulation to solve the multi-period problem of natural gas and electricity flows from a unified operation point of view was proposed. This proposal departs from a new mathematical model to describe the transient-state of the natural gas transportation system, which comprises only two nonlinear algebraic equations that solely depend on the nodal gas pressures. The proposed transient-state gas flow model was integrated into the power flow model with primary frequency regulation to assess the interdependent transient behavior of the multi-energy system

The previous description summarizes the proposals for conducting a study in a unified reference frame to assess natural gas and electricity systems' existing interdependence in both steady-state and transient-state operating regimes.

6.2 Future work

The work presented in this thesis is considered to provide a rock-solid foundation for future research related to the unified modeling and analysis of natural gas and electricity transportation systems.

Initially, it is considered that the proposed model of nodal gas flow injections could be extended with the inclusion and development of the topics below.

- To consider sectioning very long pipelines for a more precise analysis of the dynamics that governs the gas flows's behavior inside each duct [Menon05].

- To include the operating limits of the natural gas transportation system such as the following: maximum and minimum allowable operating nodal gas pressure, the gas flow limits through the pipeline and the maximum and minimum demands according to the properties and operating conditions of the network.

- To perform the calculation and automatic adjustment of the compression ratio of the compressor stations according to the needs and operating conditions of the gas network.

- To analyze gas flows from an economic context, considering price volatility and different suppliers so that, through a study similar to an economic dispatch, the fuel resources are assigned instead of using constant and reference sources.

- To propose an approach for handling the linepack of each pipeline as an energy store resource considering the pipeline maintenance, filling and commissioning times.

- To propose an approach for the analysis and detection of gas leaks using a differential scheme directly derived from the proposed nodal gas flow injection equations.

On the other hand, based on the proposed approach and the understanding of the operational interdependence between the electricity and natural gas networks, some proposals for future research are detailed below.

- To include the generation ramps, the turn on and turn off of generators, as well as the automatic voltage regulator (AVR) model, to more realistically represent the behavior of the units. Analyze the effect of these characteristics on the multi-energy system.

- To perform an integrated analysis of the multi-energy system from a context of optimal flows, with which operating costs are minimized, losses are reduced and the efficient use of natural gas is maximized. The above considering the operational limits and physical constraints of both infrastructures.

- To propose a suitable and fast approach to perform contingency analysis of multi-energy systems. The approach must evaluate the impact that disturbances that occur in one energy subsystem have on the other one and define control strategies that avoid cascading failures.

- To develop a model that quantifies the effect of integrating renewable energies on the consumption of natural gas by gas-fired generators.

- To design strategies for the dispatch of electric energy that minimize changes in the multi-energy system operation because of the intermittency of renewable generation and changes in the electric power demand

- To propose an approach to managing the linepack of each pipeline as an energy store resource to provide operational flexibility for the multi-energy system.

Appendix A

Deductions

A.1 Deduction of nodal flow injection equations

The equations of momentum and state of gases defined by (A.1) and (A.2) correspond to Newton's second law and to the relationship of pressure, temperature and density of the gas, respectively. In this case, (A.1) describes the sum of all forces acting on a gas particle inside a pipe:

$$\frac{\partial p}{\partial x} + g\rho\frac{\partial h}{\partial x} + \frac{\lambda\,|v|\,v}{2D}\rho + \frac{1}{A}\frac{\partial \dot{m}}{\partial t} + \frac{\partial\left(\rho v^2\right)}{\partial x} = 0 \tag{A.1}$$

$$\rho = \frac{p}{zR_{gas}T} \quad \text{and} \quad \rho_0 = \frac{p_0}{z_0 R_{gas} T_0}. \tag{A.2}$$

Now if (A.2) is substituted in the second term of the moment equation (A.1), which corresponds to the *force because of gravity* or *potential energy*, the following expression is obtained:

$$F_g = g\rho\frac{\partial h}{\partial x} = g\frac{p}{zR_{gas}T}\frac{\partial h}{\partial x}, \tag{A.3}$$

where "R_{gas}" is the specific gas constant defined by

$$R_{gas} = \frac{R}{M_{gas}}. \tag{A.4}$$

Furthermore,

$$R_{air} = \frac{R}{M_{air}} \quad \text{and} \quad G = \frac{M_{gas}}{M_{air}} \tag{A.5}$$

so that "R_{gas}" can be expressed as

$$R_{gas} = \frac{R_{air}}{G}. \tag{A.6}$$

Lastly, substituting (A.6) into (A.3) results in

$$F_g = g\frac{G}{R_{air}}\frac{\partial h}{\partial x}\left(\frac{p}{zT}\right). \tag{A.7}$$

Similarly, the velocity "υ" in the third term of (A.1) , which is referred to as the *shear force* or *friction force*, can be expressed as

$$\upsilon = \frac{\dot{m}}{A\rho} \tag{A.8}$$

where the mass flow "$\dot{m}$" is equal to

$$\dot{m} = \rho q_{real} \tag{A.9}$$

and in terms of standard conditions

$$\dot{m} = \rho_0 q_{st}. \tag{A.10}$$

Based on the aforementioned, the flow velocity can be expressed as

$$\upsilon = \frac{\rho_0 q_{st}}{\rho A}. \tag{A.11}$$

By substituting (A.2), (A.6) and (A.11) into the third term of the momentum equation, the friction force can be rewritten as

$$F_f = \frac{\lambda G p_0^2 zT}{2DA^2 R_{air} z_0^2 T_0^2 p}\left|q_{st}\right| q_{st}. \tag{A.12}$$

Lastly, a circular cross section of a pipeline is given by $A = \frac{\pi D^2}{4}$, so (A.12) is finally expressed as

$$F_f = \frac{8\lambda G p_0^2 zT}{\pi^2 D^5 R_{air} z_0^2 T_0^2 p}\left|q_{st}\right| q_{st}. \tag{A.13}$$

On the other hand, the fourth term of (A.1), referred to as the *inertial force*, is neglected because the mass flow "$\dot{m}$" remains constant for the steady-state operating condition.

Regarding the fifth term of (A.1), called the *convective term* or *kinetic energy*, if (A.2) and (A.11) are substituted into this term, the following equation is obtained:

$$\frac{\partial\left(\rho v^2\right)}{\partial x} = \frac{16Gp_0^2}{R_{air}z_0^2T_0^2\pi^2D^4}\frac{\partial q_{st}^2}{\partial x}\left(\frac{zT}{p}\right). \tag{A.14}$$

Lastly, by substituting (A.7), (A.13) and (A.14) into (A.1), the moment equation is given by

$$\frac{\partial p}{\partial x} + g\frac{G}{R_{air}}\frac{\partial h}{\partial x}\left(\frac{p}{zT}\right) + \frac{8\lambda Gp_0^2}{\pi^2D^5R_{air}z_0^2T_0^2}\left(\frac{zT}{p}\right)|q_{st}|\,q_{st} + \frac{16Gp_0^2}{R_{air}z_0^2T_0^2\pi^2D^4}\frac{\partial q_{st}^2}{\partial x}\left(\frac{zT}{p}\right) = 0 \tag{A.15}$$

Based on the pipeline shown in Figure 2.2 and assuming that the gas flow through this pipeline can be modeled by using the concept of gas flow injection at its inlet and outlet nodes, Eq. (A.15) can be rewritten in terms of nodal variables:

$$\begin{aligned}\frac{\partial p_{km}}{\partial x} + g\frac{G}{R_{air}}\frac{p_{k,m}}{T_{k,m}z\left(p_{k,m},T_{k,m}\right)}\frac{\partial h_{km}}{\partial x} + \frac{8\lambda_{km}Gp_0^2T_{k,m}z\left(p_{k,m},T_{k,m}\right)}{\pi^2D_{km}^5R_{air}z_0^2T_0^2p_{k,m}}|q_{st}|\,q_{st} + \\ + \frac{16Gp_0^2T_{k,m}z\left(p_{k,m},T_{k,m}\right)}{\pi^2D_{km}^4R_{air}z_0^2T_0^2p_{k,m}}\frac{\partial q_{st}^2}{\partial x} = 0\end{aligned} \tag{A.16}$$

By grouping the independent factors into general constants, G_{km}, A_{km} and B_{km}, (A.16) can be rewritten as

$$\begin{aligned}\frac{\partial p_{km}}{\partial x} + G_{km}\frac{p_{k,m}}{T_{k,m}z\left(p_{k,m},T_{k,m}\right)}\frac{\partial h_{km}}{\partial x} + A_{km}\frac{T_{k,m}z\left(p_{k,m},T_{k,m}\right)}{p_{km}}|q_{st}|\,q_{st} + \\ + B_{km}\frac{T_{k,m}z\left(p_{k,m},T_{k,m}\right)}{p_{k,m}}\frac{\partial q_{st}^2}{\partial x} = 0.\end{aligned} \tag{A.17}$$

By performing a spatially discretization of (A.17) by using the implicit Euler scheme and by taking as a reference the sum of forces acting on node "k", Eq. (A.18) and Eq. (A.19) are obtained, where $\partial x = \Delta x = L_{km}$ was assumed to be,

$$\begin{aligned}\frac{p_m - p_k}{L_{km}} + G_{km}\frac{p_k}{z\left(p_k,T_k\right)T_k}\frac{\left(h_m - h_k\right)}{L_{km}} + A_{km}\frac{z\left(p_k,T_k\right)T_k}{p_k}|q_{km}|\,q_{km} + \\ + B_{km}\left(\frac{q_{mk}^2z\left(p_m,T_m\right)T_m}{L_{km}p_m} - \frac{q_{km}^2z\left(p_k,T_k\right)T_k}{L_{km}p_k}\right) = 0\end{aligned} \tag{A.18}$$

$$\begin{aligned}\frac{p_k - p_m}{L_{km}} + G_{km}\frac{p_m}{z\left(p_m,T_m\right)T_m}\frac{\left(h_k - h_m\right)}{L_{km}} - A_{km}\frac{z\left(p_m,T_m\right)T_m}{p_m}|q_{mk}|\,q_{mk} + \\ + B_{km}\left(\frac{q_{km}^2z\left(p_k,T_k\right)T_k}{L_{km}p_k} - \frac{q_{mk}^2z\left(p_m,T_m\right)T_m}{L_{km}p_m}\right) = 0,\end{aligned} \tag{A.19}$$

in a similar way but taking as a reference the sum of forces acting on node "m", Eq. (A.20) and Eq. (A.21) are obtained,

$$\frac{p_m - p_k}{L_{km}} + G_{km}\frac{p_k}{z\left(p_k, T_k\right)T_k}\frac{\left(h_m - h_k\right)}{L_{km}} - A_{km}\frac{z\left(p_k, T_k\right)T_k}{p_k}\left|q_{km}\right|q_{km} + \\ + B_{km}\left(\frac{q_{mk}^2 z\left(p_m, T_m\right)T_m}{L_{km}p_m} - \frac{q_{km}^2 z\left(p_k, T_k\right)T_k}{L_{km}p_k}\right) = 0 \tag{A.20}$$

$$\frac{p_k - p_m}{L_{km}} + G_{km}\frac{p_m}{z\left(p_m, T_m\right)T_m}\frac{\left(h_k - h_m\right)}{L_{km}} + A_{km}\frac{z\left(p_m, T_m\right)T_m}{p_m}\left|q_{mk}\right|q_{mk} + \\ + B_{km}\left(\frac{q_{km}^2 z\left(p_k, T_k\right)T_k}{L_{km}p_k} - \frac{q_{mk}^2 z\left(p_m, T_m\right)T_m}{L_{km}p_m}\right) = 0. \tag{A.21}$$

Now if the Eq. (A.18) and Eq. (A.19) are reciprocally replaced and solved for the term "q_{km}," and respectively the Eq. (A.20) and Eq. (A.21) are solved for the term "q_{mk}," the following equations are obtained:

$$q_{km}\left|q_{km}\right| = p_k^2\left(\frac{1}{z\left(p_k, T_k\right)T_k A_{km}L_{km}} + G_{km}\frac{\left(h_k - h_m\right)\left(A_{km}L_{km} + B_{km}\right)}{z(p_k, T_k)^2 T_k^2 A_{km}^2 L_{km}^2}\right) - \\ - p_k p_m\left(\frac{1}{z\left(p_k, T_k\right)T_k A_{km}L_{km}} + G_{km}\frac{\left(h_k - h_m\right)\left(B_{km}\right)}{z\left(p_k, T_k\right)z\left(p_m, T_m\right)T_k T_m A_{km}^2 L_{km}^2}\right) \tag{A.22}$$

$$q_{mk}\left|q_{mk}\right| = p_m^2\left(\frac{1}{z\left(p_m, T_m\right)T_m A_{km}L_{km}} + G_{km}\frac{\left(h_m - h_k\right)\left(A_{km}L_{km} + B_{km}\right)}{z(p_m, T_m)^2 T_m^2 A_{km}^2 L_{km}^2}\right) - \\ - p_k p_m\left(\frac{1}{z\left(p_m, T_m\right)T_m A_{km}L_{km}} + G_{km}\frac{\left(h_m - h_k\right)\left(B_{km}\right)}{z\left(p_k, T_k\right)z\left(p_m, T_m\right)T_k T_m A_{km}^2 L_{km}^2}\right). \tag{A.23}$$

Note that the global constants G_{km}, A_{km} and B_{km}, and the length of the pipeline L_{km} are the same in the deduction of both equations, this because they correspond to gas and pipeline parameters that remain invariant at any point in the network. Hence, substituting these global constants into (A.22) and (A.23) and performing algebraic manipulations result

in

$$q_{km}^{iny}\left|q_{km}^{iny}\right| = \frac{D_{km}^5\pi^2 z_0^2 T_0^2}{8L_{km}^2\lambda_{km}^2 G p_0^2 z(p_k,T_k)^2 T_k^2}\Big[p_k^2\big(z\left(p_k,T_k\right)T_k\lambda_{km}L_{km}R_{air}+ \\ + gG\left(2D_{km}+\lambda_{km}L_{km}\right)\left(h_k-h_m\right)\big)- \\ - p_k p_m\frac{z\left(p_k,T_k\right)T_k}{z\left(p_m,T_m\right)T_m}\big(\lambda_{km}L_{km}R_{air}z\left(p_m,T_m\right)T_m+2gGD_{km}\left(h_k-h_m\right)\big)\Big] \tag{A.24}$$

$$q_{mk}^{iny}\left|q_{mk}^{iny}\right| = \frac{D_{km}^5\pi^2 z_0^2 T_0^2}{8L_{km}^2\lambda_{km}^2 G p_0^2 z(p_m,T_m)^2 T_m^2}\Big[p_m^2\big(z\left(p_m,T_m\right)T_m\lambda_{km}L_{km}R_{air}+ \\ + gG\left(2D_{km}+\lambda_{km}L_{km}\right)\left(h_m-h_k\right)\big)- \\ - p_k p_m\frac{z\left(p_m,T_m\right)T_m}{z\left(p_k,T_k\right)T_k}\big(\lambda_{km}L_{km}R_{air}z\left(p_k,T_k\right)T_k+2gGD_{km}\left(h_m-h_k\right)\big)\Big] \tag{A.25}$$

Lastly, considering $z_0 = 1$ [Menon05] and grouping several parameters of (A.24) and (A.25) as indicated in (A.26) and (A.27),

$$q_{km}^{iny}\left|q_{km}^{iny}\right| = \underbrace{\frac{D_{km}^5\pi^2 T_0^2}{8GL_{km}^2\lambda_{km}^2 p_0^2}}_{\alpha} \\ \Bigg[p_k^2\underbrace{\frac{\left(z\left(p_k,T_k\right)T_k\lambda_{km}L_{km}R_{air}+gG\left(2D_{km}+\lambda_{km}L_{km}\right)\left(h_k-h_m\right)\right)}{z(p_k,T_k)^2T_k^2}}_{\beta_{k1}} \\ - p_k p_m\underbrace{\frac{\left(z\left(p_m,T_m\right)T_m\lambda_{km}L_{km}R_{air}+2gGD_{km}\left(h_k-h_m\right)\right)}{z\left(p_m,T_m\right)T_m z\left(p_k,T_k\right)T_k}}_{\beta_{k2}}\Bigg] \tag{A.26}$$

$$q_{mk}^{iny}\left|q_{mk}^{iny}\right| = \underbrace{\frac{D_{km}^5\pi^2 T_0^2}{8GL_{km}^2\lambda_{km}^2 p_0^2}}_{\alpha} \\ \Bigg[p_m^2\underbrace{\frac{\left(z\left(p_m,T_m\right)T_m\lambda_{km}L_{km}R_{air}+gG\left(2D_{km}+\lambda_{km}L_{km}\right)\left(h_m-h_k\right)\right)}{z(p_m,T_m)^2T_m^2}}_{\beta_{m1}} \\ - p_k p_m\underbrace{\frac{\left(z\left(p_k,T_k\right)T_k\lambda_{km}L_{km}R_{air}+2gGD_{km}\left(h_m-h_k\right)\right)}{z\left(p_k,T_k\right)T_k z\left(p_m,T_m\right)T_m}}_{\beta_{m2}}\Bigg]. \tag{A.27}$$

The simplified expressions (A.28) and (A.29) are obtained, which are exclusively a function of the magnitudes of nodal pressure:

$$q_{km}^{iny}\left|q_{km}^{iny}\right| = \alpha\left[p_k^2\beta_{k1} - p_k p_m \beta_{k2}\right] \tag{A.28}$$

$$q_{mk}^{iny}\left|q_{mk}^{iny}\right| = \alpha\left[p_m^2\beta_{m1} - p_k p_m \beta_{m2}\right]. \tag{A.29}$$

A.2 Deduction of Δq equation

From the NFI equations and considering that they circulate in opposite directions, the difference between the inlet and outlet gas flow of a pipeline is given by the Eq. (A.30):

$$\Delta_q^{pipe} = q_{km}^{iny} + q_{mk}^{iny}. \tag{A.30}$$

Now assuming over the NFI equations (2.5) and (2.6) that the gas flow circulates through a completely horizontal pipe, that its compressibility condition is constant: $\Delta h = 0$ and $z = cte$, and that the direction of the gas flow is known, the expressions (A.31) and (A.32) can be obtained:

$$\left(q_{km}^{iny}\right)^2 = \frac{D_{km}^5 \pi^2 T_0^2 R_{air}}{8 L_{km}\lambda_{km} G p_0^2 T_{km} z}\left(p_k^2 - p_k p_m\right) \tag{A.31}$$

$$\left(q_{mk}^{iny}\right)^2 = -\frac{D_{km}^5 \pi^2 T_0^2 R_{air}}{8 L_{km}\lambda_{km} G p_0^2 T_{km} z}\left(p_m^2 - p_k p_m\right), \tag{A.32}$$

and therefore

$$q_{km}^{iny} = \frac{D_{km}^{2.5}\pi T_0}{p_0}\sqrt{\frac{R_{air}}{8 L_{km}\lambda_{km} G T_{km} z}}\left(p_k^2 - p_k p_m\right)^{\frac{1}{2}} \tag{A.33}$$

$$q_{mk}^{iny} = \frac{D_{km}^{2.5}\pi T_0}{p_0}\sqrt{\frac{R_{air}}{8 L_{km}\lambda_{km} G T_{km} z}}\left(-p_m^2 + p_k p_m\right)^{\frac{1}{2}}. \tag{A.34}$$

Furthermore, assuming that the temperature in the pipeline can be approximated by the linear average of the temperatures at both its ends, the following equation is obtained:

$$T_{km} = \frac{T_k + T_m}{2}. \tag{A.35}$$

On the other hand, by substituting (A.33) and (A.34) into (A.30),

$$\Delta_q^{pipe} = \frac{D_{km}^{2.5}\pi T_0}{p_0}\sqrt{\frac{R_{air}}{8L_{km}\lambda_{km}GT_{km}z}}\left[\left(p_k^2 - p_k p_m\right)^{\frac{1}{2}} + \left(-p_m^2 + p_k p_m\right)^{\frac{1}{2}}\right]. \tag{A.36}$$

Clearing and squaring both sides of the equation results in

$$\left[\frac{\Delta_q^{pipe} p_0}{D_{km}^{2.5}\pi T_0}\sqrt{\frac{8L_{km}\lambda_{km}GT_{km}z}{R_{air}}} - \left(-p_m^2 + p_k p_m\right)^{\frac{1}{2}}\right]^2 = \left(p_k^2 - p_k p_m\right). \tag{A.37}$$

Performing algebraic manipulations over (A.37) results in

$$(p_k - p_m)^2 = \frac{\left(\Delta_q^{pipe}\right)^2 p_0^2 8L_{km}\lambda_{km}GT_{km}z}{D_{km}^5\pi^2 T_0^2 R_{air}} - \frac{2\Delta_q^{pipe} p_0}{D_{km}^{2.5}\pi T_0}\sqrt{\frac{8L_{km}\lambda_{km}GT_{km}z}{R_{air}}}\left(-p_m^2 + p_k p_m\right)^{\frac{1}{2}}. \tag{A.38}$$

Clearing and squaring again results in the following expression:

$$\left[(p_k - p_m)^2 - \frac{\left(\Delta_q^{pipe}\right)^2 p_0^2 8L_{km}\lambda_{km}GT_{km}z}{D_{km}^5\pi^2 T_0^2 R_{air}}\right]^2 = \left[-\frac{2\Delta_q^{pipe} p_0}{D_{km}^{2.5}\pi T_0}\sqrt{\frac{8L_{km}\lambda_{km}GT_{km}z}{R_{air}}}\left(-p_m^2 + p_k p_m\right)^{\frac{1}{2}}\right]^2. \tag{A.39}$$

Solving the binomial

$$\begin{aligned}(p_k - p_m)^4 - 2\frac{\left(\Delta_q^{pipe}\right)^2 p_0^2 8L_{km}\lambda_{km}GT_{km}z}{D_{km}^5\pi^2 T_0^2 R_{air}}(p_k - p_m)^2 + \left(\frac{\left(\Delta_q^{pipe}\right)^2 p_0^2 8L_{km}\lambda_{km}GT_{km}z}{D_{km}^5\pi^2 T_0^2 R_{air}}\right)^2 \\ = 4\frac{\left(\Delta_q^{pipe}\right)^2 p_0^2 8L_{km}\lambda_{km}GT_{km}z}{D_{km}^5\pi^2 T_0^2 R_{air}}\left(-p_m^2 + p_k p_m\right)\end{aligned} \tag{A.40}$$

and regrouping the terms

$$\begin{aligned}(p_k - p_m)^4 + \left(\frac{\left(\Delta_q^{pipe}\right)^2 p_0^2 8L_{km}\lambda_{km}GT_{km}z}{D_{km}^5\pi^2 T_0^2 R_{air}}\right)^2 - \\ - \frac{\left(\Delta_q^{pipe}\right)^2 p_0^2 8L_{km}\lambda_{km}GT_{km}z}{D_{km}^5\pi^2 T_0^2 R_{air}}\left(2(p_k - p_m)^2 + 4\left(-p_m^2 + p_k p_m\right)\right) = 0\end{aligned} \tag{A.41}$$

and simplifying (A.41) gives rise to the following expression:

$$(p_k - p_m)^4 - \frac{\left(\Delta_q^{pipe}\right)^2 p_0^2 8L_{km}\lambda_{km}GT_{km}z}{D_{km}^5\pi^2 T_0^2 R_{air}}\left(2\left(p_k^2 - p_m^2\right)\right) + \left(\frac{\left(\Delta_q^{pipe}\right)^2 p_0^2 8L_{km}\lambda_{km}GT_{km}z}{D_{km}^5\pi^2 T_0^2 R_{air}}\right)^2 = 0. \tag{A.42}$$

Lastly, the equation that describes the difference between the gas flow at the inlet and outlet nodes is obtained from the roots of the polynomial (A.42) :

$$\Delta_q^{pipe} = \frac{D_{km}^{2.5}\pi T_0}{p_0}\sqrt{\frac{R_{air}\left(p_k - p_m\right)}{8L_{km}\lambda_{km}GT_{km}z}}\left(p_k^{\frac{1}{2}} - p_m^{\frac{1}{2}}\right) \tag{A.43}$$

Appendix B

Systems' data

B.1 Electrical networks

B.1.1 3-bus test system

Table B.1: Generator data

Bus	P^{sch} $[MW]$	Q^{sch} $[MVARs]$	P^{nom} $[MW]$	P^{min} $[MW]$	$Q^{nom,min}$ $[MVARs]$	$Q^{nom,max}$ $[MVARs]$	v_{ref} $[pu]$	K_{reg} %	Reg. State	a	b	c	Cost $\$/BTU$
1	486.55	-30.614	500	0	-150	160	1.02	4.5	yes	769.2695	0.01055	0.00211	0.9
2	350	87.278	350	0	-100	125	1.03	3	no	469.2695	0.01055	0.00211	1.1
3	617.24	174.302	650	0	-300	160	1.05	3.2	yes	569.2695	0.01055	0.00211	1

Table B.2: Transmission lines' data

From	to	$r\,[pu]$	$x\,[pu]$	$g\,[pu]$	$b\,[pu]$
1	2	0.01008	0.0504	0	0.1025
1	3	0.00744	0.0372	0	0.0775
2	3	0.00744	0.0372	0	0.0775

Table B.3: Loads' data

Bus	$P^{sch}\,[MW]$	$Q^{sch}\,[MVARs]$	K_{pf}	K_{pp}	K_{pc}	K_{pz}	K_{qf}	K_{qp}	K_{qc}	K_{qz}
1	400	30.99	0.04	0.99	0.01	0	0	0.99	0.01	0
2	650	105.35	0.01	0.98	0.02	0	0	0.98	0.02	0
3	400	123.94	0	1	0	0	0	1	0	0

Table B.4: Shunt compensators' data

Bus	$g_{sh}\,[pu]$	$b_{sh}\,[pu]$
1	0	0.19

B.2 Gas networks

B.2.1 Belgium network

Table B.5: Node data

#	Name	Pressure [bar]	Height [m]	Source [$SCMH$]	Load[$SMCH$]	Temp.[$^{\circ}K$]
1	Zeebrugge	72	10	0	0	281.15
2	Dudzele	0	10	3.50E+05	0	281.15
3	Brugge	0	10	0	1.63E+05	281.15
4	Zomergem	0	10	0	0	281.15
5	Loenhout	0	10	1.17E+05	0	281.15
6	Antwerpen	0	10	0	1.68E+05	281.15
7	Gent	0	10	0	2.19E+05	281.15
8	Voeren	0	10	9.17E+05	0	281.15
9	Berneau	0	10	0	0	281.15
10	Liège	0	10	0	2.65E+05	281.15
11	Warnand	0	10	0	0	281.15
12	Namur	0	10	0	8.83E+04	281.15
13	Anderlues	0	10	5.00E+04	0	281.15
14	Péronnes	0	10	4.00E+04	0	281.15
15	Mons	0	10	0	2.85E+05	281.15
16	Blaregnies	0	10	0	6.51E+05	281.15
17	Wanze	0	10	0	0	281.15
18	Sinsin	0	10	0	0	281.15
19	Arlon	0	10	0	9.25E+03	281.15
20	Pétange	0	10	0	8.00E+04	281.15

Table B.6: Pipelines' data

Pipeline	From	to	$L\,[Km]$	$D\,[mm]$	$\varepsilon\,[mm]$	ϵ
1	1	2	4	890	0.05	1
2	1	2	4	890	0.05	1
3	2	3	6	890	0.05	1
4	2	3	6	890	0.05	1
5	3	4	26	890	0.05	1
6	5	6	43	590.1	0.05	1
7	6	7	29	590.1	0.05	1
8	7	4	19	590.1	0.05	1
9	4	14	55	890	0.05	1
10	8	9	5	890	0.05	1
11	8	9	5	395.5	0.05	1
12	9	10	20	890	0.05	1
13	9	10	20	395.5	0.05	1
14	10	11	25	890	0.05	1
15	10	11	25	395.5	0.05	1
16	11	12	42	890	0.05	1
17	12	13	40	890	0.05	1
18	13	14	5	890	0.05	1
19	14	15	10	890	0.05	1
20	15	16	25	890	0.05	1
21	11	17	10.5	395.5	0.05	1
22	18	19	98	315.5	0.05	1
23	19	20	6	315.5	0.05	1

Table B.7: Compressor stations' data

#	From	to	η	E	CR	$T_s\,[K]$	α	β	γ
1	17	18	1	1	1.13262	281.15	0	8.33	0

B.2.2 15-node network

Table B.8: Node data

#	Name	Pressure [$psia$]	Height [ft]	Source [$SCFH$]	Load[$SFCH$]	Temp.[$^\circ R$]
1	Nod-1	1300	10	0	0	520
2	Nod-2	1278.63	10	6.87E+06	0	520
3	Nod-3	0	10	0	3.84E+06	520
4	Nod-4	0	10	0	1.22E+06	520
5	Nod-5	0	10	0	0	520
6	Nod-6	0	10	0	0	520
7	Nod-7	0	10	0	0	520
8	Nod-8	0	10	0	0	520
9	Nod-9	0	10	0	0	520
10	Nod-10	0	10	0	0	520
11	Nod-11	0	10	0	0	520
12	Nod-12	0	10	0	0	520
13	Nod-13	0	10	0	0	520
14	Nod-14	0	10	0	0	520
15	Nod-15	0	10	0	5.01E+05	520

Table B.9: Pipelines' data

Pipeline	From	to	$L\,[mi]$	$D\,[in]$	$\varepsilon\,[in]$	ϵ
1	1	3	80.5	19.56	0.001968	0.9
2	2	4	80.3	19.56	0.001968	0.9
3	3	4	55.9	19.56	0.001968	0.9
4	3	5	81.1	19.62	0.001968	0.9
5	4	7	87.9	19.62	0.001968	0.9
6	6	9	93.5	19.62	0.001968	0.9
7	8	11	99.7	16.69	0.001968	0.9
8	10	13	93.5	16.69	0.001968	0.9
9	12	14	97.9	16.69	0.001968	0.85
10	13	14	86.6	16.69	0.001968	0.9
11	13	15	79.7	16.69	0.001968	0.9
12	14	15	83.5	16.69	0.001968	0.85

Table B.10: Compressor stations' data

#	From	to	η	E	CR	$T_s\,[°R]$	α	β	γ
1	5	6	0.83	1	1.2	520	0	8.33	0
2	7	8	0.84	1	1.3	520	0	8.33	0
3	9	10	0.83	1	1.035239	520	0	8.33	0
4	11	12	0.84	1	1	520	0	8.33	0

B.2.3 Network of 11 nodes for low pressure

Table B.11: Node data

#	Name	Pressure $[bar]$	Height $[m]$	Source $[SCMH]$	Load$[SMCH]$	Temp.$[K]$
1	One	0.075	0	0	0	281.15
2	Two	0	0	0	219	281.15
3	Three	0	0	0	192	281.15
4	Four	0	0	0	175	281.15
5	Five	0	0	0	228	281.15
6	Six	0	0	0	157	281.15
7	Seven	0	0	0	43.8	281.15
8	Eight	0	0	0	206	281.15
9	Nine	0	0	0	48	281.15
10	Ten	0	0	0	42	281.15
11	Eleven	0	0	0	30	281.15

Table B.12: Pipelines' data

Pipeline	From	to	$L\,[Km]$	$D\,[mm]$	$\varepsilon\,[mm]$	ϵ
1	1	2	0.05	160	0.05	1.0
2	2	3	0.5	160	0.05	1.0
3	2	4	0.5	110	0.05	1.0
4	2	5	0.5	110	0.05	1.0
5	3	6	0.6	110	0.05	1.0
6	3	7	0.6	110	0.05	1.0
7	3	8	0.5	110	0.05	1.0
8	5	6	0.6	80	0.05	1.0
9	4	7	0.6	80	0.05	1.0
10	6	8	0.78	80	0.05	1.0
11	7	8	0.78	80	0.05	1.0
12	7	9	0.2	80	0.05	1.0
13	9	10	0.2	80	0.05	1.0
14	10	11	0.2	80	0.05	1.0

Bibliography

[Aalto08] Aalto, H. R. M. Transfer functions for natural gas pipeline systems. *In IFAC Proceedings Volumes (IFAC-PapersOnline)*, Vol. 17, pp. 889–894. 2008.

[Abdolahi07] Abdolahi, F., Mesbah, A., Boozarjomehry, R. B., and Svrcek, W. Y. The effect of major parameters on simulation results of gas pipelines. *International Journal of Mechanical Sciences*, 49(8):989–1000, 2007.

[Abeysekera16] Abeysekera, M., Wu, J., Jenkins, N., and Rees, M. Steady state analysis of gas networks with distributed injection of alternative gas. *Applied Energy*, 164:991–1002, 2016.

[Acha04] Acha, E., Fuerte-Esquivel, C. R., Ambriz-Perez, H., and Angeles-Camacho, C. *FACTS: Modelling and Simulation in Power Networks*. John Wiley & Sons, LTD, 2004.

[AGA85] AGA. Compressibility and supercompressibility of natural gas and other related hydrocarbon gases. Tech. Rep. 8, 1985.

[An03] An, S., Li, Q., and Gedra, T. W. Natural Gas and Electricity Optimal Power Flow. *In Proceedings of the IEEE Power Engineering Society Transmission and Distribution Conference*, Vol. 1, pp. 138–143. IEEE, 2003.

[Arumugam15] Arumugam, G. S. *Alternate models for natural gas transportation system performance optimization.* Ph.D. Thesis, University of Kentucky, 2015.

[Bamzah10] Bamzah, N. S. B. *Newton loop-node analysis study on gas pipeline network.* Ph.D. Thesis, Universiti Malaysia Pahang, 2010.

[Behbahani-Nejad08] Behbahani-Nejad, M. and Bagheri, A. A MATLAB Simulink Library for Transient Flow Simulation of Gas Networks. *World Academy of Science, Engineering and Technology, International Science Index 19*, 2(7):139–145, 2008.

[Bermúdez15] Bermúdez, A., González-Díaz, J., González-Diéguez, F. J., González-Rueda, Á. M., and de Córdoba, M. P. F. Simulation and Optimization Models of Steady-state Gas Transmission Networks. *Energy Procedia*, 64(C):130–139, 2015.

[Bermúdez17] Bermúdez, A., González-Díaz, J., and González-Diéguez, F. J. Existence of solution to a model for gas transportation networks on non-flat topography. *Nonlinear Analysis: Real World Applications*, 37:71–93, oct 2017.

[Beyza19] Beyza, J., Dominguez-Navarro, J. A., and Yusta, J. M. Linear-analog transformation approach for coupled gas and power flow analysis. *Electric Power Systems Research*, 168:239–249, mar 2019.

[Borraz-Sánchez10] Borraz-Sánchez, C. *Optimization methods for pipeline transportation of natural gas.* Ph.D. Thesis, University of Bergen, 2010.

[Ćalović81] Ćalović, M. and Strezoski, V. Calculation of steady-state load flows incorporating system control effects and consumer self-

regulation characteristics. *International Journal of Electrical Power & Energy Systems*, 3(2):65–74, apr 1981.

[Camaraza Medina11] Camaraza Medina, Y. and García Morales, O. F. Nuevo Modelo para la Determinación del Factor de Fricción en el régimen de flujo turbulento. *Revista de Arquitectura e Ingeniería*, 5(2):16, 2011.

[CENACE19] CENACE. Programa de Ampliación y Modernización de la Red Nacional de Transmisión y Redes Generales de Distribución del Mercado Electro Mayorista. PRODESEN 2019-2033. p. 576, 2019.

[Chaudry08] Chaudry, M., Jenkins, N., and Strbac, G. Multi-time period combined gas and electricity network optimisation. *Electric Power Systems Research*, 78(7):1265–1279, jul 2008.

[Coelho07] Coelho, P. M. and Pinho, C. Considerations about equations for steady state flow in natural gas pipelines. *Journal of the Brazilian Society of Mechanical Science and Engineering*, 29(3):262–273, 2007.

[Correa-Posada15] Correa-Posada, C. M. and Sanchez-Martin, P. Integrated Power and Natural Gas Model for Energy Adequacy in Short-Term Operation. *IEEE Transactions on Power Systems*, 30(6):3347–3355, nov 2015.

[Crane Company88] Crane Company. Flow of fluids throuh valves, fittings and pipe. Tech. rep., New York, 1988.

[De Wolf00] De Wolf, D. and Smeers, Y. The Gas Transmission Problem Solved by an Extension of the Simplex Algorithm. *Management Science*, 46(11):1454–1465, 2000.

[De Wolf17] De Wolf, D. Mathematical properties of formulations of the gas transmission problem. *Tehnički glasnik*, 11(3):133–137, 2017.

[Farzaneh-Gord16] Farzaneh-Gord, M. and Rahbari, H. R. Unsteady natural gas flow within pipeline network, an analytical approach. *Journal of Natural Gas Science and Engineering*, 28:397–409, jan 2016.

[Ferreira A.18] Ferreira A., O. and Passos F., J. New DC Power Flow Formulation Considering The Primary Frequency Regulation. *IEEE Latin America Transactions*, 16(4):1150–1157, 2018.

[Ferris97] Ferris, M. C. and Pang, J. S. Engineering and Economic Applications of Complementarity Problems. *SIAM Review*, 39(4):669–713, jan 1997.

[Geidl07] Geidl, M. and Andersson, G. Optimal Power Flow of Multiple Energy Carriers. *IEEE Transactions on Power Systems*, 22(1):145–155, feb 2007.

[Johnson35] Johnson, T. W., Berwald, W. B., Association, A. G., and of Mines, U. S. B. *Flow of Natural Gas Through High-pressure Transmission Lines: A Joint Report*. Monograph (United States. Bureau of Mines). Lord Baltimore Press, 1935.

[Ke00] Ke, S. Transient analysis of isothermal gas flow in pipeline network. *Chemical Engineering Journal*, 76(2):169–177, feb 2000.

[Kralik84] Kralik, J., Stiegler, P., Vostrý, Z., and ZáVORKA, J. Modeling the Dynamics of Flow in Gas Pipelines. *IEEE Transactions on Systems, Man and Cybernetics*, SMC-14(4):586–596, 1984.

[Liu09] Liu, C., Shahidehpour, M., Fu, Y., and Li, Z. Security-constrained unit commitment with natural gas transmission constraints. *IEEE Transactions on Power Systems*, 24(3):1523–1536, aug 2009.

[Liu11] Liu, C., Shahidehpour, M., and Wang, J. Coordinated scheduling of electricity and natural gas infrastructures with a transient model for natural gas flow. *Chaos: An Interdisciplinary Journal of Nonlinear Science*, 21(2):025102, jun 2011.

[Martinez-Mares12] Martinez-Mares, A. and Fuerte-Esquivel, C. R. A unified gas and power flow analysis in natural gas and electricity coupled networks. *IEEE Transactions on Power Systems*, 27(4):2156–2166, 2012.

[Massrur18] Massrur, H. R., Niknam, T., Aghaei, J., Shafie-Khah, M., and Catalao, J. P. Fast Decomposed Energy Flow in Large-Scale Integrated Electricity-Gas-Heat Energy Systems. *IEEE Transactions on Sustainable Energy*, 9(4):1565–1577, 2018.

[Men17] Men, X., Wang, Z., Cao, J., and Pan, X. Coupling analysis of gas-electric hybrid system based on Newton–Raphson method. *The Journal of Engineering*, 2017(13):1505–1510, 2017.

[Meng19] Meng, Q. W., Guan, Q. S., Jia, N., Zhang, L. X., and Wang, Y. S. An Improved Sequential Energy Flow Analysis Method Based on Multiple Balance Nodes in Gas-Electricity Interconnection Systems. *IEEE Access*, 7:95487–95495, 2019.

[Menon05] Menon, E. S. *Gas Pipeline Hydraulics*. CRC Press, Boca Raton, 1st ed., 2005.

[Mikolajková18] Mikolajková, M., Saxén, H., and Pettersson, F. Linearization of an MINLP model and its application to gas distribution optimization. *Energy*, 146:156–168, mar 2018.

[Modisette00] Modisette, J. L. Equation of state tutorial. *In PSIG Annual Meeting*, p. 21. Pipeline Simulation Interest Group, Savannah, Georgia, 2000.

[Mohtashami09] Mohtashami, S. and Mashhadi, H. R. Power generation scheduling of thermal units considering gas pipelines constraints. *World Academy of Science, Engineering and Technology*, 37:948–953, 2009.

[Mokhatab19] Mokhatab, S., Poe, W. A., and Mak, J. Y. *Handbook of Natural Gas Transmission and Processing*. Gulf Professional Publishing, $4^{\underline{\text{th}}}$ ed., 2019.

[Moller04] Moller, M. *Mixed integer models for the optimisation of gas networks in the stationary case*. Ph.D. Thesis, Technischen Universit at Darmstadt, 2004.

[Moritz07] Moritz, S. *A mixed integer approach for the transient case of gas network optimization*. Ph.D. Thesis, The Technical University of Darmstadt, 2007.

[Munoz03] Munoz, J., Jimenez-Redondo, N., Perez-Ruiz, J., and Barquin, J. Natural gas network modeling for power systems reliability studies. *In 2003 IEEE Bologna PowerTech - Conference Proceedings*, Vol. 4, pp. 20–27. Bologna, Italy, 2003.

[Murillo-Sánchez00] Murillo-Sánchez, C. E. *On the integration of unit commitment and optimal power flow*. Ph.D. Thesis, Cornell University, 2000.

[Narváez99] Narváez, P. C. Solución de redes de flujo para gases usando el modelo de balance de nodos y el método de linealización de ecuaciones. *Revista Ingeniería e Investigación*, 44:56–62, dec 1999.

[Okamura75] Okamura, M., O-ura, Y., Hayashi, S., Uemura, K., and Ishiguro, F. A new power flow model and solution method - Including load and generatos characteristics and effects of system control devices -. *IEEE Transactions on Power Apparatus and Systems*, 94(3):1042–1050, may 1975.

[Olatunde12] Olatunde, A. O., Adeosun, T. A., Usman, M. A., Odunlami, O. M., Olowofoyeku, M. A., Ekakitie, T. E., and Mohammed, A. M. Direct Calculation of Unsteady-State Weymouth Equations for Gas Volumetric Flow Rate with Different Friction Factors in Horizontal and Inclined Pipes. *Engineering*, 04(04):202–209, 2012.

[Olorunniwo81] Olorunniwo, F. O. *A methodology for the optimal design and capacity expansion planning of natural gas transmission networks*. Ph.D. Thesis, The University of Texaas at Austin, 1981.

[Osiadacz87] Osiadacz, A. *Simulation and analysis of gas networks*. Gulf Publishing Company, Houston, 1987.

[Pambour17] Pambour, K. A., Erdener, B. C., Bolado-Lavin, R., and Dijkema, G. P. Development of a simulation framework for analyzing security of supply in integrated gas and electric power systems. *Applied Sciences (Switzerland)*, 7(1):47, jan 2017.

[Quelhas Alves de Freitas06] Quelhas Alves de Freitas, A. M. *Economic efficiencies of the energy flows from the primary resource suppliers to the*

electric load centers. Ph.D. Thesis, Iowa State University, 2006.

[Restrepo05] Restrepo, J. and Galiana, F. Unit Commitment With Primary Frequency Regulation Constraints. *IEEE Transactions on Power Systems*, 20(4):1836–1842, nov 2005.

[Ríos-Mercado06] Ríos-Mercado, R. Z., Kim, S., and Boyd, E. A. Efficient operation of natural gas transmission systems: A network-based heuristic for cyclic structures. *Computers & Operations Research*, 33(8):2323–2351, aug 2006.

[Ríos-Mercado15] Ríos-Mercado, R. Z. and Borraz-Sánchez, C. Optimization problems in natural gas transportation systems: A state-of-the-art review. *Applied Energy*, 147:536–555, jun 2015.

[Royo01] Royo, C. B. *Generalized unit commitment by the radar multiplier method*. Ph.D. Thesis, UniversitatPolitecnica de Catalunya, 2001.

[Saadat79] Saadat, M. H. Steady state analysis of power systems including the effects of control devices. *Electric Power Systems Research*, 2(2):111–118, jun 1979.

[Schroeder01] Schroeder, D. W. A tutorial on pipe flow equations. *PSIG Annual Meeting 2001*, jan 2001.

[SENER17a] SENER. Prospectiva de gas natural 2017-2031. Tech. rep., 2017.

[SENER17b] SENER. Prospectiva del Sector Eléctrico 2017-2031. Tech. rep., 2017.

[Shi17] Shi, J., Wang, L., Wang, Y., and Zhang, J. Generalized energy flow analysis considering electricity gas and heat sub-

systems in local-area energy systems integration. *Energies*, 10(4):1–17, 2017.

[Szoplik12] Szoplik, J. The Gas Transportation in a Pipeline Network. *In Advances in Natural Gas Technology*, chap. 13. InTech, 2012.

[Tabkhi07] Tabkhi, F. *Optimisation de réseaux de transport de gaz*. Ph.D. Thesis, Institut national polytechnique de Toulouse, 2007.

[Taherinejad14] Taherinejad, M., Hosseinalipour, S. M., and Madoliat, R. Steady flow analysis and modeling of the gas distribution network using the electrical analogy. *International Journal of Engineering, Transactions B: Applications*, 27(8):1269–1276, 2014.

[Taimin Gindalan10] Taimin Gindalan, E. O. *Newton loop method in gas pipeline network*. Ph.D. Thesis, Universiti Malaysia Pahang, 2010.

[Tao98] Tao, W. Q. and Ti, H. C. Transient analysis of gas pipeline network. *Chemical Engineering Journal*, 69(1):47–52, 1998.

[Tomasgard07] Tomasgard, A., Rømo, F., Fodstad, M., and Midthun, K. Optimization models for the natural gas value chain. *Geometric Modelling, Numerical Simulation, and Optimization*, pp. 521–558, 2007.

[Tovar-Ramírez19] Tovar-Ramírez, C. A., Fuerte-Esquivel, C. R., Martínez Mares, A., and Sánchez-Garduño, J. L. A generalized short-term unit commitment approach for analyzing electric power and natural gas integrated systems. *Electric Power Systems Research*, 172:63–76, jul 2019.

[Triola09] Triola, M. F. *Mario F. Triola*. Pearson Educación de México, S.A. de C.V., México, $10^{\underline{\text{th}}}$ ed., 2009.

[University of Washington07] University of Washington. Power Systems Test Case Archive - UWEE, 2007.
URL `http://www.ee.washington.edu/research/pstca/`

[Unsihuay07] Unsihuay, C., Lima, J. W. M., and de Souza, A. Z. Modeling the Integrated Natural Gas and Electricity Optimal Power Flow. *In 2007 IEEE Power Engineering Society General Meeting*, Vol. 1, pp. 1–7. IEEE, jun 2007.

[Woldeyohannes09] Woldeyohannes, A. D., Amin, M., and Majid, A. Simulation of Natural Gas Transmission Pipeline Network System Performance. *Journal of Energy and Power Engineering*, 3(12):1934–8975, 2009.

[Woldeyohannes11] Woldeyohannes, A. D. and Majid, M. A. A. Simulation model for natural gas transmission pipeline network system. *Simulation Modelling Practice and Theory*, 19(1):196–212, jan 2011.

[Wong68] Wong, P. and Larson, R. Optimization of natural-gas pipeline systems via dynamic programming. *IEEE Transactions on Automatic Control*, 13(5):475–481, oct 1968.

[Wu00] Wu, S., Ríos-Mercado, R., Boyd, E., and Scott, L. Model relaxations for the fuel cost minimization of steady-state gas pipeline networks. *Mathematical and Computer Modelling*, 31(2-3):197–220, jan 2000.

[Zeng16] Zeng, Q., Fang, J., Li, J., and Chen, Z. Steady-state analysis of the integrated natural gas and electric power system with bi-directional energy conversion. *Applied Energy*, 184:1483–1492, dec 2016.

Index

Average flow equation, 33, 49

Brake horsepower, 49, 133

Compressibility factor, 26
Compressor stations, 49, 117, 133
Continuity equation, 22, 113
Coupling, 74, 134
Critical flow, 29

Electric generators, 62
Electric loads, 64
Equation of state, 23, 113

Frequency control, 90
Friction factor, 28
Fritzsche equation, 36
Fully turbulent flow, 30

General flow equation, 34, 49

Heat rate curve, 74

IGT equation, 35

Lacey equation, 37
Laminar flow, 29
Linepack, 31, 113

Momentum equation, 22, 112
Mueller equation, 35
Multi-period AFE model, 114, 133
Multi-period NFI model, 115, 133

Nodal flow injection equations, 24, 25, 49

Panhandle A equation, 35
Panhandle B equation, 34
Partially turbulent flow, 29
Pole equation, 37
Polyflo equation, 36

Reynolds number, 28

Spitzglass equation, 36
Spitzglass LP equation, 36

Transient natural gas flow, 112

Weymouth equation, 35